Modelling elevations, inundation extent and hazard risk for extreme flood events

by

Davor Kvočka

A thesis submitted to Cardiff University
in candidature for the degree of
Doctor of Philosophy

Cardiff, 2017

Dedicated to my parents Marija Čolić and Milenko Kvočka

Abstract

Climate change is expected to result in more frequent occurrences of extreme flood events, such as flash flooding and large scale river flooding. Therefore, there is a need for accurate flood risk assessment schemes in areas prone to extreme flooding. This research study investigates what flood risk assessment tools and procedures should be used for flood risk assessment in areas where the emergence of extreme flood events is possible. The first objective was to determine what type of flood inundation models should be used for predicting the flood elevations, velocities and inundation extent for extreme flood events. Therefore, there different flood inundation model structures were used to model a well-documented extreme flood event. The obtained results suggest that it is necessary to incorporate shock-capturing algorithms in the solution procedure when modelling extreme flood events, since these algorithms prevent the formation of spurious oscillations and provide a more realistic simulation of the flood levels. The second objective was to investigate the appropriateness of the "simplification strategy" (i.e. improving simulation results by increasing roughness parameter) when used as a flood risk assessment modelling tool for areas susceptible to extreme flooding. The obtained results suggest that applying such strategies can lead to significantly erroneous predictions of the peak water levels and the inundation extent, and thus to inadequate flood protection design. The third and final objective was to determine what type of flood hazard assessment methods should be used for assessing the flood hazard to people caused by extreme flooding. Therefore, two different flood hazard assessment criteria were modelled for three extreme flood events. The predicted results suggest that in areas prone to extreme flooding, the flood hazard indices should be predicted with physics-based formulae, as these methods consider all of the physical forces acting on a human body in floodwaters, take into account the rapid changes in the flow regime, which often occur for extreme events, and enable a rapid assessment of the degree of flood hazard to be made in a short time period.

Declaration

This work has not been submitted in substance for any other degree or award at this or any other university or place of learning, nor is being submitted concurrently in candidature for any degree or other award.

Signed . . . . Date . . . .

Statement 1

This thesis is being submitted in partial fulfilment of the requirements for the degree of PhD.

Signed . . . . Date . . . .

Statement 2

This thesis is the result of my own independent work / investigation, except where otherwise stated. Other sources are acknowledged by explicit references. The views expressed are my own.

Signed . . . . Date . . . .

Statement 3

I hereby give consent for my thesis, if accepted, to be available for photocopying and for inter-library loan, and for the title and summary to be made available to outside organisations.

Signed . . . . Date . . . .

Statement 4

I hereby give consent for my thesis, if accepted, to be available for photocopying and for inter-library loans after expiry of a bar on access previously approved by the Academic Standards & Quality Committee.

Signed . . . . Date . . . .

Acknowledgements

Table of Contents

List of Figures

List of Tables

CHAPTER 1

Introduction

1.1 Research background

From the beginning of mankind flooding has played a major role in the evolution of the civilisation. For example, regular flooding brought great wealth and prosperity to some civilisations, such as to Ancient Egypt. On the other hand, flooding also wiped out entire communities and changed the course of the human history, as it is the case with the Biblical flooding in the Black Sea region. Nowadays, flooding is the most frequently occurring natural hazard in the world, it has the greatest damage potential among all natural disasters and annually affects nearly 180 million people worldwide (Mogollón et al., 2016).

Contemporary climate impact studies suggest that climate change will have a key role in the intensification and acceleration of the hydrological cycle (Huntington, 2006, Christensen and Christensen, 2007, Kundzewicz, 2008, Durack et al., 2012). This intensified circulation of the water cycle is expected to result in the occurrence of more frequent and intense rainfall events (Beniston, 2009), which in turn is expected to result in an increase in the magnitude, severity, frequency and intensity of flooding in the near future (Allan and Soden, 2008, Lenderink and Van Meijgaard, 2008, Pall et al., 2011, Min et al., 2011, Rojas et al., 2013, Bruwier et al., 2015). In addition to more frequent future flooding, an increase in the world's population from the current level of 7.3 billion to the anticipated 9.7 billion by 2050 will intensify urbanisation (UN, 2015). It is projected that two-thirds of the world's population will live in urban areas by 2050, and that 90% of the projected urban expansion will occur in Africa and Asia (UN, 2014), i.e. in regions where the majority of the general population already live in areas highly prone to flooding (Muis et al., 2015). All this suggests that the number of citizens affected globally by flooding will drastically increase in the near future.

A flood can be described as a situation where water temporarily covers or submerges a part of land that is usually dry. Flooding may occur due to (i) meteorological and hydrological factors, such as heavy precipitation (Butler et al., 2015), snow melting (Park and Markus, 2014), glacial outburst (Galeczka et al., 2015), ice-jams (Beltaos, 2014), high tide and intense storm events (Breilh et al., 2014), (ii) human factors, such as structural failures of hydraulic structures (e.g. levees and dams) (Bergman et al., 2014), and (iii) combination of weather and human factors, such as heavy rain and land cover change (e.g. alteration of absorptive land cover with impervious surfaces) (Sajikumar and Remya, 2015) or intense precipitation and inadequate drainage systems (Fu and Butler, 2014). Based on these characteristics, flooding can be separated into different categories or types of flooding, such as coastal flooding, river flooding, flash flooding and urban flooding.

Even though flooding is the most common natural disaster, some flood events remain in the human consciousness for many generations due to their massive devastation or high death toll. These extreme flood events can sometimes have such enormous impact on the wider communities that they become the subject of folklore songs and mythical tales. Categorising past flood events as normal or extreme can be a matter of debate. However, there are some orientation guides that can be used for categorising the scale of past flood events. Based on the extensive flood database collected at the Dartmouth Flood Observatory, Brakenridge (2012) suggested two indices for characterising past flood events, i.e. flood severity and flood magnitude. The flood severity is not an exact descriptive statistic, but more of an orientation method that allows the use of expert judgment to estimate how unusual the flood or discharge was (Kundzewicz et al., 2013). Three flood severity classes were defined, which are based on the flood recurrence interval: Class 1 includes large flood events with a return period of the order 10-20 years, Class 2 includes very large flood events with a return period of between 20 and 100 years, and Class 3 includes extreme flood events with a return period equal to, or greater than, 100 years (Brakenridge, 2012, Kundzewicz et al., 2013). Severity is an important flood characteristic, but it does not provide information on other critical aspects of flooding, such as flood duration or the extent of flooding (Kundzewicz et al., 2013). Therefore, a second statistic is needed, i.e. flood magnitude. Flood magnitude is defined as a function of flood severity, flood duration and flood inundation area (Brakenridge, 2012). Flood

magnitude is designed to mimic the Richter scale for earthquakes and thus provides a continuous metric, instead of just artificially classifying floods into different flood classes (Kundzewicz et al., 2013).

Determining the scale of past flood events should therefore be based on statistical descriptors (i.e. flood severity), spatiotemporal descriptors (i.e. flood magnitude) and also on socio-economical descriptors (e.g. the extent of flood damage, human casualties, psychological impact etc.). This being the case, an extreme flood event can be simply characterised as a flood event with a small probability of occurrence, but with a significant impact on human society in terms of general damage, human casualties and overall social disruption. Taking into account all the aforementioned considerations, there are four types of floods which can give rise to an extreme flood event. These are: (i) dam-break floods (Duffaut, 2013, Bergman et al., 2014, Raška and Emmer, 2014), (ii) storm surges (Chau et al., 2013, Breilh et al., 2014, Androulidakis et al., 2015), (iii) flash floods (Moussa and Bocquillon, 2009, Martínez Ibarra, 2012, Foulds et al., 2014, Amengual et al., 2015), and (iv) extreme/large river floods (Zhi-Yong et al., 2013, Bruwier et al., 2015, Herget et al., 2015, Schröter et al., 2015, Antico et al., 2015). Among these types of flood events, flash floods and large river floods are the most common and generally give rise to the most serious extreme flood events (Ashley and Ashley, 2008, Di Baldassarre et al., 2010).

Flash floods can be defined as rapid surface water response to (i) a short, high-intensity precipitation mainly of convective origin and often orographically enhanced (Gaume et al., 2009), or (ii) a sudden release of water due to dam break, ice jam or glacial lake outbreak (Calianno et al., 2013, Worni et al., 2013). The occurrence of a flash flood is due to a combination of different complex factors, such as the characteristics of the rain (e.g., intensity, duration and time-space distribution), soil characteristics (e.g., soil moisture and permeability), basin characteristics (e.g., basin size, shape, slope, surface roughness, stream density) and land characteristics (e.g., use, cover and changes) (Rozalis et al., 2010). Even though intense precipitation is usually considered as the main factor in the occurrence of flash floods, other aforementioned factors are sometimes of greater significance in the flash flood generation process other than rainfall itself (Hill and Verjee, 2010). As a result of the

limited duration of flash flood triggering rainfall events, a flash flood usually has greatest impact on relatively small catchments (Borga et al., 2014), with the majority of such catchments being less than hundred square kilometres in size (Collier, 2007, Sene, 2008). As mainly smaller catchments are usually affected by flash flooding, response times tend to be short, e.g. ranging from few minutes (Gourley et al., 2014) to generally less than 6 hours (Marchi et al., 2010). This being the case, the sudden nature of the rapid runoff production process is a characterising feature of flash flooding (Borga et al., 2011).

Flash floods are particularly difficult to observe and predict due to their rapid occurrence, complex generation process and small spatial and temporal scales (Borga et al., 2008, Rozalis et al., 2010). Moreover, flash flood forecasting is considered to be one of the most difficult tasks in operational hydrology (Norbiato et al., 2008), since accurate flash flood prediction depends on variety of parameters, such as availability of rainfall information, accuracy and spatial resolution of the rainfall information, estimated soil moisture, surface characteristics and ability of hydrological models to represent complex flash flood generation process (Yatheendradas et al., 2008). As flash flood forecasting is faced with great observational limitations, such as ungauged river streams and limited rainfall sampling potential from scarce rain-gauge network (Borga et al., 2011), it is not surprising that flash floods remain poorly monitored events (Borga et al., 2014). Furthermore, learning from historic flash flood events is very limited due to inadequate documentation of past flash flood events (Marchi et al., 2010), and lack of flash flood data archives (Gourley et al., 2013, 2014). All the aforesaid means that decision makers and emergency response services are, in the majority of cases, faced with insufficient information about the development and scale of an on-going real-life flash flood event. This being the case, flash floods provide a minimum amount of time for timely flash-flood warnings to be prepared and issued effectively (Creutin et al., 2013).

River flooding occurs in the floodplains of rivers when a river overflows its natural banks due to intense precipitation or snow and ice melting within the catchment areas further upstream (Bariweni et al., 2012). Large river flooding is usually a result of large-scale atmospheric circulations, and can therefore affect entire regions or even

multiple countries at the same time (Jongman et al., 2014). Even though large watercourses are primarily the main source of extreme river flooding, such as the Meuse, Rhine and Oder in Europe (Kotlarski et al., 2012, Kundzewicz et al., 2013), Mississippi in the USA (Kolker et al., 2014, Therrell and Bialecki, 2015), Indus in Pakistan (Hartmann and Andresky, 2013, Shrestha et al., 2014), Niger in Africa (Michot et al., 2013, Casse et al., 2015) or Yellow River in China (Li et al., 2014a, He et al., 2015), large river flooding can also occur in relatively small catchments (Hajdukiewicz et al., 2015, Santos et al., 2015). The common feature of all large river floods is their destructibility, as these floods cause enormous economic damage wherever they occur (Jongman et al., 2014). Although in developed countries large river floods are rarely associated with casualties (Gaume et al., 2009), these floods can still lead to thousands of fatalities in parts of the world where flood warning systems are poorly developed, such as in South Asia (Kundzewicz et al., 2013).

In contrast to flash flooding, river flooding can generally be predicted a few hours or few days in advance due to development of flood forecasting systems (Merkuryeva et al., 2015). Flood forecasting strategy is based on the coupled hydro-meteorological prediction systems, where weather observations are used in combination with hydrological and hydraulic models (Wetterhall et al., 2013). Even though flood forecasting is always faced with uncertainties, such as quality of the input data, evaluation of the data, and model structure, parameters and characteristics (Kauffeldt et al., 2016), flood forecasting is an important tool for realising real-time flood warnings and providing effective emergency responses (Li et al., 2014b). Flood forecast systems are in use all over the world, and provide forecasts on local, national, regional and even global scale (Wetterhall et al., 2013). In Europe, the devastating flooding of Elbe and Danube in 2002 led to development of the European Flood Awareness System (EFAS) (Thielen et al., 2009). The EFAS provides early flood warnings for the largest European rivers, which usually result in large scale flooding, and therefore to some extent prepare the general public for upcoming flooding and reduce damage from large river floods. Additionally, information on the large river flooding can also be provided by (i) flood databases, such as Emergency Events Database (EM-DAT) run by the Catholic University of Leuven in Belgium and Active Archive of Large Flood Events run by the Dartmouth Flood Observatory (Kundzewicz et al., 2013), (ii) historic accounts of extreme flood levels (Mudelsee et

al., 2004), and (iii) historic water level marks on old buildings (Herget and Meurs, 2010). All these records provide information that enables better understanding of large river flooding, and consequently allows development of more effective flood risk management plans.

However, large river floods still remain highly destructive events due to their large scale impact, especially since little has been done in understanding national risk transfer mechanisms and flood risk dependencies across regions, which results in a lack of effective continental or even regional flood risk management schemes (Jongman et al., 2014). Even on a national level large scale floods can lead to extensive damage and casualties, particularly if the risk management schemes are based on the traditional flood protection design. Even though traditional flood protection schemes are well established, they generally suffer from fragmented flood risk management, low level of public awareness of flooding and inadequate societal discussion about flood risk (Hall et al., 2003, Jonkman et al., 2008). However, flood risk management planning has just recently shifted to a more integrated flood risk management schemes, in which flood management measures are not focused solely in flood protection, but also in reducing flood impacts by applying non-structural measures, such as land use spatial planning, insurance and flood resilient construction (Dawson et al., 2011). Nonetheless, large river flooding, together with flash flooding, still poses the greatest flood risk to the general population.

The occurrence of the natural conditions that lead to extreme flood events cannot be prevented. However, flood damage and human casualties can be minimised by adopting suitable structural and non-structural measures. Nowadays potential flood damage is generally estimated using flood simulation models. Even though developments in the field of computer science has enabled the generation and application of high-resolution flood prediction models, difficulties still remain in recreating actual extreme flood events, which in turn has a direct impact on model predictions of flood elevations, inundation extent and hazard risk. This is mostly due to the uncertainties associated with flood inundation modelling, such as uncertainty in boundary conditions, infrastructure performance, topographic and hydrological data, roughness parameters etc. However, the difference between the computer predicted flood characteristics and the actual properties is also often due to

inappropriate flood risk assessment techniques and modelling procedures. Specifically, it is common practice among flood risk assessment practitioners to simplify the computational process, which could lead to time consuming analysis or an increase in the complexity of the problem that practitioners are dealing with (Leskens et al., 2014b). This is referred to as a "simplification strategy".

Most numerical models used for flood inundation modelling by flood control management practitioners are based either on the Alternating Direction Implicit (ADI) algorithm or a form of an explicit central difference scheme. Such models are generally very accurate (numerically) in modelling floods over mild slope or nearly horizontal flow conditions. However, due to rapid changes in the flow regime that often occur with high Froude number flows (e.g. extreme floods), ADI-type models are prone to generating spurious numerical oscillations close to the sharp gradients in the solution (Liang et al., 2007b). These numerical oscillations mostly occur in the region of discontinuities, such as the emergence of a hydraulic jump or steep hydraulic gradients. While solving the hydrodynamic governing equations, the numerical schemes try to fit the solution with a function. In the presence of discontinuities, this function approximation leads to discontinuous solutions, which in turn lead to oscillations analogous to the Gibbs phenomenon (Lax, 2006). The emergence of numerical oscillations can be overcome by applying upwind difference schemes or by using higher-order accurate schemes (Hunter et al., 2008), such as shock-capturing methods.

In shock-capturing approach, the governing equations are cast in conservation form and artificial diffusion terms are applied in the solution procedure, which ensure the stability of the computational process and enable the computation of any shock waves or discontinuities as part of the numerical solution. However, shock-capturing schemes can be computationally more expensive than the ADI-type models, which often persuades practitioners in flood risk assessment to adopt the "simplification strategy". Rather than using shock-capturing models, it is believed that flood risk assessment practitioners try to smooth out numerical oscillations in the solution procedure of the ADI-type models by employing other more practical solutions, such as applying patches of high roughness in the areas where the instabilities occurred (CH2M, 2016). This then decreases the velocity and also dissipates the energy of the

flow, which in turn can dampen out the numerical oscillations. However, such simplifications can also lead to incorrect flood level predictions, as the evaluation of the modelling results is thus based on the modeller's perception of how much of the friction parameterisation tuning is needed in order to obtain satisfactory results.

For example, flash floods usually occur in short and steep river basins. The steeper the slope the less time the peak flow has to be dissipated as the hydrograph propagates down the river basin. This maintenance of the peak hydrograph (both in terms of elevations and discharges) frequently leads to near trans or super-critical flows. As mentioned, flood risk practitioners avoid using shock-capturing models due to their long simulation runs. Instead, they dampen out the numerical oscillations, which generally occur when trans or super-critical flows are modelled with conventional 1-D or 2-D models, by removing advection terms and including an artificially high bed resistance or eddy diffusion term (de Almeida et al., 2012). Even though such procedures can minimise the simulation time (in comparison to shock-capturing models) and optimise limited resources, for such conditions it is not then possible to evaluate how much of the increased dissipation is being used in physically dissipating the energy of the flow and how much is being used in numerically damping out the oscillations. This being the case, there is a great risk that the model might under-predict peak flood discharges, flood inundation extent and hence flood hazard indices.

An accurate prediction of flood depth s and velocities is fundamental for an adequate flood hazard assessment. According to the Department for the Environment, Food and Rural Affairs (DEFRA) of the UK Environment Agency, flood hazard *"describes the flood conditions in which people are likely to be swept over or to drown in a flood"* (Ramsbottom et al., 2006). The majority of the flood hazard assessment methods are based on some sort of flood hazard index, which is generally defined as a product of water depth and velocity (Cox et al., 2010). Therefore, under-predicted water depths or velocities would lead to an under-predicted flood hazard index. In turn, this would result in misleading flood hazard assessment and consequently to an ineffective response from the emergency services, as their rescue action plans would be based on false predictions. Even if it is assumed that conventional flood inundation models could accurately predict main parameters for

an extreme flood event, there is a question over whether the standard flood hazard assessment methods can adapt to a rapidly changing flow regime, which usually occurs with extreme flooding.

Currently, there are two different types of flood hazard assessment methods in use, including: (i) methods derived from the mechanical analysis, which is based on laboratory experiments with models and real human subjects, and (ii) methods derived from empirical or theoretical analysis (Xia et al., 2011). Standard flood hazard assessment methods are suitable and accurate for low-land, slowly progressing flood events. However, flood hazard assessments methods based on laboratory experiments with models and real human subjects are usually too dependent on the physical characteristics of the model or human subject, and psychological factors of the tested human subjects, while flood hazard assessments methods based on theoretical and empirical work often too excessively simplify human body structure and flow conditions (Xia et al., 2014). This suggests that for extreme flood events where the flow conditions change rapidly, standard flood hazard assessment methods should be replaced with new methods, which could adequately assess flood hazard for extreme flood events regardless of the human body characteristics and the hydraulic characteristics of the flow.

The shortcomings in the modelling of extreme flood events can be illustrated with an example from Wales, UK. The terrain across much of Wales is complex, with many short, steep river basins across the country being highly prone to flash flooding (Carter, 2009, Davies, 2010, Hough, 2012, BBC, 2013a, BBC, 2013b, Lowe, 2013). On 27th of November 2012, the town of St Asaph, located in north Wales, was devastated by flash flooding. The post-flood investigation revealed that flood defences offered protection against 1 in 30 year flood in some parts of the city and against 1 in 75 year flood in others, whereas it was previously believed that the flood defences would protect against a 1 in 100 year flood (Denbighshire County Council, 2013). Findings from this report clearly indicate limitations in the current flood risk assessment methodologies adopted in the UK and particularly for short, steep river basins highly prone to extreme flooding. Therefore, there is an urgent need to improve flood risk assessment tools for areas prone to occurrence of extreme flood events.

In summary, climate change is expected to result in an increase in the frequency of extreme flood events, such as flash flooding and large scale river flooding. Since the use of standard flood risk tools do not adequately represents the complex hydrodynamic processes associated with trans and super-critical flows that often occur with extreme flooding, there is a need for more accurate flood risk assessment designs in areas prone to extreme flooding. This can be achieved by implementation of appropriate flood inundation modelling tools and suitable flood hazard assessment techniques.

1.2 Research objectives

The main aim of this research study is to improve flood risk assessment tools for modelling in areas prone to occurrence of extreme flood events. This being the case, the key objectives of this study are as follows:

- determine what type of flood inundation models should be used for predicting the flood elevations, velocities and inundation extent for extreme flood events

- investigate the appropriateness of the "simplification strategy" when used as a flood risk assessment modelling tool for areas susceptible to extreme flooding

- determine what type of flood hazard assessment methods should be used for assessing the flood hazard to people caused by extreme flooding

Achieving these research objectives will lay foundation for producing of more accurate flood inundation extent and flood hazard risk maps for areas prone to extreme flooding, which in turn could better equip flood risk practitioners, regulatory and planning authorities in their decision making. This being the case, better and more accurate flood risk management schemes for urban communities which are highly vulnerable to extreme flooding could be developed, and thus the devastating consequences of extreme flood events could be more efficiently militated against in the future. These detailed schemes could potentially save billions of pounds that are

now spent annually in the UK for insurance claims and damage repair. These savings could then be spent in other areas relevant for society, such as education, infrastructure etc. More importantly, accurate flood risk management schemes would lead to adequate flood protection design, which would enhance the quality of life as it would provide a safer living environment for people living in urban communities in areas prone to occurrence of extreme flood events.

1.3 Thesis outline

This thesis is organised into six chapters, including:

CHAPTER 1: Introduction, which presents the wider research background and the main objectives of this research study

CHAPTER 2: Literature review, which presents an overview of the main literature applicable to this research study

CHAPTER 3: Numerical modelling, which presents the general governing equations, an overview of the numerical methods used to discretises the governing equations, some of the well-known shock-capturing schemes, and the numerical models used in this research study

CHAPTER 4: Case studies, which present the study areas and real-life flood events considered in this research study

CHAPTER 5: Flood inundation modelling of extreme flood events, which describes (i) the evaluation of different types of flood inundation models for predicting flood depths, velocities and inundation extent for extreme flood events, and (ii) the investigation of the appropriateness of the "simplification strategy" when used as a flood risk assessment tool for areas prone to occurrence of extreme flood events

CHAPTER 6: Flood hazard assessment for extreme flood events, which describes the evaluation of different types of flood hazard assessment methods for predicting the flood hazard indices in areas susceptible to extreme flooding

CHAPTER 7: Conclusions and future research, which presents the summary of the work concluded and the main findings of this research study, and provides suggestions for potential further research following from this study

CHAPTER 2

Literature review

2.1 Introduction

This chapter presents an overview of the main literature applicable to this research study. Section 2.2 presents the literature in the field of flood inundation modelling, Section 2.3 presents the literature in the field of flood hazard assessment, while Section 2.4 provides the summary of the main literature overview findings. These findings were used to determine what type of flood inundation models and flood hazard assessment methods should be considered in order to adequately test the main assumptions and potentially reach the key objectives of this research study.

2.2 Flood inundation modelling

Even though it is not possible to prevent the occurrence of the natural conditions which lead to flooding, flood damage and human casualties can be minimised by adopting suitable structural and non-structural measures. Nowadays, potential flood damage is generally estimated using hydraulic or flood inundation models. A flood inundation model is used to provide the information about the flood extent, water depth and velocity of the flow. These parameters are needed for (i) production of flood hazard and flood inundation extent maps, (ii) land use planning, (iii) designing of the flood defence structures, and (iv) development of the emergency response and evacuation plans.

The foundation for the mathematical modelling of the fluid dynamics were laid by Newton (1687), who presented mathematical formulations based on physical conservation principles, and by de Saint-Venant (1871), who formulated the mathematical equations for the present-day hydrodynamic simulations. However, it was not until the emergence of computing machines that the necessary computational resources became available to solve these equations and apply them to practical

hydro-technical engineering problems (Stelling and Verwey, 2005). The beginnings of the modern flood simulation modelling date back to the fifties and sixties (Isaacson et al., 1958, Cunge and Wegner, 1964, Martin and DeFazio, 1969, Martin and Zovne, 1971, Mahmood et al., 1975, Katopodes and Strelkoff, 1978, Cunge et al., 1980), while the widespread development of numerical codes started in the eighties (Alcrudo, 2004).

In recent years, the developments in the field of computer science have enabled the generation and application of accurate, computationally effective and high-resolution flood inundation models. Therefore, there is now a wide range of different types of modelling tools and packages, which can be used for (i) development and realisation of large-scheme objectives, such as flood risk analysis, real-time flood forecasting or flood control management, or (ii) analysis of specific events, such as flash floods, hurricanes or dam breaks. These different types of modelling objectives require different and sometimes fairly specific modelling techniques and procedures, which means that an appropriate flood simulation modelling tool has to be used to address a specific modelling problem. This being the case, the selection of an appropriate flood inundation model is dependent on number of factors, such as the type and complexity of the modelling problem, overall consultancy time for product delivery, speed of computation, completion time for a simulation, accuracy level of results, data requirements, numerical robustness and user-friendliness of the software (Stelling and Verwey, 2005). In general, the use of a specific flood inundation model depends on the nature of the modelling problem and personal preferences of the model's user.

There are several ways to categorise flood inundation models, such as according to the method of solving the hydrodynamic equations, the method of discretisation in time and space, or the type of grid or mesh. However, the most common way to categorise flood inundation models is according to their dimensionality, or the way they combine different dimensionalities. In general, flood inundation models can be divided into three main categories, i.e. one-dimensional (1D), two-dimensional (2D) and linked one-dimensional – two-dimensional (1D-2D) models. There are also three-dimensional (3D) numerical models, which can be used to predict water levels and three-dimensional velocity fields (Rezoug et al., 2010, Spada et al., 2015). However, three-dimensional flood inundation modelling at a reach scale is currently

unpractical due to a high computational cost (Zhang et al., 2016). Therefore, further developments in the field of the computational sciences are needed before such models can be fully used in the flood risk management. In addition, there is also so-called 0D modelling approach. This approach includes methods that do not involve any modelling of the physical processes of flood inundation (Pender, 2006), such as projecting river water levels horizontally over a floodplain (Pender and Néelz, 2011). The 0D modelling approach is mainly used for a broad-scale flood risk assessment, with GIS software usually being used (such as ArcGIS) for the prediction of flood depths and flood inundation extent (Pender, 2006, Di Baldassarre, 2012). However, this type of flood inundation modelling approach does not estimate velocity of the flow (Mohammadi et al., 2013), and is thus limited to applications where only final water levels are required and dynamic effects are insignificant (Neelz and Pender, 2013). This being the case, the 0D modelling approach is too simple to be used for a detailed flood risk management scheme.

Considering all above, three types of flood inundation modelling approaches (or flood inundation models) are predominately used in both research and industry for the hydrodynamic simulations, i.e. 1D, 2D and linked 1D-2D models. This being the case, these three modelling approaches will be considered more in detail in this thesis.

2.2.1 Modelling approaches

Flood modelling typically comprises two components: (i) the hydrological simulation, which quantifies the size, duration and probability of the flood event, and (ii) the hydraulic or flood inundation simulation, which employs the propagation of the flood wave across the river channel and the mapping of inundated areas (Dimitriadis et al., 2016). In hydraulic modelling, several processes need to be considered before the selection of the appropriate modelling approach, including (Di Baldassarre, 2012): (i) in-channel processes, such as the size of the flood wave, the formation of shear layer at the junction between the main flow and slower moving dead zones at the scale of the channel platform, secondary circulations at the scale of the channel cross-section, and the effect of the eddy turbulence, (ii) physical processes that occur once the floodwater overtops channel banks, such as the

momentum exchange between faster channel and slower floodplain flow, and the interaction between meandering channel flow and the floodplain flow, (iii) flow interaction between micro-topography, vegetation and structures, and (iv) water exchanges with the surrounding catchment, such as evapotranspiration and subsurface contributions to the floodplain groundwater from adjacent hill slopes.

The scale of the processes that should be considered in the selection of the appropriate flood inundation model indicates that the flood inundation modelling can be a relatively complex process. In addition to the physical complexity, it is also important to consider the computational cost required to conduct the flood simulation. This being the case, the selection of the appropriate modelling approach is often driven by the desire to find the optimal balance between the model accuracy and computational efficiency (Di Baldassarre, 2012). There are two key factors in the selection of the appropriate flood inundation modelling approach, which can enable the balance the need between the model accuracy and computational efficiency. These two factors are: (i) the considered dimensionality of the flow, i.e. describing the flow propagation as 1D or 2D process, and (ii) the level of the mathematical complexity used in the numerical simulation, i.e. applying the full shallow water equations or considering some simplifications, such as excluding momentum or advection terms from the numerical process (Neal et al., 2012).

However, it is of vital importance to completely understand the physical scale of the considered flooding problem. Even though less complexity generally leads to shorter simulation times, the decrease in dimensionality of the flow and mathematical complexity can also lead to inaccurate prediction of flood depths, velocities and inundation extent. Therefore, the selection of the appropriate flood inundation modelling approach needs to be considered thoroughly before the start of the flood inundation modelling process. This being the case, the selection of the appropriate flood inundation modelling approach should be based on several parameters, such as objectives of the work, terrain topography, availability and resolution of data, computational time, commercial software costs and hydrodynamic characteristics of the considered modelling problem (Vojinovic and Tutulic, 2009).

1D modelling approaches

One-dimensional hydrodynamic models are based on some form of the 1D Saint-Venant equations (see Chapter 3, section 3.2). In this thesis, one-dimensional flood inundation models are divided into two categories, i.e. 1D and $1D^+$ flood inundation models (Pender, 2006). The characteristics of the 1D flood inundation models are summarised in Table 2.1.

Table 2.1: The characteristics of 1D flood inundation models (Pender, 2006)

Method	Description	Potential application
1D	solution of the 1D Saint-Venant equations	design scale modelling which can be of the order of tens to hundreds of km depending on catchment
$1D^+$	1D plus a flood storage cell approach to the simulation of floodplain flow	design scale modelling which can be of the order of tens to hundreds of kilometres depending on catchment size; it also has the potential for broad scale application, if used with sparse cross- sectional data

In the 1D flood inundation approach, the considered river reach is described with a series of cross-sections, which take into account both the main channel and adjacent floodplains (see Figure 2.1). This means that the floodplain flow is part of the one-dimensional channel flow, and that the simulation of inundation is an integral part of the solution of the 1D Saint-Venant equations. The 1D flood inundation models have been widely used for modelling of flood flows, as they are computationally efficient and able to deal with large and complex river/channel systems, and variety of hydraulic structures, such as weirs, gates and sluices (Lin et al., 2006, Vojinovic and Tutulic, 2009). Nonetheless, the 1D models have many shortcomings. For example, the 1D model assumes that the floodplain flow is aligned with the river centre line (see Figure 2.1), the flow velocities are perpendicular to cross-sections and the water surface elevations are constant for the entire cross-section (see Table 2.2). However, these assumptions are often not valid. In particular, they are not valid for river reaches containing backwater areas or for naturally occurring diversion channels (Gilles and Moore, 2010). Furthermore, the 1D models also have constraints when it

comes to modelling of floodplain flows, such as (i) the inability to simulate lateral diffusion of the flood wave, (ii) the discretisation of topography as cross-sections rather than as a surface, and (iii) the subjectivity of cross-section location and orientation (Hunter et al., 2008). This being the case, the 1D models cannot accurately model floodplain flows as their predictive ability is decreased due to the assumptions and limitations in the 1D flood inundation modelling approach.
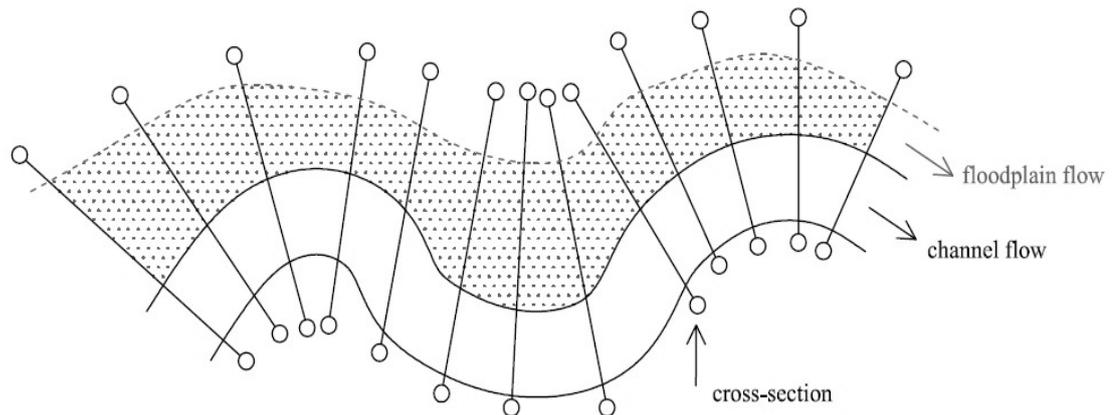
Figure 2.1: A schematic presentation of 1D modelling approach

Nonetheless, the 1D modelling approach can be enhanced to some extent by applying the Conveyance Estimation System (CES) (McGahey et al., 2006) and the Afflux Estimation System (AES) (Lamb et al., 2006) techniques. The CES technique improves the estimations of water levels, spatial velocities and boundary shear stresses at river sections, while the AES technique improves the predictions of the increase in water level upstream of a structure, which is caused by energy losses at high flows through bridges and culverts (McGahey et al., 2008). The Conveyance and Afflux Estimation System (CES/AES) software is implemented in a number of commercial packages, such as ISIS 1D and InfoWorks RS (Neelz and Pender, 2013).

In the 1D$^+$ flood inundation approach (also known as "quasi" 2D or "pseudo" 2D approach), the aforementioned 1D approach is used to model the main channel flow, while the floodplains are modelled as a storage cells or reservoirs that can cover large areas (e.g. up to several square kilometres), and whose geometry is defined as a relationship of water level versus volume (Di Baldassarre, 2012). The flow between the main channel and storage cells is modelled using weir flow based discharge

relationships. These discharge relationships are often referred to as spill units or spill links, and can be also used to link one storage cell to another. Water level in each storage cell is then computed using conservation of volume (Pender, 2006). A simple $1D^+$ model scheme is presented in Figure 2.2.
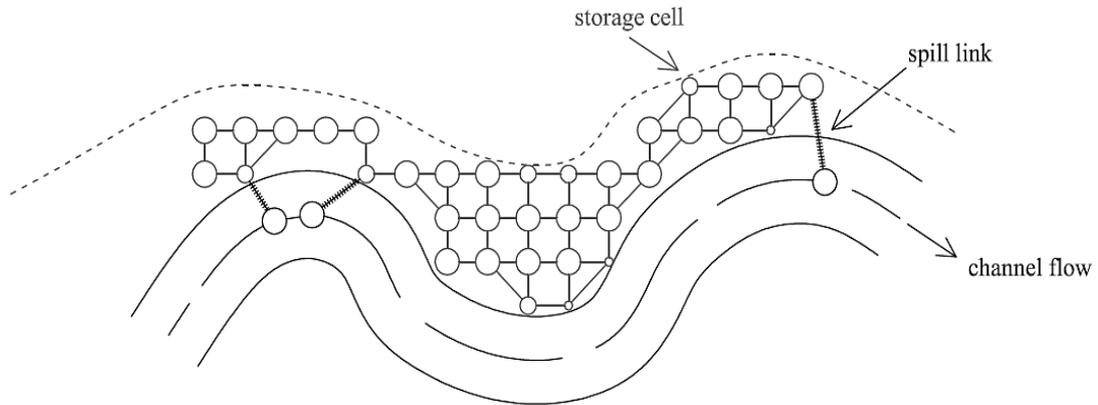
Figure 2.2: A schematic presentation of $1D^+$ modelling approach

In contrast to the 1D approach, the $1D^+$ flood inundation approach does not assume that the floodplain flow is parallel to the channel flow, which is generally more appropriate for modelling larger floodplains. This being the case, the $1D^+$ approach provides better estimations of water levels and inundation extent in the floodplains. However, the main drawback of the $1D^+$ approach is that it does not include any momentum conservation on floodplains. This means that water can be transferred instantaneously from one end of the storage cell to the other, which can consequently lead to modelling problems (Pender, 2006). Furthermore, significant errors can also occur in (i) calculation of inter-cell flows due to difficulties in defining spill discharge equations, and (ii) local predictions of water levels, if the storage cells are too large and therefore the assumption of water level horizontality cannot be met (Pender and Néelz, 2011). In addition, setting up of the $1D^+$ model can be time-consuming, and the accuracy of the model prediction can also be influenced by the way in which the floodplain is discretised (Lin et al., 2006).

The 1D modelling approaches have been widely used for modelling of flood depths, velocities and inundation extent (Horritt and Bates, 2002, Huang et al., 2007, Lindenschmidt et al., 2008, Cook and Merwade, 2009, Castellarin et al., 2011,

Doulgeris et al., 2012, Klimeš et al., 2014, Choi et al., 2015, Dimitriadis et al., 2016, Habert et al., 2016). Even though that the 1D models are extremely computationally efficient, these models have many limitations when it comes to modelling of floodplain flows. For example, 1D modelling of floodplain flows is appropriate only for narrow floodplains whose widths are typically not larger than three times the width of the main river channel (Neelz and Pender, 2009). This means that the use of the 1D models is limited to relatively small space surrounding the main river channel. Due to limitations in the modelling of floodplain flows, the developments in the digital elevation modelling (in particular LiDAR technologies) and the increase in the computational resources and power, other modelling approaches (such as use of 2D and linked 1D-2D models) have been predominantly used over 1D models in recent years (Pender and Néelz, 2011, Neal et al., 2012, Ahmadian et al., 2015).

Table 2.2: Input data, output data and computation times for different types of 1D modelling approaches (Pender, 2006)

Method	Input data	Output data	Computation time
1D	surveyed cross-sections of channel and floodplain; upstream discharge hydrographs; downstream stage hydrographs	constant water depth, cross-section averaged velocity and discharge at each cross section; inundation extent by intersecting predicted water depths with digital elevation model (DEM); downstream outflow hydrographs	minutes
1D$^+$	as 1D models	as 1D models plus water levels and inundation extent in floodplain storage cells	minutes to hours

2D modelling approaches

Two-dimensional hydrodynamic models are based on some form of the 2D shallow water equations (see Chapter 3, section 3.2). In this thesis, two-dimensional flood inundation models are divided in three categories, i.e. 2D$^-$, 2D and 2D$^+$ flood

inundation models (Pender, 2006). The characteristics of the 2D flood inundation models are summarised in Table 2.3.

Table 2.3: The characteristics of 2D flood inundation models (Pender, 2006)

Method	Description	Potential application
2D⁻	simplified version of the 2D shallow water equations; raster-based models	large-scale modelling and applications where inertial effects are not important
2D	solution of the 2D shallow water equations	design scale modelling of the order of tens of km; it may have the potential for use in broad scale modelling, if applied with very coarse grids
2D⁺	2D plus a solution for vertical velocities using continuity only	predominantly coastal modelling applications, where 3D velocity profiles are important

The 2D⁻ modelling approach can be divided into two groups, including (Neelz and Pender, 2009): (i) 2D models based on a simplified version of the 2D shallow water equations where some terms are neglected, such as models that consider inertia and diffusion but ignore advection (Bates et al., 2010), and diffusive models (Moussa and Bocquillon, 2009), and (ii) raster-based models relying on high-resolution topographic data sets (e.g. DEM) and simplified 1D representation of the flow between the raster DEM cells, such as LISFLOOD-FP (Bates and De Roo, 2000). The later approach is similar to the 1D⁺ modelling approach, because it also does not conserve momentum for the 2D floodplain simulation. However, the grid dimensions in the raster-based models are much smaller than those in a typical 1D⁺ approach, which allows finer discretisation of floodplains and thus more accurate predictions of flood depths, velocities and inundation extent (Pender, 2006).

The 2D modelling approach is based on the use of flood inundation models, which solve full 2D shallow water equations, which are presented in Section 3.2. The 2D models are based on different space-time discretisation strategies and utilise different numerical grids. The pros and cons of different numerical methods that are used in flood inundation modelling are presented in Section 3.4, while advantages and disadvantages of different types of numerical grids can be found in Section 2.2.2.

Nowadays, the 2D modelling approach is the preferred option for modelling of floodplain inundation, as 2D models enable representation of local changes in velocity, water levels and flow direction (Neelz and Pender, 2009, 2013). In addition, the 2D modelling approach conserves momentum and therefore does not encounter the limitations that characterise 1D, 1D$^+$ and 2D$^-$ modelling approaches (Pender, 2006, Neelz and Pender, 2013). However, 2D models generally require more hardware and calibration data, and tend to result in relatively longer simulation times when compared to other aforementioned modelling approaches (Apel et al., 2009, Fewtrell et al., 2011, Neal et al., 2012).

The 2D$^+$ modelling approach is based on models, such as TELEMAC-3D, which enable the predictions of velocity in all three directions. This being the case, 2D$^+$ models are predominantly used for water quality and sediment transport studies in estuaries and coastal areas (Normant, 2000, Bedri et al., 2011, 2013), as there is a need for an accurate prediction of concentration of transported quantities. In continental waters, the 2D+ modelling approach has been used for water quality studies in lakes and for study of thermal plumes in rivers (Kopmann and Markofsky, 2000, Mensencal, 2012). The 2D$^+$ modelling approach is not used in practical flood inundation modelling due to high computational cost (Neelz and Pender, 2013).

As mentioned, modelling of floodplain flows is nowadays mainly conducted by using 2D and 2D$^-$ models, which differ in the degree of the physical complexity involved in the modelling process. The degree of the physical complexity that is required to accurately predict flood depths, velocities and inundation extent is mainly dependent on the flow characteristics and type of the planning process. For example, for gradually varying flows the 2D$^-$ models generally perform as well as 2D models in terms of predicting the water depths and flood inundation extent (Hunter et al., 2007, Neelz and Pender, 2013). However, the 2D$^-$ models are much simpler and less computationally expensive, which indicates that the 2D models may be unnecessarily complex for modelling flood events with mild changes in the flow regime (Neal et al., 2012). Therefore, for modelling of gradually varying flood events where decision makers are primarily interested in flood inundation extent and maximum water depths (such as catchment flood management planning and flood risk assessment), the 2D$^-$ models appear to be the better option as they offer better balance between the

accuracy of the results and the computational cost (Apel et al., 2009, Neelz and Pender, 2013).

Table 2.4: Input data, output data and computation times for different types of 2D modelling approaches (Pender, 2006)

Method	Input data	Output data	Computation time
2D⁻	digital elevation model; upstream discharge hydrographs; downstream stage hydrographs	inundation extent; water depths; downstream outflow hydrographs;	hours
2D	as 2D⁻ models	as 2D⁻ models plus depth-averaged velocities in two horizontal directions at each computational node	hours to days
2D⁺	as 2D⁻ models plus inlet velocity distribution	as 2D⁻ models plus velocity vector at each computational cell	days

On the other hand, the 2D models appear to be much more suitable for modelling highly unsteady flows or for supporting decision makers in disaster planning and flood hazard mapping (i.e. scenarios where accurate velocity predictions are required), as these models are able to accurately predict depth-averaged velocities in two horizontal directions (see Table 2.4) (Neelz and Pender, 2013). For modelling rapidly varying or supercritical hydrodynamic processes, both 2D⁻ and 2D models are susceptible to emergence of numerical oscillations which can lead to inaccurate predictions of flood depths and inundation extent (Leopardi et al., 2002, Liang et al., 2006, Neal et al., 2012, Neelz and Pender, 2013). This being the case, for modelling of rapidly varying flows the 2D⁻ and 2D models should be replaced with shock-capturing flood inundation models. These models prevent the emergence of spurious numerical oscillations and thus enable numerically accurate predictions of flood depths, velocities and inundation extent for flood events characterised with high Froude number flows, such as flash floods. Shock-capturing models are presented in more detail in Section 3.4.

Linked 1D – 2D modelling approach

Floodplain modelling has received a great amount of attention from research community in recent years, as such modelling is a key factor in the development of an appropriate and accurate flood risk management strategies. As it was shown earlier, a variety of both 1D and 2D modelling approaches has been developed in order to find the optimal floodplain modelling approach in terms of satisfactory accuracy of the model results and reasonable computational cost. The 1D modelling approach is generally considered as the most appropriate approach for modelling flood behaviour within river channel. However, due to its limitations the 1D modelling approach is not capable of accurately predicting the flood characteristics on floodplains. On the other hand, the 2D modelling approach is regarded as the most accurate tool for modelling floodplain flows. Nonetheless, the 2D models can be computationally expensive and therefore less practical for real-time flood forecasting. This being the case, coupled 1D-2D modelling approach has been widely tested in the last decade. The idea has been to exploit the advances in data availability, improved numerical methods and enhanced computational power, and develop linked 1D-2D models which would take advantage of the benefits offered by both 1D and 2D modelling approach (Verwey, 2001, Stelling and Verwey, 2005, Lin et al., 2006, Liang et al., 2007a, Pender and Néelz, 2011).

There are virtually no limits when it comes to combining 1D and 2D modelling approaches. Therefore, the coupled 1D-2D modelling approach can be applied in many ways, such as within a channel that one wishes to model partly in 1D and partly in 2D, between a 1D drainage network model and a 2D surface flood model, and between a 1D river model and a 2D floodplain model (Pender and Néelz, 2011). In general, the main river channel is modelled in 1D while the floodplains are modelled in 2D, which results into more accurate flood inundation prediction when compared to 1D modelling approach, and significant computational savings when compared to 2D modelling approach. This being the case, linked 1D-2D modelling approach seems to be an effective flood modelling tool, and the ability to link 1D and 2D models is nowadays implemented in majority of commercial software packages (Neelz and Pender, 2013).

There are several techniques to link 1D and 2D models, such as lateral link, longitudinal link and vertical link. The lateral link is the most widely used technique for linking the 1D river and 2D floodplain models. In the lateral link approach, the simulation of over bank flow from river channel to floodplain is modelled using weir equations or depth-discharge curves, which are based on water level differences (Lin et al., 2006, Neelz and Pender, 2009, Ahmadian et al., 2015). In the longitudinal link approach, the 1D and 2D model are linked in such a way that the flow from the 1D model acts as a upstream boundary condition in the 2D model, while at the same time the water level in the 2D model at the junction is used as a downstream boundary condition in the 1D model (Danish Hydraulic Institute (DHI), 2007, Liang et al., 2007a, Pender and Néelz, 2011). For example, the narrower upstream river channel is modelled in 1D, while the wider floodplain downstream of the 1D model is modelled in 2D. In the vertical link approach, the 2D grid is placed above the 1D domain. The 1D solution is applied until the river reaches bank-full level, while the flow propagation above the bank-full level is described with the 2D model (Stelling and Verwey, 2005, Neelz and Pender, 2009, Bates et al., 2013).
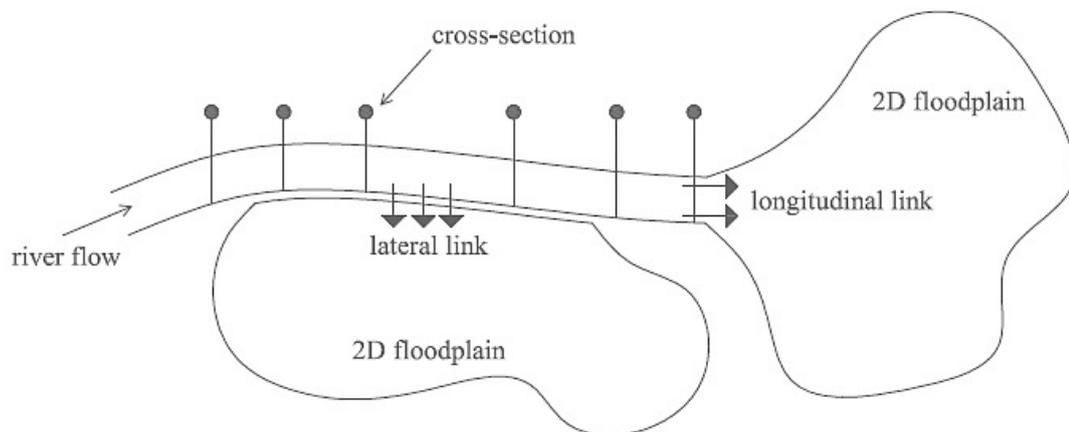
Figure 2.3: Schematic representation of the lateral and longitudinal linking mode

Even though the 1D-2D flood inundation modelling approach has been significantly improved in recent years (Chen et al., 2011, Finaud-Guyot et al., 2011, Bladé et al., 2012, Morales-Hernández et al., 2013, Liu et al., 2015, Morales-Hernández et al., 2016), there are still some constraints with the 1D-2D models. For example, two models need to be understood, which means that in general more time is spent for pre-processing and model set up when compared to other modelling approaches

(Vojinovic and Tutulic, 2009). Furthermore, a great understanding of the modelling problem is required, and in particular the nature of the volume exchange. Namely, if the volume exchange between the river and floodplain is not represented correctly, it is likely that the flood depths, velocities and inundation extent will not be modelled correctly (Morales-Hernández et al., 2016).

In addition, there is no consistent approach used in practice at the present time for the prediction of the volume exchange between the river and the floodplain. This means that different models can predict different timing of flood inundation, water levels and velocities on floodplains for the same modelling problem, because each model differently predicts the volume exchange between the river and the floodplain (Neelz and Pender, 2013). In addition, linked 1D-2D floodplain modelling for rapidly varying flows has not been thoroughly researched to present time. There are examples of use of the coupled 1D-2D models for supercritical flow simulation in crossroads of flood control channels (Ghostine et al., 2015), but up to date there was no research that would specifically test the ability of linked 1D-2D to model flood events with rapidly varying flows, such as flash floods. All in all, linked 1D-2D models are very attractive due to their computational efficiency and numerical accuracy comparable to that of 2D models for specific flood problems. Nonetheless, further research is needed in order to resolve current limitations, extend model application and potentially standardise the linking procedures.

2.2.2 Computational grids

The first step of any numerical flood inundation simulation is the grid generation process. A grid is a collection of points, where the main flow parameters (such as velocity, water depth and water level) are computed through solution of the systems of algebraic equations obtained from the discretisation processes. The grid resolution or density (i.e. the distance between the points) has a significant impact on the rate of convergence, solution accuracy and computational cost (Pender and Néelz, 2011). This being the case, the quality of the model predictions is closely related to the resolution of the computational grid (Fewtrell et al., 2011, Ozdemir et al., 2013, Savage et al., 2015).

Two different grid types are predominately used in the numerical flood inundation modelling, i.e. structured grids and unstructured grids. A structured grid is a grid based on an ordered layout of grid points. The structured grids are constructed in such manner that the grid points can be regarded as the point of intersection between the coordinate lines. This means that every point in the grid (except boundary points) is physically connected to four points on either side. In two dimensions, the grid points can be specified as a pair of integers (i,j), which can be conveniently stored as the elements of the matrices. The neighbouring points in the matrix can be directly assessed by incrementing or decrementing the array index, and can be set apart at regular or irregular intervals. This being the case, there are several types of structured grids, such as uniform or Cartesian grids (regular intervals) or curvilinear grids (irregular intervals) (see Figure 2.4).

(a)   (b)
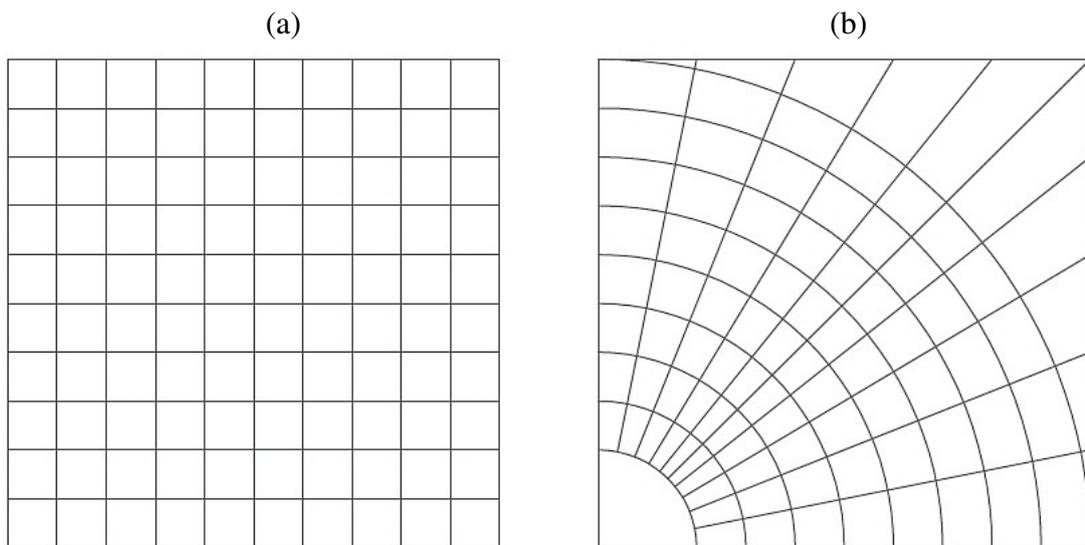
Figure 2.4: Uniform grid (a) and curvilinear grid (b)

An unstructured grid is a grid that cannot be represented on a regular matrix. Instead, it is based on an arbitrary layout of grid points, where the information about the layout must be provided. For example, the points that constitute a 2D unstructured grid are kept as lists of (x,y) coordinates, where a database provides a record on details how are these points connected to each other. In contrast to structured grids, there is no regularity in the position of grid points (see Figure 2.5). This means that unstructured grids can be refined locally to take into account fine features in the flow, while at the same time the density of grid points in the areas where the

refinement is not needed can be much smaller. These local refinements of the grid resolution can enable the optimal use of the computer power, but at the same time can also increase the computational time due to the smaller time step needed for the solution procedure in the areas with higher grid resolution (Pender and Néelz, 2011).
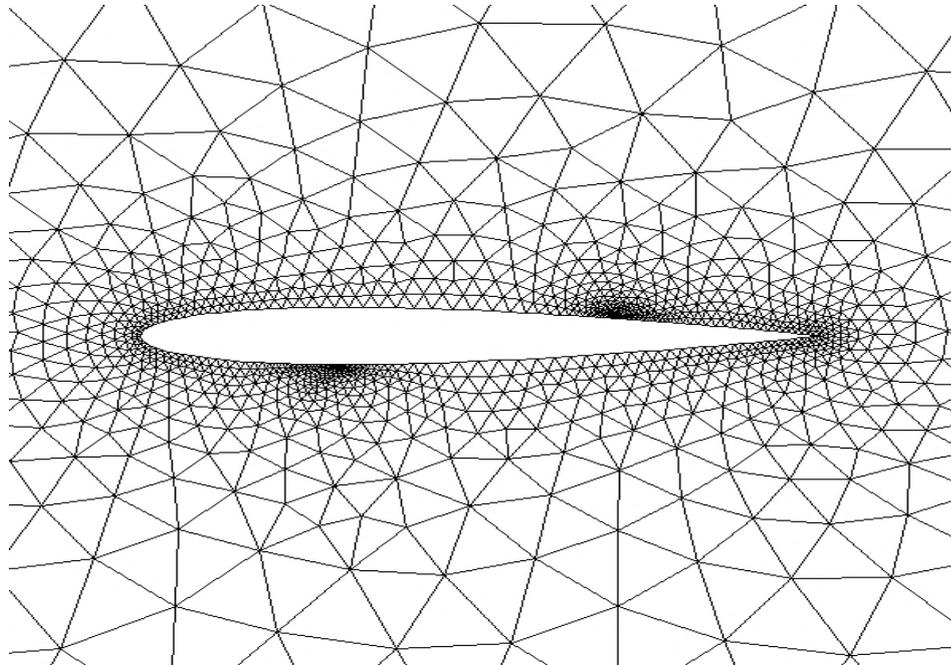
Figure 2.5: Unstructured grid

Structured grids have an evident advantage over unstructured grids, i.e. the construction of the structured gird is straightforward. On the other hand, the construction of the unstructured grid is far more complicated and can be time-consuming process, if there are many local grid refinements involved in the grid generation process. Furthermore, solver based on structured grids generally run much faster than solvers based on unstructured grids. However, unstructured grids are extremely flexible. For example, in structured grids it is necessary to cluster points far away from the area of interest in order to achieve a desired resolution in specific part of the domain. On the other hand, the unstructured grids can be easily applied to follow complex floodplain contours and flow geometry without any need to extend the limits of the grid (Potter et al., 2012). The selection of the grid type is directly related to the selected spatial discretisation strategy. For example, the finite difference method can only be applied to structured grids, whereas the finite volume

and finite element methods can be applied to both structured and unstructured grids (Neelz and Pender, 2009).

As mentioned, the quality of the grid can have a great impact on the accuracy of the numerical model, i.e. the grid generation process plays an important role in the numerical flood modelling. This is particularly important for flood inundation modelling in urban areas, as flood pathways are narrow in size due to complex urban topography. This being the case, accurate and high-resolution topographical information is needed in order to adequately represent complex flow characteristics of urban flooding. A more accurate flood inundation can be obtained by applying small scale grids. However, such high-resolution grids can lead into extremely long computational times, which eventually make the flood simulation process infeasible (Tsubaki and Fujita, 2010). Simplified grid generation techniques could be used, such as sub-grid modelling or reduced complexity modelling (Brasington and Richards, 2007). However, the grid resolution from these approaches is too small to accurately resolve the detailed and complex flow structure in urban areas (Tsubaki and Fujita, 2010). Therefore, there is a need to further develop automatic grid generation techniques, which would optimise the grid generation process and reduce the labour cost for data preparation. Even though there were significant advances in recent years in the field of the automatic grid generation (Owen and Shephard, 2003, Cobby et al., 2003, Begnudelli and Sanders, 2006, Sanders, 2007, Liang et al., 2008, Tsubaki and Fujita, 2010, Stelling, 2012), these techniques are currently still not used to their full potential in the field of the flood inundation modelling (Neelz and Pender, 2009, 2013).

2.2.3 Model parameterisation

The model parameterisation in the flood inundation modelling is generally reduced to setting of the friction coefficient, i.e. the value of the Manning's coefficient. In addition, the eddy viscosity is usually considered as a secondary parameter. However, the eddy viscosity is often ignored because it usually has a limited effect on the model predictions due to the dominance of the friction. Furthermore, there is also no methodology that would enable the calibration of the viscosity in flood inundation models (Neelz and Pender, 2009). Nonetheless, if the eddy viscosity is

not ignored in the flood inundation modelling process, it can be dealt with by using a constant viscosity coefficient, the Smagorinsky viscosity formulation or the two equation k–e model (Pender and Néelz, 2011).

The parameterisation of the bed roughness is one of the more important issues in the flood inundation modelling, because the predictions of water depths, velocities and inundation extent are highly dependent on the values of the friction parameters adopted in the models based on the shallow water equations (Pender and Néelz, 2011). For example, the presence of high vegetation and associated woody debris on the floodplain increases the hydraulic roughness, which consequently slows down the flood flow and enhances flood storage (Thomas and Nisbet, 2007), and vice versa. The flood inundation models can be parameterised by using engineering judgement informed by experience, calibration, or an ad hoc combination of both experience and calibration (Neelz and Pender, 2009). Nonetheless, it has been debated in the literature which of these options is the most suitable one (Beven, 2000, Cunge, 2003, Fewtrell et al., 2008, Savage et al., 2015).

The parameterisation of friction in 1D models benefits from decades of hydrometric data collection and user experience in model calibration and validation. This being the case, the flood propagation is nowadays predicted with high degree of accuracy with 1D models for many engineering applications. The parameterisation of friction in 2D models is, however, a bit more difficult due to the lack of hydrometric data, spatially varying topographic characteristics of floodplains (e.g. roads, different type of vegetation etc.), and more complex hydrodynamic processes associated with the floodplain flows (Pender and Néelz, 2011). For example, if the water depths and velocities are small in the floodplains when compared to those in the main channel (i.e. the floodplains act like a storage), then the predictions of flood depths, velocities and inundation extent are much more dependent on the friction values in the main channel than they are on the friction values on the floodplains (Pappenberger et al., 2005). On the other hand, when the velocities on the floodplains are higher, then the model predictions are not dependent solely on the frictions values on the floodplains, but also on the correct prediction of flood discharge (Neelz and Pender, 2009). Due to these limitations, elaborate spatially-distributed friction models for floodplain friction parameterisation have been proposed and applied in recent years (Cobby et

al., 2003, Mason et al., 2003, 2007, Hunter et al., 2007, Fewtrell et al., 2008, 2011, Ozdemir et al., 2013, Croissant et al., 2014). These approaches rely on the information provided by remote-sensing observations (such as LiDAR), from which spatially-distributed details on vegetation thickness and density can be extracted, and thus friction parameters needed for the flood inundation modelling can be obtained (Pender and Néelz, 2011).

As an appropriate parameterisation of flood inundation models is essential for an accurate flood inundation modelling process, it is therefore important to completely understand the nature of the modelling problem and the limitations of the model one is using. However, it often occurs that flood risk practitioners misinterpret the information from the models they are using, which is usually due to the difference in the perception of flood risks between model developers and flood risk practitioners (Faulkner et al., 2007, Janssen et al., 2009, Timmerman et al., 2010, Wood et al., 2012). Namely, the modellers generally frame flood risk issues using scientific knowledge and expertise, and assume that with more detailed model information analysis will improve and better decisions can be made. On the other hand, flood risk assessment practitioners often lack the time and resources to perform such complex analyses. This being the case, flood risk assessment practitioners tend to discard model information that seem to increase the complexity of the problem they already have to deal with, and often apply solutions that they do not necessarily understand completely (Leskens et al., 2014a). For example, viscosity coefficient can be used to introduce additional artificial viscosity to the flow, which consequently can enhance model stability (Pender and Néelz, 2011). However, the question is whether such solution can be applied for all modelling problems and how much of an additional artificial viscosity can be introduced without affecting model predictions? This lack of consideration of model information and applying of practical solutions in the modelling process in order to save time, or decrease the complexity and uncertainty of the modelling problem, is often referred to as a "simplification strategy" (Leskens et al., 2014a).

The issue with the "simplification strategy" is that its use is based on the user's experience rather than on some scientific or technical background. This means that flood risk assessment practitioners will apply solutions that they probably cannot

fully justify. However, these solutions would still, in their opinion, provide satisfactory results, and thus would not be considered as inappropriate. For example, the majority of commercial hydraulic software packages are based either on the Alternating Direction Implicit (ADI) finite difference scheme or the explicit finite volume scheme (Neelz and Pender, 2013), which means that these types of models are generally the model-of-choice for the majority of flood risk practitioners. These models are generally very accurate (numerically) in modelling floods over mild slope or nearly horizontal flow conditions. However, when used for modelling of rapidly varying flood events (such as flash floods) where rapid changes in the flow regime (such as hydraulic jumps) often occur, then these models are prone to generating spurious numerical oscillations close to the sharp gradients in the solution, and thus can lead to inaccurate results (Liang et al., 2007c, Neelz and Pender, 2013). As mentioned, the use of more complex models (such as shock-capturing models) would deal with these oscillations. However, the high computational cost required by such models persuades flood risk assessment practitioners to revert to the ADI-type models and apply other solutions, such as applying patches of high roughness to slow water down in the areas in the modelling domain where instabilities occurred (e.g. where Froude number was greater than 1) (CH2M, 2016). This being the case, the flood risk assessment in areas prone to occurrence of rapidly varying flood events is thus based on the flood risk assessment practitioner's perception of how much of the friction parameterisation tuning is needed in order to obtain satisfactory results.

However, water depths and velocities, and flood wave arrival time are particularly sensitive to the specification of surface friction parameters (Mason et al., 2003, Begnudelli and Sanders, 2007, Fewtrell et al., 2008, Ozdemir et al., 2013). This means that flood hazard assessment and development of emergency evacuation plans are thus indirectly related to the values of friction parameters used in the flood inundation modelling process. As mentioned, including an artificially high bed resistance or eddy diffusion term can dampen out numerical simulations (de Almeida et al., 2012). However, it is practically impossible to evaluate how much of the increased dissipation is being used in physically dissipating the energy of the flow and how much is being used in numerically damping out the oscillations. Therefore, it is highly questionable whether applying of the "simplification strategy" (i.e. manipulating with the friction coefficients) when modelling extreme flood events is a

smart thing to do, since model results can be completely misleading. This being the case, there is a need to explore in detail the use of such strategies in practical flood risk assessment, as there is practically no literature or wider debate on this matter at the moment.

2.3 Flood hazard assessment

According to the Department for the Environment, Food and Rural Affairs (DEFRA) of the UK Environment Agency, flood hazard *"describes the flood conditions in which people are likely to be swept over or to drown in a flood"* (Ramsbottom et al., 2006). In the case of a flood event, three fairly wide-ranging sets of characteristics generally have a direct impact on the degree of danger to people, including: (i) characteristics of the flood, such as flood depth and velocity, (ii) characteristics of the location, such as being indoors or outdoors, or being in urban or rural area, and (iii) characteristics of the general population, such as gender, age, health and body physique (Jonkman et al., 2002). Among these characteristics, flood depth and velocity are the main factors in determining the degree of flood hazard (Abt et al., 1989), since these two factors have the greatest influence on the human balance in the floodwater.

In floodwaters, people predominantly lose stability due to two hydrodynamic mechanisms, i.e. toppling or moment instability and sliding or friction instability (Jonkman and Penning-Rowsell, 2008, Cox et al., 2010, Xia et al., 2014). Sliding instability occurs when the drag force is larger than the frictional resistance between a person's footwear and the substrate surface (Jonkman and Penning-Rowsell, 2008).The occurrence of the sliding instability mechanism depends on the body weight, clothing and footwear type of a person standing in the floodwater, buoyancy and the ground surface conditions (Cox et al., 2010). Toppling instability occurs when a human body pivots around the heel, as the moment induced by the oncoming flow exceeds the resisting moment generated by the effective body weight (Abt et al., 1989). The occurrence of the toppling instability mechanism depends on the buoyancy, body positioning and weight distribution of a person standing in the floodwater (Cox et al., 2010).

People can also loose stability in floodwaters due to floating, i.e. when the floodwater depth exceeds the height of a person standing in the floodwater. Once a human body is influenced by floating, the body cannot be effected anymore by sliding or the toppling instability mechanism (Xia et al., 2014). Additionally, people can also lose stability to other unfavourable conditions, including: (i) bottom conditions, such as unevenness and obstacles, (ii) flow conditions, such as floating debris, water temperature, poor visibility, unsteady flow, flow aeration, animals, (iii) human vulnerability, such as standing or moving, experience and training, clothing and footwear, physical attributes including mass, height, muscular development or disabilities, psychological factors, age etc., and (iv) other factors, such as wind, lighting, visibility and waves (Jonkman and Penning-Rowsell, 2008, Cox et al., 2010).

Flood hazard assessment methods are classically divided into two groups, i.e. methods derived from mechanical analysis based on experimental studies and methods based on empirical or theoretical studies. However, a new type of flood hazard assessment methods was introduced recently, which includes methods that are completely physically based and experimentally calibrated.

2.3.1 Methods derived from mechanical analysis based on experimental studies

This section presents the flood hazard assessment methods derived from mechanical analysis based on experimental studies. The short summary of the considered methods is outlined in Table 2.5, while the more detail discussion on individual studies is presented below. The following studies were considered: Foster and Cox (1973), Abt et al. (1989), Takahashi et al. (1992), Karvonen et al. (2000) and Jonkman and Penning-Rowsell (2008).

Table 2.5: Comparison of flood hazard assessment methods derived from mechanical analysis based on experimental studies. Partially adapted from Cox et al. (2010)

Study	Foster and Cox (1973)	Abt et al. (1989)	Takahashi et al. (1992)	Karvonen et al. (2000)	Jonkman and Penning-Rowsell (2008)
Setup	flume	flume	funnelled basin	moving platform	sluice-controlled flood relief channel
Surface	painted timber	concrete, turf, gravel, steel	metal load cell	steel grating	concrete
Test subjects	children	adults with safety equipment	adults	adults with safety equipment	professional stuntman
Number of test subjects	6	20	3	7	1
Subject action	standing, walking, turning, sitting	standing, turning, walking	standing	standing, turning, walking	standing, walking
Failure mechanism	subject feels unsafe or loses footing	subject loses footing	subject loses footing	subject loses footing	subject loses footing
Considered instability mechanisms	/	toppling instability	toppling and sliding instability	toppling instability	toppling and sliding instability
Proposed stability criteria	/	see Equation (2.1)	see Equations (2.3) and (2.4)	see Equations (2.5), (2.6) and (2.7)	see Equations (2.8) and (2.9)

Foster and Cox (1973)

Experiments by Foster and Cox (1973) were conducted in 6 m long, 0.6 m wide and 0.75 m deep flume. The base of the flume was made of timber and there were sluice gates at each end of the flume, which were used to control the water height and

velocity within the flume. The test group consisted of 6 male children, which were 9-13 years old, 1.27-1.45 m tall and weighed from 25 to 37 kg. All children wore shorts during the different stages of the experiment in order to minimalize the effect of the clothing drag on the child's stability. However, water levels never reached the height of the shorts and therefore the effect of the clothing drag was negligible during the experiment. Within the flume, children were tested in different body positions and body movements, such as standing, sitting, walking and turning. Additionally, tests were performed with children both facing the oncoming flow and with their backs turned against the oncoming flow. Safety criteria developed within this study were based on child's perception of security, which means that the critical instability was identified when the child felt unsafe and not when the actual body stability was lost. This being the case, stability thresholds were strongly based on the psychological tendency of the child.

Based on the performed tests and observations, Foster and Cox (1973) outlined four conditions that could affect child's stability in floodwaters, including (Cox et al., 2010): (i) physical attributes, such as age and body characteristics (e.g. weight, height and muscular development), (ii) psychological factors, such as awareness and reaction time, (iii) hydraulic conditions, such as water depth and velocity, and (iv) other factors, such as bottom friction, type of clothing and possible impact of floating debris. Foster and Cox (1973) generally concluded that relatively low flow depths in combination with high velocities could lead to a loss of child's stability in the floodwaters. Furthermore, it was also noted that moving in the flow reduces standing stability, and that stability is the lowest when the child is seated. The latter conclusion is very important as it indicates that once standing stability has been lost, it is very difficult for a person to get back to the standing position and thus escape to safety (Cox et al., 2010).

The study of Foster and Cox (1973) was a pioneering research in the field of investigating human stability in floodwaters. Although it laid the foundation for further investigations, the study of Foster and Cox (1973) has two main shortcomings. First, the study focused solely on children safety in floodwaters. It is difficult to apply the safety criteria developed for children to the rest of the general population, because children are one of the most vulnerable sub-population groups

due to not being yet fully physically or emotionally developed. Therefore, projecting stability criteria for children to adults is not straightforward and cannot be done as easily as it might seem. Second, stability thresholds were based on the psychological tendency of the child. As it was indicated earlier, psychological factors play an important role in defying the stability thresholds for children. However, it is difficult to imagine that an average adult would feel unsafe as quickly as an average child does. This means that the any flood hazard criteria based on the study of Foster and Cox (1973) would have tendency to under-predict flood hazard indices for adults. This being the case, the flood hazard maps based on such criteria would show much higher flood hazard risk than it would be in reality. Although this might seem as a positive thing from viewpoint of flood safety, it would also cause difficulties when it comes to the development of urban communities, flood protection design and flood rescue plans. All in all, the study of Foster and Cox (1973) set guidelines for the future researches, but any safety criteria based on the study of Foster and Cox (1973) would not be representative for the entire general population, and thus would not enable a detailed flood hazard assessment.

Abt et al. (1989)

Experiments by Abt et al. (1989) were conducted in a 61 m long, 2.44 m wide and 1.22 m deep flume. Two different flume gradients were considered within this study, i.e. 0.5 and 1.5 per cent. Furthermore, four different types of materials were used to cover the bottom of the flume, i.e. steel, smooth concrete, gravel and turf. The test group consisted of 20 adult males and females, which were 1.52-1.83 m tall and weighed from 41 to 91 kg. All test subjects wore similar clothing in order to establish a consistent database. The main motivation behind the experiments conducted by Abt et al. (1989) was to determine the approximate hydraulic conditions (i.e. the value of water depth and velocity) in which person would lose stability in floodwater.

Even though four different surface conditions were considered within this study, no significant effect on the human stability was noted. This is probably due to the fact that water depth in the flume was relatively high (i.e. water depth was greater than 1 m) during the majority of the experiment. When the water depth is relatively high, the friction between the sole of the footwear and the ground surface becomes less

important, because toppling (moment) instability prevails over sliding (friction) instability. If the flume tests were undertaken at lower depths in combination with high velocities, a noticeable difference in human stability on different surfaces would most likely be observed (Cox et al., 2010).

Based on the collected data, Abt et al. (1989) derived the following expression to define the stability threshold for a person standing in the floodwater:

$$dv = 0.0929[e^{0.001906hm+1.09}]^2 \qquad (2.1)$$

where dv is the depth-velocity product (m^2/s), m is the weight of a person (kg) and h is the height of a person (m).

It should be noted that Equation (2.1) was obtained using linear regression of the observed data, and that the resulting coefficient of determination (R^2) was relatively low, i.e. it had value of 0.48. Furthermore, Abt et al. (1989) also reported that experiment had some constraints, such as optimal experiment conditions, the presence of the safety equipment, healthy test subjects and the ability of the test subject to learn how to manoeuvre in flow with time. All these artificially increase the stability threshold for a person standing in the floodwater. This means that the test subjects lost their stability later than an average person probably would in the case of a real-life flood event. In addition, the most vulnerable sub-population groups (such as children) were not considered in this study. The study of Foster and Cox (1973) has shown that the stability thresholds for children are greatly dependent on the psychological tendency of a child. Therefore, the stability expression proposed by Abt et al. (1989) would probably predict lower flood hazard indices, if children were also considered as test subject. Considering all above, there are some doubts regarding the accuracy of the expression proposed by Abt et al. (1989), as this expression most likely too optimistically assesses flood hazard indices for real-life flood events. This being the case, any flood hazard assessment based on the expression proposed by Abt et al. (1989) could be very misleading in terms of predicting flood hazard indices for a potential real-life flooding.

Takahashi et al. (1992)

Takahashi et al. (1992) investigated the safety of people on breakwaters (i.e. a harbour structure for protecting from storm waves) against overtopping sea waves, with particularly focusing on the safety of harbour workers. Experiments by Takahashi et al. (1992) were conducted in large current basin, which was 50 m long and 20 m wide. The test group consisted of 3 adult, male harbour personnel, which were 1.64-183 m tall and weighed from 64 to 73 kg. Test subject were standing on component load cells, which were used to measure forces acting on human body subjected to flow, such as drag and friction force. During the experiments, test subjects wore three different types of clothing and two pairs of shoes with different types of soles. Also, different types of ground surfaces were tested, such as smooth and rough concrete, and concrete covered with algae and seaweed.

While standing on the platform, test subjects were exposed to different combinations of flow depths and flow velocities. The angle of subject's body against the current (i.e. 0, 45 and 90 degrees) and the distance between the subject's feet (i.e. 0, 25 and 50 cm) varied for each test. One series of testing lasted until the test subject lost balance or stability due to the force of the flow. Based on the experiment results, Takahashi et al. (1992) established that current force acting on human body in floodwater is proportional to the flow velocity squared. This force can be expressed as a drag force, which is dependent on the angle of subject's body against the current, the distance between the subject's feet and the water depth (Endoh and Takahashi, 1994), and is written as:

$$F = \frac{w_0}{2g} C_D \cdot A \cdot U^2 \tag{2.2}$$

where F is the current or drag force, w_0 is the specific weight of the sea water, g is the gravitational acceleration (m/s^2), C_D is the drag coefficient, A is the projected area of the body against overtopping flow (m^2) and U is the current velocity during wave overtopping (m/s).

Depending on the height and the velocity of the flow, resulting current or drag force can lead to occurrence of either toppling or friction instability mechanism, and thus to loss of person's stability. Furthermore, the measurements of friction and drag coefficient showed that (i) the friction coefficients are dependent on the surface conditions (for example, the value of friction coefficients for smooth concrete under wet condition were typically around 0.6, while typical values of frictions coefficient for rough concrete under wet conditions were around 1), and (ii) the drag coefficients are dependent on the subjects characteristics and the clothing being worn, with typical value of the drag coefficient being between 0.6 and 1.1

Measurements of friction coefficients, water depths and velocities of the flow, and resultants forces on the subject's body enabled Takahashi et al. (1992) to calculate drag coefficients and human stability when exposed to overtopping sea waves. This enabled the development of a computational model for human stability in the floodwater (i.e. the loss of balance model), which was presented by Endoh and Takahashi (1994). For any given height and weight of a person, the model calculates drag and friction forces. Based on these forces, an estimation of the critical sliding or toppling stability in a given water depth can be made, i.e. the model estimates the critical water depth in which a person would lose their balance due to the overtopping sea wave (Endoh and Takahashi, 1994). The toppling instability mechanism is expressed as:

$$F \cdot h_G \geq W_0 \cdot l_G \tag{2.3}$$

where F is the current or drag force, h_G is the vertical distance from the floor to the point where the resultant force acts, W_0 is the weight of a human body in the overtopping flow and l_G is the horizontal distance between the centre of the gravity and the fulcrum of the moment.

The sliding instability mechanism is expressed as:

$$F \geq \mu s \cdot W_0 \tag{2.4}$$

where F is the current or drag force, μs is the coefficient of friction between the shoes and the ground and W_0 is the weight of a human body in the overtopping flow.

Even though model results agreed well with the experimental data, it should be taken into account that the research of Takahashi et al. (1992) focused exclusively on the effect of the overtopping waves on breakwaters. On breakwaters, safety does not depend solely on the characteristics of the sea wave, but also on other factors, such as the height and the type of the fence and the distance of the person from the edge of the breakwater (Cox et al., 2010). Furthermore, there were only three test subjects included in the experiment, which could raise some questions whether the test group was large enough to obtain fully representative set of data. This, consequently, also raises doubts about the accuracy of the proposed model, since such small dataset was used to calibrate the model. Finally, the proposed model was developed for a specific situation, i.e. safety of people on breakwaters against overtopping sea waves. This being the case, it is hard to say if the proposed stability model would be similarly accurate in the case of a river or coastal flooding. Considering all above, it appears that the model proposed by Takahashi et al. (1992) most likely could not adequately predict flood hazard indices for the most common types of flooding, such as riverine flooding.

Karvonen et al. (2000)

Experiments by Karvonen et al. (2000) were conducted as a part of the Development of Rescue Actions Based on Dam-Break Flood Analysis project (RESCDAM) (Maijala et al., 2001). In their part of the RESCDAM project, Karvonen et al. (2000) concentrated on testing the stability and manoeuvrability of humans in floodwaters, with particular focus on producing stability thresholds that could be used by the rescues authorities to organise a safe rescue action in the case of a dam-break flood. Experiments were conducted in a 130 m long, 11 m wide and approximately 5.5 m deep basin, which was equipped with a towing carriage. The test group consisted of seven adults (5 males, 2 females), with two of the test subjects being professional rescue personnel. Test subjects were between 1.6-1.95 m tall and weighed from 48 to 100 kg. All test subjects wore Gore Tex survival suits, helmets and were tethered

with a safety rope. Additionally, test subject were also provided with a handle and a second safety rope, which could be used when a test subject lost their balance.

In contrast to previous studies where test subject were facing the on-coming flow, a moving steel platform was used to replicate the flow in the basin. This platform was installed on the towing carriage and was vertically adjustable, which allowed the simulation of different water depths and velocities. The test subjects were asked to perform three different manoeuvres, i.e. to walk into the flow, to walk perpendicular to the flow and to walk facing downstream to the flow. The velocity and depth of the platform were steadily increased until the test subject lost stability or manoeuvrability (see Figure 2.6). This procedure was repeated until at least four different water depths were tested.

Figure 2.6: Test subject during the experimental procedure (Karvonen et al., 2000)

According to Karvonen et al. (2000), the main factors affecting the conditions of the flow and environment can be divided into three categories: (i) bottom surface characteristics, such as uneven/smooth, slippery/non-slippery and with obstacles/without obstacles, (ii) water characteristics, such as floating debris/no floating debris, cold/warm, ice/no ice and poor visibility/good visibility, and (iii) human characteristics, such as age, disabilities, health and cognitive abilities. Based on the data collected in their experiment, Karvonen et al. (2000) proposed three

stability expressions. These stability expressions define the approximate limits of human stability in different conditions of the flow and environment, including: good conditions (i.e. Equation (2.5)), normal conditions (i.e. Equation (2.6)), and poor conditions (i.e. Equation (2.7)). The expressions are written as:

$$dv = 0.006hm + 0.3 \qquad (2.5)$$

$$dv = 0.004hm + 0.2 \qquad (2.6)$$

$$dv = 0.002hm + 0.1 \qquad (2.7)$$

where dv is the depth-velocity product (m^2/s), m is the weight of a person (kg) and h is the height of a person (m).

Even though Karvonen et al. (2000) proposed stability thresholds for humans in floodwaters, the authors also report that their experiment had some constraints, such as excessive safety features, the use of survival suits, which increases buoyancy and cross-sectional area of a person, and the use of quite slippery surface. This being the case, the stability expressions proposed by Karvonen et al. (2000) are faced with similar shortcomings as the expression proposed by Abt et al. (1989), i.e. they most likely too optimistically assesses flood hazard indices for real-life flood events. In addition, it is also hard to evaluate how the proposed expressions would apply to children, as they were not considered as test subject in the experiment. Therefore, the expressions proposed by Karvonen et al. (2000) should probably be used only as an orientation guide and not as an exact flood hazard assessment method.

Jonkman and Penning-Rowsell (2008)

Jonkman and Penning-Rowsell (2008) based their research on the experiment conducted at the Flood Hazard Research Centre (FHRC), Middlesex University, United Kingdom. The experiment was conducted in the Cattlegate Flood Relief Channel, which is a part of the River Lee Navigation. The water depths and velocities in the channel were controlled by the sluice gates some 75 meters upstream of the site of the test. In the experiment undertaken by the FHRC, a professional

stuntman was used as a test subject. The stuntman was 1.7 m tall and weighed 68kg. The stuntman wore rubber soled shoes and a dry suit, which was tightly drawn around his legs in order to prevent the artificial increase of the cross-sectional area of the subject's legs due to the trapped air. The test subject was not tethered with a safety rope or supported in any other way. This being the case, the test subject could move freely and allowed to readjust his body position in the flow (see Figure 2.7). The test subject was also connected with the experiment controllers via wireless radio and was therefore able to report his reactions while manoeuvring in the water. During the tests, the test subject undertook different manoeuvres within the channel, such as walking and standing. Also, different body positions were tested, such as leaning forward in order to lower the centre of gravity and thus increase stability.

Figure 2.7: Stuntman during the experiment in the Cattlegate Flood Relief Channel (Jonkman and Penning-Rowsell, 2008)

Based on the FHRC experiment results, Jonkman and Penning-Rowsell (2008) concluded that low water depths in combination with high flow velocities are more dangerous than it had been suggested in earlier studies, such as in Abt et al. (1989). This conclusion is based on the characteristics of sliding instability, which appears to occur earlier than toppling instability for low depth / high velocity flood waters. Furthermore, Jonkman and Penning-Rowsell (2008) derived equations for both toppling and sliding instability for humans standing in floodwaters. The following simplifications were applied in the derivation process: (i) the effect of buoyancy was not included, (ii) human body was represented by a simple block, and (iii) static models, constant flow velocity and uniform velocity profile were assumed. The

experimental datasets of Abt et al. (1989), Karvonen et al. (2000) and the FHRC experiment were used to validate the performance of the proposed expressions.

The toppling instability mechanism is expressed as:

$$dv = \left(\frac{2mg\cos\alpha\,L}{C_D B \rho}\right)^{0.5} \tag{2.8}$$

where dv is the depth-velocity product (m^2/s), m is the weight of a person (kg), g is gravitational acceleration (m/s^2), α is person's angle of tilt into flowing water (degrees), L is the height of a human (m), C_D is the drag coefficient, B is the average body width exposed normal to the flow (m) and ρ is the density of the flow (kg/m^3).

The sliding instability mechanism is expressed as:

$$dv^2 = \frac{2\mu g}{C_D B \rho} \tag{2.9}$$

where dv^2 is the depth-velocity squared product (m^3/s^2), μ is the coefficient of static friction, g is gravitational acceleration (m/s^2), C_D is the drag coefficient, B is the average body width exposed normal to the flow (m) and ρ is the density of the flow (kg/m^3).

Derived equations show that dv (depth times velocity) product is related to the toppling instability mechanism (see Equation (2.8)), whereas dv^2 (depth times the velocity squared) product is more closely related to sliding instability mechanism see Equation (2.9)). However, these derivations are based on over-simplified human body structure and characteristics of the flow, and exclude the effect of buoyancy. Furthermore, the conclusions of Jonkman and Penning-Rowsell (2008) are based on the experiment with very small test group (i.e. only one test subject) and on the experiments which had several constraints (see Abt et al. (1989) and Karvonen et al. (2000)). In addition, it could be argued how representative is the data based on the experiment using a professional stuntman, since he most likely is both physically and

mentally (e.g. facing fear) more capable than an average person. Considering all above, it is questionable whether the expressions proposed by Jonkman and Penning-Rowsell (2008) can accurately assess the danger to people due to flooding. This being the case, these two expressions should probably be used only for a rough estimation of flood hazard indices.

2.3.2 Methods based on empirical or theoretical studies

This section presents the flood hazard assessment based on empirical or theoretical studies. The short summary of the considered methods is outlined in Table 2.6, while the more detail discussion on individual studies is presented below. The following methods were considered: Keller and Mitsch (1993), Lind et al. (2004) and Ramsbottom et al. (2006).

Table 2.6: Comparison of flood hazard assessment methods based on empirical or theoretical studies. Partially adapted from Cox et al. (2010)

Study	Keller and Mitsch (1993)	Lind et al. (2004)	Ramsbottom et al. (2006)
Analysis type	theoretical	empirical	empirical
Human body representation	vertical cylinder	rigid circular cylinder, square parallelepiped, composite cylinders	/
Considered instability mechanisms	sliding instability	toppling instability	/
Calibration means	friction and drag coefficients	experimental data	experimental data
Considered experimental data	/	Abt et al. (1989) and Karvonen et al. (2000)	Abt et al. (1989) and Karvonen et al. (2000)
Proposed stability criteria	see Equation (2.10)	see Equation (2.14)	see Equation (2.16)

Keller and Mitsch (1993)

Keller and Mitsch (1993) conducted completely theoretical study of human stability in floodwaters. Two simplifications were applied in the study, including: (i) a uniform velocity profile along the vertical direction was assumed, and (ii) the human body shape was idealised to the shape of a vertical cylinder. Based on the representation of the human body as a vertical cylinder, a friction coefficient of 0.3 and a drag coefficient of 1.2 were selected for this study. Keller and Mitsch (1993) considered both toppling and sliding instability mechanism. Toppling instability was reached when the moment induced by the flow around a pivot point at the base of the cylinder exceeded the moment due to subject weight, while sliding instability was reached when the drag force due to flow exceeded the frictional resistance between the bottom of the cylinder and ground surface (Cox et al., 2010).

Keller and Mitsch (1993) reported that sliding instability is the dominant instability mechanism for flows where water depths is less than 0.55 m, while toppling instability is the dominant instability mechanism for flows where water depth is greater than 0.55 m. Furthermore, Keller and Mitsch (1993) proposed a formula for human stability in floodwaters, which is derived from the equilibrium of forces acting on a flooded person, i.e. buoyancy, weight, frictional resistance and drag force. The formula is based on the mechanism of sliding instability, and is written as:

$$v_{cr} = \sqrt{\frac{2F_R}{\rho_f C_d A}} \qquad (2.10)$$

where v_{cr} is critical velocity (m/s), F_R is restoring force due to friction, ρ_f is the density of the flow (kg/m^3), C_d is the drag coefficient and A is the submerged area projected normal to the flow (m^2).

According to the proposed formula, a person standing in the floodwater loses stability due to the sliding instability mechanism, if the velocity of the flow is higher than the critical velocity. The expression proposed by Keller and Mitsch (1993) is, however, highly dependent on the selection of friction and drag coefficients. In their

study, Takahashi et al. (1992) reported that friction coefficient values generally range between 0.6 and 1.0, while drag coefficients values generally range between 0.6 and 1.1. Taking this into account, it appears that a low value of friction coefficient (i.e. 0.3) and a conservative value of drag coefficient (i.e. 1.2) were adopted in the study of Keller and Mitsch (1993). Furthermore, the friction and drag coefficients used in the study of Keller and Mitsch (1993) were adopted without any evident sensitivity assessment. This being the case, it could be questioned whether adequate values of the friction and drag coefficients were adopted in the derivation process, and how this affects the predictive ability of the proposed formula. Considering all mentioned, the formula proposed by Keller and Mitsch (1993) should probably be used only for a rough estimation of the risk to people due to flooding.

Lind et al. (2004)

Lind et al. (2004) considered three mechanical human stability models, which were used to simulate the toppling instability mechanism for a human body immersed in floodwaters. The human body was approximated by (i) a rigid circular cylinder, (ii) a square parallelepiped and (iii) composite cylinders, where one circular cylinder was used to represent the torso and two circular cylinders were used to represent the legs. On the basis of these three mechanical models four empirical expressions were derived, which define stability threshold for a human standing in floodwaters. These four expressions are written as:

$$hv_{cr} = K\left[m\left(1 - \frac{h}{H}\right)\right]^{\frac{1}{2}} \tag{2.11}$$

$$hv_{cr} = K \cdot m^{\frac{1}{2}} \tag{2.12}$$

$$hv_{cr} = K \cdot m \tag{2.13}$$

$$hv_{cr} = K \tag{2.14}$$

where hv_{cr} is the critical flow regime (m²/s), m is the weight of a person (kg), H is the height of a person (m), h is the water depth (m) and K is an empirical coefficient which can be estimated from the experimental data.

The tests based on these three mechanical models showed that human instability in floodwaters depends on the speed and depth of the flow, and the height and weight of the human standing in the floodwater. Furthermore, Lind et al. (2004) also noted that drag, drag factor and person's gender have great impact on human stability in floodwaters. On the other hand, the influence of ground surface and moderate slope were noted as negligible. Lind et al. (2004) suggested that the simplest expression (i.e. Equation (2.14)) should be generally used for the assessment of human stability in floodwaters. In the Equation (2.14), the estimation of the critical flow regime depends solely on the empirical calibration coefficient K. In the flood hazard assessment analysis, different values of the empirical coefficient K should be used for males and females, and for different type of clothing. The empirical calibration coefficients K were evaluated by using the data collected by Abt et al. (1989) and Karvonen et al. (2000).

However, the authors themselves noted that these two datasets should not be aggregated in the application process, as these datasets are too small, not random and consequently not representative enough. Furthermore, Lind et al. (2004) also reported that by controlling the weight and height parameters in Equation (2.11), the influence of person's gender on the human stability in floodwaters is annihilated. This, however, contradicts earlier suggestions that different values of the coefficient K should be used for different sub-population groups, such as men, women and children. In addition, the authors also suggested that different datasets should be used for different locations and time of year, such as summer or winter. All in all, it appears that empirical expressions presented by Lind et al. (2004) are highly dependent on the quality of the experimental data, and that calibration of the proposed expressions can be a fairly complicated process. This being the case, the expressions proposed by Lind et al. (2004) should only be used for a rough approximation of the actual flood hazard indices due to the aforementioned limitations.

Ramsbottom et al. (2006)

Ramsbottom et al. (2003) developed a methodology for assessing and mapping the risk to people caused by flooding, with this methodology being developed for the Department for the Environment, Food and Rural Affairs (DEFRA) and the UK Environment Agency. Based on testing various empirical formulae by comparing the predictions to experimental datasets obtained from laboratory studies conducted by Abt et al. (1989) and Karvonen et al. (2000) (Cox et al., 2010), Ramsbottom et al. (2003) proposed an empirical formula, which assesses the flood hazard to people as follows:

$$HR = d(v + 1.5) + DF \qquad (2.15)$$

where HR is the flood hazard rating (m^2/s), d is the water depth (m), v is the velocity of the flow (m/s) and DF is the debris factor (m^2/s). The debris factor can have a value of 0, 1 or 2, depending on the location of the flood.

In the review of the original study, Ramsbottom et al. (2006) revised the initially proposed formula (i.e. Equation (2.15)), wherein: the velocity coefficient was reduced from 1.5 to 0.5, while the values for the debris factor were reduced from the initial values of 0, 1 and 2 to values of 0, 0.5 and 1. This being the case, the revised formula is given as:

$$HR = d(v + 0.5) + DF \qquad (2.16)$$

where HR is the flood hazard rating (m^2/s), d is the water depth (m), v is the velocity of the flow (m/s) and DF is the debris factor (m^2/s).

Based on the revised formula (i.e. Equation (2.16)), Ramsbottom et al. (2006) proposed various flood hazard classifications. These are outlined in Table 2.7.

Table 2.7: Flood hazard to people (Ramsbottom et al., 2006)

HR	Degree of flood hazard	Description
0 – 0.75	low	**Caution** *Flood zone with shallow flowing water or deep standing water*
0.75 – 1.5	moderate	**Dangerous for some (i.e. children)** *Danger: Flood zone with deep or fast flowing water*
1.5 – 2.5	significant	**Dangerous for most people** *Danger: flood zone with deep fast flowing water*
> 2.5	extreme	**Dangerous for all** *Extreme danger: flood zone with deep fast flowing water*

The revised empirical expression (i.e. Equation (2.16)) proposed by Ramsbottom et al. (2006) has some shortcomings, including (Cox et al., 2010): (i) the flow regime values from the experimental datasets were averaged and thus some training (i.e. the ability of the test subject to learn how to manoeuvre in the flow with time) was incorporated in the derived expression; however, this is usually not the case with the general population, as majority of people does not have the experience of standing or manoeuvring in floodwaters, (ii) the assigned values for the debris factor were not based on or supported by any sort of experimental testing, and (iii) the proposed expression has no upper depth limit and therefore large depth/low velocity flood flows are not necessarily considered as hazardous, i.e. the flow conditions in which a person would be floating and thus completely dependent upon swimming ability are not automatically classed as dangerous.

Nevertheless, flood hazard maps issued by the governing authorities in the UK (i.e. DEFRA) are based on the flood hazard assessment method presented by Ramsbottom et al. (2006). Furthermore, the criterion presented by Ramsbottom et al. (2006) is also well established outside the UK (Penning-Rowsell et al., 2005, Kaźmierczak and Cavan, 2011, Purwandari et al., 2011, Foudi et al., 2015).This being the case, the formula presented by Ramsbottom et al. (2006) is widely considered as an accurate criterion for assessing and mapping hazard to people due to flooding.

2.3.3 Physically based and experimentally calibrated methods

This section presents the physically based and experimentally calibrated flood hazard assessment methods. The short summary of the considered methods is outlined in Table 2.8, while the more detail discussion on individual studies is presented below. The following methods were considered: Xia et al. (2014) and Milanesi et al. (2015).

Table 2.8: Comparison of physically based and experimentally calibrated flood hazard assessment methods

Study	Xia et al. (2014)	Milanesi et al. (2015)
Physical background	considers drag force, frictional force, gravitational force, buoyancy force and normal reaction force	considers body weight, the fluid dynamic force, buoyancy and frictional force
Human body representation	model human body based on the real human prototype	human body is approximated with three cylinders
Considered instability mechanisms	toppling and sliding instability	toppling and sliding instability
Calibration means	experimental data	experimental data
Considered experimental data	own experimental data, Foster and Cox (1973), Abt et al. (1989), Karvonen et al. (2000), Jonkman and Penning-Rowsell (2008)	Foster and Cox (1973), Abt et al. (1989), Takahashi et al. (1992), Karvonen et al. (2000), Jonkman and Penning-Rowsell (2008), Xia et al. (2014)
Proposed stability criteria	see Equations (2.17) and (2.18)	see Equations (2.20) and (2.24)

Xia et al. (2014)

Xia et al. (2014) derived a new method for assessing human stability in floodwaters, which is based on extensive theoretical and experimental studies. The formulae proposed by Xia et al. (2014) are based on the mechanisms of toppling and sliding instability, and were derived by considering all forces acting on a human body in floodwater, i.e. drag force, frictional force, gravitational force, buoyancy force and normal reaction force. Furthermore, the formulae introduced by Xia et al. (2014) also take into account the effect of a non-uniform upstream velocity profile on the stability of a person standing in a floodwater, and consider the impact of the body buoyancy for rapidly varying water depths.

Two formulae were proposed by Xia et al. (2014). Firstly, the incipient velocity for a human body in floodwater experiencing sliding instability is given as:

$$U_c = \alpha \left(\frac{h_f}{h_p}\right)^{\beta} \sqrt{\frac{m_p}{\rho_f h_p h_f} - \left(a_1 \frac{h_f}{h_p} + b_1\right)\frac{(a_2 m_p + b_2)}{h_p^2}} \qquad (2.17)$$

where U_c is the incipient velocity, h_f is the water depth (m), h_p is the height of a person (m), m_p is the weight of a person (kg), ρ_f is the density of water (kg/m^3), α and β are empirical coefficients and a_1, a_2, b_1 and b_2 are coefficients based on the characteristics of a human body.

Secondly, the incipient velocity for a human body in floodwater experiencing toppling instability is given as:

$$U_c = \alpha \left(\frac{h_f}{h_p}\right)^{\beta} \sqrt{\frac{m_p}{\rho_f h_f^2} - \left(\frac{a_1}{h_p^2} + \frac{b_1}{h_f h_p}\right)(a_2 m_p + b_2)} \qquad (2.18)$$

where U_c is the incipient velocity, h_f is the water depth (m), h_p is the height of a person (m), m_p is the weight of a person (kg), ρ_f is the density of water (kg/m^3), α

and β are empirical coefficients and a_1, a_2, b_1 and b_2 are coefficients based on the characteristics of a human body.

Finally, the degree of flood hazard can be quantified with the following expression:

$$HR = MIN\left(1, \frac{U}{U_c}\right) \qquad (2.19)$$

where HR is the flood hazard rating, U is the velocity of the flow and U_c is the incipient velocity.

Xia et al. (2014) then undertook laboratory experiments to calibrate the proposed formulae, i.e. to calibrate the parameters α and β in Equations (2.17) and (2.18). The tests were conducted in 60 m long, 1.2 m wide and 1 m deep horizontal flume, with a cement based bed and two glass sides. A scale model human body was used for this experiment, which strictly followed the principles of geometric, kinematic and dynamic stability (Chanson, 2004). This means that flow conditions (such as velocity, drag and friction coefficients) and characteristics of the human body (such as density) were ideally similar to those of prototype. This being the case, the prototype 1.70 m in height and 60 kg in weight was scaled down to the model human body 0.3 m in height and 0.334 kg in weight. The tests were performed with the model body both facing the on-coming flow and with its back turned against the on-coming flow (see Figure 2.8). For each test, the water depth and the corresponding depth-averaged velocity were recorded when the flooded model body started to become unstable, with the corresponding instability mode of sliding or toppling being identified for each test.

Figure 2.8: Two different postures of the model human body in the flume (Xia et al., 2014)

Based on the conducted experimental tests, Xia et al. (2014) determined the values of α and β for typical adult and child based on the model human body, and thereafter proposed stability thresholds. Furthermore, Xia et al. (2014) also calibrated proposed stability formulae with the experimental data for real human bodies (i.e. real human test subjects) obtained in the aforementioned experimental studies, such as data collected by Foster and Cox (1973), Abt et al. (1989), Karvonen et al. (2000), Jonkman and Penning-Rowsell (2008). The main focus was, however, on the data collected by Abt et al. (1989) and Karvonen et al. (2000), because many other studies (such as Lind et al. (2004), Ramsbottom et al. (2006) and Jonkman and Penning-Rowsell (2008)) were calibrated using these two datasets. Comparison of all data revealed that stability thresholds based on the scaled model human body are lower than those based on the real human body. The difference in threshold values occurred because the real human test subjects were able to readjust themselves according to the flow conditions and therefore longer maintained stability, whereas the model human body could not readjust to the flow conditions and thus earlier (i.e. at lower velocities) lost stability.

From the viewpoint of flood hazard assessment, the stability thresholds based on the model human body tend to be safer to use in practice than the stability thresholds based on the real human bodies. Stability thresholds based on the real human body could potentially be dangerous, since the ability to manoeuvre and readjust body position in floodwaters depends on several factors, such as the person's gender, age, physical and psychological characteristics. Therefore, it could be hazardous to apply the stability thresholds based on the real human body in the practical flood hazard assessment, as it is almost impossible to imagine that the majority of the general population would be able to adapt to the flow conditions in the same way as the test subjects in the experimental studies of Abt et al. (1989) and Karvonen et al. (2000). Namely, these two studies included only healthy and physically fit subjects that were facing the on-coming flow in controlled and safe environments, and were able to learn how to manoeuvre in the flow after few tests. However, this is completely opposite to the real-world conditions, and thus it can be debated how realistic are any flood hazard formulae based on these datasets.

The main difference between the majority of the aforementioned flood hazard formulae and this physically based and experimentally calibrated method is in the way they take into account forces induced by flow conditions. In Equations (2.17) and (2.18), it can be seen that the overturning force on the body is proportional to the water depth times the velocity squared (i.e. hv^2), whereas for the majority of the aforementioned formulae (see for example Equations (2.1), (2.5), (2.8), (2.14) and (2.16)) the overturning force on the body is proportional to the water depth times velocity only (i.e. hv). This means that the physically based and experimentally calibrated method can be much more influenced by higher velocities and momentum. This being the case, the physically based and experimentally calibrated method proposed by Xia et al. (2014) is most likely highly adaptable to abrupt changes in the flow regime, and can probably rapidly and with high level of accuracy assess the degree of flood hazard risk in a short time period. This characteristic, however, could be particularly important for flood hazard assessment of extreme flood events due to high-velocity flows associated with such flood events. It should be noted that Jonkman and Penning-Rowsell (2008) have also proposed an expression where the overturning force on the body is proportional to the hv^2 product (see Equation (2.9)).

However, Jonkman and Penning-Rowsell (2008) associated the hv^2 product only with the sliding instability mechanism.

A further advantage of the physically based and experimentally calibrated formulae proposed by Xia et al. (2014) is that they can be adjusted to a specific body type. For example, by applying a biomechanical model, such as the 3D biomechanical model presented by Nikolova and Toshev (2007), Equations (2.17) and (2.18) can assess the stability of people according to their height, weight and body parameter characteristics, i.e. length, mass and the corresponding volume of a particular body part, such as legs, torso, arms etc. This means that stability thresholds can be defined specifically for: (i) different sub-population groups of the general population, such as males, females and children, and (ii) that stability thresholds can be defined explicitly for different geographic regions or countries, such as Europe, America or the Far East etc.

All in all, Xia et al. (2014) presented a completely new approach for assessing human stability in floodwaters, which is physically based and thus independent of the flow characteristics. Considering all mentioned above, it appears that the flood hazard assessment method presented by Xia et al. (2014) can assess flood hazard risk to people with high level of accuracy.

Milanesi et al. (2015)

Milanesi et al. (2015) developed a simple conceptual model of human stability through the description of the involved forces, considering sliding, toppling, and drowning related to high water levels. The model presented by Milanesi et al. (2015) is based on a simplified representation of human body, i.e. the human body is approximated with three cylinders, two paired cylinders for the legs and a single cylinder for the torso. Similarly to criterion presented by Xia et al. (2014), the model presented by Milanesi et al. (2015) also considers all forces acting on human body in floodwater, i.e. body weight, the fluid dynamic force, buoyancy and the friction force. In addition, the model presented by Milanesi et al. (2015) introduces one novelty, i.e. the model can account for the effect of the local slope, which widens the

potential application of the model to different environments, such as mountain regions. The model accounts for both sliding and toppling instability mechanisms, with both instability mechanisms being based on the equilibrium of forces.

Firstly, the equilibrium condition with respect to the sliding instability is expressed as:

$$D + W_P \leq T \tag{2.20}$$

where D is the drag force, W_P is the weight component parallel to the slope and T is the friction force between the sole of the human body and the ground, with the forces considered in the equilibrium being defined as:

$$D = \frac{1}{2}\rho C_c sin^3 \alpha U^2 A_s \tag{2.21}$$

$$W_P = W \sin \vartheta \tag{2.22}$$

$$T = \mu w \tag{2.23}$$

where ρ is the density of the flow, C_c is the drag coefficient for a circular cylinder, α is the angle of inclination of the cylinder against the flow, U is the averaged velocity of the flow, A_S is the wetted frontal area, W is the body weight, ϑ is the angle of the slope, μ is the friction coefficient and w is the effective weight.

Secondly, the equilibrium condition with respect to the sliding instability is expressed as:

$$D\xi_{L,D} + W_P\xi_G + B_N\eta_{Gs} + L\eta_{L,D} \leq W_N\eta_G \tag{2.24}$$

where D is the drag force, $\xi_{L,D}$ is the distance from the ground to the point of action of the drag force, W_P is the weight component parallel to the slope, ξ_G is the distance from the ground to the point of action of the weight component parallel to the ground, B_N is the buoyancy force, η_{Gs} is the distance from the heel to the point of action of the buoyancy force, L is the lift force, W_N is the weight component normal

to the slope and η_G is the distance from the heel to the point of action of the weight component normal to the ground, with the forces considered in the equilibrium being defined as:

$$B_N = \rho g V_s \cos \vartheta \tag{2.25}$$

$$L = \frac{1}{2} \rho C_c \sin^2 \alpha \cos \alpha \, U^2 A_s \tag{2.26}$$

$$W_N = W \cos \vartheta \tag{2.27}$$

where ρ is the density of the flow, g is the gravitational acceleration, V_s is the submerged body of the volume, ϑ is the angle of the slope, C_c is the drag coefficient for a circular cylinder, α is the angle of inclination of the cylinder against the flow, U is the averaged velocity of the flow, A_S is the wetted frontal area and W is the body weight.

In addition to sliding and toppling instability mechanisms, a third risk condition was also introduced, i.e. maximum admissible water depth h_d. The maximum admissible water depth accounts for the risk of drowning, and might be assumed as a function of the height of the neck. This means that a person is considered safe until water does not reach the height of the neck. Finally, the limiting safety depth, as a function of the flow velocity U, is provided by the minimum of the sliding (h_s), toppling (h_t), and drowning depths (h_d), and is written as:

$$h = min[h_s(U); h_t(U); h_d] \tag{2.28}$$

The proposed model needs to be calibrated to identify the geometry of the body and the dynamics actions. The quantities regarding human body dimensions and the drag coefficients have to be obtained from literature, while the friction coefficient can be estimated from the experimental values obtained in the previous studies, such as the studies of Takahashi et al. (1992), Keller and Mitsch (1993) and Jonkman and Penning-Rowsell (2008). Based on the calibration parameters and Equation (2.28), three different flood hazard classes are obtained, i.e. low, medium and high. The lowest stability threshold is generally based on the body characteristics of the 7 years

old child, while the upper threshold limit is based on the mean sized adult. The proposed model was also validated against experimental datasets obtained from the previous experimental studies, such as datasets collected by Foster and Cox (1973), Abt et al. (1989), Takahashi et al. (1992), Karvonen et al. (2000), Jonkman and Penning-Rowsell (2008) and Xia et al. (2014). The evaluation of the model performance was based on the calculated value of the relative root mean square error (rRMSE). The model generally agreed very well with the experimental datasets, which indicates that the flood hazard assessment method presented by Milanesi et al. (2015) could assess the potential flood hazard indices with high level of accuracy.

All in all, Milanesi et al. (2015) presented a simple physically based flood hazard assessment method, which takes into account the inclinations of the ground slope and requires a calibration of only one parameter (i.e. friction coefficient). In comparison to the method proposed by Xia et al. (2014), the model presented by Milanesi et al. (2015) can be currently seen as more advanced due to the two aforementioned characteristics. However, the method proposed by Xia et al. (2014) has more room for improvement, as it considers human body characteristics (and thus the effect of the resulting physical forces) much more in detail. This means that with further improvements (such as accounting for the effect of the ground slope) the method proposed by Xia et al. (2014) could predict flood hazard indices with even higher degree of accuracy. Nonetheless, the model presented by Milanesi et al. (2015) should be at the moment regarded as the state-of-the-art flood hazard assessment method,. Furthermore, the model presented by Milanesi et al. (2015) clearly indicates that the research in this field is shifting towards the development of methods that take into account the physical interpretation of the processes which affect human stability in floodwaters.

2.4 Summary

The purpose of this literature review is to establish the basic theoretical framework behind this research study, and to determine what methodologies should be adopted in order to adequately test the main assumptions and potentially reach the key objectives of this research study.

Flood inundation modelling

In the Section 2.2, the literature in the field of flood inundation modelling is reviewed. In general, three modelling approaches are predominately used in the field of flood inundation modelling, i.e. 1D, 2D and linked 1D-2D modelling approach. The 1D models are generally considered as the most appropriate models for modelling flood behaviour within river channels. These models are computationally very efficient, but they also have many limitations when it comes to modelling of floodplain flows. The fully 2D models generally provide the most accurate prediction of flood depths, velocities and inundation extent, but these models can be computationally demanding and can result into long simulation runs. The 2D models with lower degree of the physical complexity (i.e. 2D⁻ modelling approach) tend to be much faster than fully 2D models, but these models are not appropriate for modelling of all types of flood events. The linked 1D-2D models take advantages offered by both 1D and 2D flood inundation models. However, these models can be limited by incorrect representation of the volume exchange between the river and floodplain, and suffer from lack of standardisation of the linking procedures. In addition, none of these modelling approaches are generally appropriate for modelling flood events with rapidly changing flow conditions, such as dam-break or flash flood scenarios. As mentioned earlier, flood inundation models with shock-capturing ability need to be used for modelling such flood events.

Flood depths, velocities and inundation extent are computed through the solution of the systems of algebraic equations obtained from the discretisation processes (see Section 3.3), with these computations being conducted on a collection of points called grids. Two different grid types are predominately used in the numerical flood modelling, i.e. structured grids and unstructured grids. The selection of the grid type is directly related to the selected spatial discretisation strategy (see Section 3.3), with the quality of the grid (i.e. grid resolution) having a generally significant impact on the accuracy of the predicted results.

Finally, parameterisation of friction is one of the more important issues in the flood inundation modelling, since water depths and velocities, and flood wave arrival time

are particularly sensitive to the specification of surface friction parameters. Furthermore, the tuning of roughness parameters can also be used as a "simplification strategy" in order to dampen out the numerical oscillations, which often occur with the modelling of extreme flood events. However, there are no guidelines to suggest how much tuning (i.e. artificially increasing the value of the roughness parameter) is needed in order to improve on the accuracy of the simulations results to an acceptable level. This being the case, such a strategy might be seen as dangerous, as it can lead to inaccurate predictions of flood depths, velocities and inundation extent and consequently can result to inadequate flood protection design.

Based on the reviewed literature in Section 2.2 and by considering the first key objectives of this study (i.e. what type of flood inundation models should be used for predicting the flood elevations, velocities and inundation extent for extreme flood events), two different flood inundation models were selected for this research study. The first model selected for this study is the 2D Depth Integrated Velocity and Solute Transport (DIVAST) model. The DIVAST model adopts the ADI finite difference method for solving the hydrodynamic equations, and was used to derive the underlying numerical engine of the well-known commercial model ISIS 2D (now Flood Modeller Pro). As mentioned earlier, the ADI method is also adopted in many other commercial 2D flood inundation models. This being the case, the DIVAST model represents the type of flood inundation model which is widely used in the flood risk management community for predicting the water depths, velocities and flood inundation extent, and as such should be considered in this research study. The second model selected for this study is the 2D DIVAST-TVD (Total Variation Diminishing) shock-capturing model. The DIVAST-TVD model adopts the MacCormack-TVD scheme, a type of modern shock-capturing method that can produce highly accurate numerical solutions even for problems containing strong shock waves or discontinuities. This model feature could be significantly relevant for this research study, since we are exploring what type of flood inundation models should be used in areas prone to extreme flooding. As mentioned, extreme flood events are generally characterised by rapidly varying flows and abrupt changes in the flow regime (such as hydraulic jumps), which can lead to the emergence of numerical oscillation in the flood inundation simulation process. Therefore, the

shock-capturing ability of the DIVAST-TVD model should prevent the emergence of the aforementioned numerical oscillations and consequently provide accurate predictions of flood depths, velocities and inundation extent for extreme flood events. This being the case, the DIVAST-TVD should also be used for flood inundation modelling within this study.

All in all, both DIVAST and DIVAST-TVD model appear to have all the necessary characteristics relevant for this research study. Therefore, these two models should be tested in order to determine what type of flood inundation models should be used for predicting the flood levels, velocities and inundation extent in areas prone to occurrence of extreme flood events, i.e. standardly used flood inundation models, such as the DIVAST model, or flood inundation models with shock-capturing ability, such as the DIVAST-TVD model.

In addition, the appropriateness of the "simplification strategy" when used as a flood risk assessment modelling tool for areas susceptible to extreme flooding (i.e. the second key objective of this research study) was also investigated. It was expected that simulation performed with the DIVAST model (i.e. the ADI-type model) would lead to inaccurate predictions of water levels and flood inundation extent. This being the case, the simulation results obtained with the DIVAST model were improved by artificially increasing the bed roughness. This means that the value of the roughness coefficient (i.e. the value of Manning's n) was gradually increased in each additional simulation until the predictions of depths and inundation extent obtained with the DIVAST model did not match the actual observations. The aim of this particular task was to investigate how much improvement of the initial results is actually needed in order to reach an acceptable level of accuracy, and to determine whether such an improvement lies within reasonable limits.

Flood hazard assessment

In Section 2.3, the literature in the field of assessing of the human stability in floodwaters (i.e. assessing flood hazard indices) is reviewed. In the case of a flood event, three sets of characteristics have a direct impact on the degree of danger to people, i.e. characteristics of the flood (such as flood depth and velocity),

characteristics of the location (such as indoors/outdoors or urban area/ rural area) and characteristics of the general population (such as gender, age, health and body physique). Among these characteristics, the flood depth and velocity are the main factors in determining the stability thresholds for humans in floodwaters. In floodwaters, people predominantly lose stability due to toppling (moment) or sliding (friction) instability mechanism. In addition, people can also loose stability due to floating or other adverse conditions, i.e. bottom surface conditions (such as unevenness and obstacles), flow conditions (such as floating debris and unsteady flow), and human vulnerability (such as physical and psychological factors).

Flood hazard assessment methods are classically divided into two groups, i.e. methods derived from mechanical analysis based on experimental studies and methods based on empirical or theoretical studies. However, a new type of methods has been developed recently, which includes methods that are completely physically based and experimentally calibrated. The main characteristics of the flood hazard assessment methods considered within this thesis are presented in Table 2.5 (see Section 2.3.1), Table 2.6 (see Section 2.3.2) and Table 2.8 (see Section 2.3.3).

Based on the reviewed literature in Section 2.3 and by considering the third key objectives of this study (i.e. what type of flood hazard assessment methods should be used for assessing the flood hazard to people caused by extreme flooding), two different flood hazard assessment methods were selected for this research study. The first flood hazard assessment method selected for this study is the empirically based method proposed by Ramsbottom et al. (2006). The method developed for DEFRA is used by the governing and planning authorities in the UK (and abroad) to produce flood hazard maps. This being the case, this method is regarded as an official flood hazard assessment method in the UK for assessing the flood hazard indices, and as such should be considered in this research study. The second flood hazard assessment method selected for this study is the physically and experimentally calibrated method proposed by Xia et al. (2014). Even though this method is not yet widely established due to being just recently presented, it is, however, completely independent of the flow characteristics. This feature could be significantly relevant for this research study, since we are exploring what type of flood hazard assessment

methods should be used in areas prone to extreme flooding. As mentioned, extreme flood events are often characterised with rapidly varying flows and abrupt changes in the flow regime, such as hydraulic jumps. Since the method proposed by Xia et al. (2014) is independent of the flow characteristics, it could adapt to the aforementioned violate flow characteristics, and thus predict flood hazard indices for extreme flood events with high level of accuracy. This being the case, the method proposed by Xia et al. (2014) should also be used for predicting flood hazard indices within this study.

All in all, both empirically based method developed for DEFRA and physically based and experimentally calibrated method presented by Xia et al. (2014) appear to have all the necessary characteristics relevant for this research study. Therefore, these two methods should be tested in order to determine what type of flood hazard assessment methods should be used for assessing flood hazard indices in areas prone to extreme flooding, i.e. standard flood hazard assessment methods, such as the method developed for DEFRA, or recently introduced, physically based and experimentally calibrated methods, such as the method proposed by Xia et al. (2014).

CHAPTER 3

Numerical modelling

3.1 Introduction

This chapter presents some of the main aspects of the numerical modelling associated with flood inundation models. Section 3.2 provides an overview of the general governing equations that describe the motion of the flood flow, Section 3.3 describes the numerical methods which are used to discretise the main governing equations, Section 3.4 presents some of the well-known shock-capturing schemes, Section 3.5 describes the numerical models used in this research study, and finally Section 3.6 provides a brief summary of the details presented in this chapter.

3.2 Governing equations

All characteristics of water, and therefore all changes that occur during a simulation process, can be described with four equations, including (Rajar, 1980): (i) continuity equation, (ii) dynamic or momentum equation, (iii) equation of state, and (iv) conservation of energy (i.e. Bernoulli's principle). However, for majority of practical hydro-environmental engineering problems all characteristics of water (e.g. flood flow) can be described solely by continuity and dynamic or momentum equation.

The continuity equation describes the conservation of mass, which demands that the net fluid mass entering a control volume in a specific time interval equals the amount by which the mass of the control volume changes during this specific time interval. The continuity equation can be written as (Rajar, 1980):

$$\frac{\partial \rho}{\partial t} + \frac{\partial \rho u}{\partial x} + \frac{\partial \rho v}{\partial y} + \frac{\partial \rho w}{\partial z} = 0 \tag{3.1}$$

where ρ is the density of the fluid and u, v, and w are the velocity components in each of the principal Cartesian axes x, y, and z.

However, for the majority of cases in flood inundation modelling it is assumed that the flow is incompressible (i.e. the density of the fluid does not change over time), and thus Equation (3.1) can be written as:

$$\frac{\partial u}{\partial x} + \frac{\partial v}{\partial y} + \frac{\partial w}{\partial z} = 0 \tag{3.2}$$

where u, v, and w are the velocity components in each of the principal Cartesian axes x, y, and z.

The dynamic or momentum equations describe the conservation of momentum, and are thus used to describe the motion of fluids. They are also known as the Navier-Stokes equations and are used to model a wide range of natural phenomenon, such as weather, the movement of air in the atmosphere, ocean currents, air flow around a wing, water flow in channels and pipes etc. The Navier-Stokes equations originate from the application of Newton's second law to the fluid motion, along with the assumption that the stress in the fluid is the sum of the viscous and pressure term. The Navier-Stokes equations can be written as (Rajar, 1980):

$$\begin{aligned} \frac{\partial u}{\partial t} + \frac{\partial u}{\partial x}u + \frac{\partial u}{\partial y}v &+ \frac{\partial u}{\partial z}w \\ &= X - \frac{1}{\rho}\frac{\partial P}{\partial x} + v\left(\frac{\partial^2 u}{\partial x^2} + \frac{\partial^2 u}{\partial y^2} + \frac{\partial^2 u}{\partial z^2}\right) + \frac{v}{3}\frac{\partial}{\partial x}\left(\frac{\partial u}{\partial x} + \frac{\partial v}{\partial y} + \frac{\partial w}{\partial z}\right) \end{aligned} \tag{3.3}$$

$$\begin{aligned} \frac{\partial v}{\partial t} + \frac{\partial v}{\partial x}u + \frac{\partial v}{\partial y}v &+ \frac{\partial v}{\partial z}w \\ &= Y - \frac{1}{\rho}\frac{\partial P}{\partial y} + v\left(\frac{\partial^2 v}{\partial x^2} + \frac{\partial^2 v}{\partial y^2} + \frac{\partial^2 v}{\partial z^2}\right) + \frac{v}{3}\frac{\partial}{\partial y}\left(\frac{\partial u}{\partial x} + \frac{\partial v}{\partial y} + \frac{\partial w}{\partial z}\right) \end{aligned} \tag{3.4}$$

$$\begin{aligned} \frac{\partial w}{\partial t} + \frac{\partial w}{\partial x}u + \frac{\partial w}{\partial y}v &+ \frac{\partial w}{\partial z}w \\ &= Z - \frac{1}{\rho}\frac{\partial P}{\partial z} + v\left(\frac{\partial^2 w}{\partial x^2} + \frac{\partial^2 w}{\partial y^2} + \frac{\partial^2 w}{\partial z^2}\right) + \frac{v}{3}\frac{\partial}{\partial z}\left(\frac{\partial u}{\partial x} + \frac{\partial v}{\partial y} + \frac{\partial w}{\partial z}\right) \end{aligned} \tag{3.5}$$

where t is time, u, v, and w are the velocity components in each of the principal Cartesian axes x, y, and z, ρ is the density of the fluid, P is the pressure, X, Y and Z are the external body forces and ν is the kinematic viscosity defined as

$$\nu = \frac{\mu}{\rho} \qquad (3.6)$$

where μ is the dynamic viscosity.

In most hydro-environmental engineering problems, the fluid flow propagates over large geographical domains and is often characterised by turbulent fluctuations. This poses a great problem, as it is extremely difficult to obtain the numerical solution of the Navier–Stokes equations for turbulent flow. In very simple geometrical configurations, the Navier-Stokes equations can be solved directly by using direct numerical simulation (DNS) (Moin and Mahesh, 1998). However, for more complex geometries (i.e. practical engineering problems) the DNS becomes impractical. In the direct numerical simulations, the whole range of spatial and temporal scales of the turbulence must be resolved in highly densified computational mesh, which must satisfy the Kolmogorov micro dimension requirement (Kolmogorov, 1962). Kolmogorov's theory describes how energy is transferred from larger to smaller eddies, and consequently defines the size of the smallest eddies that are responsible for dissipating the energy, i.e. Kolmogorov micro scales. This means that the mesh dimension needs to satisfy the micro dimension requirement in order to satisfy the resolution requirement for small eddies. For example, for 3D problems the number of mesh nodes must be in the order of 10^9–10^{11}, where both the mesh dimension and time step are constantly getting smaller with the increase of Reynolds number (Ding and Wu, 2012). This being the case, for practical hydro-environmental engineering problems such fine grid resolution and small time step would result into computational time so long that the numerical simulation itself would be infeasible (Vos and Farokhi, 2015).

In order to increase the minimum spatial and temporal scales, the Navier-Stokes equations can be averaged in time to obtain the so-called Reynolds-averaged Navier-Stokes (RANS) equations (Durbin and Reif, 2010). The Reynolds-averaged Navier-Stokes equations are derived by first decomposing the dependant variables in the Navier-Stokes equations into time-mean and fluctuation components (see Figure 3.1), and then time averaging the entire equation (Tannehill et al., 1997).
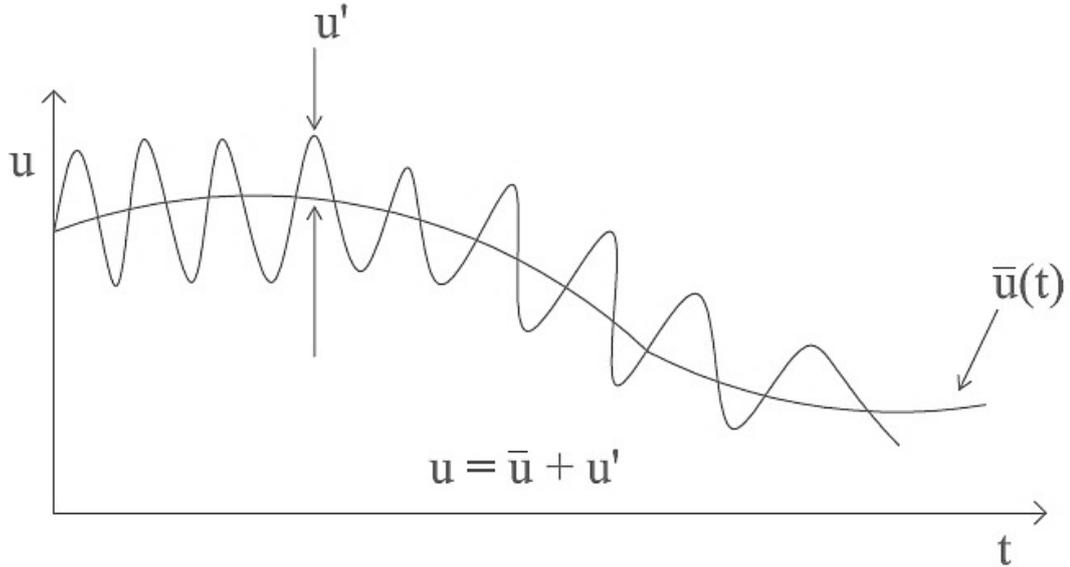
Figure 3.1: Decomposition of the changing flow variable, where u is the flow variable, ū is the time-mean component of the flow variable and u' is the fluctuation component of the flow variable

The Reynolds-averaged continuity equation can be written as (Boye, 2014):

$$\frac{\partial \bar{u}}{\partial x} + \frac{\partial \bar{v}}{\partial y} + \frac{\partial \bar{w}}{\partial z} = 0 \qquad (3.7)$$

where the mean notation (‾) indicates the time-mean component of a specific value and u, v, and w are the velocity components in each of the principal Cartesian axes x, y, and z.

The Reynolds-averaged Navier-Stokes equations can be written as (Boye, 2014):

$$\rho \left(\frac{\partial \bar{u}}{\partial t} + \bar{u}\frac{\partial \bar{u}}{\partial x} + \bar{v}\frac{\partial \bar{u}}{\partial y} + \bar{w}\frac{\partial \bar{u}}{\partial z} \right) = \rho \bar{X} - \frac{\partial \bar{P}}{\partial x} + \frac{\partial \sigma_{xx}{'}}{\partial x} + \frac{\partial \tau_{yx}{'}}{\partial y} + \frac{\partial \tau_{zx}{'}}{\partial z} \qquad (3.8)$$

$$\rho \left(\frac{\partial \bar{v}}{\partial t} + \bar{u}\frac{\partial \bar{v}}{\partial x} + \bar{v}\frac{\partial \bar{v}}{\partial y} + \bar{w}\frac{\partial \bar{v}}{\partial z} \right) = \rho \bar{Y} - \frac{\partial \bar{P}}{\partial y} + \frac{\partial \tau_{xy}{'}}{\partial x} + \frac{\partial \sigma_{yy}{'}}{\partial y} + \frac{\partial \tau_{zy}{'}}{\partial z} \qquad (3.9)$$

$$\rho \left(\frac{\partial \bar{w}}{\partial t} + \bar{u}\frac{\partial \bar{w}}{\partial x} + \bar{v}\frac{\partial \bar{w}}{\partial y} + \bar{w}\frac{\partial \bar{w}}{\partial z} \right) = \rho \bar{Z} - \frac{\partial \bar{P}}{\partial z} + \frac{\partial \tau_{xz}{'}}{\partial x} + \frac{\partial \tau_{yz}{'}}{\partial y} + \frac{\partial \sigma_{zz}{'}}{\partial z} \qquad (3.10)$$

where the mean notation ($^{-}$) indicates the time-mean component of a specific value, the derivative notation ($'$) indicates the fluctuation component of a specific value, t is time, u, v, and w are the velocity components in each of the principal Cartesian axes x, y, and z, ρ is the density of the fluid, P is the pressure, X, Y and Z are the external body forces and the complete turbulent stress tensor is written as

$$\begin{bmatrix} \sigma_{xx}' & \tau_{xy}' & \tau_{xz}' \\ \tau_{yx}' & \sigma_{yy}' & \tau_{yz}' \\ \tau_{zx}' & \tau_{zy}' & \sigma_{zz}' \end{bmatrix} = - \begin{bmatrix} \rho\overline{u'u'} & \rho\overline{u'v'} & \rho\overline{u'w'} \\ \rho\overline{v'u'} & \rho\overline{v'v'} & \rho\overline{v'w'} \\ \rho\overline{w'u'} & \rho\overline{w'v'} & \rho\overline{w'w'} \end{bmatrix} \qquad (3.11)$$

with the expressions $\rho\overline{u'u'}$, $\rho\overline{u'v'}$ and $\rho\overline{u'w'}$ being known as Reynolds stresses (Launder et al., 1975).

The Reynolds-averaged Navier-Stokes equations are often supplemented with turbulence models (such as k-ε turbulence models), which deal with the effects of the turbulent fluctuations on the mean flow (Rodi, 1993). Such models are widely used in practical and industrial fluid mechanics (Shimada and Ishihara, 2002, Pinson et al., 2006, Ji et al., 2012, Freeman and Roy, 2014, Okaze et al., 2015, Mirzaei et al., 2015). However, these models are currently inapplicable to practical flood simulation modelling due to high computational cost. For example, Oertel (2015) modelled a small river reach (ca. 300 m) in FLOW-3D model, which implements the RANS equations and k-ε turbulence model. The simulation of this short river section took up to 2 days in FLOW-3D, while on the other side the simulation of much longer river reach (ca. 30 km) took around 13 hours in 2D model (Oertel, 2015). This

clearly indicates that the application of RANS models is, at the moment, completely impracticable due to high computational cost. In addition, the Large-eddy simulations (LES) technique can be used to address the turbulences effecting the mean flow (Deardorff, 1970). Even though this approach produces better results, it is even more computationally expensive than the RANS methods (Cheng et al., 2003, Mihaescu et al., 2008, Khan and Joshi, 2015), and thus also generally unusable in practical flooding problems.

Besides the problem of turbulence, there is also the problem of the air-water interface movement with the Navier-Stokes and Reynolds-averaged Navier-Stokes based models. The free surface moves with the velocity of the fluid particles located at the boundary, which means that the position of the free surface is one of the unknowns in the computational process. However, the equations of motions only apply to the space occupied by the fluid, which is not known a prior and therefore present an additional difficulty in the applying of the aforementioned models to the practical engineering problems (Delis and Kampanis, 2009). There are several methods that can be used to circumvent the free surface problem, such as the Volume of Fluid (VOF) method (Hirt and Nichols, 1981), and Marker-and-Cell (MAC) methods (Harlow and Welch, 1965).

However, these methods are generally very computationally demanding. For example, Biscarini et al. (2010) modelled free surface flows induced by a dam break, where they compared the 2D shallow water approach to fully three-dimensional simulations. The fully 3D simulations were based on the solution of the complete set of RANS equations coupled to the VOF method. The spatial domain was a 200 m long and 200 m wide region, with a dam in the middle. The simulation of this dam break test case took 15 min for the 2D model, and 2 h for the fully 3D model. This indicates that the 2D model may be at least one order of magnitude faster than the fully 3D model (Biscarini et al., 2010). This being the case, the application of the aforementioned methods (e.g. VOF etc.) to practical flood simulation modelling (e.g. modelling of large, complex domains) is currently infeasible due to high computational cost.

All in all, application of fully 3D Navier-Stokes equations to model practical hydro-environmental problems is currently impractical due to the high computational cost required to solve the Navier-Stokes equations for such problems. This being the case, a reasonable simplification of the Navier-Stokes equations is needed in order to apply them to practical flood simulation modelling. The usual approach is to depth-average the Navier-Stokes equations, which leads to derivation of the 2D shallow water equations (SWE), and with further simplifications to the 1D Saint-Venant equations.

2D Shallow water equations

The 2D shallow water equations (also called 2D Saint-Venant equations) are a set of partial differential equations, which can be applied to model floods, tsunamis, atmospheric flows, storm surges, flows around structures and planetary flows. In general, the shallow water equations describe a thin layer of fluid, which is bounded from below by the bottom topography and from above by the free surface, and are valid for problems in which the horizontal length scale is much greater than the vertical length scale. The derivation of the shallow water equations is based on several assumptions, including: (i) the vertical velocity component w is a lot smaller than the horizontal velocity components u and v and therefore can be ignored, (ii) the vertical pressure gradients are hydrostatic, i.e. the pressure gain is linear with the water depth, (iii) the horizontal velocity across the water layer is constant, (iv) the bottom slope is small so that the sinus of the slope angle can be approximated to the angle itself, and (v) the friction formulae are based on the uniform flow conditions (Alcrudo, 2002, Institute of River and Coastal Engineering, 2006, Dawson and Mirabito, 2008). Besides these assumptions, two additional conditions are also important in the derivation process of the shallow water equations: (i) the implementation of the kinematical boundary conditions at the free surface and at the bottom topography (see Figure 3.2), and (ii) the application of the Leibniz integral rule and the fundamental theorem of calculus (i.e. corollary or integration theorem) (Institute of River and Coastal Engineering, 2006).
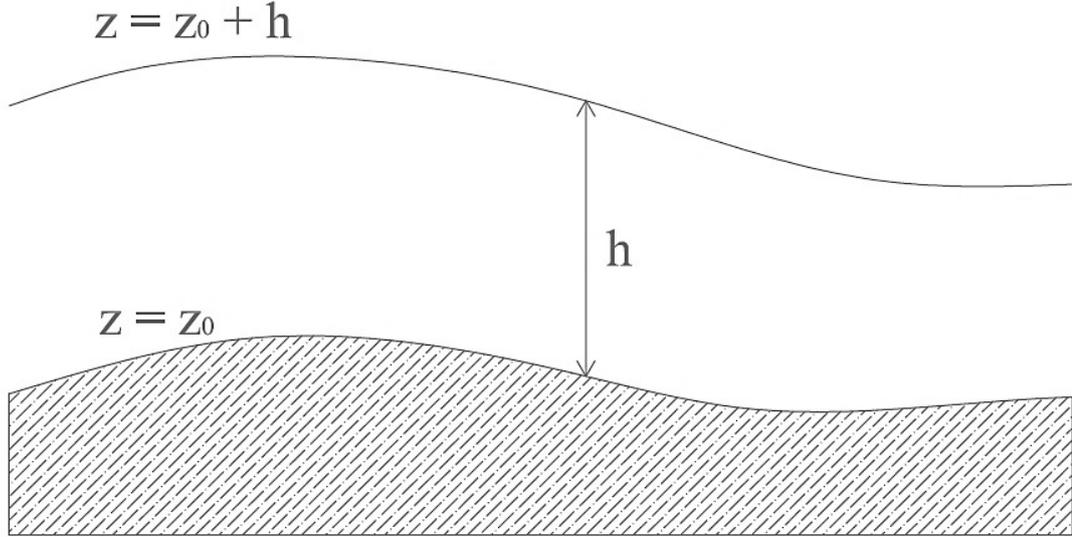
Figure 3.2: A typical water column used in the SWE derivation process

By taking into account the initial assumptions, the kinematic boundary conditions and the necessary mathematical procedures, the shallow water equations can be derived by depth-integrating the continuity and the Navier-Stokes equations, and can be written as (Institute of River and Coastal Engineering, 2006):

$$\frac{\partial h}{\partial t} + \frac{\partial q_x}{\partial x} + \frac{\partial q_y}{\partial y} = 0 \tag{3.12}$$

$$
\begin{aligned}
\frac{\partial u}{\partial t} &+ u\frac{\partial u}{\partial x} + v\frac{\partial u}{\partial y} \\
&= X - g\frac{\partial}{\partial x}(z_0 + h) + \frac{1}{h\rho}\frac{\partial}{\partial x}(h\tau_{xx}) + \frac{1}{h\rho}\frac{\partial}{\partial y}(h\tau_{xy}) - \frac{1}{h}\frac{\tau_{so,x}}{\rho} + \frac{1}{h}\frac{\tau_{wind,x}}{\rho}
\end{aligned}
\tag{3.13}
$$

$$
\begin{aligned}
\frac{\partial v}{\partial t} &+ u\frac{\partial v}{\partial x} + v\frac{\partial v}{\partial y} \\
&= Y - g\frac{\partial}{\partial y}(z_0 + h) + \frac{1}{h\rho}\frac{\partial}{\partial x}(h\tau_{xy}) + \frac{1}{h\rho}\frac{\partial}{\partial y}(h\tau_{yy}) - \frac{1}{h}\frac{\tau_{so,y}}{\rho} + \frac{1}{h}\frac{\tau_{wind,y}}{\rho}
\end{aligned}
\tag{3.14}
$$

where t is time, h is the water depth, q_x and q_y are the discharges per unit width in the x and y directions, u and v are the velocity components in the principal Cartesian axes x and y, X and Y are the external body forces, g is the gravitational acceleration, $z_0 + h$ is the water surface elevation, ρ is the density of the water, are τ_{so} and τ_{wind} are the bed and wind shear stresses and τ_{ij} are the viscous shear stresses defined as

$$\tau_{ij} = \rho v \left(\frac{\partial u_i}{\partial x_j} + \frac{\partial u_j}{\partial x_i} \right) \tag{3.15}$$

where v is the kinematic viscosity.

As a result of the aforementioned assumptions used in the derivation process, the shallow water equations are not the exact mathematical representation of the floodwater propagation. Nonetheless, the majority of the 2D flood inundation models currently used both in industry and research are based upon the shallow water equations due to their relatively low computational cost and general accuracy (Jha et al., 2000, Yoon and Kang, 2004, Mignot et al., 2006, Marche et al., 2007, Bates et al., 2010, Franchello, 2010, Neelz and Pender, 2013, Wang and Geng, 2013, Sánchez-Linares et al., 2015, Izem et al., 2016).

1D Saint-Venant equations

Even though 1D models were not considered within this study, a brief presentation of the main 1D governing equation is included in this chapter in order to provide at least a minimal theoretical framework behind the 1D modelling approaches presented in Section 2.2.1.

The floodwaters in nature generally vary in all three spatial coordinate directions (i.e. longitudinal, lateral and transverse) and with time. However, in many practical hydro-environmental engineering problems the spatial variations in lateral and transverse directions can be neglected, and thus the flow can be approximated as a one-dimensional process along the longitudinal direction. This being the case, the characteristics of the flow can be described with a set of one-dimensional partial differential equations, i.e. the Saint-Venant equations. The one-dimensional Saint-Venant equations are a simplification of the 2D shallow water equations and were first derived by de Saint-Venant (1871). The derivation of the Saint-Venant equations is based on several assumptions, including: (i) the flow is one-dimensional, i.e. the velocity is uniform over the cross-section and the water level across the section is horizontal, (ii) the streamline curvature is small and the vertical accelerations are negligible, hence the hydrostatic pressure distribution prevails, (iii)

the effect of boundary friction and turbulence can be accounted for through resistance laws analogous to those used for steady-state flow, i.e. the resistance relationship for steady flow is also applicable for unsteady flow, (iv) the average channel bed slope is small so that the cosine of the slope can be replaced by unity, (v) the water level slope or gradient in the x-direction is constant along the cross section, (vi) channel boundaries are considered fixed and therefore not susceptible to erosion or deposition, and (vii) fluid is incompressible (Stelling and Verwey, 2005, Litrico and Fromion, 2009). By considering these basic assumptions, the Saint-Venants equations can be derived from the Navier-Stokes equations, and can be written as (Litrico and Fromion, 2009):

$$\frac{\partial A}{\partial t} + \frac{\partial Q}{\partial x} = 0 \tag{3.16}$$

$$\frac{\partial Q}{\partial t} + \frac{\partial}{\partial x}\left(\frac{Q^2}{A}\right) + gA\left(\frac{\partial h}{\partial x} + S_f - S_b\right) = 0 \tag{3.17}$$

where t is time, A is the wetted area, Q is the discharge across-section, g is the gravitational acceleration, h is the water depth, S_b is the bed slope and S_f is the frictions slope defined as

$$S_f = \frac{Q^2 n^2}{A^2 R^{4/3}} \tag{3.18}$$

where n is the Manning coefficient and R is the hydraulic radius.

Even though one-dimensional flows do not actually exits in nature, the 1D flood inundation models based upon the Saint-Venants equations are one of the most popular models among hydraulic engineers. This being the case, the 1D flood inundation models have been applied successfully in many practical hydraulic engineering problems, such as modelling of open channel flow, sewer modelling, river flow forecasting, dam-break analysis and reservoir emptying (Gouta and Maurel, 2002, Yoshida and Dittrich, 2002, Horritt and Bates, 2002, Stelling and Verwey, 2005, Trigg et al., 2009, Litrico and Fromion, 2009, Saleh et al., 2013, Li et al., 2015, Dimitriadis et al., 2016, Habert et al., 2016).

3.3 Numerical methods

The first step in numerical modelling consists of converting the governing equations into discrete difference equations, which would be suitable for numerical computing. This means that the partial differential equations (such as the shallow water equations) are replaced by a set of algebraic equations, which calculate the main variables at a finite set of points in the space-time domain (Neelz and Pender, 2009). This process of converting the partial differential equations into a set of algebraic equations is called discretisation, and there are numerous methods that can be used for the space-time discretisation of the governing equations.

The great majority of numerical methods used for the spatial discretisation can be divided into three categories, including (Tannehill et al., 1997): (i) the finite difference methods, (ii) the finite element methods, and (iii) the finite volume methods.

The finite difference method is based upon the application of a local Taylor expansion to approximate the differential equations (Peiró and Sherwin, 2005). The Taylor series is used to transform the partial differential equations into an algebraic system of equations, which describe the derivatives of a variable as the differences between the values of the variable at neighbouring points. The accuracy of the approximations can be controlled by the order to which the Taylor series expansions are developed, i.e. to the order of the so-called truncation (Neelz and Pender, 2009). The main advantage of the finite difference method is its straightforward and well defined implementation, which enables simple application of the finite difference based flood models to practical problems (Alcrudo, 2002). However, the popularity of the finite difference method is decaying progressively in recent years. This is most likely due to it being less flexible from the geometric point of view, since the finite difference method is usually applied on a structured grid (Alcrudo, 2004, Neelz and Pender, 2009). As it will be presented in more detail later, structured grids are less flexible than unstructured grids, and thus less convenient for modelling of flood events in complex domains. Nonetheless, flood inundation models based on the finite difference method are still quite popular among flood risk practitioners, as they are

compatible with high-resolution digital terrain models created from LiDAR (Light Detection And Ranging) and sonar surveys (Neelz and Pender, 2013).

In the finite element method, the domain is divided into a finite number of small sub-domains, called finite elements, where each sub-domain is represented by a set of element equations from the original problem. After the whole domain is divided into a collection of sub-domains, all sets of element equations are systematically recombined into a global system of equations, which has known solution techniques and can be calculated from the initial values (Zienkiewicz and Taylor, 1977). The sub-division of the domain into smaller parts provides flexibility to (i) accurately represent complex geometries, (ii) include dissimilar material properties, (iii) easily represent the total solution, and (iv) capture in the solution process all local effects (Reddy, 1993). Furthermore, a rigorous mathematical foundation is considered to be the main advantage of the finite element method, as it allows a posteriori error estimation and thus better understanding of method's accuracy (Alcrudo, 2004, Hervouet, 2007). On the other hand, complex mathematical procedure also results into large run-times, as lot of computational time is being consumed at every time step in the numerical procedure (Ferziger and Peric, 2002). In addition, the finite element method is also conceptually more difficult than other methods (Alcrudo, 2002). This being the case, the finite element method has not been used as much as other approaches in numerical flood simulation modelling (Neelz and Pender, 2013).

The finite volume method is a discretisation method based on the integral form of the conservation laws. First, the domain is divided into a certain number of so-called finite control volumes. After the control volumes have been defined, the integral balance equations are formulated for each control volume. These integrals are approximated by numerical integration, while the obtained function values and derivatives are afterwards approximated by interpolation with nodal values (Schäfer, 2006). Finally, all equations are assembled in a discrete algebraic system and then solved. The finite volume method is highly popular in numerical flood simulation modelling due to guaranteeing (i) the conservation of the mass and momentum, (ii) being applicable to all types of meshes, and (iii) being considerably intuitive and conceptually simple (Alcrudo, 2004). The finite volume method is as flexible as the finite element method, but the computational cost of the finite volume method is

much smaller due to the size of matrix in the finite element method (Wang, 2011). Furthermore, the efficiency of the finite volume method is similar to that of the finite difference method, while for the complex geometries the finite volume method can even be more accurate than the finite difference method (Boye, 2014). Due to all aforementioned advantages, the finite volume method is the most widely used method in the area of the flood inundation modelling (Pender and Néelz, 2011).

The great majority of numerical methods used for the time discretisation can also be divided into three categories, including (Chadwick et al., 2013): (i) explicit schemes, (ii) implicit schemes, and (iii) semi-implicit schemes.

In explicit (forward-looking) schemes, dependent variables at the current time step (Δt_n) are computed by using the quantities calculated at the previous time step (Δt_{n-1}), which makes these schemes simple to program and thus highly popular among researchers and software developers (Neelz and Pender, 2009). However, explicit schemes are conditionally stable and thus cannot guarantee numerical stability across all flow conditions. Numerical stability can be defined as a property of a numerical method that ensures damping out any disturbance which can occur during the computational process (Szymkiewicz, 2010). The most common sign of numerical instability is the emergence of unphysical numerical oscillations in the numerical solution. Therefore, the conditional stability means that a particular condition must be satisfied in order to ensure a stable solution. In order to provide the stability for explicit schemes, the model time step must be small enough to satisfy the Courant-Friedrichs-Lewy (CFL) condition (Courant et al., 1967), which can be written as:

$$\frac{v \Delta t}{\Delta x} \leq C \qquad (3.19)$$

where v is the magnitude of the velocity, Δt is the time step, Δx is the length interval and C is the dimensionless number called the Courant number.

The Courant number is typically set to 1 for explicit schemes. However, satisfying the CFL condition for explicit schemes can result into selection of the model time step that is very small compared to the physics behind the problem under

consideration (Hunter et al., 2007). Furthermore, it can also lead to an excessively large number of time steps, which can make the computational process completely impracticable (Ryaben'kii and Tsynkov, 2006).

In implicit (backward-looking) schemes, dependant variables are computed by using the quantities calculated at the previous time step (Δt_{n-1}) as well as the quantities calculated at the present time step (Δt_n), with a matrix or an iterative technique being used to obtain the solution. Implicit schemes couple together all cells within the computational procedure. This enables the transmission of hydraulic effects across the entire computational domain, but on the other hand also results in increased complexity of the model code and computational cost (Hunter et al., 2007). However, implicit schemes are unconditionally stable and allow larger model time steps, which are generally more compatible with the physical phenomenon under consideration (such as the evolution of a flood event). These advantages often outweigh the difficult implementation and high cost per time step of the implicit time-stepping procedure (Chadwick et al., 2013). Even though implicit schemes are unconditionally stable, this does not mean that they will provide an accurate solution for every modelling problem. Therefore, time steps are often limited (i.e. the CFL condition is satisfied) in order to provide a numerically accurate solution (Pender and Néelz, 2011). Nonetheless, implicit schemes are less sensitive to numerical stability than explicit schemes and therefore larger values of the Courant number can be considered, i.e. Courant numbers up to 8 can be used.

A semi-implicit scheme is a hybrid between an implicit and explicit scheme, where some time derivatives are treated explicitly and some are treated implicitly. The terms should be split in such a way that the largest time step for the semi-implicit discretisation is significantly larger than for a corresponding explicit discretisation. This means that larger time-steps can be employed when compared to standard explicit discretisation, and therefore the computer time needed to solve the equations can be greatly reduced (Fulton, 2004). At the same time, the semi-implicit schemes produce numerically accurate solutions due to being unconditionally stable (Rosatti et al., 2011). This being the case, the semi-implicit schemes are computationally efficient without sacrificing accuracy. However, similar to implicit schemes semi-

implicit schemes are also mathematically complex and thus often complicated to design (Fulton, 2004).

Based on the selected space-time discretisation strategy, different numerical schemes can be constructed, such as explicit finite difference schemes (Liang et al., 2010, Ransom and Younis, 2016), semi-implicit finite difference schemes (Acosta et al., 2015, Ahmadian et al., 2015), implicit finite volume schemes (Wu and Lin, 2015, Yu et al., 2015), explicit finite volume schemes (Zhou et al., 2013, Vacondio et al., 2014), semi-implicit finite volume (Frolkovič et al., 2015, Dumbser and Casulli, 2016), and implicit finite element schemes (Villaret et al., 2013). In industry, the majority of the commercial flood inundation software packages are based either on the Alternating Direction Implicit (ADI) finite difference scheme or the explicit finite volume scheme (Neelz and Pender, 2013).

3.4 Shock-capturing schemes

Even though the majority of the aforementioned numerical schemes generally work well and are computationally effective, these regular schemes do not respond well when it comes to modelling of flood scenarios with rapidly varying flows or high Froude number flows, such as dam-breaks or flash floods (Neelz and Pender, 2013). These flood events are often characterised with abrupt changes in the flow regime (such as hydraulic jumps or steep hydraulic gradients), which act as discontinuities (shocks) in the numerical procedure. These can lead to the generation of spurious numerical oscillations and consequently to highly erroneous simulation results. The emergence of numerical oscillations can be prevented by applying the so-called shock-capturing methods. In shock-capturing approach, the governing equations are cast in conservation form and artificial diffusion terms are applied in the solution procedure, which ensure the stability of the computational process and enable the computation of any shock waves or discontinuities as part of the numerical solution. In general, shock-capturing can be divided into two groups, including: (i) classical shock-capturing schemes (see Section 3.4.1), and (ii) modern or high-resolution shock-capturing schemes (see Section 3.4.2).

The shock-capturing schemes are usually associated with higher computational cost when compared to numerical models typically used in flood inundation modelling (Liang et al., 2006, Neal et al., 2012, de Almeida et al., 2012). However, the advances in computational power enabled the development of generally efficient shock-capturing schemes, which also persuaded commercial software developers to include flood inundation models with shock-capturing ability in their software packages (Neelz and Pender, 2013). Despite all developments in recent years in the field of the flood inundation modelling, shock-capturing models are at the moment used mainly for modelling of dam-break and tsunami scenarios (Kesserwani and Liang, 2012, Ma et al., 2012, Ouyang et al., 2013, Tsakiris and Bellos, 2014, Ransom and Younis, 2015, Hou et al., 2015, Aureli et al., 2015). However, shock-capturing models are generally not used for practical flood simulation modelling of other types of rapidly varying flood events, such as flash floods or large river floods. This is mainly due to the lack of qualitative research, which would emphasise the advantages of the flood inundation models with shock-capturing ability for modelling flood events with rapidly varying flows. Consequently, such research would also define in which cases the shock-capturing models ought to be used regardless of the general perception about these models, such as the complex structure and high computational cost.

3.4.1 Classical shock-capturing schemes

In classical shock-capturing methods, the numerical dissipation is distributed linearly (i.e. the same amount of dissipation at all grid points) or through adjustable parameters. The main drawback of classical shock-capturing methods is that they are accurate only for smooth or weak shock solutions, whereas in the presence of strong shock waves these methods result in oscillatory solutions (Yee, 1989). Some of the well-known classical shock-capturing methods include the Lax-Wendroff method (Lax and Wendroff, 1960), the MacCormack method (MacCormack, 1969), and the Beam-Warming method (Warming and Beam, 1976).

The application of the three-aforementioned classical shock-capturing methods in flood inundation modelling can be presented by considering a rectangular channel of

unit width. The Saint-Venant equations for a rectangular channel of unit width can be written as (Machalinska-Murawska and Szydłowski, 2014):

$$\frac{\partial \mathbf{U}}{\partial t} + \frac{\partial \mathbf{F}}{\partial x} + \mathbf{S} = 0 \quad or \quad \mathbf{U}_t + \mathbf{F}_x + \mathbf{S} = 0 \tag{3.20}$$

with vectors **U**, **F** and **S** being given as

$$\mathbf{U} = \begin{bmatrix} h \\ uh \end{bmatrix} \tag{3.21}$$

$$\mathbf{F} = \begin{bmatrix} uh \\ u^2h + 0.5gh^2 \end{bmatrix} \tag{3.22}$$

$$\mathbf{S} = \begin{bmatrix} 0 \\ -gh\left(S_0 - S_f\right) \end{bmatrix} \tag{3.23}$$

where t is time, x is the distance, h is the water depth, u is the velocity of the flow, g is the gravitational acceleration, S_0 is the bed slope and S_f is the friction slope defined as

$$S_f = \frac{n^2 u|u|}{R^{4/3}} \tag{3.24}$$

where n is the Manning coefficient and R is the hydraulic radius.

As indicated in Section 3.2, the derivation of the Saint-Venant equations is based on the assumption of hydrostatic-pressure distribution, incompressibility of water, sufficiently small bottom slope of the channel, and negligible wind stress and Coriolis force. This being the case, Equation (3.20) can be expressed in quasi-linear form as (Rahimpour and Tavakoli, 2011):

$$\frac{\partial \mathbf{U}}{\partial t} + \mathbf{M}\frac{\partial \mathbf{U}}{\partial x} + \mathbf{S} = 0 \tag{3.25}$$

The matrix $\mathbf{M}$ in the Equation (3.25) is the Jacobian matrix, and is written as (Rahimpour and Tavakoli, 2011):

$$\mathbf{M} = \begin{bmatrix} 0 & 1 \\ -u^2 + gD & 2u \end{bmatrix} \tag{3.26}$$

where u is the velocity of the flow, g is the gravitational acceleration, and D is the hydraulic depth.

The matrix $\mathbf{M}$ has independent and real eigenvectors and therefore it can be written in diagonalized form as (Rahimpour and Tavakoli, 2011):

$$\mathbf{M} = \frac{1}{2c} \begin{bmatrix} 1 & -1 \\ u + \sqrt{gD} & -(u - \sqrt{gD}) \end{bmatrix} \begin{bmatrix} \lambda_1 & 0 \\ 0 & \lambda_2 \end{bmatrix} \begin{bmatrix} -(u - \sqrt{gD}) & 1 \\ -(u + \sqrt{gD}) & 1 \end{bmatrix} \tag{3.27}$$

where the λ_i are eigenvalues of matrix $\mathbf{M}$ defined as

$$\lambda_1 = u + \sqrt{gD} \tag{3.28}$$

$$\lambda_2 = u - \sqrt{gD} \tag{3.29}$$

Finally, the matrix $\mathbf{M}$ can now be split into positive and negative component, and can be written as follows (Rahimpour and Tavakoli, 2011):

$$\mathbf{M} = \mathbf{M}^+ + \mathbf{M}^- \tag{3.30}$$

where

$$\lambda_i^+ = max(\lambda_i, 0) \tag{3.31}$$

$$\lambda_i^- = \lambda_i + \lambda_i^+ \tag{3.32}$$

The Lax-Wendroff method

Lax-Wendroff method is an explicit finite-difference scheme, which ensures second order accuracy of derivation approximation in both time and space. A two-step version of the original scheme is usually employed in numerical flood inundation modelling. At the first step, the Lax method is applied at the midpoint $x_{i+1/2}$ for a half-time step (Machalinska-Murawska and Szydłowski, 2014):

$$U_{i+1/2}^{n+1/2} = \frac{1}{2}(U_{i+1}^n + U_i^n) - \frac{\Delta t}{2\Delta x}(F_{i+1}^n + F_i^n) - \frac{1}{4}\Delta t(S_{i+1}^n + S_i^n) \qquad (3.33)$$

Next, the fluxes **F** and source terms **S** are calculated at intermediate points of space and time as (Machalinska-Murawska and Szydłowski, 2014):

$$F_{i+1/2}^{n+1/2} = F\left(U_{i+1/2}^{n+1/2}\right) \qquad (3.34)$$

$$S_{i+1/2}^{n+1/2} = S\left(U_{i+1/2}^{n+1/2}\right) \qquad (3.35)$$

At the second step, values of the midpoint variables values are used for final calculation (Machalinska-Murawska and Szydłowski, 2014):

$$U_i^{n+1} = U_i^n - \frac{\Delta t}{\Delta x}\left(F_{i+1/2}^{n+1/2} + F_{i-1/2}^{n+1/2}\right) - \frac{1}{2}\Delta t\left(S_{i+1/2}^{n+1/2} + S_{i-1/2}^{n+1/2}\right) \qquad (3.36)$$

The Lax-Wendroff scheme is an explicit scheme, which means that is must satisfy the Courant-Friedrich-Lewy (CFL) criterion in order to be stable (Machalinska-Murawska and Szydłowski, 2014):

$$Cr = \frac{|u| + \sqrt{gh}}{\Delta x/\Delta t} \leq 1 \qquad (3.37)$$

where Cr is the Courant number, t is time, x is the distance, h is the water depth, u is the velocity of the flow and g is the gravitational acceleration.

The MacCormack method

The MacCormack method is a variation of the two-step Lax–Wendroff method, which removes the necessity of computing unknowns at the mid points (e.g. $x_{i+1/2}$). The MacCormack method is a predictor-corrector method: the predictor step calculates a rough approximation of the desired variable, whereas the corrector step refines the initial approximation. The MacCormack method for Equation (3.20) can be written as (Machalinska-Murawska and Szydłowski, 2014):

$$\boldsymbol{U}_i^p = \boldsymbol{U}_i^n - \frac{\Delta t}{\Delta x}(\boldsymbol{F}_{i+1}^n - \boldsymbol{F}_i^n) + \Delta t \boldsymbol{S}_i^n \qquad (3.38)$$

$$\boldsymbol{U}_i^c = \boldsymbol{U}_i^n - \frac{\Delta t}{\Delta x}(\boldsymbol{F}_i^p - \boldsymbol{F}_{i-1}^p) + \Delta t \boldsymbol{S}_i^p \qquad (3.39)$$

where the superscript p refers to the predictor step, the superscript c refers to the corrector step and n is the time level.

Finally, the solution at the next time level n + 1 can be written as (Machalinska-Murawska and Szydłowski, 2014):

$$\boldsymbol{U}_i^{n+1} = \frac{1}{2}(\boldsymbol{U}_i^p + \boldsymbol{U}_i^c) \qquad (3.40)$$

The MacCormack scheme is an explicit scheme, which means that is must satisfy the Courant-Friedrich-Lewy (CFL) criterion in order to be stable (see Equation (3.37)).

The Beam-Warming method

The Beam-Warming method is a second order accurate implicit scheme, and thus unconditionally stable (see Section 3.3). More specifically, the Beam-Warming method is a spatially factored, non-iterative ADI scheme that uses implicit Euler scheme to perform the time integration (Warming and Beam, 1976).

The finite-difference approximation for flow variables $\mathbf{U}$ (see Equation (3.20)) at the higher time level (i.e. $\mathbf{U}^{n+1}$) can be written as (Rahimpour and Tavakoli, 2011):

$$U^{n+1} = U^n + \frac{\Delta t}{2}\left[\left(\frac{\partial U}{\partial t}\right)^{n+1} + \left(\frac{\partial U}{\partial t}\right)^{n}\right] \tag{3.41}$$

The value of $\mathbf{U}_t$ from Equation (3.20) can be substituted into Equation (3.41), which yields (Rahimpour and Tavakoli, 2011):

$$U^{n+1} = U^n - \frac{\Delta t}{2}\left[\left(\frac{\partial F}{\partial x} + S\right)^{n+1} + \left(\frac{\partial F}{\partial x} + S\right)^{n}\right] \tag{3.42}$$

The next step is to linearize terms $\mathbf{F}^{n+1}$ and $\mathbf{S}^{n+1}$, which can be done by applying the Taylor series expansion. The Taylor series expansion of $\mathbf{F}^{n+1}$ and $\mathbf{S}^{n+1}$ can be written as (Rahimpour and Tavakoli, 2011):

$$F^{n+1} = F^n + M(U^{n+1} - U^n) \tag{3.43}$$

$$S^{n+1} = S^n + B(U^{n+1} - U^n) \tag{3.44}$$

where $\mathbf{M}$ and $\mathbf{B}$ are the Jacobians of $\mathbf{F}$ and $\mathbf{S}$ with respect to $\mathbf{U}$.

The matrix $\mathbf{M}$ in Equation (3.26) is replaced in the Equation (3.43), and thus B is given as (Rahimpour and Tavakoli, 2011):

$$B = \begin{bmatrix} 0 & 0 \\ -gS_0 - \dfrac{4gn^2u|u|}{R^{4/3}} & \dfrac{gn^2|u|}{R^{4/3}} \end{bmatrix} \tag{3.45}$$

where g is the gravitational acceleration, S_0 is the bed slope, n is the Manning coefficient, u is the velocity of the flow and R is the hydraulic radius.

The substitution of Equations (3.43) and (3.44) into Equation (3.42) yields (Rahimpour and Tavakoli, 2011):

$$U^{n+1} - U^n = -\frac{\Delta t}{2}\left[\frac{\partial(M^n U^{n+1})}{\partial x} - \frac{\partial(M^n U^n)}{\partial x} + B^n(U^{n+1} - U^n)\right] - \Delta t\left(M\frac{\partial U}{\partial x} + S\right)^n \tag{3.46}$$

and finally

$$U^{n+1} + \frac{\Delta t}{2}\left[\frac{\partial(M^n U^{n+1})}{\partial x} + B^n U^{n+1}\right] = U^n + \frac{\Delta t}{2}\left[\frac{\partial(M^n U^n)}{\partial x} + B^n U^n\right] - \Delta t\left(M\frac{\partial U}{\partial x} + S\right)^n \tag{3.47}$$

Introducing the split form of matrix **M** as given in Equations (3.31) and (3.32), Equation (3.47) can be written as (Rahimpour and Tavakoli, 2011):

$$\left[I + \frac{\Delta t}{2}\left(\frac{\partial M^+}{\partial x} - \frac{\partial M^-}{\partial x} + B\right)^n\right]U^{n+1}$$
$$= \left[I + \frac{\Delta t}{2}\left(\frac{\partial M^+}{\partial x} - \frac{\partial M^-}{\partial x} + B\right)^n\right]U^n - \Delta t\left[(M^+ + M^-)\frac{\partial U}{\partial x} + S\right]^n \tag{3.48}$$

where **I** is a unit matrix defined as $\mathbf{I} = \alpha(2\times2)$.

The space derivatives associated with positive and negative components of **M** are approximated by backward and forward space differences, and are defined as (Rahimpour and Tavakoli, 2011):

$$\frac{\partial(M^+ U)}{\partial x} = \frac{M_i^+ U_i - M_{i-1}^+ U_{i-1}}{\Delta x} \tag{3.49}$$

$$\frac{\partial(M^- U)}{\partial x} = \frac{M_{i+1}^- U_{i+1} - M_i^- U_i}{\Delta x} \tag{3.50}$$

3.4.2 Modern shock-capturing schemes

In modern shock-capturing methods, the numerical dissipation is distributed non-linearly. This means that the amount of the dissipation varies from one gird point to another and is supported with automatic feedback mechanisms, which remove the necessity of implementation of any adjustable parameters. In contrast to classical methods, these modern methods produce highly accurate numerical solutions even for problems containing strong shock waves (Yee, 1989). Some of the well-known modern shock-capturing methods include the Monotonic Upstream-Centered Schemes for Conservation Laws (MUSCL) based on the Godunov approach (van Leer, 1977, 1979), the Total Variation Diminishing (TVD) methods (Harten, 1983), methods based on the approximate Riemann solver, such as Roe's Riemann solver (Roe, 1981), and the Essentially Non-Oscillatory (ENO) methods (Harten et al., 1987).

The majority of the aforementioned schemes are schemes known as Godunov methods. The Godunov type methods are non-oscillatory schemes that incorporate the solution (exact or approximate) to Riemann's initial-value problem or a generalisation of it (van Leer, 1997). Godunov's scheme can be presented by considering the following solution of the (system of) hyperbolic conservation laws (Sweby, 2001):

$$u_i + f(u)_x = 0 \tag{3.51}$$

Godunov's method considers the numerical values of the solution u_i^n to be the cell averages of the analytic solution $u(x, t)$ at time interval n (Sweby, 2001):

$$u_i^n = \frac{1}{\Delta x} \int_{x_{i-1/2}}^{x_{i+1/2}} u(x, n\Delta t) dx \tag{3.52}$$

Therefore, we have a piecewise constant data representation. At each cell boundary, the resulting Riemann problem is then solved and the union of all Riemann solutions

averaged over each cell to give the updated numerical solution values (Sweby, 2001). Godunov scheme can be recast into Eulerian form by integrating Equation (3.51) over the cell $[x_{i-1/2}, x_{i+1/2}] \times [n\Delta t, (n+1)\Delta t]$ (Sweby, 2001):

$$\int_{t^n}^{t^{n+1}} \int_{x_{i-1/2}}^{x_{i+1/2}} u(x, n\Delta t)dx\, dt = -\int_{t^n}^{t^{n+1}} \int_{x_{i-1/2}}^{x_{i+1/2}} f_x\big(u(x,t)\big)dx\, dt \qquad (3.53)$$

If we now define a numerical flux as:

$$f_{i-1/2}^n = f(u_{i-1}^n, u_i^n) = \frac{1}{\Delta t}\int_{t^n}^{t^{n+1}} f\left(u\big(x_{i-1/2}, t\big)\right) dx dt \qquad (3.54)$$

then we can write Godunov's method in conservation form (Sweby, 2001):

$$u_i^{n+1} = u_i^n - \frac{\Delta t}{\Delta x}\big(f_{i+1/2}^n - f_{i-1/2}^n\big) \qquad (3.55)$$

Monotonic Upstream-Centered Schemes for Conservation Laws (MUSCL)

MUSCL methods have been first introduced by Van Leer (1979) in order to provide a more accurate approximation of the conservation equation solutions. In his MUSCL scheme, van Leer (1977, 1979) replaced Godunov's piecewise constant representation with a piecewise linear one, where the piecewise linear representation was constructed to maintain conservation by defining cell representation to be (Sweby, 2001):

$$u_i(x) = u_i^n - \frac{\Delta_i u}{\Delta x}(x - x_i) \qquad (3.56)$$

where u_i^n is the Godunov cell average (see Equation (3.52)) and the slope $\frac{\Delta_i u}{\Delta x}$ must be defined.

Three possibilities were proposed for $\Delta_i u$, including (van Leer, 1977):

1. centred differencing of the piecewise constant cell averages

$$\Delta_i u = \frac{1}{2}(u_{i+1} - u_i)$$

2. differencing of the underlying continuous function

$$\Delta_i u = \left(u\left(x_{i+1/2}, t^n\right) - u\left(x_{i-1/2}, t^n\right)\right)$$

3. maintaining the first moment of the underlying analytical solution

$$\Delta_i u = \frac{12}{(\Delta x)^2} \int_{x_{i-1/2}}^{x_{i+1/2}} u(x, t^n)(x - x_i)dx$$

However, calculation of the slopes in any of these fashions could lead to the increase in total variation diminishing of the data representation, which in turn can result into occurrence of spurious oscillations (Sweby, 2001). In order to avoid the increase in total variation, van Leer (1977) limited the gradients of slopes by defining a monotonised slope as (Sweby, 2001):

$$(\Delta_i u)_{mono} = \begin{cases} min\left\{2\left|\Delta u_{i-\frac{1}{2}}\right|, |\Delta_i u|, 2\left|\Delta u_{i+\frac{1}{2}}\right|\right\} sgn\Delta_i u \\ \quad if \ sgn\Delta u_{i-\frac{1}{2}} = sgn\Delta u_{i+\frac{1}{2}} = sgn\Delta_i u \\ 0 \quad otherwise \end{cases} \quad (3.57)$$

which may be applied to any definition of $\Delta_i u$ and where $\Delta u_{i-1/2} = u_i - u_{i-1}$.

For his first choice of slope, van Leer (1977) also gave an improved limiting as (Sweby, 2001):

$$(\Delta_i u)_{mono} = \begin{cases} \frac{2\Delta u_{i-1/2}\Delta u_{i+1/2}}{\Delta u_{i-1/2} + \Delta u_{i+1/2}}, if \ sgn\Delta u_{i-1/2} = sgn\Delta u_{i+1/2} \\ 0 \quad\quad\quad\quad\quad otherwise \end{cases} \quad (3.58)$$

This slope limiting has much in common with flux limiters, and if we define

$$r_{i-1/2} = \Delta u_{i-1/2}/\Delta u_{i+1/2} \quad (3.59)$$

then Equation (3.58) can be written as (Sweby, 2001):

$$(\Delta_i u)_{mono} = \frac{r_{i-1/2} + |r_{i-1/2}|}{1 + |r_{i-1/2}|} = \emptyset VL(r_{i-1/2}) \tag{3.60}$$

where $\emptyset VL(r)$ is van Leer's flux limiter.

Total Variation Diminishing (TVD) methods

First orders methods (such as Godunov's) tend to be very diffusive, i.e. they smear the discontinuities that often arise in the solution of conservation laws. However, such methods (e.g. classical higher shock-capturing schemes, see Section 3.4.1) are prone to producing spurious numerical oscillations in the presence of strong shock waves, which can result into breakdown of the numerical solution. Godunov (1959) showed that this course of events was inevitable for constant coefficient schemes, as these schemes could not be both monotonicity preserving and higher than first order accurate (Sweby, 2001). One of the proposed solutions was the adoption of total variation as a monitor of spurious oscillations. Lax (1973) showed that for scalar conservation laws, the total variation (TV) of physically possible solutions does not increase in time. The total variation is given by (Sweby, 2001):

$$TV(u) = \int |u_x| dx \tag{3.61}$$

and the total variation for discrete case is

$$TV(u_i^n) = \sum_i |u_{i+1}^n - u_i^n| \tag{3.62}$$

According to Harten (1983), numerical method is said to be total variation diminishing if:

$$TV(u_i^{n+1}) \le TV(u_i^n) \tag{3.63}$$

The central idea in constructing a TVD scheme is to attempt to develop a higher-order method that will avoid oscillations and exhibit properties similar to those of a monotone scheme. For such schemes, the solution is first order near discontinuities and higher order in smooth regions, with the transition to higher order being accomplished by the use of slope limiters on the dependent variables or flux limiters (Tannehill et al., 1997).

Roe's Riemann solver

In order to solve the Riemann problem for non-linear conservation laws, an iterative procedure is usually required. However, this iterative procedure must be used at every cell boundary and at every time step, which in turn can be computationally expensive. Therefore, approximate Riemann solvers that do not employ iteration are often used to simplify the process and reduce overhead. This simplification can be achieved by approximating the Riemann states and applying physical flux, or by approximating the numerical flux directly (Sweby, 2001).

Perhaps the simplest approximate Riemann solver is Roe's Riemann solver (Roe, 1981). The system of conservation laws (see Equation (3.51)) may be written in quasi-linear form as (Sweby, 2001):

$$u_t = A(u)u_x \qquad (3.64)$$

where A(u) is the Jacobian matrix defined as $\frac{\partial f}{\partial u}$.

In each interval (u_{i-1}, u_i), Equation (3.64) is linearized by replacing the Jacobian by interval-wise constant matrices $\hat{A}(u_{i-1}, u_i)$, which for any two adjacent states u_L, u_R must satisfy the following (Sweby, 2001):

1. $\hat{A}(u_L, u_R)$ is diagonalisable with real eigenvalues (hyperbolicity)
2. $\hat{A}(u_L, u_R) \rightarrow A(u)$ as $u_L, u_R \rightarrow u$ (consistency)
3. $f(u_L) - f(u_R) = \hat{A}(u_L, u_R)(u_L - u_R)$ (conservation)

The first two conditions are readily satisfied if $\hat{A}$ is taken to be the Jacobian evaluated at an averaged state, i.e. $\hat{A}(u_L, u_R) = A(\bar{u})$. However, a straight arithmetic average will generally not satisfy the third condition and therefore a geometric average is often used instead, with this geometric average being in the form of the arithmetic mean of an auxiliary vector known as the parameter vector (Sweby, 2001).

Once the Jacobian matrix $\hat{A}$ has been obtained, it is diagonalized as (Sweby, 2001):

$$\hat{A} = \bar{X}\bar{\Lambda}\bar{X}^{-1} \tag{3.65}$$

where $\bar{\Lambda}$ is the diagonal matrix whose entries are the absolute values of the eigenvalues (Tannehill et al., 1997).

This diagonalization results in a set of decoupled linear advection equations in each interval, with the flux differences $f_R - f_L$ in each interval being decomposed onto local eigenvectors as follows (Sweby, 2001):

$$\Delta f = f_R - f_L = \sum_{k=1}^{n} \tilde{\alpha}^{(k)} \bar{\lambda}^{(k)} \tilde{x}^{(k)} \tag{3.66}$$

where $\bar{\lambda}^{(k)}$, $\tilde{x}^{(k)}$ and $\tilde{\alpha}^{(k)}$ are the eigenvalue, eigenvector and coefficient for Δu that correspond to the *kth* characteristic field of the Jacobian matrix $\hat{A}$.

Roe's original scheme updated the solution by upwinding and directly adding the flux difference components from Equation (3.66). Nonetheless, Roe's scheme may also be placed in the framework of inter-cell fluxes by integration around the half cell $(x_{i-1/2}, x_i) \times (t^n, t^{n+1})$, which results in the flux (Sweby, 2001):

$$f_{i-1/2} = \frac{1}{2}(f_{i-1} + f_i) - \frac{1}{2}\sum_{k=1}^{n} \tilde{\alpha}_{i-1/2}^{(k)} \left| \bar{\lambda}_{i-1/2}^{(k)} \right| \tilde{x}_{i-1/2}^{(k)} \tag{3.67}$$

with the Jacobian matrix $\tilde{A}$ being identified with the cell interfaces.

The resulting individual approximate Riemann problems are linear, which means that their solution contains only discontinuities and not expansion fans (Sweby, 2001). This being the case, Roe's original method is not entropy satisfying (Tannehill et al., 1997), and therefore a number of entropy fixes have since been proposed (Harten and Hyman, 1983, Roe and Pike, 1985, Roe, 1992).

Essentially Non-Oscillatory (ENO) methods

The idea of MUSCL was further extended by constructing a piecewise parabolic data representation (Colella and Woodward, 1984). This parabolic data representation is (i) limited in such a way to avoid overshoots and undershoots, and (ii) incorporates a discontinuity detection mechanism to sharpen any discontinuities of the data fans (Sweby, 2001). The data representation is then advanced using either a Lagrangian step followed by a remap, or in conservation form, resulting in the third order Piecewise parabolic method (PPM) (Sweby, 2001).

The idea of polynomial data representation was then extended even further and resulted in the development of the so-called the Essentially Non-Oscillatory (ENO) schemes (Harten et al., 1986, 1987, Harten and Osher, 1987, Shu and Osher, 1988). The technique behind the ENO scheme is similar to the technique employed in the MUSCL and PPM schemes, with the main difference being that (i) the data representation constructed from the cell averages $\{u_i^n\}$ does not damp the values of local extrema (e.g. the MUSCL and PPM schemes do), and (ii) the data reconstruction is even allowed occasionally to accentuate these local features (Sweby, 2001).

The Essentially Non-Oscillatory (ENO) scheme starts from the cell averages $\bar{u}^n = \{u_i^n\}$ and constructs the approximate function $u_{\Delta x}(x, t^n) = R(x, \bar{u}^n)$, where $R(x, \bar{u}^n)$ is a piecewise polynomial in x of degree p – 1 satisfying (Sweby, 2001):

1. $R(x, \bar{u}^n) = u(x, t^n) + O(\Delta x^p)$ where the functions are smooth

2. $R(x, \bar{u}^n)$ is conservative, i.e. $\frac{1}{\Delta x} \int_{x_{i-1/2}}^{x_{i+1/2}} R(x, \bar{u}^n) dx = u_i^n$

3. $R(x, \bar{u}^n)$ is essentially non-oscillatory, i.e. $TV(R(\cdot, \bar{u}^n)) \leq TV(u(\cdot, t^n)) + O(\Delta x^p)$

Both MUSCl (p = 2) and PPM (p = 3) fit into this framework, except that they have the more restrictive condition of $TV\big(R(\cdot, \bar{u}^n)\big) \leq TV\big(u(\cdot, t^n)\big)$. After the reconstruction of the data, the solution to the conservation law in Equation (3.51) with initial data $u_{\Delta x}(\cdot, t^n)$ is calculated, and the solution re-averaged to obtain updated cell averages u_i^{n+1} (Sweby, 2001).

According to Sweby (2001), the key step of ENO is in the reconstruction of the data, which can be summarised as follows:

1. the interpolant $R(x, \bar{u}^n)$ is built up in stages using Newton interpolation, where a local linear interpolant in the cell $\big(x_{i-1/2}, x_{i+1/2}\big)$ may initially be constructed by either using u_{i+1} and u_i or u_i and u_{i-1}

2. the pair with smallest difference is chosen, with the process being repeated for each cell

3. a quadratic interpolant for each cell is constructed by adding an additional interpolation point, which can be either the value to the left or right of the previous stencil. For example: if u_{i+1} and u_i had been chosen to form the linear interpolation for our cell, then we add in either u_{i+2} or u_{i-1}. The one which gives the smoothest interpolation (as monitored by comparison of divided differences) is chosen

4. the process is done for each cell and the method is applied recursively until the desired degree of interpolation is reached

An advanced variant of ENO is so-called Weighted ENO (WENO), where a linear combination of the candidate stencils for interpolation is taken (Liu et al., 1994). ENO can be shown to be Total Variation Bounded (TVB), i.e. $TV(u^n) \leq CTV(u^0)$. This means theoretically that solutions still converge as for TVD schemes, and practically that small oscillations on the scale of truncation error may appear; however, these oscillations usually vanish if the solution is adequately solved (Sweby, 2001).

3.5 Numerical models

As indicated in Section 2.4, the flood simulations conducted within this research were conducted using the DIVAST and DIVAST-TVD numerical models. The DIVAST model is a widely used, open source ADI-type flood inundation model developed by Falconer (1986). The DIVAST model has been acquired by consulting companies and government organisations for application to over 100 hydro-environmental impact assessment studies worldwide. The DIVAST model has also been extensively calibrated and verified against laboratory and field data, with details of model refinements and verification tests being well documented in the literature (Falconer and Lin, 2003, Bockelmann et al., 2004, Falconer et al., 2005, Lin et al., 2006, Hunter et al., 2008, Gao et al., 2011, Ahmadian et al., 2012, Ahmadian and Falconer, 2012, Sparks et al., 2013, Wang and Lin, 2013, Ahmadian et al., 2015). This being the case, only a brief presentation of the DIVAST model is included in this section, while the detailed description of the model can be found in Boye (2014).

The DIVAST-TVD model is a shock-capturing flood inundation model introduced by Liang et al. (2006). The DIVAST-TVD model is an effective tool for analysing storm surges, dam-break scenarios, flash floods etc., i.e. any flow scenario that could involve rapidly varying flow conditions or abrupt changes in the flow regime, such as hydraulic jumps, bores etc. As this thesis revolves around shock-capturing flood inundation modelling, the DIVAST-TVD model will be presented in more detail in this section. Additional information about the development and extensive verifications of the DIVAST-TVD model can be in the literature (Liang et al., 2006, 2007a, 2007b, 2007c, Hunter et al., 2008, Liang et al., 2010, 2014).

3.5.1 The DIVAST model

The DIVAST model is a two-dimensional, depth-integrated, time-variant model, which was primarily developed for predicting the hydrodynamics in estuaries and coastal waters. It is suitable for water bodies that are dominated by near horizontal, unsteady flows and do not display significant vertical stratification. The model simulates two-dimensional currents, water surface elevations and various water

quality parameters within the modelling domain as functions of time, taking into account the hydrodynamic characteristics governed by the bed topography and boundary conditions (Falconer, 1986).

DIVAST has been developed in order to simulate the hydrodynamic, solute and sediment transport processes in rivers, estuaries and coastal waters. The hydrodynamic module solves the Reynolds averaged, depth integrated Navier–Stokes equations. The governing equations for the hydrodynamic processes can be written as (Falconer, 1986):

$$\frac{\partial \eta}{\partial t} + \frac{\partial p}{\partial x} + \frac{\partial q}{\partial y} = q_m \tag{3.68}$$

$$\begin{aligned}\frac{\partial p}{\partial t} + \frac{\partial \beta p U}{\partial x} + \frac{\partial \beta p V}{\partial y} &= fq - gH\frac{\partial \eta}{\partial x} + \frac{\rho_a}{\rho}C_w W_x\sqrt{W_x^2 + W_y^2} \\ &\quad - \frac{gp\sqrt{p^2 + q^2}}{H^2 C^2} + \varepsilon\left[2\frac{\partial^2 p}{\partial x^2} + \frac{\partial^2 p}{\partial y^2} + \frac{\partial^2 q}{\partial x \partial y}\right]\end{aligned} \tag{3.69}$$

$$\begin{aligned}\frac{\partial q}{\partial t} + \frac{\partial \beta q U}{\partial x} + \frac{\partial \beta q V}{\partial y} &= fp - gH\frac{\partial \eta}{\partial y} + \frac{\rho_a}{\rho}C_w W_y\sqrt{W_x^2 + W_y^2} \\ &\quad - \frac{gq\sqrt{p^2 + q^2}}{H^2 C^2} + \varepsilon\left[2\frac{\partial^2 q}{\partial x^2} + \frac{\partial^2 q}{\partial y^2} + \frac{\partial^2 p}{\partial x \partial y}\right]\end{aligned} \tag{3.70}$$

where η is water surface elevation above datum, q_m is source discharge per unit horizontal area (m^3/s/m^2), p and q are discharges per unit width in the x and y directions, U and V are depth averaged velocity components in the x and y directions, H is total water depth, h is water depth between bed level and datum, β is momentum correction factor for a non-uniform vertical velocity profile, f is Coriolis parameter, ρ_a is air density, ρ is density of fluid, W_x and W_y are wind velocities in x and y directions, C is Chezy roughness coefficient, C_w is air/fluid resistance coefficient and ε is depth averaged turbulent eddy viscosity.

In this study, the Coriolis, wind and viscous forces were omitted from the flood inundation simulations conducted with the DIVAST model. In addition, friction term was redefined in such a way that the Chezy coefficient was based on the Manning's roughness parameter. This means that the Chezy coefficient was defined as:

$$C = \frac{h^{1/6}}{n} \tag{3.71}$$

where C is Chezy roughness coefficient, h is the depth of the water and n is Manning's roughness parameter.

In the DIVAST model, an Alternating Direct Implicit (ADI) method has been adopted for solving the hydrodynamic equations. Adopting the finite difference method and a space staggered grid, the governing equations are split into two sets of one-dimensional equations, which are then solved at two half time steps. The system of equations to be solved in the first and second half time steps can be described as a tri-diagonal system of equations, and is solved efficiently using a simplified form of Gaussian elimination, i.e. the Thomas algorithm. The x-direction system of equations is solved in the first half time step, while the y-direction system of equations is solved in the second half time step. This means that the solution of a full two-dimensional matrix is not required, and a one-dimension set of equations is solved implicitly for each half time step. The numerical scheme for the hydrodynamics is basically second order accurate, both in time and space, with no stability constraints due to the time centred implicit character of the ADI technique. However, it has been recognised that the time step needs to be restricted so that a reasonable computational accuracy can be achieved (Chen, 1992). This being the case, a Courant number restriction for accuracy of the hydrodynamic module has been implemented in the DIVAST model, with the maximum Courant number being suggested as (Stelling et al., 1986):

$$Cr = 2\Delta t \sqrt{gH\left(\frac{1}{\Delta x^2} + \frac{1}{\Delta y^2}\right)} \leq 4\sqrt{2} \tag{3.72}$$

where Cr is Courant number, Δt is the time step, g is the gravitational acceleration, H is total water depth and Δx and Δy are spatial parameters.

As indicated in Section 3.3, implicit schemes are less sensitive to numerical stability than explicit schemes and therefore larger values of the Courant number can be considered, i.e. Courant numbers up to 8 can be used. Nonetheless, a Courant number was set to 1 in the DIVAST model in this study. This value was selected in order to be consisted with the Courant number selected for the explicit scheme considered in this study (i.e. the DIVAST-TVD model). As indicated in Section 3.3, the Courant number is typically set to 1 for explicit schemes.

3.5.2 The DIVAST-TVD model

The DIVAST-TVD model is a shock-capturing flood inundation model, which has been developed in order to simulate the rapidly varying hydrodynamic processes in rivers and coastal waters by solving the shallow water equations. By neglecting the Coriolis, wind and viscous forces, the shallow water equations can be written in the following form (Liang et al., 2007b):

$$\frac{\partial \zeta}{\partial t} + \frac{\partial q_x}{\partial x} + \frac{\partial q_y}{\partial y} = 0 \tag{3.73}$$

$$\frac{\partial q_x}{\partial t} + \frac{\partial \left(\frac{\beta q_x^2}{H}\right)}{\partial x} + \frac{\partial \left(\frac{\beta q_x q_y}{H}\right)}{\partial y} = -gH\frac{\partial \zeta}{\partial x} - \frac{g q_x \sqrt{q_x^2 + q_y^2}}{H^2 C^2} \tag{3.74}$$

$$\frac{\partial q_y}{\partial t} + \frac{\partial \left(\frac{\beta q_x q_y}{H}\right)}{\partial x} + \frac{\partial \left(\frac{\beta q_y^2}{H}\right)}{\partial y} = -gH\frac{\partial \zeta}{\partial y} - \frac{g q_y \sqrt{q_x^2 + q_y^2}}{H^2 C^2} \tag{3.75}$$

where t is the time, ζ is the water surface elevation above datum, q_x and q_y are the discharge per unit width in the x and y directions, β is the momentum correction factor for a non-uniform vertical velocity profile, g is gravitational acceleration, H (= h + ζ) is the total water column depth (where h is the water depth relative to datum) and C is the Chezy roughness coefficient. As in the DIVAST model, the Chezy

coefficient in the DIVAST-TVD model was also based on the Manning's roughness parameter (see Equation (3.71)).

The conservative form of the shallow water equations is usually deployed to insure the conservation of mass and momentum after the discretisation of equations. For example, Equations (3.73) - (3.75) can be rearranged in the following conservative form (Liang et al., 2006):

$$\frac{\partial \boldsymbol{X}}{\partial t} + \frac{\partial \boldsymbol{F}}{\partial x} + \frac{\partial \boldsymbol{G}}{\partial y} = \boldsymbol{S} + \boldsymbol{T} \tag{3.76}$$

where

$$\boldsymbol{X} = \begin{bmatrix} H \\ q_x \\ q_y \end{bmatrix} \tag{3.77}$$

$$\boldsymbol{F} = \begin{bmatrix} q_x \\ \dfrac{\beta q_x^2}{H} + \dfrac{gH^2}{2} \\ \dfrac{\beta q_x q_y}{H} \end{bmatrix} \tag{3.78}$$

$$\boldsymbol{G} = \begin{bmatrix} q_y \\ \dfrac{\beta q_x q_y}{H} \\ \dfrac{\beta q_y^2}{H} + \dfrac{gH^2}{2} \end{bmatrix} \tag{3.79}$$

$$\boldsymbol{S} = \begin{bmatrix} 0 \\ gH\dfrac{\partial h}{\partial x} - \dfrac{g q_x \sqrt{q_x^2 + q_y^2}}{H^2 C^2} \\ 0 \end{bmatrix} \tag{3.80}$$

$$\boldsymbol{T} = \begin{bmatrix} 0 \\ 0 \\ gH\dfrac{\partial h}{\partial y} - \dfrac{g q_y \sqrt{q_x^2 + q_y^2}}{H^2 C^2} \end{bmatrix} \tag{3.81}$$

with $\boldsymbol{X}$ representing the independent variables η, q_x, and q_y, $\boldsymbol{F}$ and $\boldsymbol{G}$ representing the flux terms, and $\boldsymbol{S}$ and $\boldsymbol{T}$ representing the source terms.

Majority of the shock-capturing models choose the formulation given by Equations (3.77) - (3.81) in their solution strategy, but this formulation can induce numerical imbalances associated with the treatment of the bed-slope term (Liang et al., 2006). However, this imbalance can be alleviated by following Rogers et al. (2003), who proposed that Equations (3.77) - (3.81) can be transformed into Equation (3.76) in such a way that η (instead of H), q_x and q_y are taken as the independent functions. This then yields (Liang et al., 2006):

$$\boldsymbol{X} = \begin{bmatrix} \eta \\ q_x \\ q_y \end{bmatrix} \tag{3.82}$$

$$\boldsymbol{F} = \begin{bmatrix} q_x \\ \dfrac{\beta q_x^2}{h+\eta} + \dfrac{g\eta^2}{2} + gh\eta \\ \dfrac{\beta q_x q_y}{h+\eta} \end{bmatrix} \tag{3.83}$$

$$\boldsymbol{G} = \begin{bmatrix} q_y \\ \dfrac{\beta q_x q_y}{h+\eta} \\ \dfrac{\beta q_y^2}{h+\eta} + \dfrac{g\eta^2}{2} + gh\eta \end{bmatrix} \tag{3.84}$$

$$\boldsymbol{S} = \begin{bmatrix} 0 \\ g\eta\dfrac{\partial h}{\partial x} - \dfrac{gq_x\sqrt{q_x^2+q_y^2}}{(h+\eta)^2 C^2} \\ 0 \end{bmatrix} \tag{3.85}$$

$$\boldsymbol{T} = \begin{bmatrix} 0 \\ 0 \\ g\eta\dfrac{\partial h}{\partial y} - \dfrac{gq_y\sqrt{q_x^2+q_y^2}}{(h+\eta)^2 C^2} \end{bmatrix} \tag{3.86}$$

The latter formulation of the shallow water equations (i.e. Equations (3.82) - (3.86)) is also used in the DIVAST-TVD model. Using the Strang operator-splitting technique (Strang, 1968), the solution to Equation (3.76) is obtained by solving two one-dimensional problems (Liang et al., 2006):

$$\frac{\partial \boldsymbol{X}}{\partial t} + \frac{\partial \boldsymbol{F}}{\partial x} = \boldsymbol{S} \tag{3.87}$$

$$\frac{\partial \boldsymbol{X}}{\partial t} + \frac{\partial \boldsymbol{G}}{\partial y} = \boldsymbol{T} \tag{3.88}$$

with the explicit discretisation of Equations (3.87) and (3.88) for rectangular grid being written as (Liang et al., 2006):

$$\boldsymbol{X}_{i,j}^{n+1} = L_x \boldsymbol{X}_{i,j}^n \tag{3.89}$$

$$\boldsymbol{X}_{i,j}^{n+1} = L_y \boldsymbol{X}_{i,j}^n \tag{3.90}$$

where L_x and L_y are the finite-difference operators and the subscript, while subscript of $\boldsymbol{X}$ represent the spatial and temporal grid levels.

The finite-difference solution to Equation (3.76) can thus be approximated by (Liang et al., 2006):

$$\boldsymbol{X}_{i,j}^{n+2} = L_x L_y L_y L_x \boldsymbol{X}_{i,j}^n \tag{3.91}$$

As indicated in Section 3.4.1, the MacCormack method is a predictor-corrector scheme: the predictor step calculates a rough approximation of the desired variable, whereas the corrector step refines the initial approximation. In the DIVAST-TVD model, the MacCormack scheme is utilised to solve consecutively the two one-dimensional hyperbolic equations in each time step. For example, the discretization scheme for Equation (3.87) is given as (Liang et al., 2006):

$$\boldsymbol{X}_i^p = \boldsymbol{X}_i^n - (\boldsymbol{F}_i^n - \boldsymbol{F}_{i-1}^n) \cdot \frac{\Delta t}{\Delta x} + \boldsymbol{S}^n \cdot \Delta t \tag{3.92}$$

$$\boldsymbol{X}_i^c = \boldsymbol{X}_i^n - \left(\boldsymbol{F}_{i+1}^p - \boldsymbol{F}_i^p\right) \cdot \frac{\Delta t}{\Delta x} + \boldsymbol{S}^p \cdot \Delta t \tag{3.93}$$

where the superscripts p and c denote the predictor and corrector steps, Δx and Δt are the spatial and time steps.

The standard MacCormack scheme has second-ordered accuracy (MacCormack, 1976). It is well known that all schemes of accuracy greater than one will generate spurious numerical oscillations in the regions where the gradient is high (Godunov, 1959). Therefore, a symmetric five point TVD term is appended to the corrector step of the MacCormack scheme to prevent non-physical oscillations. As indicated in Section 3.4, total variation diminishing schemes prevent the emergence of numerical oscillations through added non-linear artificial dissipation terms.

The TVD term implemented in the DIVAST-TVD model was first presented by Davis (1984), who proposed a total variation diminishing scheme where a symmetric five point TVD term is added to the Lax-Wendroff scheme. The symmetric five point TVD term is used to adjust the introduced numerical diffusion: a second-order accurate MacCormack scheme is deployed where the solution is smooth, whereas a first-order accurate upwind scheme is deployed to avoid spurious numerical oscillations (Liang et al., 2007b).

In the DIVAST-TVD model, the MacCormack-TVD scheme is defined as (Liang et al., 2006):

$$X_i^{n+1} = \frac{\left(X_i^p + X_i^c\right)}{2} + [G(r_i^+) + G(r_{i+1}^-)] \cdot \Delta X_{i+1/2}^n - [G(r_{i-1}^+) + G(r_i^-)] \cdot \Delta X_{i-1/2}^n \tag{3.94}$$

where

$$X_{i+1/2}^n = X_{i+1}^n - X_i^n \tag{3.95}$$

$$X_{i-1/2}^n = X_i^n - X_{i-1}^n \tag{3.96}$$

and

$$r_i^+ = \frac{\langle \Delta X_{i-1/2}^n, \Delta X_{i+1/2}^n \rangle}{\langle \Delta X_{i+1/2}^n, \Delta X_{i+1/2}^n \rangle} \tag{3.97}$$

$$r_i^- = \frac{\langle \Delta \boldsymbol{X}_{i-1/2}^n, \Delta \boldsymbol{X}_{i+1/2}^n \rangle}{\langle \Delta \boldsymbol{X}_{i-1/2}^n, \Delta \boldsymbol{X}_{i-1/2}^n \rangle} \tag{3.98}$$

The point brackets in the numerator and denominator of Equations (3.97) and (3.98) denote the scalar product of the two vectors within the brackets. The function G( ) is defined as (Liang et al., 2006):

$$G(x) = 0.5 \times C \times [1 - \varphi(x)] \tag{3.99}$$

where the flux limiter function is given as

$$\varphi(x) = max(0, min(2x, 1)) \tag{3.100}$$

and variable C as

$$C = \begin{cases} Cr \times (1 - Cr), & Cr \leq 0.5 \\ 0.25, & Cr > 0.5 \end{cases} \tag{3.101}$$

with the Cr being the local Courant number defined as

$$C_r = \frac{\left(\left| \frac{q_x}{H} \right| + \sqrt{gH} \right) \Delta t}{\Delta x} \tag{3.102}$$

where Cr is local Courant number, q_x is the discharge per unit width in the x direction H (= h + ζ) is the total water column depth (where h is the water depth relative to datum), g is the gravitational acceleration, Δt is the time step and Δx is the spatial parameter.

The DIVAST-TVD model optimisation

As indicated in Section 3.4, the shock-capturing models are usually associated with higher computational cost when compared to numerical models typically used in flood inundation modelling (Liang et al., 2006, Neal et al., 2012, de Almeida et al.,

2012). Therefore, simple optimisation procedures for the DIVAST-TVD code were implemented in order to increase the clarity of the code and overall efficiency of the model performance.

Refinements of the model syntax

The original DIVAST-TVD code was a mix of Fortran 77 and 95 with GNU extensions. This being the case, the first step in the optimisation process was to convert the original code to strict FORTRAN 90 language standard, which unified the code syntax and ensured full portability of the code across different compilers and hardware.

Secondly, following Whittaker (2014) the DIVAST-TVD model code was moved from a single source file to a modular distributed system, which means that each logical part of the program (such as hydrodynamic calculation) was written in a separate module. Dividing the code into modules and further use of those modules makes the interface of the procedure explicit. An explicit interface allows a FORTRAN compiler to check for consistency between the actual arguments in a call and the dummy arguments of the procedure, which results in protection against variety of programming mistakes (Whittaker, 2014). In addition, when code is divided into modules it is very simple to implement new features into the existing code, as new features can simply be added to main procedure by declaring the *use* statement for newly written module (Ellis et al., 1994). This being the case, the division of the code into modules enhanced the clarity of the code, and resulted in easier comprehension of program flow, faster program compilation and easier further development of the model.

An additional minor change in the code structure was made; this is the use of the *implicit none* statement, which (i) prevents potential confusion in variable types, as programmer is forced to strictly declare all variables, and (ii) enables much easier detection of typographic errors (Ellis et al., 1994). This simple change helped to reduce accidental programming errors and thus saved a lot of time during the code writing and compilation process.

These improvements did not strictly optimise the code in terms of significantly decreasing the programme execution and running time. Nonetheless, they had a high impact on increasing the clarity, functionality, maintainability and accessibility of the code. This in turn enabled easier implementations of new features into the existing DIVAST-TVD code, such as the module for the prediction of flood hazard indices.

Increasing the model efficiency

After the refinement of the model syntax, the next step in the optimisation process was to increase the model efficiency (e.g. to decrease model running time). One of the things that can have a great impact on the model performance is the order in which memory is accessed. The storage order depends on the particular language standard being used. For example, consider the following matrix:

$$A = \begin{bmatrix} a_{11} & a_{12} & a_{13} \\ a_{21} & a_{22} & a_{23} \end{bmatrix} \tag{3.103}$$

In FORTRAN codes, the array storage is column-major ordered, which means that the matrix A will be arranged as (a_{11}, a_{21}, a_{12}, a_{22}, a_{13}, a_{23}) when stored in memory as a linear array (Knuth, 1974). This being the case, accessing the elements of the matrix A column-wise is the most efficient, as it allows the central processor unit (CPU) to reuse data already loaded into the cache and minimise the number of comparatively costly memory fetches (Anderson et al., 1995). This means that the performance of the code can be easily improved just by paying attention to the loop ordering. Therefore, the original DIVAST-TVD code was rewritten in such manner that (almost) every loop in the code is now column-major ordered.

Nowadays code performance is generally significantly enchased by applying parallel computing methods, such as CPU parallel optimisation, for example OpenMP (Dagum and Menon, 1998) and MPI (Gropp et al., 1999), or graphic processing unit (GPU) parallelisation (Kirk, 2007). However, parallel computing is generally time-consuming and requires a relatively strong computing background. Nonetheless, the model execution and running time can be greatly decreased simply by considering computer characteristics (e.g. processor characteristics) and compiler optimisation

properties (such as loop optimisation and inter-procedural optimisation). This means that by including optimisation procedures in the compiler settings, the efficiency of the model execution can be vastly increased. For example, Intel Fortran Compiler was used for optimisation of the DIVAST-TVD code within this research study. In this research study, three optimisation settings or optimisation flags provided by the Intel Fortran Compiler were included in the optimisation process: the O3 flag (i.e. general optimisation), the Qipo flag (i.e. inter-procedural optimisation), and the QxHost flag (i.e. Intel processor-specific optimisation) (Intel, 2013).

In order to measure the impact of the aforementioned refinements (i.e. the changes in the DIVAST –TVD code structure and the implementation of the optimisation procedures), the optimised version of the DIVAST-TVD code was benchmarked against the original version of the DIVAST-TVD code. The hardware and software used in the benchmarking test are detailed in Table 3.1. The 2004 Boscastle flash flood simulation was used for the benchmarking test, with the main model parameters being presented in Table 3.2.

Table 3.1: The hardware and software used in the benchmarking test between the original and the optimised code

CPU model	Intel Core™ i5 – 3210M
CPU clock frequency	2.50 GHz
CPU cores/threads	2/4
Memory	6 GB
Memory clock frequency	1600 MHz
Operating system	Windows 10, 64 bit operating system
Compiler	Intel Fortran Compiler XE 13.1

The results of the benchmarking test are presented in Table 3.3. In Table 3.3, it can be seen that with these relatively simple refinements (e.g. changes in the model syntax and implementation of the optimisation procedures) a speed up of 8.096 was achieved. This means that the optimised version of the DIVAST-TVD code was eight times faster than the original version of the DIVAST-TVD code. This being the

case, the simple refinements (e.g. the changes in the DIVAST –TVD code structure and the implementation of the optimisation procedures) significantly decreased model running time. All in all, the simple optimisation procedure presented in this sub-section can be applied quickly and practically without any prior knowledge of coding, and thus provides a relatively good alternative to more computationally sophisticated and time-demanding optimisation methods, such as parallel computing.

Table 3.2: Model parameters used in the benchmarking test between the original and the optimised version of the DIVAST-TVD code

Domain size	665 x 235 m
Grid size	1 m
Number of grid cells	156275
Simulation time	7200 s
Time step	0.04 s

Table 3.3: The results of the benchmarking test between the original and the optimised version of the DIVAST-TVD code

Model version	**Simulation time**	**Speed up**
Original DIVAST-TVD code	9h 16min 30s	/
Optimised DIVAST-TVD code	1h 8min 44s	8.096

3.6 Summary

Nowadays potential flood damage is generally estimated using numerical flood inundation models. These models enable the simulation of the flood flow propagation over a piece of land, which can be mathematically described with the well-known, three-dimensional Navier-Stokes equations. However, application of fully 3D Navier-Stokes equations to model practical hydro-environmental problems is currently impracticable due to high computational cost. Therefore, the 3D Navier-Stokes equations are usually depth-averaged in order to derive the 2D shallow water equations and 1D Saint-Venant equations, which are used in flood inundation models to describe the characteristics of the flow.

In order to be suitable for numerical computation, the main governing equations are discretised in space and time, i.e. the partial differential equations are converted into a set of algebraic equations. Three spatial discretisation methods are predominately used in numerical flow propagation modelling, i.e. finite difference method, finite element method and finite volume method, while the time integration is generally conducted using explicit, implicit or semi-implicit schemes. Based on the selected space-time discretisation strategy, different numerical schemes can be constructed that can be used to compute flood depths, velocities and inundation extent. However, these regular schemes do not respond well when it comes to modelling of flood scenarios with rapidly varying flows or high Froude number flows (such as dam-break or flash flood scenarios), and are susceptible to the emergence of spurious numerical oscillations, which can lead to highly erroneous simulation results. For such flood scenarios flood inundation models with shock-capturing ability need to be used. These models apply artificial diffusion terms in the solution procedure, which ensure the stability of the computational process and enable the computation of any shock waves or discontinuities as part of the numerical solution.

Finally, two numerical models were presented in this chapter, including; (i) a model based on the ADI scheme, i.e. the DIVAST model, and (ii) a model based on the MacCormack-TVD shock-capturing scheme, i.e. the DIVAST-TVD model. In addition, modifications of the DIVAST-TVD code were also described in this chapter, which included refinements of the model syntax and implementation of simple optimisation procedures that increase model efficiency.

CHAPTER 4

Case studies

4.1 Introduction

This chapter presents three case studies of extreme flood events that were considered in this research. These case studies are: (i) the 2004 Boscastle flash flood (England, UK), (ii) the 2007 Železniki flash flood (Slovenia), and (iii) the 2010 Kostanjevica na Krki extreme river flood (Slovenia).

The main focus of this research is on the 2004 Boscastle flash flood, because this flood event is one of the best recorded flash floods in the history of the UK, and therefore a large amount of data exists which can be used to verify the results obtained in this study. The 2007 Železniki flash flood was one of the most severe flash flood events in Europe in the last 20 years, and as such has been substantially studied both in Slovenia and in a wider research community across Europe. This being the case, the 2007 Železniki flash flood is a good case study, which can be used to assess the performance of different methodologies considered in this research. In contrast, the 2010 Kostanjevica na Krki extreme river flooding received practically no attention in the research community, even though it was one of the largest flooding events in the history of Slovenia. Nonetheless, measurements from the stream gauge stations and quite substantial hydrological reports issued by the Slovenian Environment Agency exist, which provide all the relevant information necessary to set up and validate a numerical flood simulation.

Considering more than one case study should be of great benefit for this research. First, model predictions from three different case studies should provide enough output results in order to conclusively confirm or reject the main research assumptions. Second, considering multiple case studies enables testing the main research assumption on different types of extreme flood events, such as flash flooding and extreme river flooding in this research. This means that any research

outcomes can be generalised, as conclusions would not be dependent on characteristics of a particular flood event (such as type of terrain, response time etc.). This being the case, the research itself gains credibility, and consequently any practical applications based on the research outcomes could be applied to a wider range of flooding problems without major doubts in the proposed solutions.

4.2   The 2004 Boscastle flash flood

Boscastle is a picturesque village and small fishing port on the north coast of Cornwall, south-west England, UK. Being completely surrounded by sea, the climate of the south-west England is strongly affected by the maritime influences (i.e. the influence of the ocean on the land, which regulates the region's temperature) that balance the seasonal temperature range of the south-west England (Phillips and McGregor, 2001). Besides being governed by the general circulation of the atmosphere and the progression of the seasons, the variations in mean monthly temperature and rainfall in Cornwall are additionally influenced by sea temperature variations. Furthermore, local sea temperatures play an important role in determining the potential for shower activity, and have the ability to perpetuate and amplify weather anomalies (Phillips and Mcgregor, 2002). Due to these specific climate characteristics, long sea fetch to the west and the orographic trigger of the moorland areas in the inland (i.e. Cornwall and West Devon), the south-west England is highly prone to high-intensity precipitation events (Bleasdale, 1963, Clark, 1995, Phillips and McGregor, 2001).

The village of Boscastle is situated at the end of a steep, short and narrow valley that was cut by the River Valency. The River Valency has a catchment area of approximately 18 km^2, which is characterised by steeply incised tributaries and impermeable bedrock overlain by thin soils (Fenn et al., 2005, Roseveare and Trapmore, 2008). The small catchment area above Boscastle concentrates rainwater from surrounding steep hillslopes into a relatively narrow space, which descends towards the end of the valley and the location of Boscastle. Due to steep gradient, shallow soils and shape of the catchment, the village of Boscastle is particularly vulnerable to localised high-intensity rainfall events. Namely, these catchment

characteristics increase the velocity and volume of the river runoff during a high-intensity storm event, which can result in extremely rapid propagation of large amounts of water to the nearby sea, and the village of Boscastle (see Figure 4.1). All this makes the village of Boscastle particularly vulnerable to flash flooding.
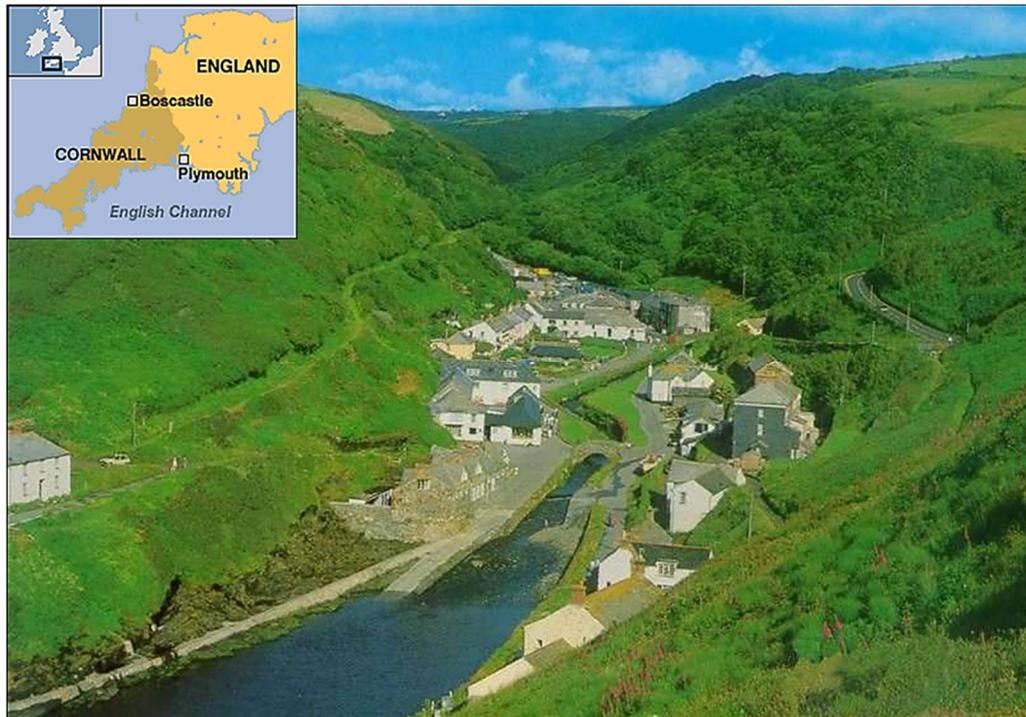
Figure 4.1: The village of Boscastle (Retrieved: November 3, 2014 from http://ayresriverblog.com/2011/08/12/uk-boscastle-2004-flash-flood-footage/)

In the first two weeks of August 2004, most of north Cornwall received above average rainfall, with Boscastle receiving about 25% more than normal (Golding et al., 2005). In addition, a slow-moving weakly baroclinic low pressure system spread over the UK on the 16th of August 2004 (Warren et al., 2014). Due to this unstable cyclonic situation, heavy showers developed in parts of south-west England by late morning on the same day. Furthermore, convergence effects between onshore winds and local topography lead to the repeated development of intense storm cells in the west and north Cornwall, particularly in the area around Boscastle (Burt, 2005). In addition, these storm cells repeatedly generated and propagated in much the same area over several hours, which meant that the heaviest precipitation fell on the same coastal catchments throughout the entire period of the storm event (Burt, 2005, Golding et al., 2005). This being the case, River Valency rose rapidly during the

afternoon on the 16th of August 2004 and resulted in the devastation of the village of Boscastle (see Figure 4.2). The 2004 Boscastle flash flood occurred due to combination of: (i) intense precipitation on the day of the flood, (ii) limited infiltration capacity of the soil due to the previous two weeks of above average rainfall and (iii) the steep gradient of the terrain around Boscastle. In the period of approximately 4 hours, over 250 mm of rainfall fell in the relative proximity of Boscastle (Burt, 2005). This extreme precipitation resulted in a 1 in 400 year flood event (Golding et al., 2005), while the total peak discharge was estimated to be between 150 and 180 m^3/s (Roca and Davison, 2010).

Figure 4.2: The 2004 Boscastle flash flood (Retrieved: November 3, 2014 from http://www.metoffice.gov.uk/learning/learn-about-the-weather/weather-phenomena/case-studies/boscastle)

The Boscastle study domain (see Figure 4.3) was 235 m wide, 665 m long and divided into square cells, with each square cell having an area of 1 m^2. The topographical data for the hydraulic model were collected after the flood using the LiDAR mapping technique, and can be seen in Figure 4.4. The roughness coefficients for the Boscastle study domain were estimated in the post-flood survey, which is in detail presented in HR Wallingford (2005). Since the computational domain was relatively small and had a short river reach, friction variation was

considered not to have any significant effect on the flood level predictions, and therefore a uniform Manning's coefficient of 0.040 was applied across the entire domain.

Figure 4.3: Sketch map of the Boscastle study domain (adopted from Google Maps)
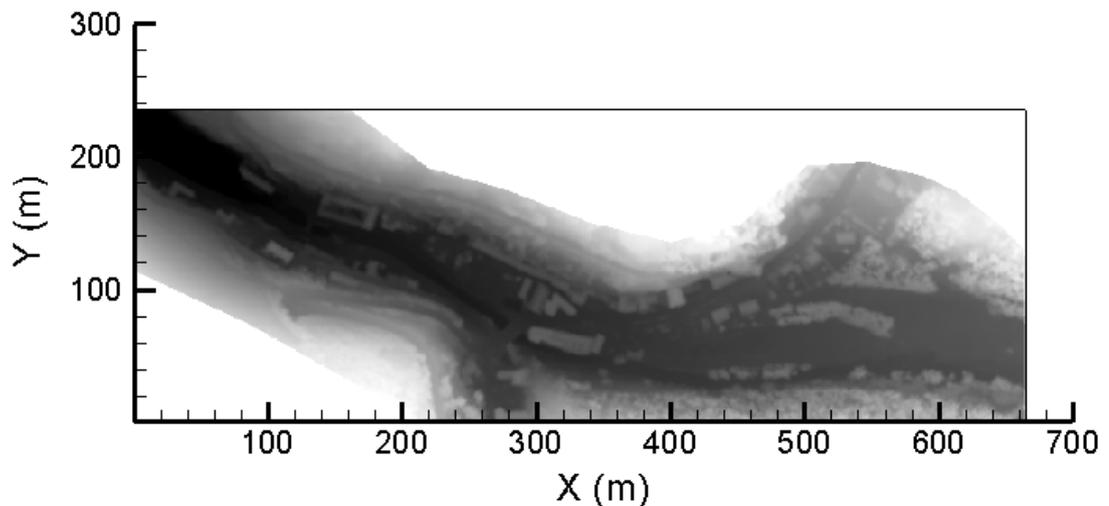
Figure 4.4: Representation of the topographical data for the Boscastle study domain

The eastern boundary of the domain was set as an inflow boundary for the River Valency. The considered hydrograph was based on the hydrological simulation conducted by HR Wallingford (2005), with the peak discharge being 140 m^3/s (see Figure 4.5). The western boundary was set as the seaward boundary, where the conditions were governed by the tide. According to HR Wallingford (2005), the actual tide level at the peak of the flood was approximately 0.8 m AOD (above ordnance datum), whereas the highest tide level of around 3.5 m AOD was measured approximately one hour after the peak of the flood had passed through the village of

Boscastle. Even thought there was a high tide during the flooding in Boscastle, the tide did not have any effect on the actual flood levels in the centre of the village (HR Wallingford, 2005). Therefore, the tidal water level variations were not included in the studies, and a prescribed water level of 3.5 m AOD was specified as the seaward boundary condition. In addition, a post-flood field survey was undertaken shortly after the 2004 Boscastle flash flood (HR Wallingford, 2005). The post-flood observations collected within this survey were used to validate the performance of different types of models considered in this research (see Chapter 5, section 5.2).
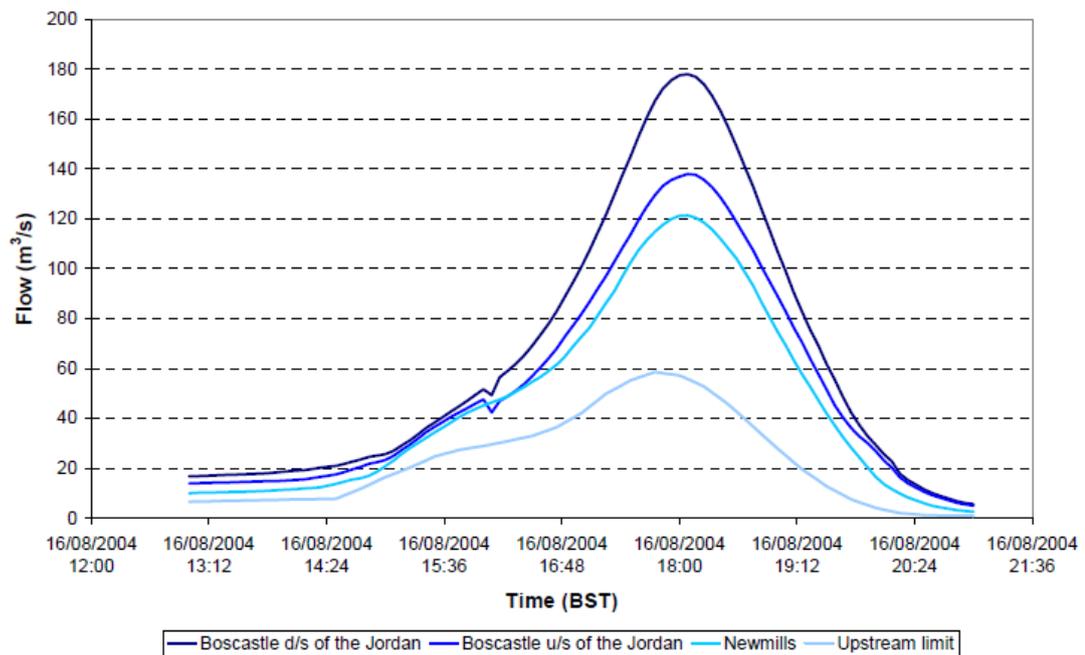
Figure 4.5: Hydrological simulation by HR Wallingford (2005), which was used to derive the inflow hydrograph for the Boscastle flood simulation

There are two bridges in the centre of village, i.e. the Lower Bridge and the B3263Road Bridge. According to eye-witness accounts, both bridges were blocked during the early stages of the flood event (HR Wallingford, 2005). To account for this in the hydraulic model, both bridges were modelled as being completely blocked, i.e. no flow propagated under either of the two bridges. In reality there would still have been some flow propagating through the bridges, but the amount of the propagating flow would have been relatively small. Therefore, there was no need to account for this in the hydraulic model, as the flow propagating through the bridges would not have had any considerable effect on flood level predictions.

Figure 4.6: Debris blocking the Lower Bridge (HR Wallingford, 2005)

4.3 The 2007 Železniki flash flood

Železniki is a small town in the north-west part of Slovenia. The north-west Slovenia is characterised by the extension of the Julian Alps, where many mountain peaks rise above 2000 m. This region has the highest mean value of precipitation in the entire Alps mountain range system, with the mean annual precipitation reaching values up to 3300 mm (Frei and Schär, 1998). The precipitation decreases from the west to the east, due to the rain shadow effect of the mountain ranges. The majority of precipitation in the north-western Slovenia is generally recorded before the arrival of a cold front associated with the Mediterranean cyclone (Vrhovec et al., 2004). The heavy prefrontal convection is triggered by the forced ascent over steep southern slopes of the Alps and as the warm and moist air lifts above the level of free convection (Zanon et al., 2010).

Figure 4.7: The town of Železniki (Retrieved: March 21, 2016 from http://www.publishwall.si/zelezniki/search/-/photos/0/2013/01)

The town of Železniki is situated in the long and narrow Selca Valley (see Figure 4.7), which stretches along the River Selška Sora. The Selca Valley, and in particular the Selška Sora catchment area upstream of Železniki, is characterised by a steep topographical terrain, high-gradient channels and relatively thin soils on the hillslopes (i.e. 0-50 cm) (Zanon et al., 2010). The rainfall events in the Selška Sora catchment area upstream of Železniki are strongly influenced by the orography, with the annual precipitation ranging between 1700 and 2300 mm (Marchi et al., 2009). Due to these topographical and meteorological characteristics, the Selška Sora catchment area upstream of Železniki is often hit by flash flooding, with at least 12 remarkable flash flood events being recorded in the last century (Komac et al., 2008). As the town of Železniki is the administrative centre, economic hub and the largest settlement in the Selca Valley, it is therefore considered as an area of high flood risk and particularly vulnerable to flash flooding.

On the 18th of September 2007, a region of low air pressure moved over western and middle Europe towards the Alps. In addition to a low-pressure weather system, a high valley of cold air moved over Western Europe towards the east, meanwhile a south-western wind was getting stronger over Slovenia. As a result of these complex weather conditions, an extensive convective system formed over the north-western part of Slovenia, which led to the occurrence of an extreme rainfall event that affected approximately one third of the country (Slovenian Environment Agency, 2008). More than 300 mm of rainfall was recorded on some rain-gauge stations within six hours after the start of the storm, with the return period of the highest precipitation being more than 100 years (Kobold et al., 2008).

In Železniki, the observed maximum daily amount of rainfall was around 220 mm, which was the highest recorded amount of rainfall since the beginning of the measurements in 1930 (Grillakis et al., 2010). Furthermore, the cumulated areal rainfall in the Selška Sora catchment area upstream of Železniki was the second largest rainstorm for duration between 15 and 20 hours in the list of 25 extreme flash floods that occurred in Europe in the period between 1994 and 2008 (Marchi et al., 2010). The accumulated rainfall resulted in a flood event that by far exceeded the 100-year return period of maximal floods, with the estimated peak discharge being around 300 m^3/s (Marchi et al., 2009, Zanon et al., 2010). In addition, River Selška Sora exceeded the highest water level recorded so far, with the highest water level reaching up to 551 cm (Rusjan et al., 2009). The flash flood triggered by the intense precipitation devastated the town of Železniki: three people lost their lives, while the damage due to flooding was estimated to be €100 million (Bouilloud et al., 2009).

Figure 4.8: The 2007 Železniki flash flood (Retrieved: March 21, 2016 from https://mojalbum.com/culto/zelezniki-poplave-2007/foto/9457818)

The Železniki study domain (see Figure 4.9) was 1966 m long, 1285 m wide and divided into square cells, with each cell having an area of 1 m^2. Topographical data for the Železniki study domain was collected during the national project of LiDAR scanning of the Slovenian surface (see Ministry of the Environment and Spatial Planning of the Republic of Slovenia, 2015), and can be seen in Figure 4.10. The roughness coefficients for the Železniki study domain were evaluated by Lamovec et al. (2012), with the evaluation being based on the field conditions. Taking into account relatively short river reach, it was once again predicted that friction variation would not have had any significant effect on the flood level predictions. This being the case, a uniform Manning's coefficient of 0.040 was applied across the entire domain. The western boundary of the domain was set as an inflow boundary for the River Selška Sora. The considered hydrograph was based on the hydrological simulation conducted by Rusjan et al. (2009), with the peak discharge being 280 m^3/s (see Figure 4.11). The eastern boundary of the study domain was set as the downstream boundary, with a water level time series being specified as the downstream boundary condition (see Slovenian Environment Agency, 2015b).

Figure 4.9: Železniki study domain (adopted from Google Maps)
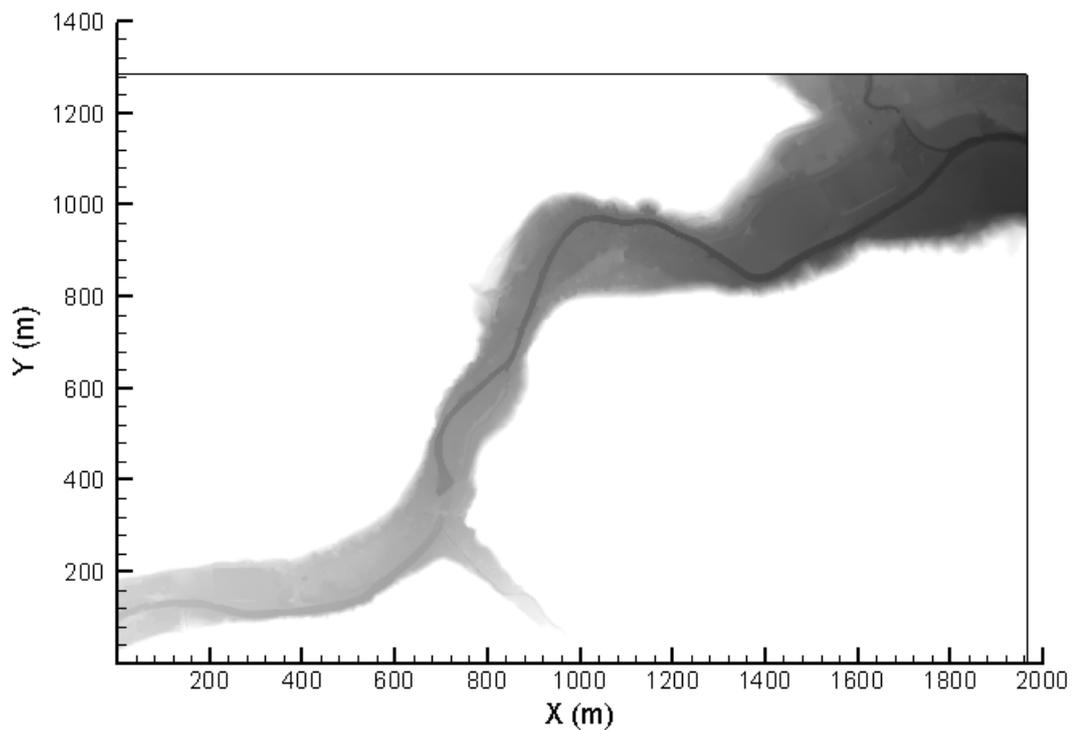
Figure 4.10: Representation of the topographical data for the Železniki study domain

In the post-event survey after the 2007 Železniki flash flood, several eye-witnesses were interviewed in order to reconstruct the time evolution of the flood, e.g. the timing of onset and end of rainfall, the presence of hail, the time of rise, peak and

recession of the flood, and the nature of the flow process (i.e. water flood or debris flow) (Zanon et al., 2010). Even though there were reports of backwater effects due to channel obstruction in the area upstream of Železniki, it was concluded that these effects did not have any effect on the peak discharge and the flood propagation further downstream, i.e. in the town of Železniki (Marchi et al., 2009). Although large amounts of sediment and woody debris were transported during the flood, there were no reports suggesting that any blockages formed in the town of Železniki. This being the case, there was no need to specifically model any of the aforementioned effects in the hydraulic model for the Železniki study domain.
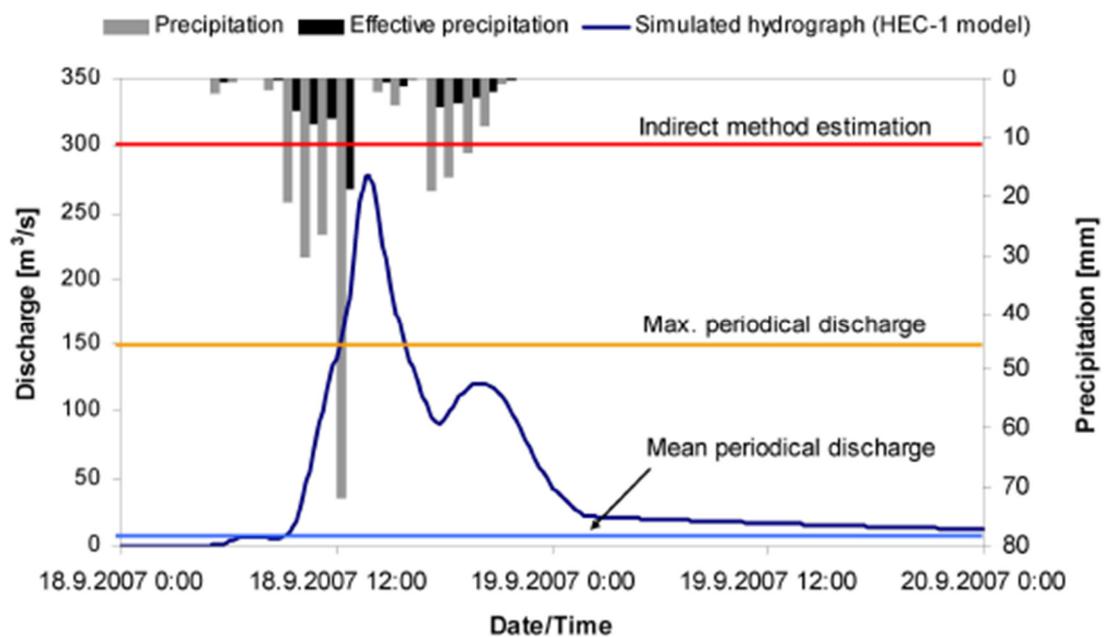
Figure 4.11: Hydrological simulation by Rusjan et al. (2009), which was used to derive the inflow hydrograph for the Železniki flood simulation

4.4 The 2010 Kostanjevica na Krki extreme river flood

Kostajevica na Krki is one of the oldest and smallest towns in Slovenia. It is located in the south-eastern part of Slovenia, near the border with Croatia. The centre of the town lies on a small artificial island, which is surrounded by the River Krka (see Figure 4.12), and is protected as a cultural town with historical monuments.

Figure 4.12: The town of Kostanjevica na Krki (Retrieved: March 23, 2016 from https://www.rtvslo.si/kultura/razstave/arhitekturni-obraz-kostanjevice-na-krki-od-zasnove-iz-13-stoletja-do-plecnika/287808)

River Krka is a distinctly karst river in its upper reach and is deeply incised in the karst bed rock, which means that there are almost no (wider) floodplains along the main channel and thus flooding there is scarce (Komac et al., 2008). However, River Krka becomes a typical low-land river in its lower reach, with its floodplains significantly widening out in the proximity of the town of Kostanjevica na Krki (Šifrer et al., 1980). In Slovenia, lowland floods generally occur in lower reaches of major watercourses, such as River Sava and River Krka. The flooding in these areas occurs due to the difference between the water inflow rate and the drainage capacity of the river channel during intense and prolonged precipitation. Namely, water rapidly propagates from the nearby higher ground to the main river channel, which very quickly reaches a maximum flow rate. This being the case, the rapidly increasing water volume in the main river channel eventually overtops the channel banks resulting in the flooding of the surrounding floodplains (Komac et al., 2008). The River Krka basin is generally hit by flooding several times per year, the typical duration of an individual flood event is between 1 and 3 days, and the maximum flood levels can measure up to 4 meters in height on floodplains (Perko, 1998). As the town of Kostanjevica na Krki is located on the wide floodplain of the River Krka,

it is frequently endangered by flooding. Furthermore, due to frequent flooding, and its rich historical and cultural heritage, the town is also promoted as the "Venice of Lower Carniola".

During the period between 17th - 19th September 2010, Slovenia was hit by heavy and extensive precipitation, which led to a sharp rise in the water levels in watercourses all over the country (Slovenian Environment Agency, 2010a). In the territory of Slovenia an average of 170-180 mm of rainfall fell over 48 hour period, which was the highest amount of rainfall accumulated in a two-day period over the past 60 years (Slovenian Environment Agency, 2010b). This intense precipitation resulted in state-wide flooding, where 137 municipalities (i.e. 60% of territory) were affected. The damage was estimated to be €240 million, with the floods being characterised by exceptionally high water levels, long duration and great variety of different flood types, such as flash floods, lowland (riverine) floods, karst floods and urban flooding (Komac and Zorn, 2013).

The River Krka started flooding on the evening of 18th September, and on the 19th September the town of Kostanjevica na Krki was flooded (see Figure 4.13) (Kobold, 2011). The data from the nearby stream gauge station at Podbočje revealed that the peak discharge of 468 m^3/s occurred on 20th of September (Slovenian Environment Agency, 2010a). This was the highest measured discharge for the River Krka since the beginning of measurements in 1926, and statistically corresponds to nearly a 1 in 1000 year flood event (Kobold, 2011, Slovenian Environment Agency, 2013). The maximum recorded water level of River Krka in the nearby stream gauge station at Podbočje was 457 cm, while the depth of the flood water in the Kostanjevica na Krki town centre was approximately 120 cm (Slovenian Environment Agency, 2010a).

Figure 4.13: The 2010 Kostanjevica na Krki extreme river flood (Retrieved: March 23, 2016 from http://www.24ur.com/novice/slovenija/pregled-najhujsih-poplav-v-sloveniji-najbolj-smrtonosne-so-bile-na-celjskem-leta-1954.html)

The Kostanjevica na Krki study domain (see Figure 4.14) was 705 m long, 641m wide and divided into square cells, with each cell having an area of 1 m^2. The topographical data for the Kostanjevica na Krki study domain was collected during a national project of LiDAR scanning of the Slovenian surface (see Ministry of the Environment and Spatial Planning of the Republic of Slovenia, 2015), and can be seen in Figure 4.15. The roughness coefficients for the Kostanjevica na Krki study domain were estimated within this research by using the land use maps and orthophoto images of the considered computational domain. Furthermore, the estimation of roughness parameters was also based on the expert opinions of the personnel at the Faculty of Civil and Geodetic Engineering of University of Ljubljana, Slovenia, who conducted hydraulic studies for similar sites on the River Krka. Similar to the two aforementioned case studies, friction variation was predicted not to have any significant effect on the flood level predictions, and therefore a uniform Manning's coefficient of 0.030 was applied across the entire domain. The western boundary of the domain was set as an inflow boundary for the River Krka, with the peak discharge being 467 m^3/s. The area where the River Krka leaves the

study domain was set as the downstream boundary, with a water level time series being specified as the downstream boundary condition (see Figure 4.16).
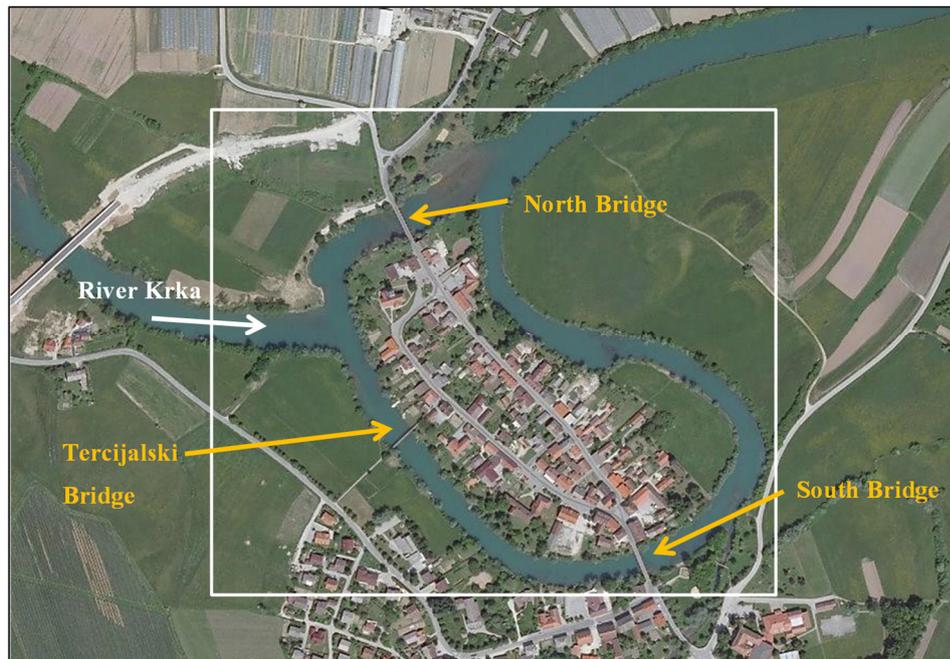
Figure 4.14: Kostanjevica na Krki study domain (adopted from Google Maps)
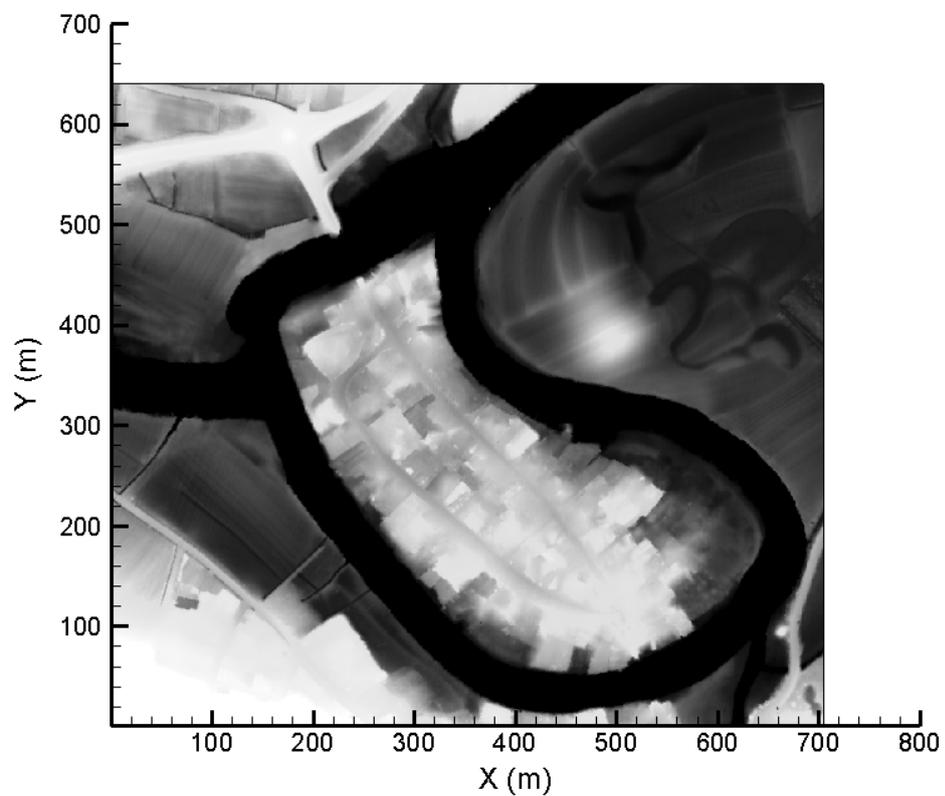
Figure 4.15: Representation of the topographical data for the Kostanjevica na Krki study domain
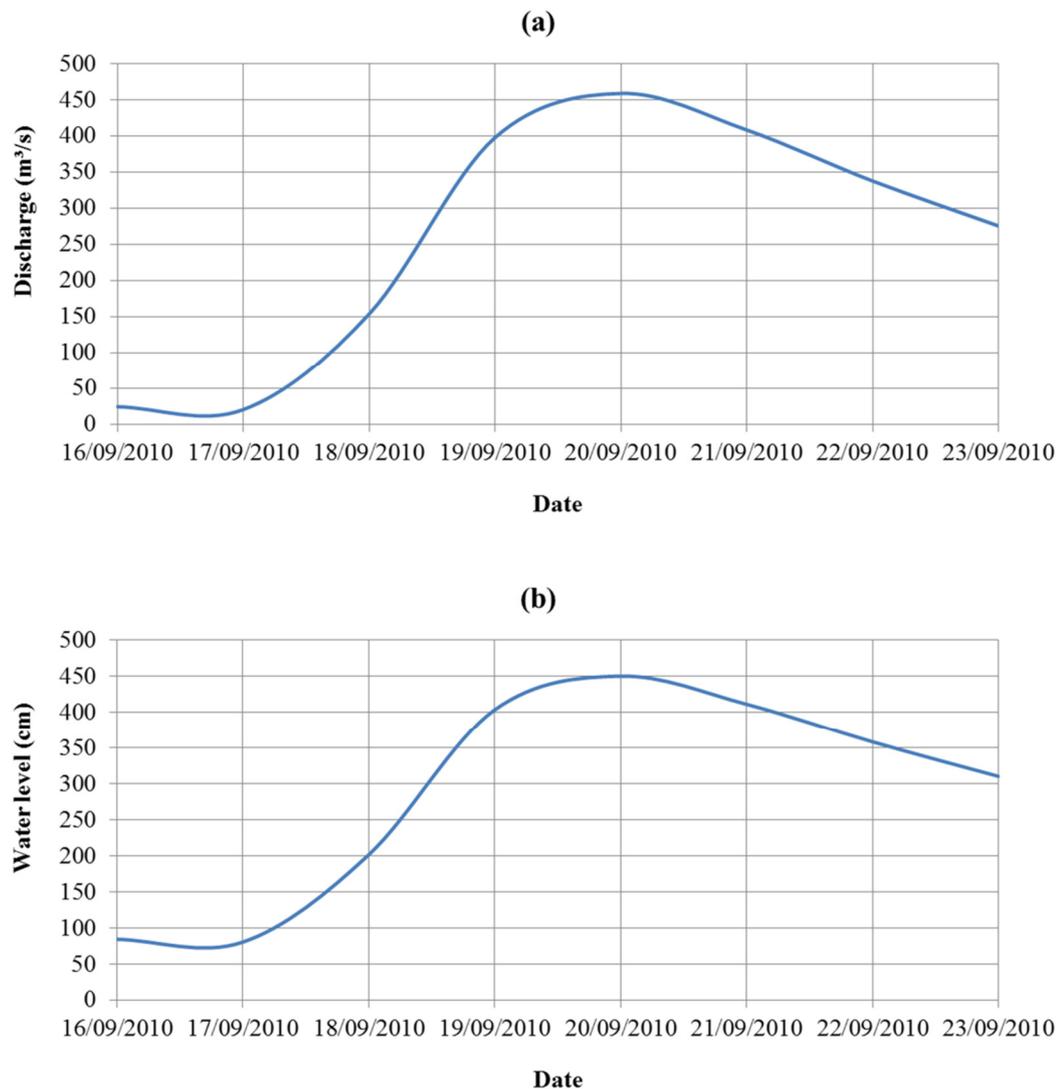
Figure 4.16: Upstream (a) and downstream (b) boundary condition for the Kostanjevica na Krki flood simulation (adopted from Slovenian Environment Agency (2015a))

Three wooden bridges connect the old town centre with the surrounding area, i.e. the North Bridge, the South Bridge and the Tercijalski Bridge. There were no official reports or eye-witness accounts suggesting that any of the three bridges were blocked during the time of the flood event. This being the case, there was no need to specifically model bridges in the hydraulic model for the Kostanjevica na Krki study domain (e.g. limited propagation of the flow through the bridges due to debris blockage etc.).

4.5 Summary

Three different case studies were presented in this chapter, i.e. the 2004 Boscastle flash flood (England, UK), the 2007 Železniki flash flood (Slovenia), and the 2010 Kostanjevica na Krki extreme river flood (Slovenia). The common feature of all three considered flood events is intense and heavy precipitation. On the other hand, these three considered flood events occurred in two completely different types of river basins. Both flash floods occurred in short, narrow and steep river basin, while the extreme river flood occurred in generally flat and wide river basin. This indicates that extreme flood events can occur practically anywhere, and that the occurrence of extreme flooding is due to a combination of different complex factors, such as characteristics of the rain and catchment characteristics. Therefore, considering two different types of extreme flood events that occurred in two different types of river basins should be very beneficial for this study, as any potential conclusions should be independent of specific parameters that lead to occurrence of extreme flood events. This being the case, any potential research outcomes could be generalised, and thus applicable to any area (i.e. type of terrain) where the occurrence of extreme flood event is possible.

CHAPTER 5

Flood inundation modelling of extreme flood events

5.1 Introduction

This chapter presents the evaluation of different types of flood inundation models for predicting flood elevations, velocities and inundation extent for extreme flood events. Furthermore, it also presents the investigation of the appropriateness of the "simplification strategy" often used when modelling flood events characterised with high Froude number flows, i.e. applying high roughness coefficients in order to dampen out numerical oscillations and improve model predictions. Section 5.2 describes the research process and the methods implemented, Section 5.3 presents the main findings and evaluation of the modelling results, and finally Section 5.4 provides the summary of the main findings.

5.2 Methodology

The first key objective of this research study was to determine what type of flood inundation models should be used for predicting flood elevations and inundation extent for extreme flood events. This being the case, the well documented 2004 Boscastle flash flood event was simulated using three different flood inundation prediction model structures, including: (i) the shock-capturing flood inundation model (i.e. the TVD simulation case), (ii) the regular ADI-type flood inundation model (i.e. the ADI simulation case), and (iii) the regular ADI-type flood inundation model with no advection terms (i.e. the SI simulation case). For the TVD simulation case, the full shock-capturing ability of the DIVAST-TVD model was included. For the ADI simulation case, the flood simulations were undertaken using the DIVAST model, a regular ADI-type flood prediction model. For the SI simulation case, the advection terms were excluded in the DIVAST model, and thus the DIVAST model worked on the principle of the "local inertial" or "simplified inertial" approach (Hunter et al., 2007, Bates et al., 2010, de Almeida et al., 2012).

The objective of the comparisons was therefore to establish the main differences between these three modelling approaches when simulating flood events where abrupt changes of flow occur, such as for the case of flash flooding or dam-break scenarios. In order to compare the computational ability of these three different modelling approaches, all three simulation cases were run under the same conditions, i.e. the same boundary conditions, Manning's coefficient and the same model time-step. The initial assumption was made that only the TVD simulation case would generate numerically accurate results, whereas the ADI and SI simulation cases were likely to give less numerically accurate flood level and inundation extent predictions. The latter two simulation cases did not have appropriate mechanisms to absorb numerical oscillations, which often occur for rapidly varying flows (Liang et al., 2006, Moussa and Bocquillon, 2009, Neal et al., 2012), and were thus susceptible to produce erroneous results.

Simulation results were compared to actual post-flood field measurements and observations. As mentioned in section 4.2, a survey of flood marks was undertaken after the 2004 Boscastle flash flood event (HR Wallingford, 2005). The peak water levels during the flood are frequently marked by a collection of floating branches or rubbish that were carried by the flow, with these marks being referred to as wrack marks. Although there are some reservation regarding the accuracy of the wrack marks (e.g. wrack marks may not always correspond to the highest water levels), the wrack marks still provide the best indication of actual flood levels (HR Wallingford, 2005). This being the case, wreck marks were used to validate the performance of the three different flood inundation model structures.

The second key objective of this research study was to investigate the appropriateness of the "simplification strategy" when used as a flood risk assessment modelling tool for areas susceptible to extreme flooding. As it was indicated in Section 2.2.3, flood risk assessment practitioners often apply "simplification strategy" in order to save time and resources, or to decrease the complexity of the modelling problem they are dealing with. As mentioned, the ADI-type models (i.e. the model-of-choice for majority of flood risk assessment practitioners) are prone to emergence of spurious numerical oscillations when modelling rapidly varying flood events (such as flash floods and dam-break floods), and thus generally produce

numerically inaccurate results for such flood events (Liang et al., 2006, Neal et al., 2012, Neelz and Pender, 2013). In order to dampen out numerical oscillations, it is believed that flood risk assessment practitioners often apply a form of "simplification strategy" by implementing an artificially high bed resistance coefficient in the flood inundation modelling process. The increased roughness parameter should decrease the velocity of the flow and therefore result into more gradually changing flow regime. This being the case, the numerical stability of the model should increase and thus resolve the problem with the emergence of numerical oscillations in the model solution.

In order to test this assumption (i.e. the appropriateness of this "simplification strategy"), attempts have been made within this research to improve on the simulation results for the ADI simulation case. This means that additional simulations were conducted with the model structure used in the initial ADI simulation case, where the value of roughness parameter (i.e. Manning's n) was gradually increased for each simulation run. The idea was to keep increasing the value of the roughness parameter until the model predictions generally matched the observed values. This being the case, more than 30 additional simulations were conducted with the ADI model structure. Only the relevant results are presented in this thesis due to the large number of additional simulations.

5.3 Predictions of flood levels and inundation extent

As stated earlier, all three simulation cases were run for the same conditions, i.e. with the same upstream and downstream boundary conditions, Manning's coefficient of 0.040 across the entire study domain, model time-step of 0.04 s and the Courant number set to 1. The differences between these three different model structures can be readily identified by a direct comparison of the flood level predictions against observed wrack marks that were obtained from a post-flood survey of flood marks (HR Wallingford, 2005). The collected data is reproduced in Table 5.1, while Figure 5.1 shows the position of the surveyed wrack marks in the village of Boscastle.
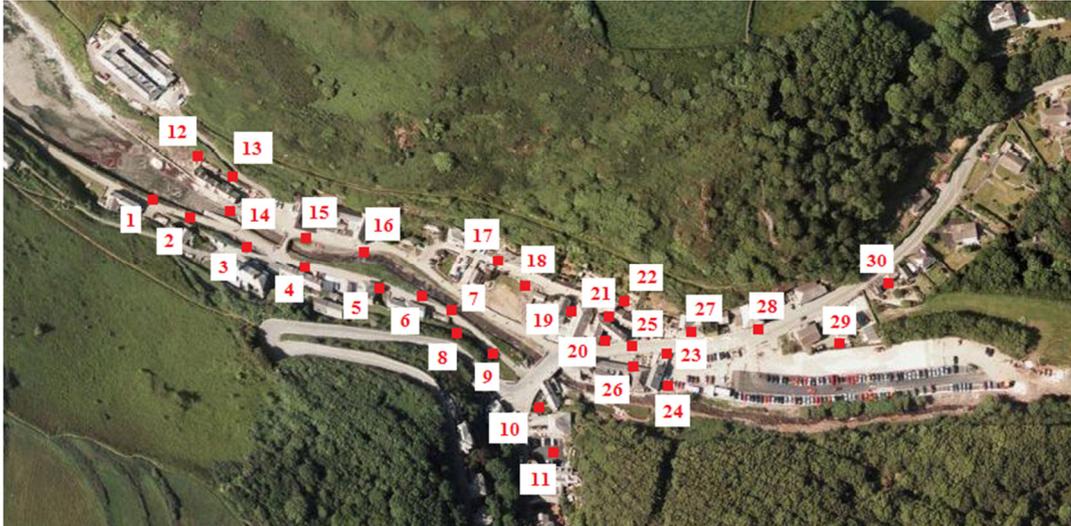
Figure 5.1: Locations post-flood surveyed wrack marks in the village of Boscastle (adopted from Google Maps and HR Wallingford (2005))

Figure 5.2 shows a comparison between the observed flood levels (i.e. wrack marks) and the predicted flood levels for three different model configurations, i.e. the TVD, ADI and SI simulation cases. In Figure 5.2, it can be seen that results for the TVD simulation case generally fit the post-flood surveyed wrack marks. Nonetheless, the results from the TVD simulation case differ more obviously at marked positions 4, 19, 23 and 27. At marking positions 4 and 27 the TVD simulation case slightly over-predicts the flood levels. However, according to the comments made by the observers (see Table 5.1) the maximum flood level at marked positions 4 and 27 were probably higher than those recorded. This suggests that at these two marked positions the results from the TVD simulation case do not differ too significantly from the actual flood levels occurring during the event. At the marked positions 19 and 23, the TVD simulation case over-predicts the flood level by nearly 1 m. However, this big difference in the flood level predictions is most likely due to the too simple modelling approach for this particular section. The marked positions 19 and 23 were selected between buildings where the space was very limited. To get more accurate results for such a small space, a more densely distributed grid would be necessary to represent these areas more accurately (Ozdemir et al., 2013). Overall, the TVD simulation case results appear to reproduce the wrack marks most accurately.

131

Table 5.1: Post-flood measurements of flood levels (HR Wallingford, 2005)

Marking position	Estimated elevation (m AOD)	Comment to observation	Marking position	Estimated elevation (m AOD)	Comment to observation
1	6.1	Gravel washed away and trash mark	16	9.99	Trash caught on wall
2	6.33	Vegetation marked and flattened	17	10.84	Trash caught on wall
3	8.01	Trash on road and flattened vegetation	18	11.53	Max level may have been higher
4	8.28	Max level probably higher	19	11.35	Internal water level on window
5	9.64	Max level possibly higher	20	12.58	Debris on wall
6	9.79	Levels on windows ties in with trash caught on trees	21	12.53	Damp line on wall
7	9.98	Max level possibly higher	22	12.46	Debris caught on cable. Max level estimated
8	11.18	/	23	12.76	Trash on steps and railing
9	10.64	Mark possibly caused by surge	24	13.58	/
10	12.99	Trash mark	25	13.38	Maximum level reached by resident
11	13.86	Mud caught on vegetation	26	13.46	Maximum level reached by resident
12	8.25	Water spilled over wall	27	13.16	Maximum level possibly higher
13	8.38	/	28	14.34	Level given by landlord as underside of window
14	8.48	Trash mark on road and side of road	29	15.05	Level Marked by resident
15	9.34	Water level possibly lower	30	16.27	Level indicated by friend of owner. Still water level
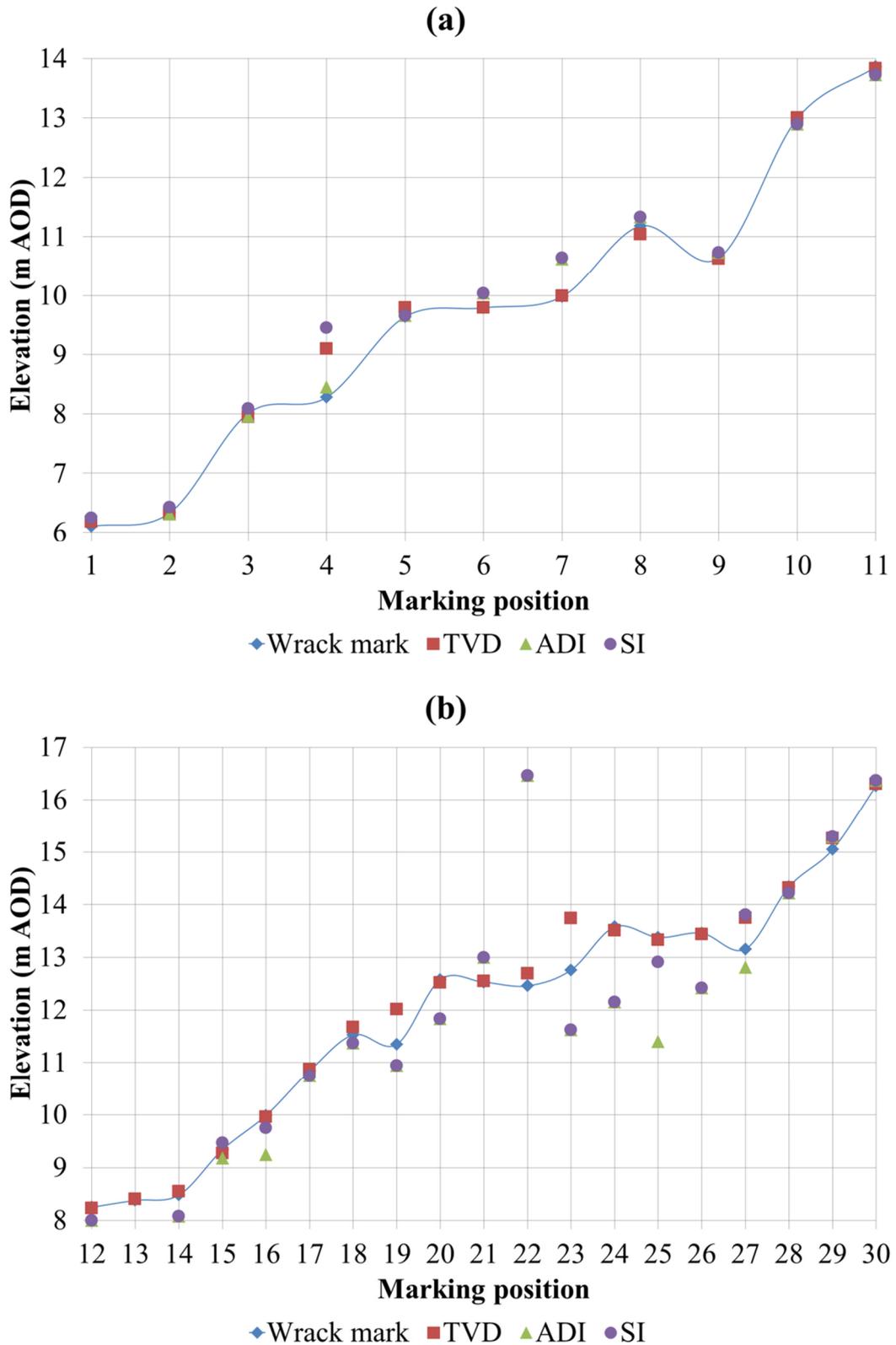
Figure 5.2: Comparison between predicted flood levels for the TVD, ADI and SI simulation cases and post-flood surveyed wrack marks: (a) shows comparisons of the marking positions on the western side of the flood pathway (marks 1-11), while (b) shows the comparisons on the eastern side of the flood pathway (marks 12-30)

Figure 5.2 also shows that the SI simulation case generally under-predicted the peak flood levels, with more significantly under-predicting the peak flood levels in at least 8 marking positions (i.e. at marking positions 12, 14, 19, 20, 23, 24, 25 and 26). The inaccuracy in this approach was as expected, since the "simplified inertia" approach is too basic for simulating the extreme flood events. The advection terms can be neglected without any major influence on the predicted water levels if the Froude number is well below 0.5, whereas at flows with higher Froude numbers discontinuities and errors start to appear (Katopodes and Schamber, 1983, Hunter et al., 2007, Neal et al., 2012). Models based on the simplified version of the shallow water equations (e.g. diffusion wave models, kinematic wave models, inertial models) can be used to simulate extreme flooding to a limited extent (Moussa and Bocquillon, 2009), but such models are generally erroneous for examples where the depth and velocity changes are very rapid (Neal et al., 2012, Neelz and Pender, 2013), something which often occurs during a flash flood. Overall, the results suggest that the SI simulation predictions are numerically inaccurate, and as such would lead to erroneous flood inundation maps.

Figure 5.2 further shows that the ADI simulation case also generally under-predicted the peak flood levels, with more significantly under-predicting the peak flood levels in at least 10 marking positions (i.e. at marking positions 12, 14, 16, 19, 20, 23, 24, 25, 26 and 27). The inaccuracy in this approach was as expected, since the ADI-type models are also too basic for simulating high Froude number flows (Liang et al., 2006, Neal et al., 2012, Neelz and Pender, 2013). For example, Figure 5.3 shows the maximum Froude number values at different stages of the Boscastle flood simulation. It can be seen from Figure 5.3 that the super critical flow regime occurred almost immediately after the start of the simulation. As mentioned, super critical flow conditions are often characterised with abrupt changes in the flow regime, such as hydraulic jumps. These act as discontinuities in the numerical solution procedure, which usually lead to the generation of spurious numerical oscillations for the ADI-type numerical schemes. These oscillations can be easily seen by observing a time-series of depth predictions from a point located in an area where Froude numbers were high (i.e. near or above 1). Figure 5.4a shows the maximum Froude number values for the Boscastle flood simulation, with black circle

marking the area where the observation point was located, while Figure 5.4b shows a part of the depth time-series recorded in the selected point.
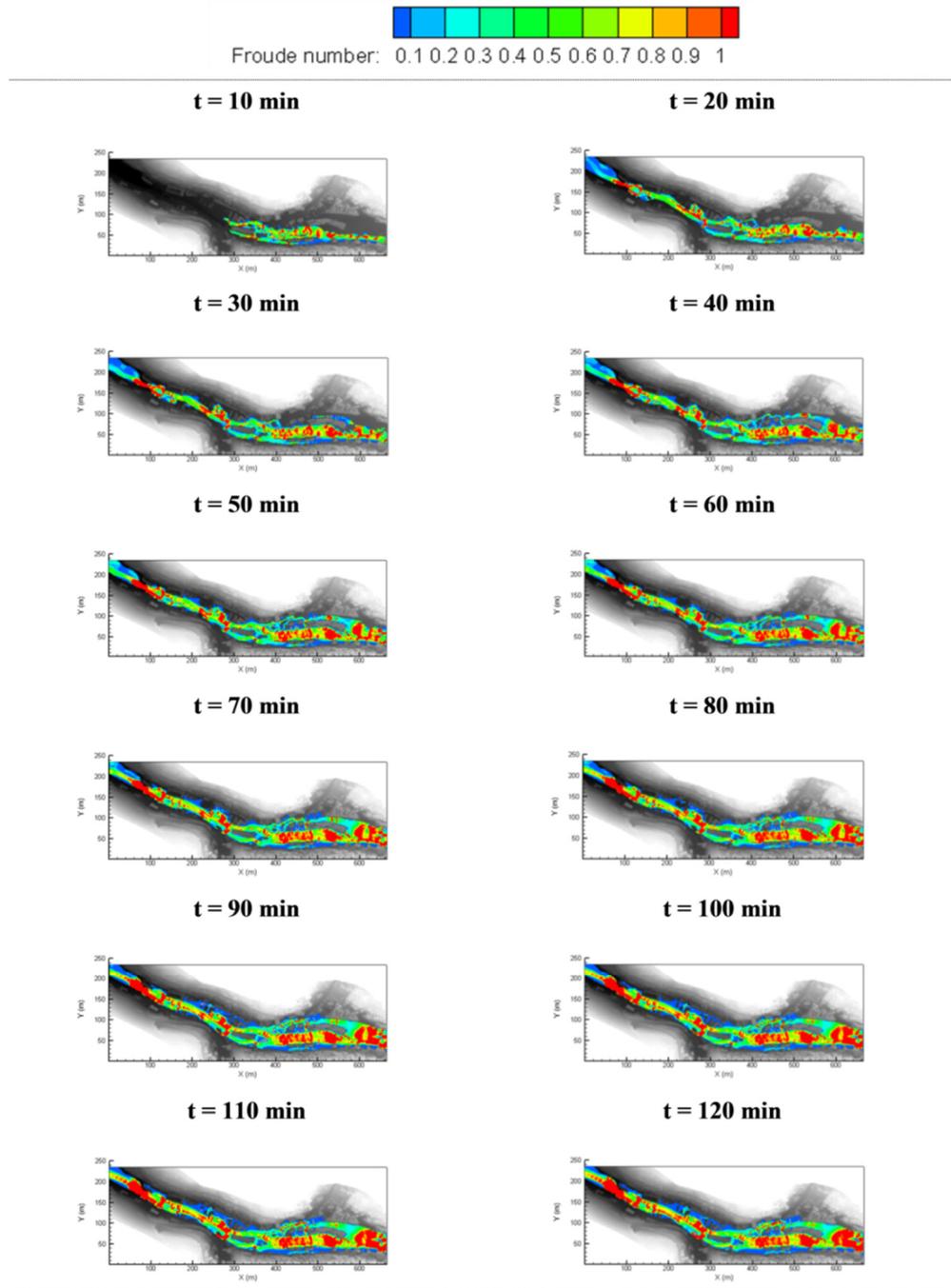
Figure 5.3: Maximum Froude number values at different stages of the 2004 Boscastle flash flood simulation

In Figure 5.4b, it can be nicely seen the presence of numerical instabilities, which quickly lead to a complete dissipation of the flood wave in this point (i.e. all depth

prediction after 15 minutes of the simulation are equal to zero). When the area marked in the black circle is compared to the same area in Figure 5.6, it can be seen that there is very limited flood extent predicted in this region by the ADI model configuration (see Figure 5.6). This only further indicates that ADI-type models are prone to occurrence of numerical instabilities when modelling high Froude number flows (e.g. flash floods), which consequently leads to erroneous results, i.e. under-prediction of the peak flood elevations. All in all, the presented results clearly suggest that the ADI simulation results are numerically inaccurate, and thus would lead to production of inaccurate flood inundation extent maps for areas prone to occurrence of high Froude number flows, such as the Boscastle flood simulation considered in this study.
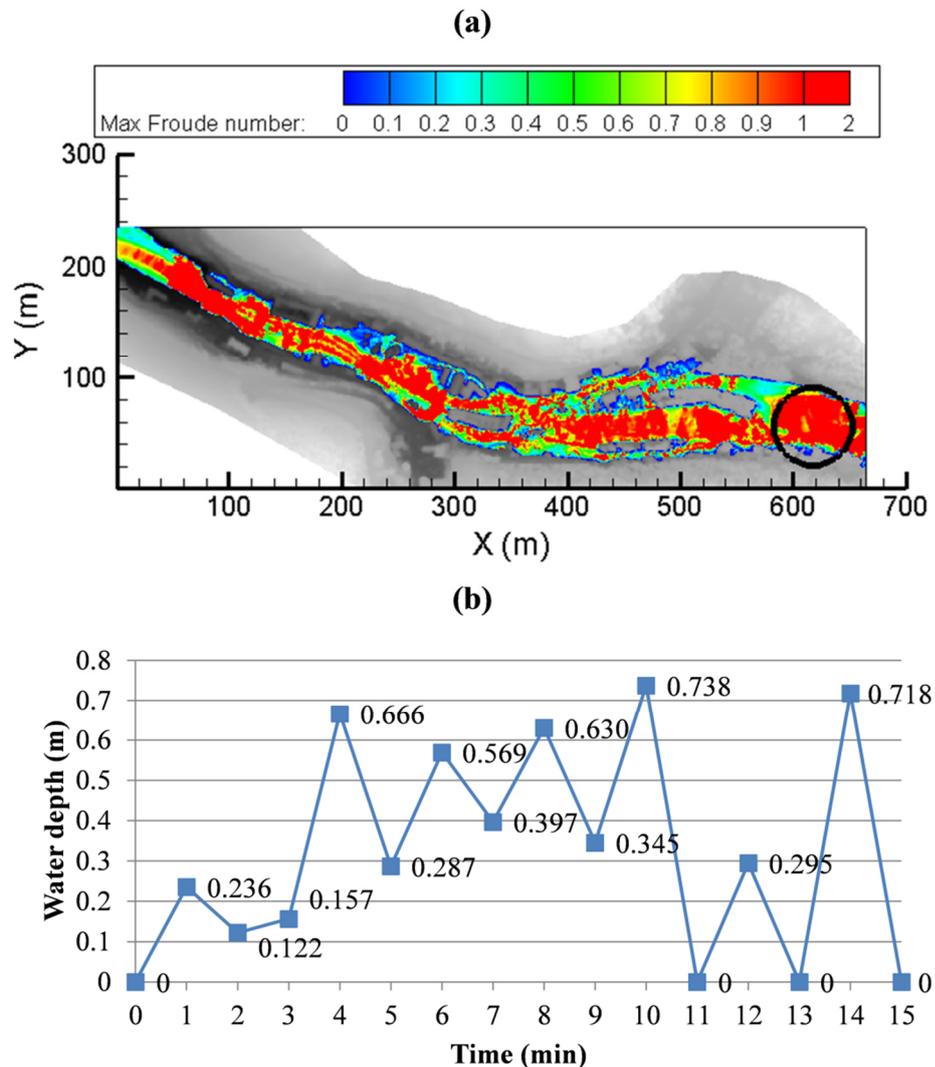
Figure 5.4: Location of the selected monitoring point (a) and the numerical instabilities in the ADI simulation case (b) at the selected point

The difference between the simulation results becomes more obvious when the water depths and the inundation extent from all three simulation cases are compared. Figure 5.5 (i.e. SI simulation case), Figure 5.6 (i.e. ADI simulation case), and Figure 5.7 (i.e. TVD simulation case) show the predicted maximum water depths and inundation extent for each simulation case. When these results were compared to results obtained in other studies, such as HR Wallingford (2005), Roca and Davison (2010) or Xia et al. (2011), it could be seen that the TVD simulation case generally accurately predicted the flood depths and inundation extent, whereas the SI and ADI simulation cases inaccurately predicted flood depths and inundation extent. As stated earlier, the ADI and SI simulation cases inaccurately predicted the main hydrodynamic parameters due to the numerical instabilities (i.e. spurious numerical oscillations) caused by abrupt changes in the flow regime, which often occur with extreme flood events. These numerical oscillations have swamped the flood wave prediction, and therefore resulted in erroneous flood level and inundation extent predictions. These results again confirm the initial assumption, i.e. the ADI and simplified models are inappropriate for simulating extreme flood events, such as the flash flood scenario considered in this study.
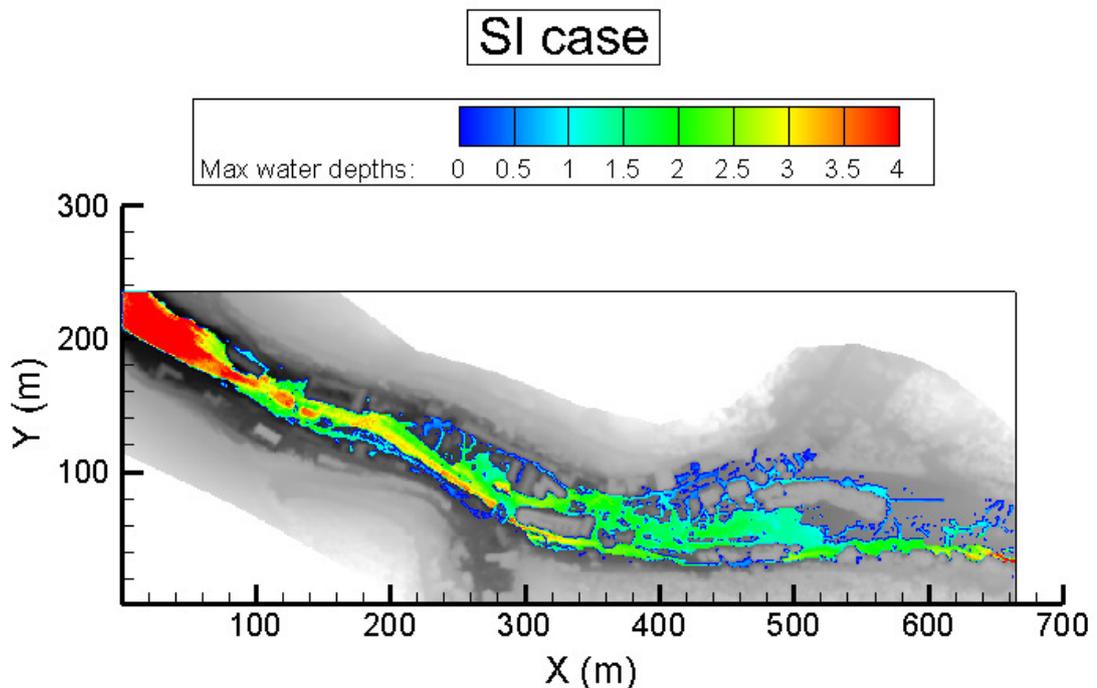
Figure 5.5: Predicted maximum water depths for the SI simulation case
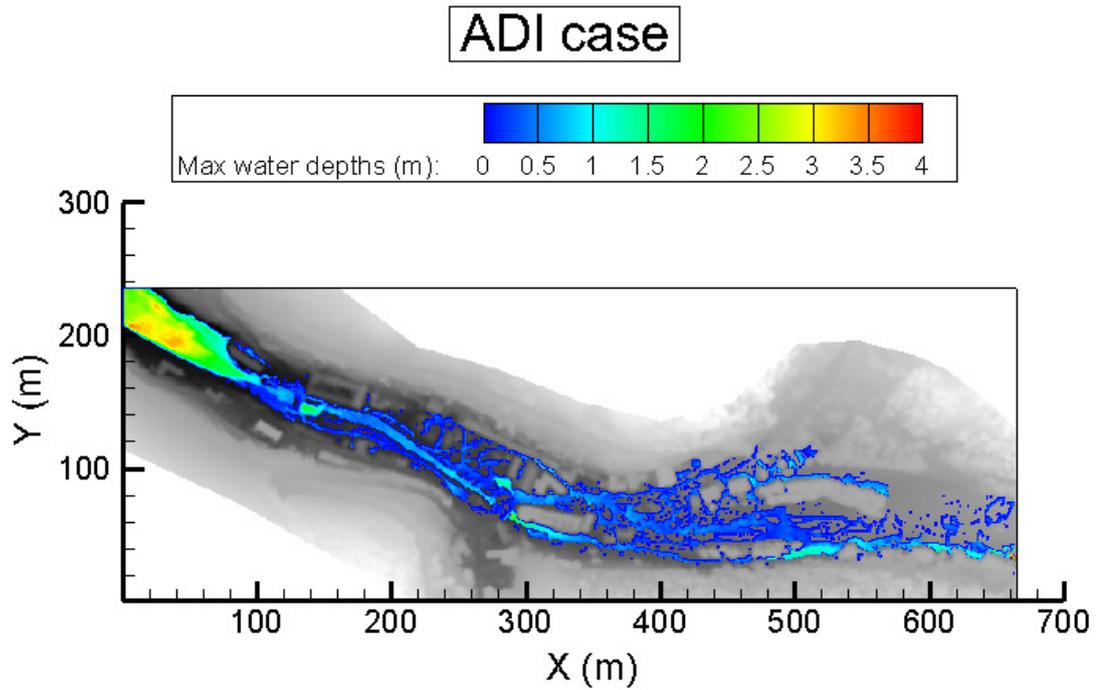
Figure 5.6: Predicted maximum water depths for the ADI simulation case
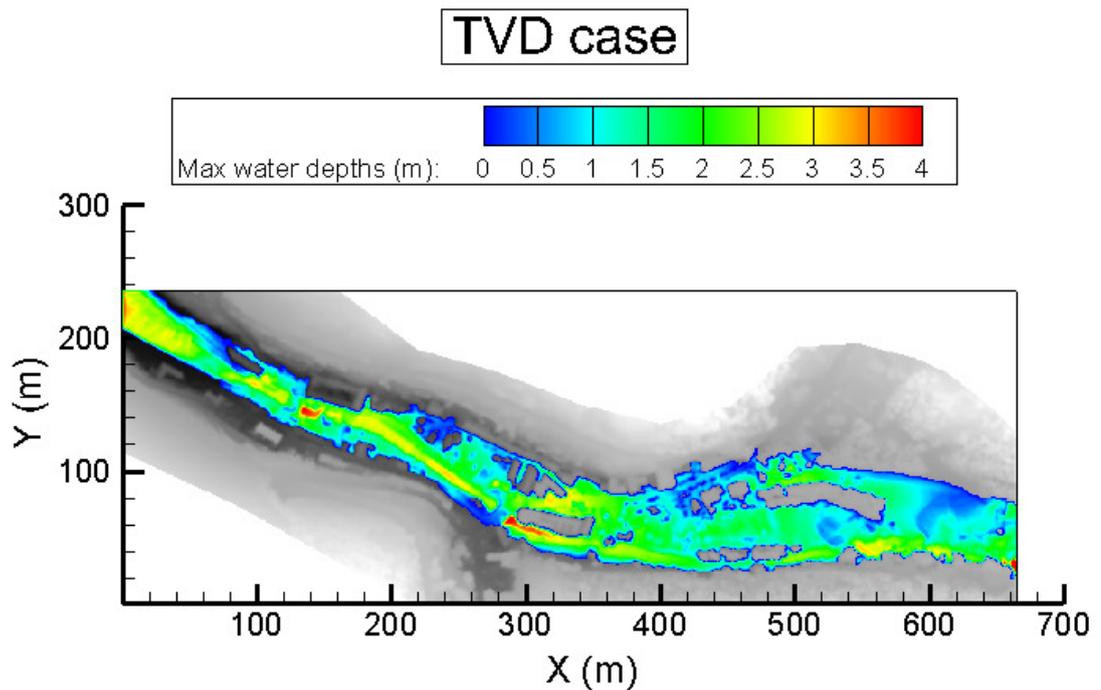
Figure 5.7: Predicted maximum water depths for the TVD simulation case

In addition to the comparisons presented above, the Nash-Sutcliffe model efficiency coefficient (NSE) was used to measure the predictive capability of the TVD, ADI and SI simulation cases, and provide the last evaluation of the simulation results

presented in this section. The NSE was introduced by Nash and Sutcliffe (1970), and is based on the following equation:

$$NSE = 1 - \frac{\sum_{i=1}^{n}(O_i - S_i)^2}{\sum_{i=1}^{n}(O_i - \bar{O})^2} \tag{5.1}$$

where O_i is the observed data, S_i is the simulated data and $\bar{O}$ is the mean of the observed data.

Nash–Sutcliffe efficiencies can range from $-\infty$ to 1. An efficiency of 1 (i.e. NSE = 1) corresponds to a perfect match between the predicted data and the observed data. An efficiency of 0 (NSE = 0) indicates that the model predictions are as accurate as the mean of the observed data. An efficiency of less than zero (NSE < 0) indicates that the mean of the observed data are a better predictor than the model. Most importantly, the closer the model efficiency is to 1, the more accurate is the model. The NSE efficiencies for the TVD, ADI and SI simulation cases were calculated using 30 pairs of observed-simulated values, with the observed values being presented in Table 5.1. Calculation of the NSE coefficients revealed that the TVD configuration had an efficiency of 0.9863, the ADI configuration had an efficiency of 0.8530, while the SI configuration had an efficiency of 0.8684. These coefficient values showed that the TVD model structure outperformed the other two model structures in predicting the peak flood levels, with the NSE coefficient being nearly equal to 1. This being the case, it appears that the TVD predictions almost matched the observed data perfectly, whereas the ADI and SI simulation cases were less numerically accurate.

5.3.1 Simplification strategy

Although results presented above highlight that simplified and ADI-type models are not appropriate for flood simulations of extreme flood events, these models (especially the ADI-type) are still the model of choice for most practitioners working in this field. Namely, these models execute the simulations much quicker than the more numerically accurate shock-capturing models (Liang et al., 2006, de Almeida et

al., 2012). For example, all three simulation cases were completed on a personal computer (processor Intel® Core™ i5-3210M CPU 2.50GHz, 6 GB RAM). The TVD simulation case was completed in 1h 8min, whereas the ADI and the SI simulation cases were completed in less than 10 minutes. The differences in computational times are quite substantial even for a small domain, such as the Boscastle domain considered in this study. Therefore, it is reasonable to assume that the differences in the computational times would be even greater for flood simulations for much larger urban areas.

Even though the ADI simulation case was completed much faster than the TVD simulation case, the above results have highlighted that the ADI simulation results can be completely misleading in terms of determining the extent of the flood inundation impact for extreme flood events. As mentioned, this is due to the emergence of spurious oscillations, which tend to swamp the flood wave prediction and thus result in erroneous flood level and inundation extent predictions. However, it is believed that the oscillatory results are often improved by increasing the Manning's coefficient during the flood risk assessment process, with some of the friction then smoothing out the numerical oscillations. Therefore, additional flood simulations with the ADI-type model (i.e. ADI simulation case) were performed to test the appropriateness of this methodology when modelling extreme flood events, such as the 2004 Boscastle flash flood event considered in this study.

As stated earlier, more than 30 additional simulations of the ADI model structure were carried out. The value of the Manning's coefficient was gradually increased for each simulation run until the modelled water depths and inundation extent were not similar to those obtained using the TVD simulation case, as the TVD simulation case predictions almost matched the observed data perfectly. It was noted that higher, but still relatively reasonable values of Manning's coefficient (e.g. values of up to around 0.15) did not significantly improve the simulation results. This suggested that for this extreme flood event the ADI-type models were not capable of accurately predicting the main parameters for rapidly varying flows, even when higher roughness coefficients were applied. Therefore, unrealistically high values of Manning's coefficient were used to manipulate the ADI-type model simulation results to an acceptable level.

Figure 5.8 shows the predicted maximum water depths and the inundation extent for the ADI simulation cases, for Manning's coefficients of 0.1, 0.2, 0.3, 0.4, 0.5 and 0.6. The results from these simulations were then compared to the TVD simulation case, which employed a more realistic value of Manning's coefficient (i.e. 0.040) and reproduced the wrack marks most accurately. It can be seen that higher value of the Manning's coefficient leads to greater water depths, and with a value of the Manning's coefficient of 0.6, the ADI simulation case produced similar results to the TVD simulation case. It should be added here that such high values of Manning's coefficient also result in unrealistically low flood velocities for an extreme flood event, such as a flash flood. However, as there are no records of actual flood velocities for the 2004 Boscastle flood, it was not possible to validate the model predicted flood velocities within this study.

Even though the ADI simulation case with a Manning's value of 0.6 generally matched the TVD simulation case, this should not be considered as proof of appropriateness of the ADI-type models for simulating extreme flood events. There is no known procedure in determining the value of the Manning's coefficient which will improve on the accuracy of the simulations results to an acceptable level. If flood risk assessment practitioners improve on their final flood elevation result by increasing the value of the Manning's coefficient, their effort to improve on the final results is based on bare speculation, especially if it is taken into account that maximum values of a Manning's coefficient for open channels is about 0.20 (Chow, 1959). In setting the Manning's coefficient values as high as 0.6, or thereabouts, the corresponding flood simulation results have no scientific or engineering basis, as such large values of the Manning coefficient can rarely be justified on technical grounds. Therefore, these results strongly suggest that the "simplification strategy", in any form, is not appropriate for flood risk assessment of urban areas where the emergence of extreme flood events is possible.
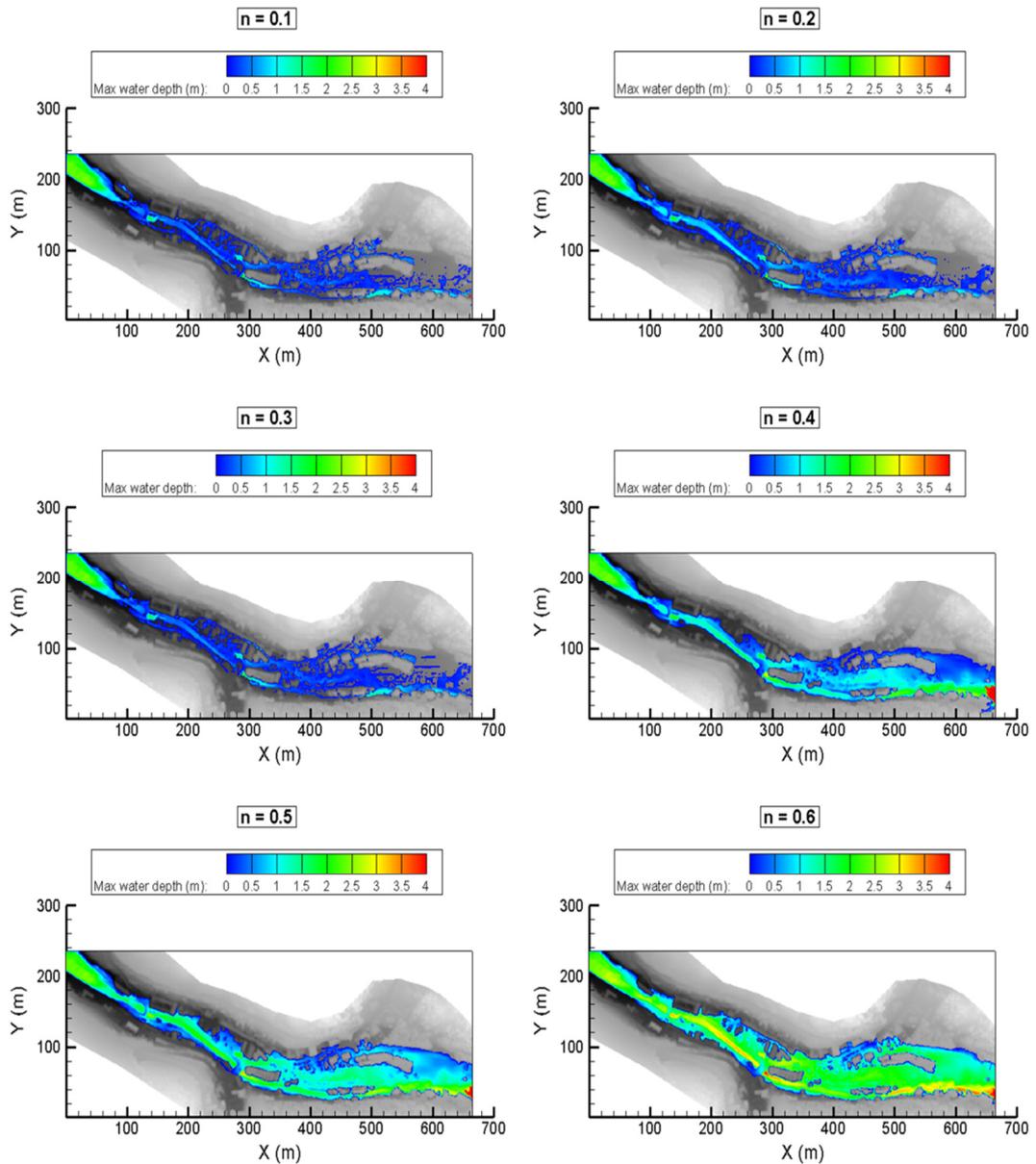
Figure 5.8: Predicted maximum water depths and inundation extent for the ADI simulation cases with different values of Manning's coefficient

5.4 Summary

Two key research objectives were addressed in this chapter. The first key objective of this research study was to determine what type of flood inundation models should be used for predicting the flood elevations, velocities and inundation extent for extreme flood events. This being the case, the well documented 2004 Boscastle flash flood was simulated using three different model structures of the DIVAST and DIVAST-TVD flood inundation models, including: (i) a shock-capturing flood

inundation model (i.e. the TVD simulation case), (ii) a regular ADI-type flood inundation model (i.e. the ADI simulation case), and (iii) a flood inundation model based on the "simplified-inertia" approach (i.e. the SI simulation case). Simulation results from these three different model structures were compared to post-flood measurements, based mainly on observed wrack marks. Direct comparisons between the predicted flood levels and observed wrack marks, showed that the shock-capturing model structure (i.e. the TVD simulation case) was significantly more accurate in terms of numerical model predictions of the flood peak elevations, as compared to the water elevations predicted using the two other model structures considered in this study (i.e. the ADI and the SI simulation cases).

The second key objective of this research study was to investigate the appropriateness of the "simplification strategy" when used as a flood risk assessment modelling tool for areas susceptible to extreme flooding. Therefore, attempts have been made to improve on the simulation results for the ADI simulation case by increasing the value of the Manning's coefficient. More than 30 additional simulations were conducted with the ADI model structure, where the value of the Manning's coefficient was gradually increased until the modelled elevations and inundation extent were not similar to those of the TVD simulation case. The ADI simulation case produced similar results to the TVD simulation case when the value of the Manning's coefficient was set to 0.6, i.e. this improvement was based on using an artificially high Manning's coefficient. This clearly indicates that adopted "simplifications strategy" should not be considered as an appropriate flood risk assessment modelling tool when modelling extreme flood events (such as the 2004 Boscastle flash flood considered in this study) or in areas prone to occurrence of extreme flooding.

All in all, the results presented in this chapter indicate that shock-capturing schemes are more appropriate for modelling of flood events characterised with abrupt changes in the flow regime and/or high Froude number flows (i.e. Froude number near or greater than 1) than ADI-type or simplified models. Shock-capturing models apply artificial diffusion terms in the solution procedure, which ensure the stability of the computational process and enable the computation of any shock waves or discontinuities as part of the numerical solution. Therefore, shock-capturing models

can produce more reliable results when modelling rapidly varying or high Froude number flows when compared to the ADI-type or simplified models. Namely, these models require additional modifications of the modelling procedure in order to obtain stable solution for rapidly varying flows, such as applying of patches of high roughness in order to decrease the velocity of the flow and thus dissipate the energy of the flow, which in turn can dampen out the numerical oscillations. However, these modifications are consequently always based on the modeller's perception of how much improvement is needed, which therefore means that such modelling results can generally be considered as highly speculative.

CHAPTER 6

Flood hazard assessment for extreme flood events

6.1 Introduction

This chapter presents an investigation of what type of flood hazard assessment methods should be used for predicting flood hazard indices in areas prone to occurrence of extreme flood events. As noted in Section 2.4, two flood hazard assessment criteria were selected for predicting flood hazard indices in this research study: (i) a classical and widely used empirically based method developed for DEFRA by Ramsbottom et al. (2006) (see Section 2.3.2), and (ii) a recently introduced physically based and experimentally calibrated method presented by Xia et al. (2014) (see Section 2.3.3). The two selected flood hazard assessment methods were: (i) validated against different experimental datasets, including datasets based on experiments using real humans as test subjects and datasets based on experiments using a scaled model human body, and (ii) used to assess flood hazard indices for three different extreme flood events presented in Chapter 4, i.e. the 2004 Boscastle flash flood (England, UK), the 2007 Železniki flash flood (Slovenia), and the 2010 Kostanjevica na Krki extreme river flood (Slovenia). In addition, Section 6.2 describes the research process and the methods implemented, Section 6.3 presents the main findings and evaluation of the obtained results, and finally Section 6.4 provides the summary of the main findings.

6.2 Methodology

The third key objective of this study was to determine what type of flood hazard assessment methods should be used for assessing the flood hazard posed on people during extreme flooding. The initial assumption was made that the physically based and experimentally calibrated method would more accurately assess the flood hazard indices for people than the empirically derived method when the flood hazard is

assessed for extreme flood events. In order to test this assumption, two different validation procedures were undertaken.

Firstly, both flood hazard assessment criterion were validated against two different types of experimental data, i.e. the data based on the experiments including real human test subjects and the data based on the experiments using model human bodies. The experiments, including real human test subjects, conducted by Abt et al. (1989) and Karvonen et al. (2000) were considered for this study. There are several other studies where real humans as test subjects have been used, such as the studies conducted by Foster and Cox (1973), Takahashi et al. (1992) and Jonkman and Penning-Rowsell (2008). However, the focus in this study is on the experimental data by Abt et al. (1989) and Karvonen et al. (2000), as these two datasets were included in the derivation process of the empirically based method considered in this study, and have the largest amount of experimental observations among the available experimental datasets.

In the experiments conducted by Abt et al. (1989) and Karvonen et al. (2000), the water depth and the corresponding velocity were recorded when the human test subject lost manoeuvrability or stability in the flume due to the flow conditions. The authors of these two studies did not specifically record which instability mechanism led to the loss of stability of the test subject during a particular test. Nonetheless, it can be established from the recorded data that it was only in a few tests that stability was lost due to sliding, whereas in the vast majority of the tests the stability was lost due to toppling (Jonkman and Penning-Rowsell, 2008, Xia et al., 2014). In contrast to experiments with real human test subjects, Xia et al. (2014) used a scaled human body (i.e. a dummy) for their experiments. As indicated in Section 2.3.3, the scaled human body strictly followed the principles of geometric, kinematic and dynamic scaling. This meant that the flow conditions were ideally similar to those in the prototype (Chanson, 2004), i.e. density, drag and friction coefficient of the selected human body model were approximately equal to those of the prototype (Xia et al., 2014). This being the case, the prototype, at 1.70 m in height and 60 kg in weight, was scaled down to a model human body of 0.3 m in height and 0.334 kg in weight, with the model human body strictly following the geometric similarity in each dimension. For each test, the water depth and the corresponding velocity were

recorded at the moment when the model human body started to become unstable. Also, the instability mechanism (e.g. toppling or sliding), which led to instability of the model human body, was identified for each test.

As mentioned in Section 2.3.3, the physically based and experimentally calibrated method considered in this study can be adjusted to a specific body type. The characteristics of a specific body type in Equations (2.17) and (2.18) (see Section 2.3.3) are represented with coefficients a_1, b_1, a_2 and b_2. More precisely, the coefficients a_1, b_1, a_2 and b_2 form part of an expression, which represents the effect of the buoyancy force as a function of the human height and mass for a given water depth (Xia et al., 2014). These coefficients can be determined from the characteristics of the human body, e.g. the human height and mass, and the volume and mass of the body segment parameters, such as legs, arms, torso etc. For example, based on the body segment characteristics of a typical Bulgarian body (Nikolova and Toshev, 2007), the values of a_1 and b_1 were assumed to be 0.612 and 0.388, while according to the body structure of an American body (Drillis et al., 1964), the value of the coefficients a_1 and b_1 were 0.737 and 0.263, respectively (Xia et al., 2014). For the coefficients a_2 and b_2, these can be obtained from the relationship between the total body volume and the corresponding mass of a human body. Hence, the values of the coefficients a_2 and b_2 for a typical Bulgarian body, for example, were assumed to be $0.9748 \times 10^{-3} \, \text{m}^3/\text{kg}$ and $- 0.7111 \times 10^{-3} \, \text{m}^3$. In addition, the coefficients a_1, b_1, a_2 and b_2 are constant, which means that the same values of these coefficients apply for both instability mechanisms, as given by Equations (2.17) and (2.18). The value of the coefficients a_1, b_1, a_2 and b_2 for the model human body used in this study were: $a_1 = 0.633$, $b_1 = 0.367$, $a_2 = 1.015 \times 10\text{-}3 \, \text{m}^3/\text{kg}$ and $b_2 = - 4.927 \times 10\text{-}3 \, \text{m}^3$ (Xia et al., 2014).

Two parameters are needed to calibrate the physically based and experimentally calibrated method considered herein, i.e. parameters α and β (see Equations (2.17) and (2.18)). These two parameters can be evaluated from the relevant experimental data, and are influenced by the shape of the test subject, the friction coefficient between the soles and the ground surface, the drag coefficient, the effect of a non-uniform velocity distribution along the vertical direction, and the effect of the ability of a test subject to adjust its position in the flow (Xia et al., 2014). Hence, the values

of the parameters α and β are different for each body type and for each instability mechanism. However, as the height, mass and the values of the aforementioned coefficients are constant for a particular human body, the values of parameters α and β can be evaluated by statistical analysis from the relevant experimental data (Xia et al., 2014). As we were modelling sites in Slovenia and in the UK, it would be reasonable to calibrate Equations (2.17) and (2.18) for the body characteristics of people living in these two countries. Unfortunately, these calibrations are not possible at present due to the lack of body segment parameter data needed to undertake the calibration process. Alternatively, Equations (2.17) and (2.18) could be calibrated for a typical Bulgarian body, since the necessary body segment parameter data exists (Nikolova and Toshev, 2007). These data can be used to represent a model human body based on the typical Bulgarian body prototype, with the model human body being used for the experimental tests and thus for calibration of Equations (2.17) and (2.18). However, as the difference in size and body characteristics between a typical Bulgarian body and the body considered in the study of Xia et al. (2014) are relatively small, it was decided to use the values of the parameters α and β obtained in the study by Xia et al. (2014) for the calibration of Equations (2.17) and (2.18) in this research study. This saved valuable resources and time that would otherwise be spent on experimental procedures, yet still enabled satisfactory quality of the final results as the potential computational error is in an acceptable range. The values of the parameters α and β used in this study for the calibration of Equations (2.17) and (2.18), for both the model human body considered by Xia et al. (2014) and the real human body (i.e. data collected in the experiments considering real human test subjects) are presented in Table 6.1.

Table 6.1:The values of the parameters α and β used to calibrate the physically based and experimentally calibrated method for the model human body and real human body (Xia et al., 2014)

Parameter	Model human body		Real human body	
	Toppling instability	Sliding instability	Toppling instability	Sliding instability
α	3.472	7.975	7.867	10.253
β	0.188	0.018	0.462	0.139

Secondly, the assessed flood hazard indices from both methods were compared at different stages of three extreme flood events, including one extreme river flood event and two flash flood events. In order to focus solely on the hydrodynamic conditions of the flow that can lead to loss of stability in floodwaters, any external factors that present a risk to people in floodwaters (such as floating debris) were omitted from the flood hazard assessment process. As mentioned, the physically based and experimentally calibrated method considered in this study can assess the hazard to people by considering both the sliding and toppling instability mechanisms. This being the case, the limiting stability threshold for the physically based and experimentally calibrated method was defined as the minimum of the toppling and sliding incipient velocities:

$$HR = MIN\left(1, \frac{U}{MIN\left(U_{toppling}, U_{sliding}\right)}\right) \tag{6.1}$$

where HR is the flood hazard rating, U is the velocity of the flow, $U_{toppling}$ is the toppling incipient velocity and $U_{sliding}$ is the sliding incipient velocity.

The empirically derived method categorises flood hazard into four flood hazard classifications, namely: low, moderate, significant and extreme. On the other hand, the physically based and experimentally calibrated method considered in this study quantifies flood hazard by mimicking the principle of bivalence, i.e. there is only one threshold that defines whether the stability of a person in floodwater is lost or not. This means that there is only one flood hazard class, i.e. extreme. However, in order to allow a more detailed comparison to be undertaken between the two flood hazard assessment methods, the assessed degree of flood hazard according to the physically based and experimentally calibrated method was divided into three additional flood hazard classifications that correspond to the flood hazard classifications of the empirically derived method, i.e. low, moderate and significant. The subdivision of the quantifying flood hazard criteria of the physically based and experimentally calibrated method, which ranges between 0 and 1, was undertaken in such a manner that the ratio of the threshold values that separate the subdivided flood hazard classes was identical to the ratio of the threshold values that separate the flood hazard classes

of the empirically based method. Therefore, if the threshold values in the empirical method are 0.75, 1.5 and 2.5, then the corresponding values for the physically based and experimentally calibrated method would be 0.3, 0.6 and 1. The subdivision of the physically based and experimentally calibrated method into three additional flood hazard classifications, corresponding to the flood hazard classifications of the empirically derived method, should enable better evaluation of how the two flood hazard assessment methods adapt to the violent nature of extreme flood events and thus provide more meaningful results.

In this study, extreme flood events were simulated with rapid changes occurring in the flow regime and the Froude numbers being relatively high. Therefore, there was a need to determine what type of flood simulation model should be used for predicting flood depths, velocities and inundation extent, which were needed for an accurate flood hazard assessment process and production of flood hazard risk maps. The shock-capturing DIVAST-TVD model was used for predicting flood depths, velocities and inundation extent for both flash flood scenarios, as it was shown in Section 5.3 that only shock-capturing flood simulation model produces numerically accurate predictions of flood depths and velocities when simulating flash flood events. In order to be consistent, the DIVAST-TVD model was also used for predicting depths, velocities and inundation extent in the extreme river flood scenario.

6.3   Predictions of flood hazard indices

As mentioned, two different validation procedures were considered in this study. First, both methods were validated against different experimental datasets, including datasets based on experiments using real humans as test subjects and datasets based on experiments using a scaled model human body. Second, both methods were used to assess flood hazard indices for three different extreme flood events, i.e. the 2004 Boscastle flash flood (England, UK), the 2007 Železniki flash flood (Slovenia), and the 2010 Kostanjevica na Krki extreme river flood (Slovenia).

6.3.1 Comparison with the experimental datasets

Figure 6.1 shows a comparison of the flood hazard prediction ability of the two methods with the experimental observations of Abt et al. (1989), while Figure 6.2 shows a comparison of the flood hazard prediction ability of the two methods with the experimental observations of Karvonen et al. (2000). As mentioned, in the experiments conducted by Abt et al. (1989) and Karvonen et al. (2000), the dominant mode of instability was due to the toppling instability mechanism (Jonkman and Penning-Rowsell, 2008, Xia et al., 2014). Therefore, only Equation (2.18) was used for the comparisons with the empirically derived method. Table 6.2 shows the values of the parameters α and β used for the calibration of Equation (2.18) when the two datasets are considered separately.

Figure 6.1: Comparison of the flood hazard prediction ability of the two methods with the experimental observations of Abt et al. (1989)

Figure 6.2: Comparison of the flood hazard prediction ability of the two methods with the experimental observations of Karvonen et al. (2000)

Table 6.2: The values of the parameters α and β used to calibrate the Equation (2.18) separately for each of the two datasets (Xia et al., 2014)

Parameter	Data by Abt et al. (1989) Equation (2.18)	Data by Karvonen et al. (2000) Equation (2.18)
α	8.855	4.825
β	0.473	0.160

In both Figure 6.1 and Figure 6.2 the blue circles represent the depth and velocity when stability was lost, i.e. the flow conditions which led to instability of the test subject. In Figure 6.1, it can be seen that the empirically derived method classified all experimental observations into two flood hazard classes, i.e. moderate hazard and significant hazard. The majority of the experimental observations (i.e. the point in the experiments when the real human test subject was losing, or completely lost, stability) were classified as significant hazard, which indicated that the empirical method generally accurately assessed the flood hazard indices. Figure 6.1 also shows that the physically based and experimentally calibrated method agreed well with the

experimental observations, as 38 out of 58 experimental observations can be found above the stability threshold (red line), which indicated that stability was lost, and with at least 15 experimental observations being in the relative proximity of the stability threshold, which indicated that subject was close to losing stability, i.e. was greatly endangered by the flow conditions.

In Figure 6.2, it can be seen that the empirically derived method classified the majority of the experimental observations in the moderate flood hazard class, which was regarded as the stability threshold for children. This indicated that the empirically derived method underestimated the flood hazard indices for the dataset of Karvonen et al. (2000). On the other hand, Figure 6.2 also shows that the physically based and experimentally calibrated method agreed well with the experimental observations, as 21 out of 29 of the experimental observations fall above the stability threshold (red line), which indicated that stability was lost. In addition, Figure 6.1 and Figure 6.2 also show that in practically all test runs the stability of the real human test subjects was lost in the sub-critical flow regime. Therefore, it is hard to evaluate the prediction ability of the empirically derived method for high Froude number flows, which often occur with extreme flood events. Nonetheless, it can be seen from Figure 6.1 and Figure 6.2 that the physically based and the experimentally calibrated method performed better than the empirically derived method.

In contrast, the results are somewhat different when both datasets are merged. For example, Figure 6.3 shows a comparison of the flood hazard prediction ability of the two methods with the experimental data from both aforementioned experimental studies. The blue circles and orange squares represent the depth and velocity when stability was lost, i.e. the flow conditions which led to instability of the test subject. In Figure 6.3, it can be seen that the empirically derived method classified all data into two flood hazard classes, i.e. moderate hazard and significant hazard. This means that nothing changed from the perspective of the empirically derived method when compared to the results presented in Figure 6.1 and Figure 6.2. On the other hand, Figure 6.3 also shows that there was some change in the predictive ability of the physically based and experimentally calibrated method. It can be seen in Figure 6.3 that the physically based and experimentally calibrated method classified 57 out of 87 experimental observations as extreme hazard. However, there are now 48

experimental observations (compared to 38 in Figure 6.1) from the dataset by Abt et al. (1989), and only 9 experimental observations (compared to 20 in Figure 6.2) from the dataset by Karvonen et al. (2000) above the stability threshold (red line) of the physically based and experimentally calibrated method.
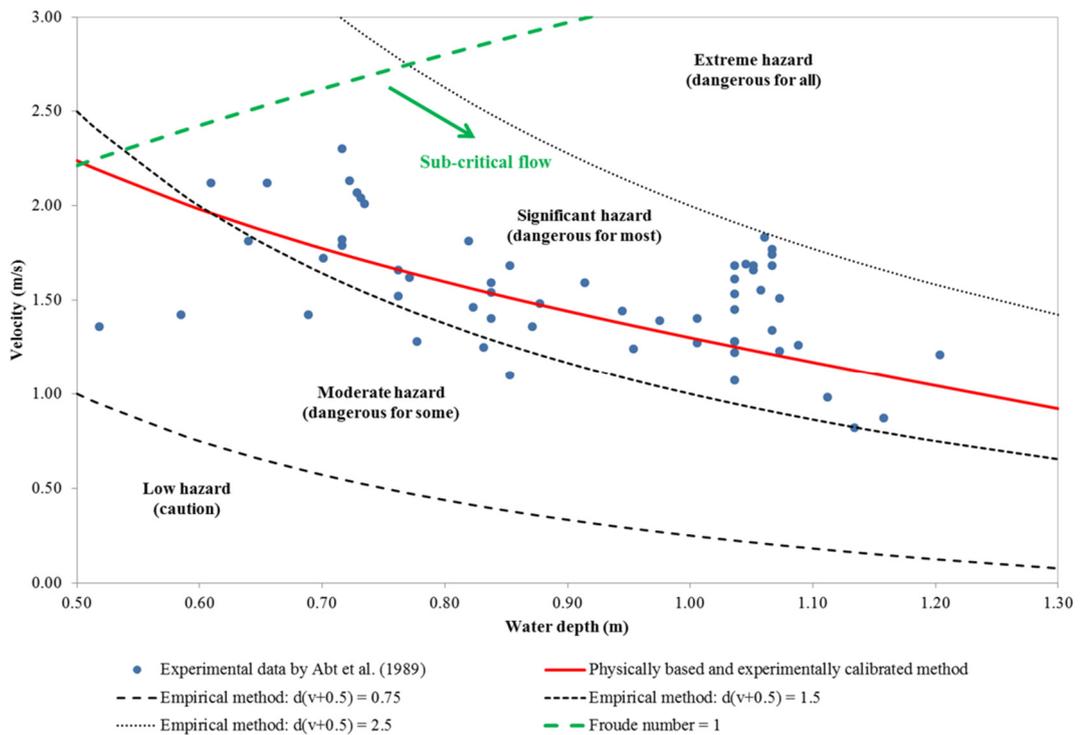

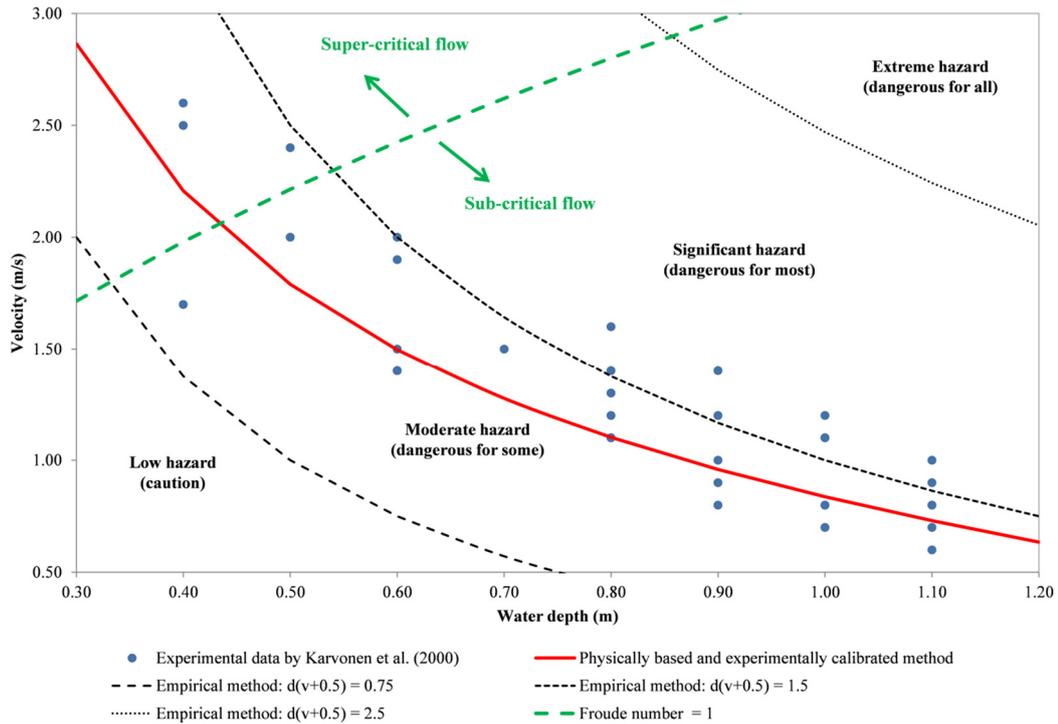Figure 6.3: Comparison of the flood hazard prediction ability of the two methods with the experimental observations of Abt et al. (1989) and Karvonen et al. (2000)

The results in Figure 6.3 show that the predictive ability of the physically based and experimentally calibrated method is closely related to the body characteristics of the test subjects, which agrees with the observations of other authors, such as Xia et al. (2014) and Milanesi et al. (2015). As the two datasets were merged, the body characteristics of an average test subject changed. Furthermore, the effect of buoyancy on an average test subject also changed, which in turn changed the values of the calibrating parameters α and β (see Table 6.3), and thus the stability threshold of the physically based and experimentally calibrated method considered in this research study.

Table 6.3: The values of the parameters α and β used to calibrate the Equation (2.18) when the two datasets are merged (Xia et al., 2014)

Parameter	Data by Abt et al. (1989) and Karvonen et al. (2000)
	Equation (2.18)
α	7.867
β	0.462

For example, average height and weight of a test subject in the study of Abt et al. (1989) were 178 cm and 76 kg, while for a test subject in the study of Karvonen et al. (2000) they were 174.6 cm and 73.6 kg, respectively. However, when both datasets are merged the average test subject is 177.1 cm in height and weighs 75.3 kg. Therefore, an average test subject is now a bit smaller and weighs less than an average test subject in the study of Abt et al. (1989), and a bit taller and heavier than an average test subject in the study of Karvonen et al. (2000). This explains why there are more experimental observations of Abt et al. (1989) above the stability threshold (red line) of the physically based and experimentally calibrated method when compared to Figure 6.1, and why there are less experimental observations for Karvonen et al. (2000) above the stability threshold (red line) when compared to Figure 6.2.

On the other hand, the results in Figure 6.3 also indicate that there are some reservations regarding the experimental data based on real human test subjects. For example, Lind et al. (2004) noted that these two datasets should not be aggregated in the application process, because these datasets are too small, not random and consequently not representative enough. In addition, Abt et al. (1989) reported that their experiments had some constraints, such as optimal experiment conditions, the presence of the safety equipment, healthy test subjects and the ability of the test subject to learn how to manoeuvre in the flow with time. Similar findings were reported by Karvonen et al. (2000), who noted that their experiments also had some shortcomings, such as excessive safety features, the use of survival suits, which increased the buoyancy and cross-sectional area of a person, and the use of a slippery surface. It is therefore reasonable to assume that these experiments did not represent the actual response of a person in the event of real-life flooding.

In general, an average person has probably never been directly faced with rising floodwaters, which means that such a person does not know how to readjust the body position in order to maintain stability for longer, as a real human test subject would after a few test runs (i.e. training). Furthermore, it is important to point out that not all people in the general population are healthy or physically fit, and are not therefore able to adequately face the dangers due to flooding. This being the case, including only healthy and relatively young test subjects in the experimental studies leads to safety criteria that exclude some of the most vulnerable groups of the general population, such as frail and/or elderly citizens, and people with physical disabilities. Finally, one of the key factors that have a major effect on human stability in floodwaters is human psychology. If a human test person is attached with safety ropes, and therefore feels completely safe, then the psychological factors, such as shock or fear, do not play a significant role in maintaining or losing stability in floodwaters. However, the psychological factors are sometimes even more influential than physical ability. For example, in the study presented by Cox et al. (2004) two child test subjects were similar in size and thus should have had similar safety characteristics. Nonetheless, as these two child test subjects were of different age and physiological development, they had differing safety characteristics. This highlights the importance of demographic and psychological characteristics, as they can have a significant impact on a person's response time and consequently on a person's ability to adequately react to the dangers due to flooding. Therefore, it is reasonable to conclude that any stability thresholds based on experimental data collected using real human test subjects could be misleading, and could lead to hazardous and unsafe situations in the case of a real-life flooding (Chanson et al., 2014). This being the case, the predictive ability of both methods was also validated against the experimental data of Xia et al. (2014).

As mentioned, Xia et al. (2014) used a scaled human body (i.e. a dummy) for their experiments. This meant that the scaled human body could not readjust its position or learn how to manoeuvre itself in the flow with time, and it could not be influenced by any sort of safety feature. This being the case, the experimental results obtained in this study tend to be more conservative from a flood risk point of view when compared to the experimental data obtained in the studies using real human test subjects (Xia et al., 2014). Figure 6.4 shows a comparison of the flood hazard

prediction ability of the two methods using the experimental data of Xia et al. (2014). The blue circles identify the conditions when stability was lost due to the toppling instability mechanism, i.e. the flow conditions which led to instability of the human model due to the momentum.
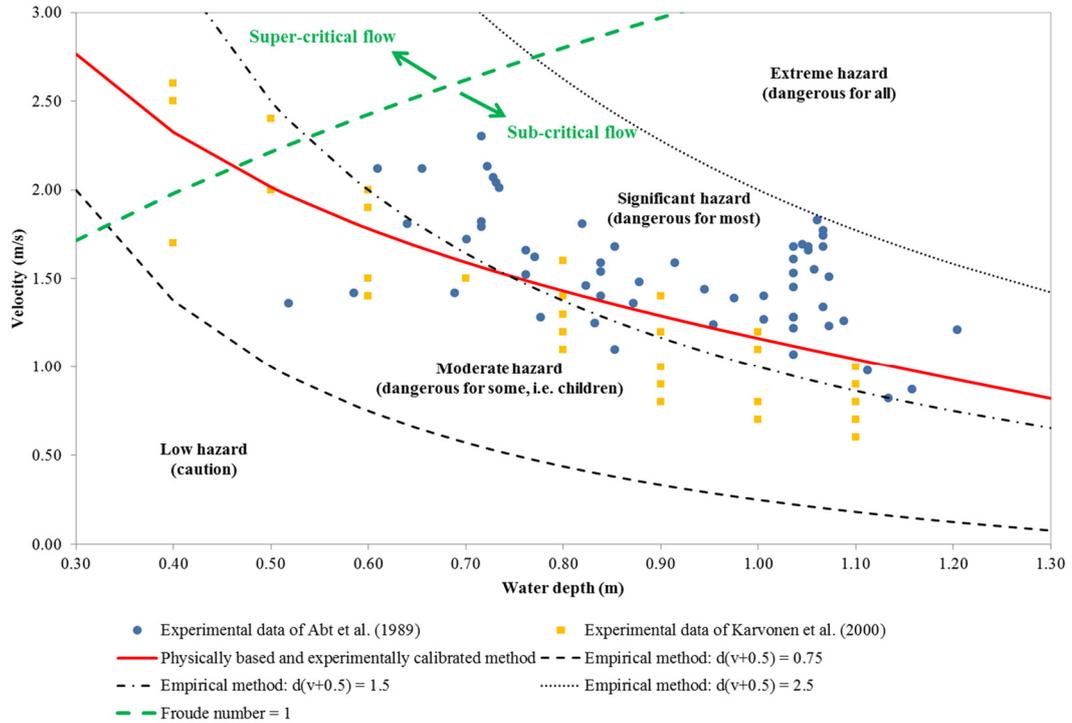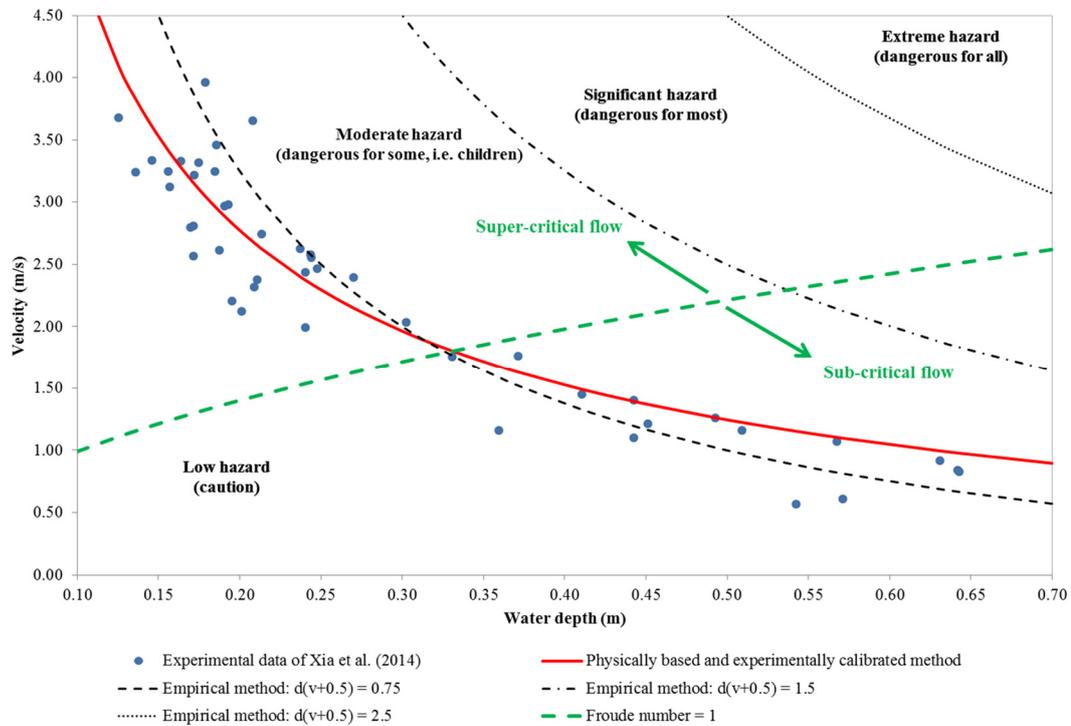

Figure 6.4: The comparison of the flood hazard prediction ability of the two methods with the experimental observations of Xia et al. (2014)

In Figure 6.4, it can be seen that the empirically derived method classified the majority of the data as of low hazard, which indicates that the empirically derived method generally under-predicts the flood hazard indices. This is probably due to the fact that the experimental data of Abt et al. (1989) and Karvonen et al. (2000) were used in the derivation process for the empirical method and therefore the ability of the test subjects to learn how to manoeuvre in the flow is incorporated in the empirically derived method (Cox et al., 2010). However, as mentioned earlier this means that the flood hazard assessment with the empirically derived method tends to be too optimistic regarding safety. Furthermore, it can also be seen that the empirically derived method showed a higher flood hazard index (i.e. moderate hazard) for the tests where the stability was lost in the sub-critical flow regime, whereas almost all tests in which the stability was lost in the super-critical flow

regime were classified as low hazard. This indicates that the empirically derived method, despite the potential shortcomings, still better assesses flood hazard indices for relatively slowly changing flow conditions than for the high Froude number flows, i.e. for the rapidly varying velocities that often occur with extreme flood events.

Figure 6.4 also shows that the physically based and experimentally calibrated method agreed well with the experimental observations, as 20 out of 46 experimental observations can be found above the stability threshold (red line), which indicated that stability was lost. In addition, the vast majority of the remaining experimental observations can be found in the relative proximity of the stability threshold, which indicated that the model was close to losing stability, i.e. was greatly endangered by the flow conditions. In Figure 6.4, it can also be seen that the physically based and experimentally calibrated method adapts well to high Froude number flows, which are generally characterised with abrupt changes in the flow regime and often occur with extreme flood events. For example, 17 out of 31 experimental observations in the super-critical flow regime can be found above the stability threshold (red line), with the majority of the remaining experimental observations in the super-critical flow regime being in the relative proximity of the stability threshold. This being the case, the physically based and experimentally calibrated method assesses the flood hazard indices much better for super-critical flows when compared to the empirically derived method.

In summary, the comparisons of the two methods with the experimental data have shown that the physically based and experimentally calibrated method is highly adaptable to the characteristics of a particular human body, which allows more accurate assessment of flood hazard indices to be made when compared to the empirically based method. Furthermore, the physically based and experimentally calibrated method also generally agreed better with the observations which recorded the loss of stability in the super-critical flow regime when compared to the empirically based method. Therefore, the results obtained in the comparisons with the experimental observations suggests that the methods derived from a physics-based analysis, such as the physically based and experimentally calibrated method considered in this study, would be more appropriate for flood hazard assessment of

extreme flood events than the classically used methods, such as the empirically based method considered in this study.

6.3.2 Comparisons of the flood hazard indices assessed in the numerical simulations of extreme flood events

Three extreme flood events were considered in this study, including: (i) the 2010 Kostanjevica na Krki large river flood, (ii) the 2004 Boscastle flash flood, and (iii) the 2007 Železniki flash flood. As the empirical method considered in this study is based on the experimental data of Abt et al. (1989) and Karvonen et al. (2000) (i.e. real human body), the calibrating parameters α and β used to calibrate the physically based and experimentally calibrated method for the numerical simulations of extreme flood events were also based on the same datasets, i.e. a real human body (see Table 6.2). This being the case, neither of the considered methods was ideal in terms of being able to predict accurately to the calibration dataset. As mentioned earlier, the DIVAST-TVD model was used for predicting depths, velocities and inundation extent for both flash flood scenarios, as it was shown in Section 5.3 that only shock-capturing flood simulation model produces numerically accurate predictions of flood depths and inundation extent when simulating flash flood events. In order to be consistent, the DIVAST-TVD model was also used for predicting the main parameters in the extreme river flood scenario.

The 2010 Kostanjevica na Krki extreme river flood

Figure 6.5 and Figure 6.6 show a comparison between the empirically derived and the physically based and experimentally calibrated flood hazard assessment method for the 2010 Kostanjevica na Krki extreme river flood event. A step-by-step presentation of the assessed flood hazard shows that both methods were assessing a relatively similar degree of flood hazard for the first half of the simulation, i.e. for the first 36 hours (see Figure 6.5). This is not surprising, as the flood was gradually increasing in intensity during the first half of the simulation period and therefore both methods could easily replicate the relatively gradual changes in the flow regime. However, the flooding becomes much more intense during the second part of the

simulation (i.e. over the last 36 hours), as it can be seen in Figure 6.7. Figure 6.7 shows the predicted Froude number values for the last 36 hours of the 2010 Kostanjevica na Krki extreme river flood simulation.

In Figure 6.7, it can be seen that Froude numbers are relatively high, with Froude number values reaching up to 1 at final stages of the 2010 Kostanjevica na Krki extreme river flood simulation. This clearly reflects on the flood hazard assessment predictions, as it can be seen in Figure 6.6. In the last 36 hours of the 2010 Kostanjevica na Krki flood simulation scenario, the physically based and experimentally calibrated method assessed a higher degree of flood hazard at every time mark when compared to the flood hazard assessment obtained with the empirically derived method. These results were expected, as the physically based and experimentally calibrated method is based on being linked to the momentum of the flow, which is proportional to the square of the velocity, as compared to the empirically derived formulation, which is far less sensitive to the velocity of the flood flow. These results suggest that the empirically derived flood hazard assessment method cannot accurately assess the degree of flood hazard for high Froude number flows, or violent flood events, such as the 2010 Kostanjevica na Krki extreme river flood considered in this study. Furthermore, the results also suggest that flood hazard assessment methods based on a physics-based analysis, such as the physically based and experimentally calibrated method considered in this study, should be used for flood hazard assessment of extreme flood events and where the flood velocity of flow is relatively high.
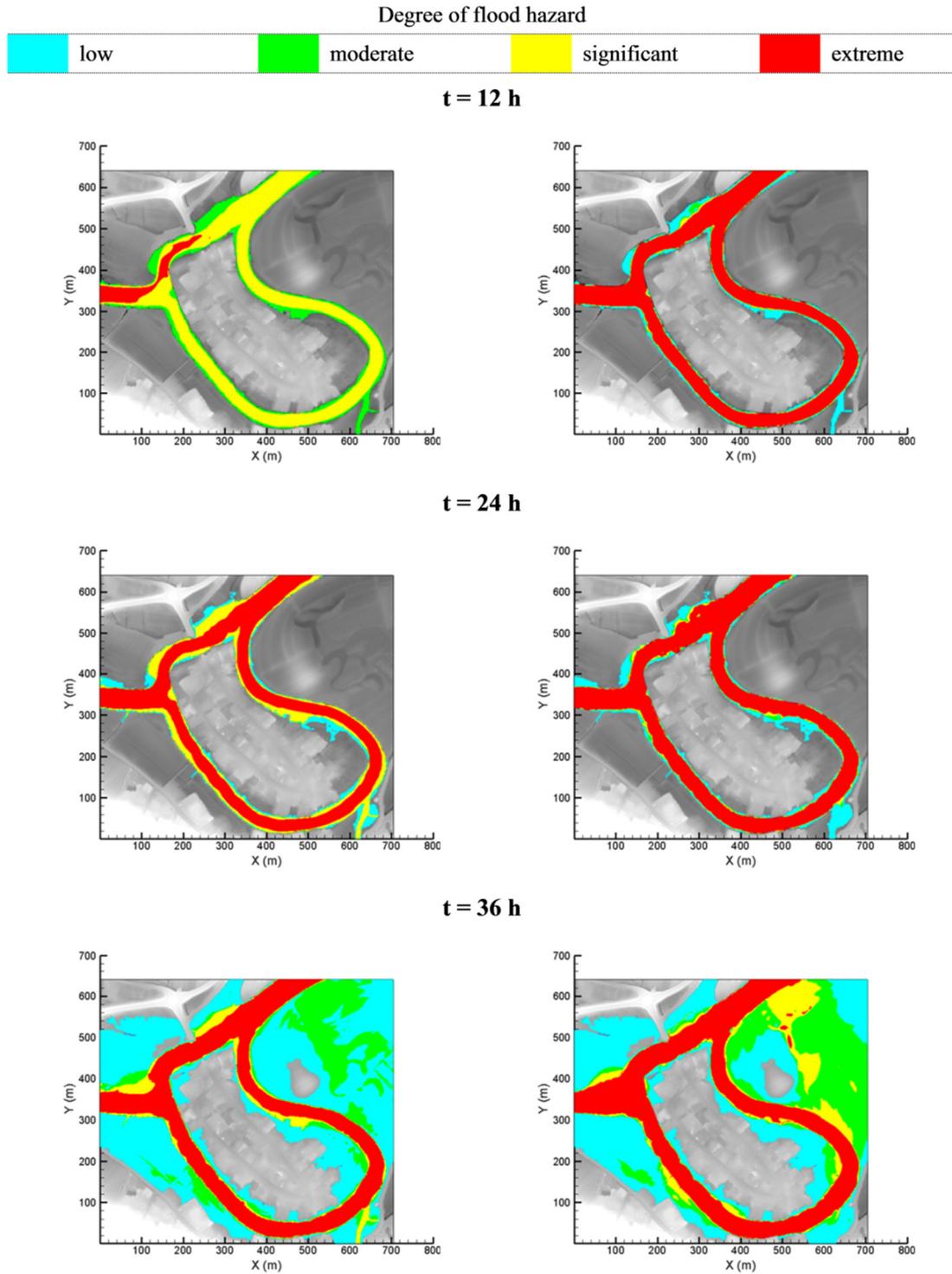
Figure 6.5: Flood hazard rating at 12, 24 and 36 hours after the start of the 2010 Kostanjevica na Krki extreme river flood simulation according to the empirically derived method (left) and the physically based experimentally calibrated method (right)

Figure 6.6: Flood hazard rating at 48, 60 and 72 hours after the start of the 2010 Kostanjevica na Krki extreme river flood simulation according to the empirically derived method (left) and the physically based experimentally calibrated method (right)

Figure 6.7: Maximum Froude number values for the last 36 hours of the 2010 Kostanjevica na Krki extreme river flood simulation

The 2004 Boscastle flash flood

Figure 6.8 shows the comparison between the empirically derived and the physically based and experimentally calibrated method flood hazard assessment method for the 2004 Boscastle flash flood event. Step-by-step presentation of the assessed flood hazard shows that the results from the two selected methods differ from the beginning of the flood simulation. In Figure 6.8, it can be seen that the physically based and experimentally calibrated method predicted higher flood hazard indices at every stage of the simulation when compared to the results obtained with the empirically derived method. These results were expected, as the physically based and experimentally calibrated method is much more influenced by higher velocities and momentum, associated with higher Froude number flows and which occur more frequently with flash floods. This can be clearly seen in Figure 6.9, which shows the predicted Froude number values for the 2004 Boscastle flash flood simulation. In Figure 6.9, it can be seen that Froude numbers are relatively high, with Froude number values reaching up to 1 from early stages of the 2004 Boscastle flash flood simulation. On the other hand, the empirically derived method is rather a simple approach for flash flood events, or other extreme flood events where the Froude number is relatively high, with the method being a function of the velocity only, vis-à-vis the square of the velocity for the physics based method. All in all, these results agree well with the results obtained for the Kostanjevica na Krki extreme river flood event, and further indicate that the flood hazard assessment methods based on a physics-based analysis, such as the physically based and experimentally calibrated method considered in this study, should be used for flood hazard assessment of extreme flood events.
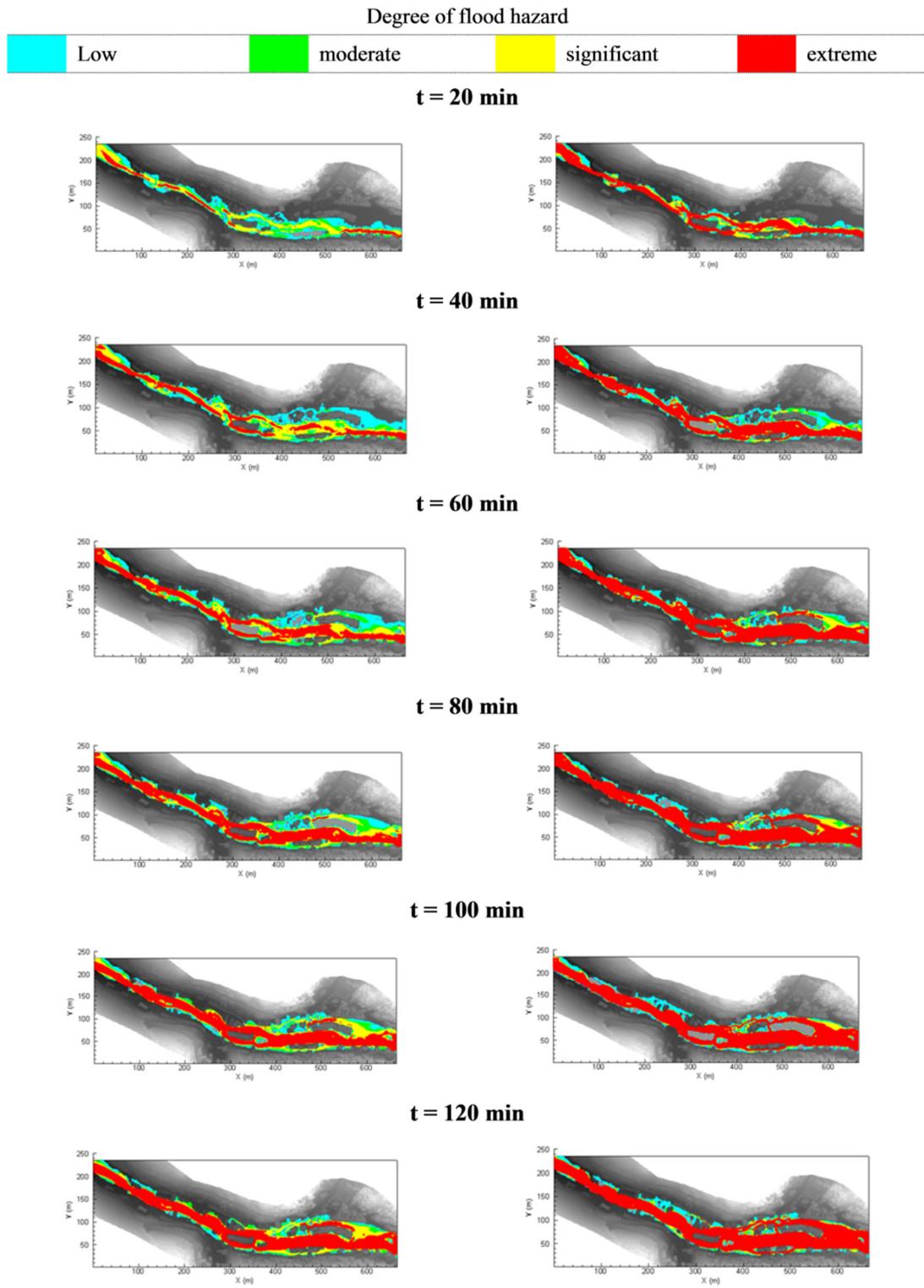
Figure 6.8: Flood hazard rating at different stages of the 2004 Boscastle flash flood simulation according to the empirically derived method (left) and the physically based experimentally calibrated method (right)
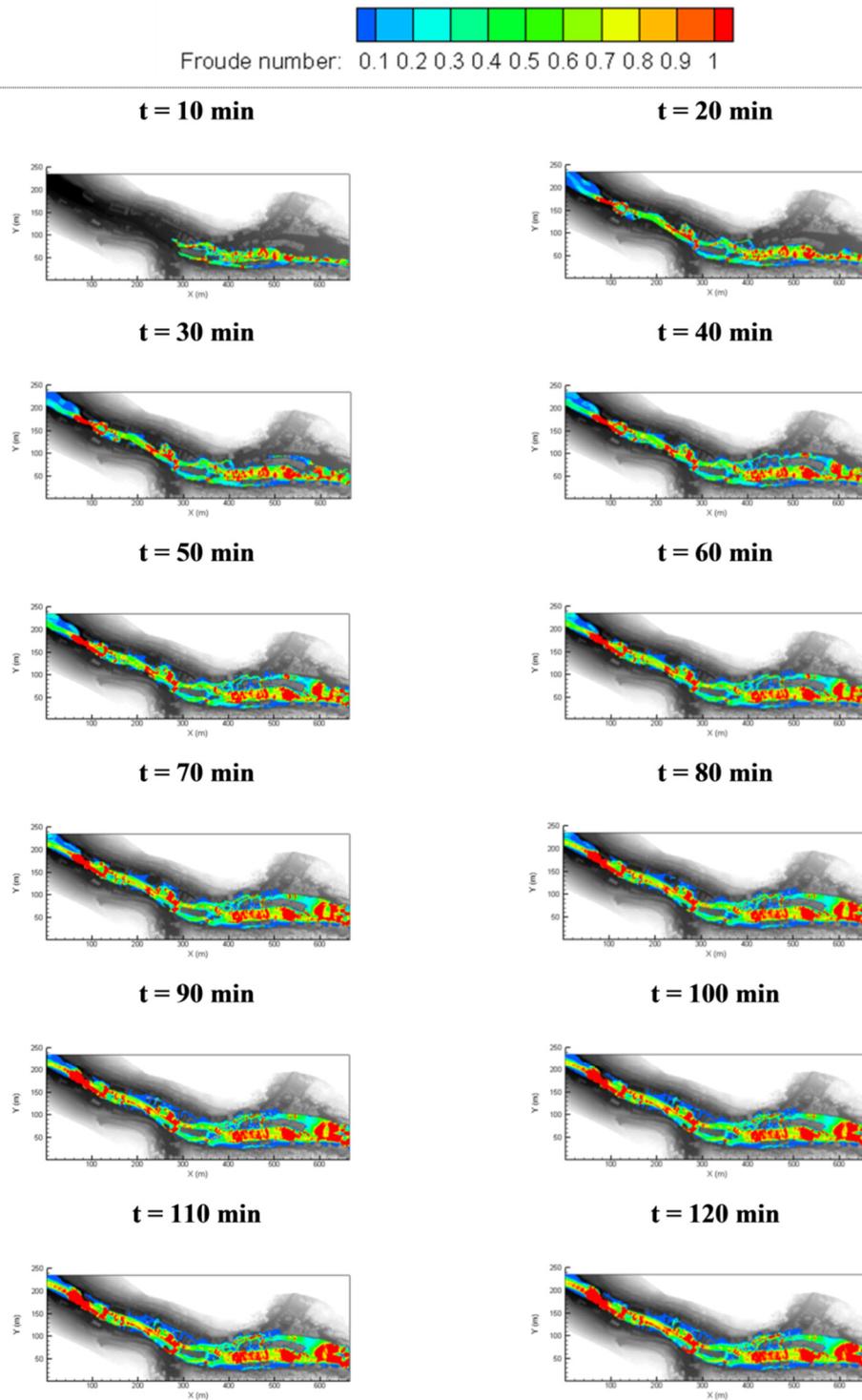
Figure 6.9: Maximum Froude number values for the 2004 Boscastle flash flood simulation

The 2007 Železniki flash flood

Figure 6.10 and Figure 6.11 show a comparison between the empirically derived, and the physically based and experimentally calibrated flood hazard assessment method for the 2007 Železniki flash flood event. A step-by-step presentation of the assessed flood hazard shows the same course of events as can be seen for the 2004 Boscastle flash flood simulation scenario, i.e. the physically based and experimentally calibrated method predicted a higher degree of flood hazard at every stage of the simulation when compared to the results obtained with the empirically derived method. This is not surprising, as the 2007 Železniki flash flood was characterised with high Froude number flows, which often occur with extreme flooding. This can be clearly seen in Figure 6.12, which shows the predicted Froude number values for the 2007 Železniki flash flood simulation. In Figure 6.12 it can be seen that Froude numbers are relatively high, with Froude number values reaching up to 1 from early stages of the 2007 Železniki flash flood simulation. Overall, the results obtained for the 2007 Železniki flash flood event agree well with the results obtained for the 2004 Boscastle flash flood event. These results again indicate that flood hazard assessment methods based on a physics-based analysis, such as the physically based and experimentally calibrated method considered in this study, should be used for flood hazard assessment in areas prone to occurrence of extreme flood events.
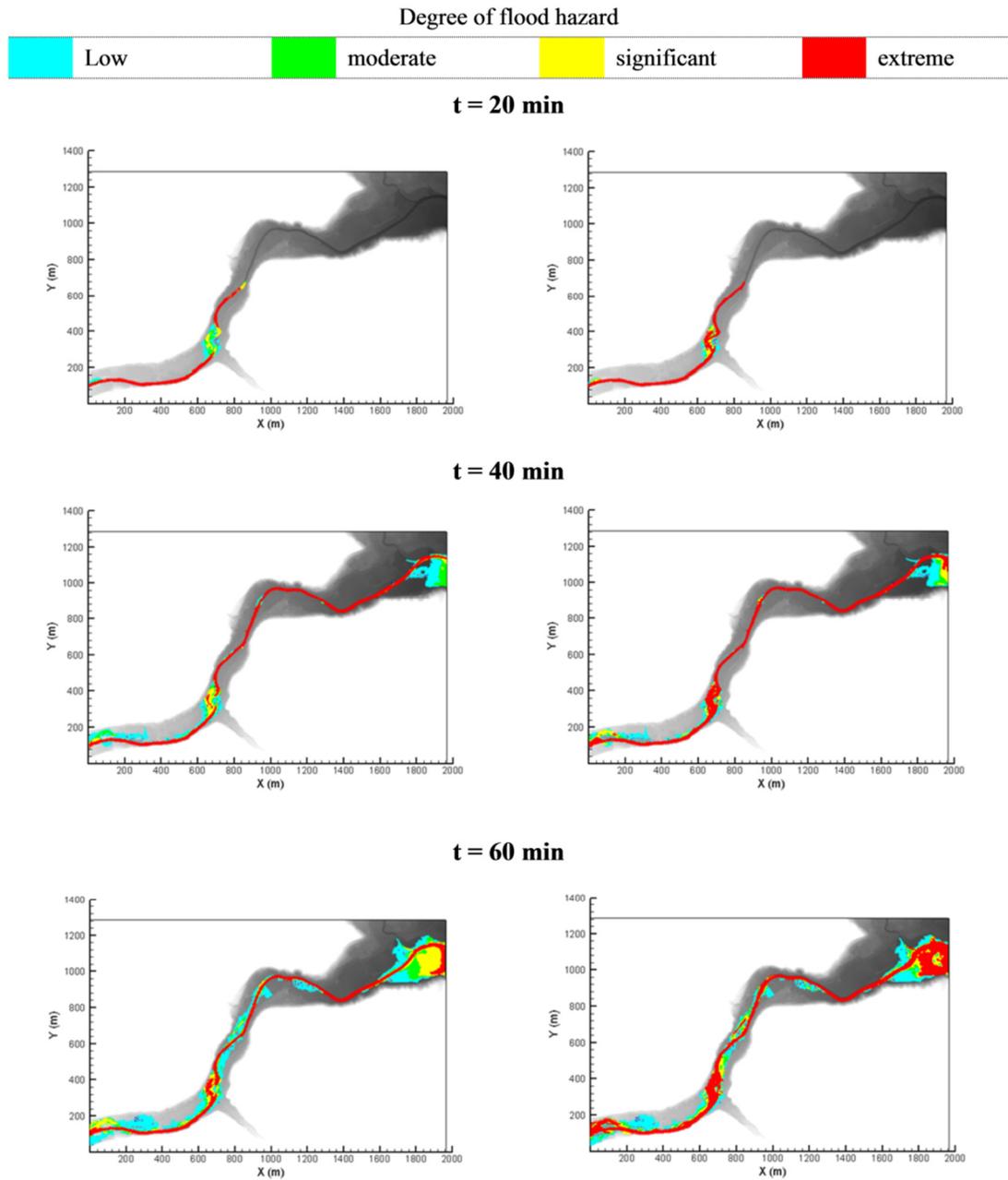
Figure 6.10: Flood hazard rating at 20, 40 and 60 minutes after the start of the 2007 Železniki flash flood simulation according to the empirically derived method (left) and the physically based method and experimentally calibrated method (right)
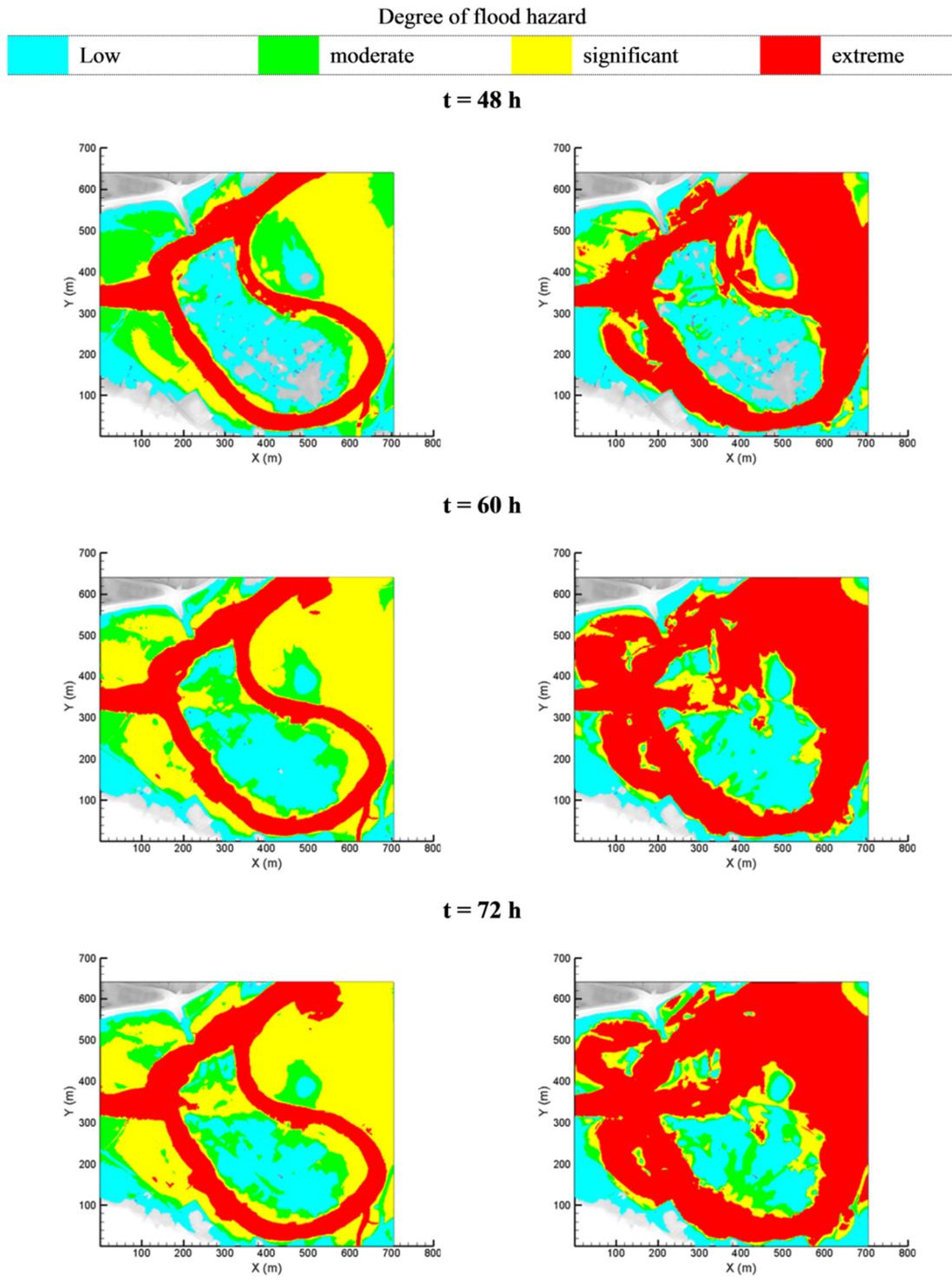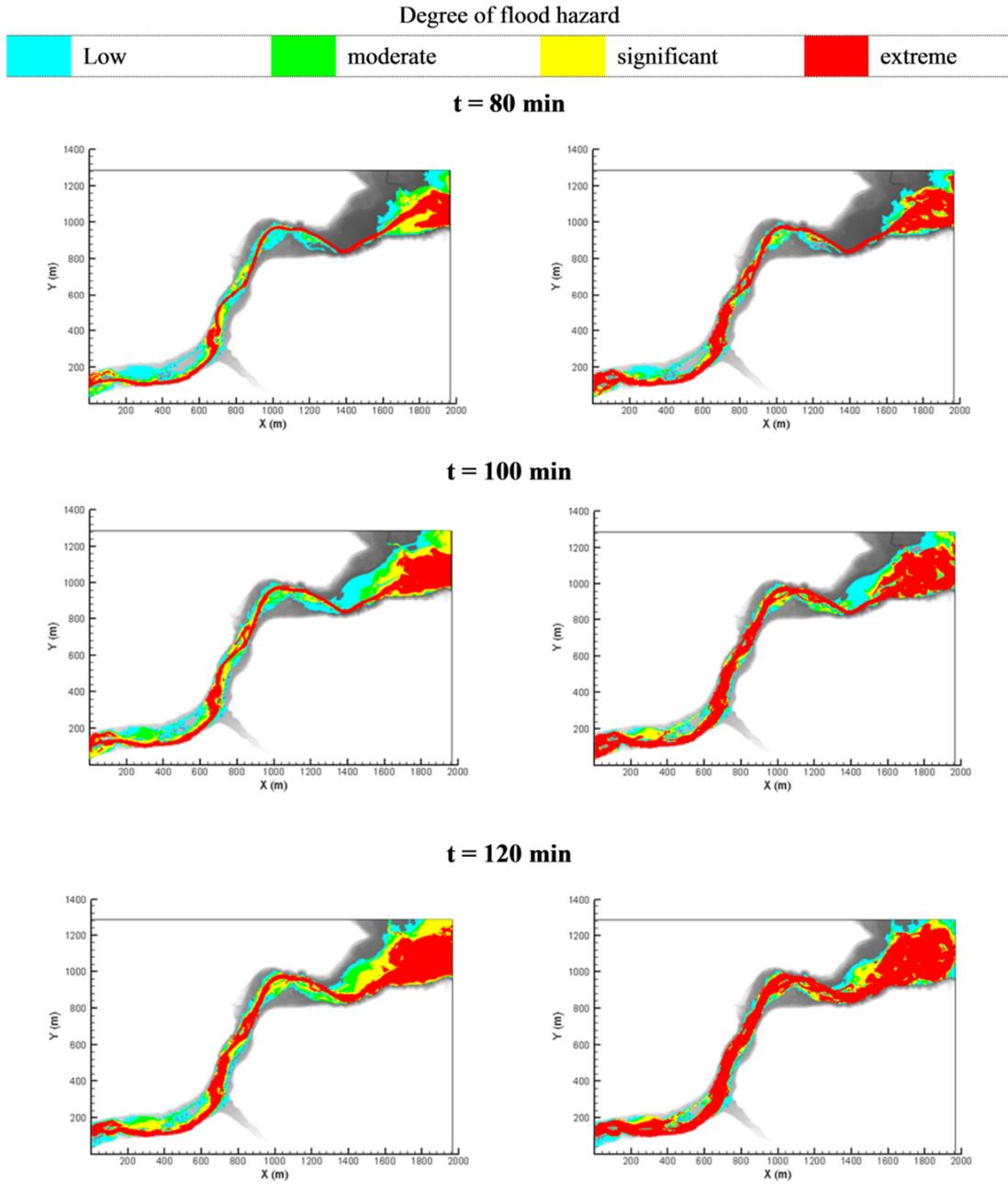
Figure 6.11: Flood hazard rating at 80, 100 and 120 minutes after the start of the 2007 Železniki flash flood simulation according to the empirically derived method (left) and the physically based experimentally calibrated method (right)

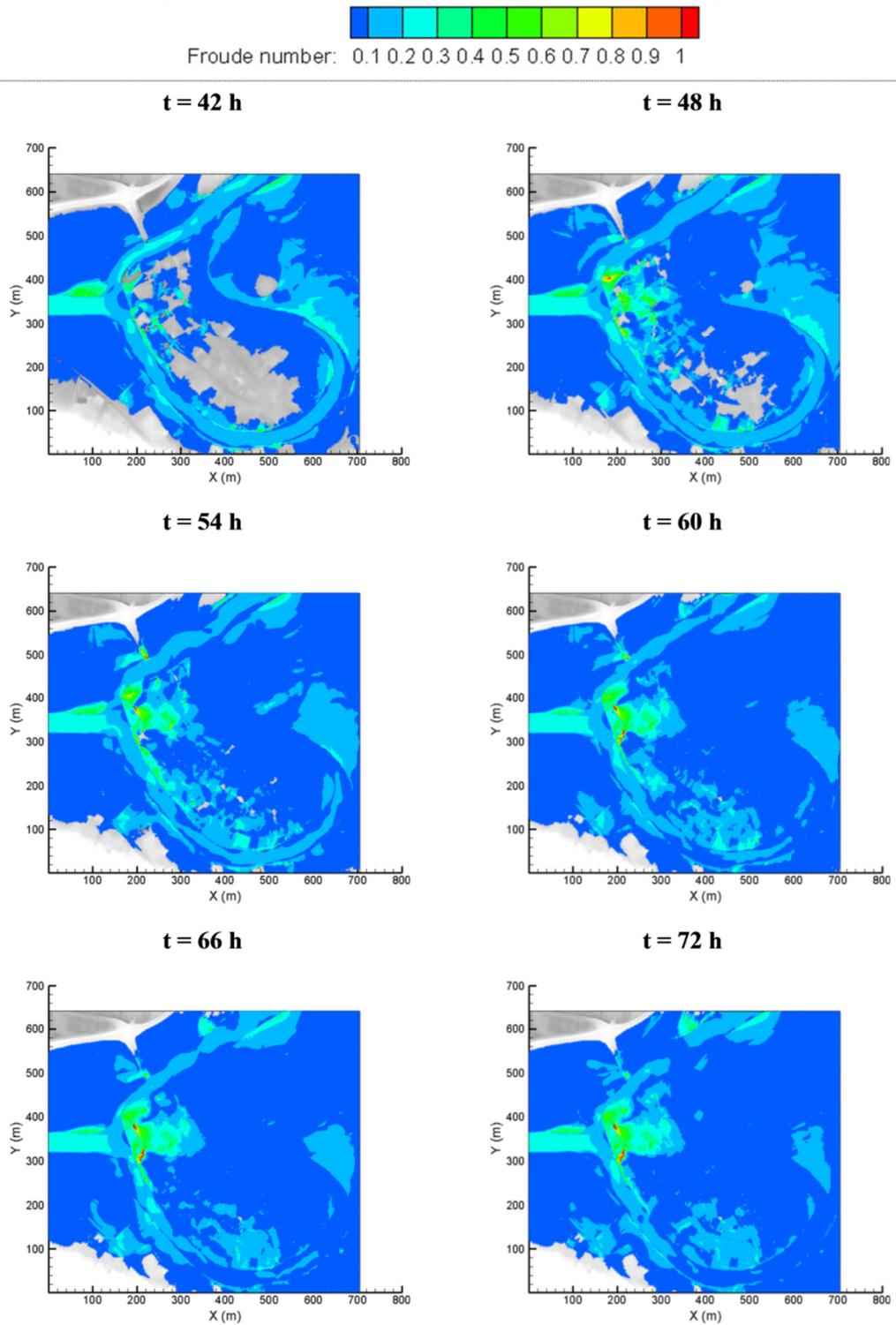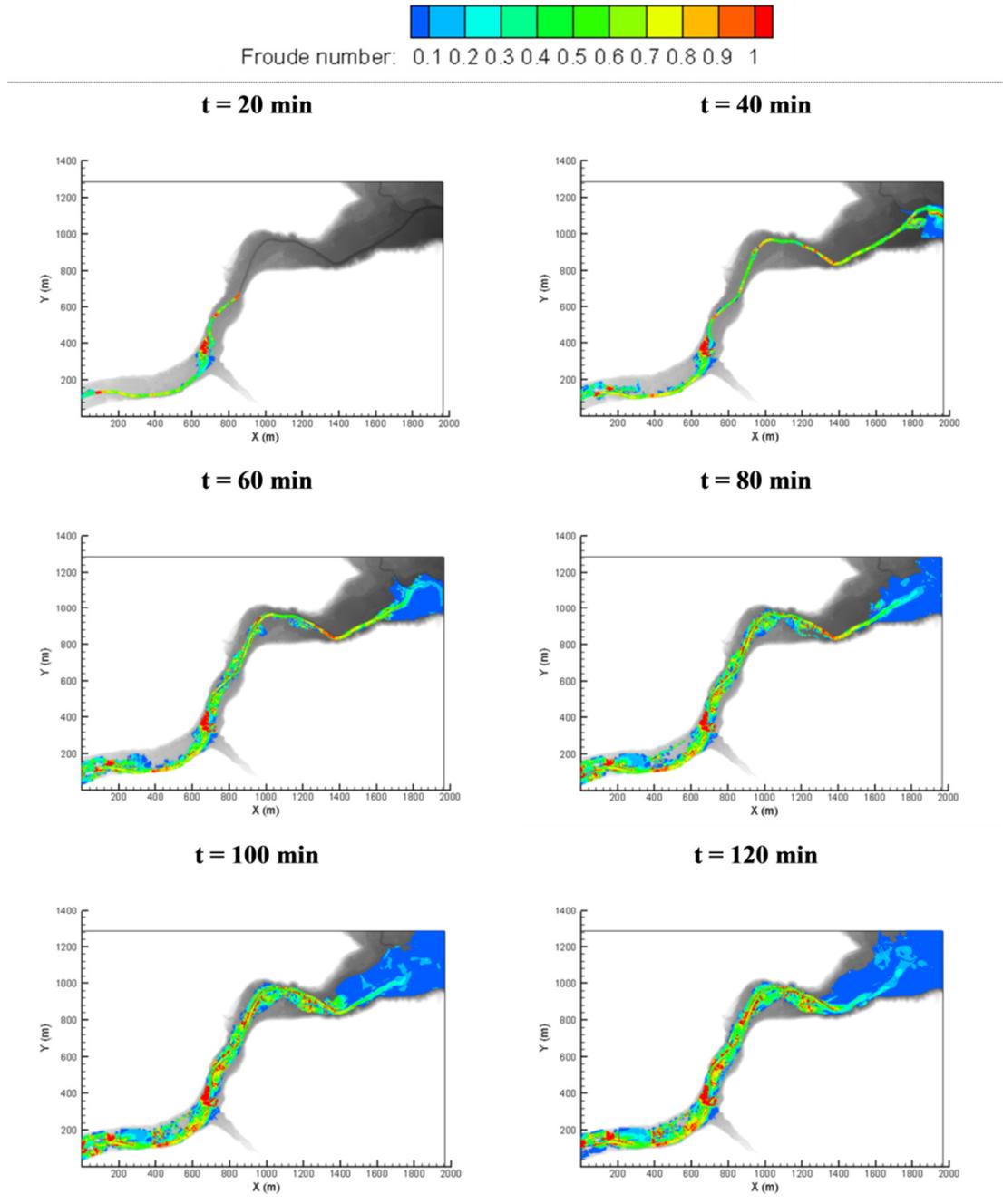Figure 6.12: Maximum Froude number values for the 2007 Železniki flash flood simulation

It should be noted that the empirically derived flood hazard assessment method considered in this study is well established in the UK, and that flood hazard maps issued by the governing authorities in the UK (i.e. DEFRA) are based on this criterion. The formulae based on empirical or quasi-theoretical studies, such as the empirically derived method considered in this study, are suitable and accurate for low land floods, with a low Froude number. However, for flood events where the velocity conditions change rapidly and the Froude numbers are relatively large, such as during flash floods or extreme river floods (see Figure 6.7, Figure 6.9 and Figure 6.12) then these methods fail to accurately predict flood hazard indices. Instead, a flood hazard assessment in areas prone to flash flooding, or in areas known for large scale and violent river flooding, should be undertaken using flood hazard assessment methods based on a physics-based analysis, because these methods are able to efficiently take into account rapid changes in the flow regime and enable a rapid assessment of the degree of flood hazard risk in a short time period.

Although the differences between the tested two flood hazard assessment methods might seem insignificant for some cases, the difference in the accuracy could be a crucial factor when it comes to real life rescue actions and the need to decide on the priority areas for the emergency services etc. The rescue services can acquire much more accurate and meaningful information from the step-by-step presentation of the development of a potential flood event, or from a video simulation of flood propagation, using the physics-based approach for flood hazard prediction, as compared to standard flood hazard maps. This is particularly important in the case of violent flood events, such as flash flooding, as it allows such flood hazards to be more accurately determined and for the emergency services etc. to determine how much time they have for a rescue operation, as well as determining the optimum rescue routes from a flood prone region. Therefore, flood hazard assessment methods based on a physics-based analysis, such as the physically based and experimentally calibrated method considered in this thesis, could provide an additional response time and more efficient deployment of the rescue services, particularly during the most critical stages of flooding.

Even though the use of more sophisticated flood hazard assessment methods can improve the prediction of flood hazard indices, the precondition for an adequate

flood hazard assessment is still an accurate flood inundation modelling. Firstly, there is a need to use appropriate flood inundation models and flood risk assessment techniques when modelling specific flood events, such as flash flooding (see Chapter 4). Secondly, an important factor in flood inundation modelling, and thus flood hazard assessment processes, is also the selected grid size. In the study conducted by Smith and Wasko (2012), it was shown that model resolutions of up to 10 m were adequate for representing peak flood levels, whereas model resolutions of 2m or less were required to represent the complex flow patterns in urban areas. This being the case, a change in the grid resolution can have a significant effect on the predicted flow velocities, flow directions, flow discharge distributions and ultimately on the prediction of flood hazard indices (Smith and Wasko, 2012). Therefore, any flood hazard assessment should not be focused exclusively on the selection of an appropriate flood hazard assessment method, but it should also take into account the complexity of the modelling area and the nature of the considered flood flow (e.g. the expected hydraulic characteristics of the considered flood flow).

6.4 Summary

The third key research objective was addressed in this chapter, i.e. what type of flood hazard assessment methods should be used for assessing the flood hazard to people caused by extreme flooding has been considered. Two flood hazard assessment methods were tested, including: (i) a widely used, empirically derived method developed for DEFRA by Ramsbottom et al. (2006), and (ii) a recently introduced, physically based and experimentally calibrated method proposed by Xia et al. (2014). These two flood hazard assessment methods were first evaluated against three different experimental datasets, including two datasets based on testing real human subjects and one dataset based on experiments using model human bodies, and later used to assess the flood hazard rating for three extreme flood events, i.e. the 2010 Kostanjevica na Krki extreme river flood, the 2004 Boscastle flash flood and the 2007 Železniki flash flood. The obtained results show that in areas prone to extreme flooding, the flood hazard indices should be predicted with methods derived from a physics-based analysis, such as the physically based and experimentally calibrated method considered in this study. Such methods have a number of benefits since they:

(i) consider all of the physical forces acting on a human body in floodwaters, (ii) are able to efficiently take into account rapid changes in the flow (or velocity) regime, something that usually occurs during flash flooding or extreme river flooding, and (iii) enable a rapid assessment of the degree of flood hazard risk in a short time period, a feature particularly important when assessing flood hazard indices for high Froude numbers flows, such as for the three extreme flood events considered in this study. This being the case, flood hazard assessment methods based on a physics-based analysis, such as the physically based and experimentally calibrated method considered in this study, could significantly improve the flood response and rescue plans currently in use for areas susceptible to occurrence of extreme flood events.

CHAPTER 7

Conclusions and future research

7.1 General conclusions

The research presented in this thesis has been directed towards improving flood risk assessment tools for modelling in areas susceptible to the occurrence of extreme flood events, and thus laying the foundation for production of more accurate flood inundation extent and flood hazard risk maps for areas prone to extreme flooding.

Namely, climate change will have a key role in the intensification and acceleration of the hydrological cycle, which in turn is expected to result into more frequent occurrence of extreme flood events, such as flash flooding and large scale river flooding. These flood events are often associated with trans and super-critical flows, and abrupt changes in the flow regime, such as emergence of hydraulic jumps. However, standard flood risk tools do not adequately represent such complex hydrodynamic processes, which can result in misleading predictions of flood depths, velocities and inundation extent and therefore in inadequate flood risk design. In addition, there is also a constant growth in the world's population, with more and more urban communities being developed in high-frequency flood zones and areas susceptible to occurrence of extreme flood events. This being the case, there is a need for more accurate flood risk assessment designs in areas prone to extreme flooding, which can be achieved by the implementation of appropriate flood inundation modelling tools and suitable flood hazard assessment techniques.

The first research objective of this study was to determine what type of flood inundation models should be used for predicting the flood elevations, velocities and inundation extent for extreme flood events. In order to reach this research objective, the well documented 2004 Boscastle flash flood was simulated using of two different types of flood inundation models, i.e. the ADI-type DIVAST model and the shock-capturing DIVAST-TVD model. Three different model structures were considered in

this study, including: (i) a shock-capturing flood inundation model (i.e. the TVD simulation case), (ii) a regular ADI-type flood inundation model (i.e. the ADI simulation case), and (iii) a flood inundation model based on the "simplified inertial" approach (i.e. the SI simulation case). Simulation results from these three different model structures were compared to post-flood measurements, which were based mainly on observed wrack marks.

Direct comparisons between the predicted flood levels and observed wrack marks showed that the shock-capturing model structure (i.e. the TVD simulation case) was more accurate in terms of numerical model predictions of the flood peak elevations, as compared to the water elevations predicted using the two other model structures considered in this study (i.e. the ADI and the SI simulation cases). The ADI and SI model configurations lacked the shock-capturing ability and thus inaccurately predicted the main hydrodynamic parameters due to the spurious numerical oscillations caused by abrupt changes in the flow regime. This being the case, the numerical oscillations have swamped the flood wave prediction, and consequently resulted in erroneous flood level and inundation extent prediction. In addition, the Nash-Sutcliffe model efficiency coefficient was used to measure the predictive capability of the TVD, ADI and SI simulation cases, and was calculated using 30 pairs of observed-simulated values. The calculation of the NSE coefficients further confirmed that the TVD simulation case significantly outperformed the ADI and SI simulation cases, with an NSE coefficient of 0.9863, as compared to values of 0.8530 and 0.8684 respectively. The NSE coefficient close to 1 indicated that the TVD simulation case results matched almost perfectly to the observed data, whereas the ADI and SI simulation cases were less numerically accurate.

The second research objective of this study was to investigate the appropriateness of the "simplification strategy" when used as a flood risk assessment modelling tool for areas susceptible to extreme flooding. In order to reach this research objective, attempts have been made within this study to improve on the simulation results for the ADI simulation case by increasing the value of the Manning's coefficient. More than 30 additional simulations were conducted with the ADI model structure, where the value of the Manning's coefficient was gradually increased until the modelled elevations and inundation extent were similar to those of the TVD simulation case.

However, the improvements were based on using an artificially high Manning's coefficient to give an acceptable level of accuracy, i.e. the ADI simulation case produced similar results to the TVD simulation case when the value of the Manning's coefficient was set to 0.6. As only unrealistically high roughness coefficients improved simulation results to an acceptable level, these improvements should not stand as proof of appropriateness of ADI-type models for simulating rapidly varying flood events. Instead, these improvements should stand as a caution against using this undesirable practice, since setting blindly unrealistically high values of Manning's coefficients to improve the results could have a devastating consequence in predicting the real extreme flood elevations and inundation extent, particularly when designing flood defence structures.

The third and final research objective of this study was to determine what type of flood hazard assessment methods should be used for assessing the flood hazard to people caused by extreme flooding. In order to achieve this research objective, two flood hazard assessment methods were tested, i.e. a widely used, empirically derived method introduced by Ramsbottom et al. (2006), and a recently introduced, physically based and experimentally calibrated method developed by Xia et al. (2014). The two selected flood hazard assessment methods were: (i) validated against experimental data, including two datasets based on testing real human subjects and one dataset based on experiments using model human bodies, and (ii) used to assess flood hazard indices for three different extreme flood events, namely: the 2010 Kostanjevica na Krki extreme river flood (Slovenia), the 2004 Boscastle flash flood (England, UK) and the 2007 Železniki flash flood (Slovenia).

The obtained results show that in areas prone to extreme flooding, the flood hazard indices should be predicted based on methods derived from a physics-based analysis, such as the physically based and experimentally calibrated method considered in this study. These formulations: (i) consider all of the physical forces acting on a human body in floodwaters, e.g. drag force, frictional force, gravitational force, buoyancy force and normal reaction force, (ii) take into account the rapid changes in the flow (or velocity) regime, which often occur for extreme flood events, and (iii) enable a rapid assessment of the degree of flood hazard risk in a short time period, a feature particularly important when assessing flood hazard indices for high Froude numbers

flows. Furthermore, the recently introduced flood hazard assessment methodologies derived from a physics-based analysis, such as the method presented by Xia et al. (2014) considered in this study, or the methodology proposed by Milanesi et al. (2015), can be adjusted to: (i) a specific body type, such as Asian, Caucasian or African-American, (ii) a specific region, such as Europe, USA or China, and (iii) a specific sub-population group, such as men, women or children. This being the case, the criterion derived from a physics-based analysis, such as the physically based and experimentally calibrated method considered in this study, can provide valuable information on the response time and enable more efficient rescue operations. Namely, these criteria are highly adaptable to extreme flood conditions and human body characteristics, and can therefore provide an accurate real-time assessment of the risk to people caused by real-time extreme flooding.

All in all, the main finding of this research can be summarised as following:

- shock-capturing flood inundation models should be used for predicting flood elevations, velocities and inundation extent for extreme flood event scenarios that are characterised with high Froude number flows (i.e. Froude number near or above 1) and/or abrupt changes in the flow regime, such as hydraulic jumps; shock-capturing models apply artificial diffusion terms in the solution procedure, which ensure the stability of the computational process and enable the computation of any shock waves or discontinuities as part of the numerical solution; these model features enable more reliable predictions of flood depths, velocities and inundation extent for rapidly varying flood events (e.g. flash floods) when compared to the ADI-type models, which are prone to the generation of spurious numerical oscillation in the model solution for such modelling scenarios; namely, ADI-type models usually need additional modification of the modelling domain in order to obtain stable solution when modelling high Froude number flows or flood scenarios with abrupt changes in the flow regime (e.g. hydraulic jumps), such as applying of patches of high roughness in order to decrease the velocity of the flow and thus dissipate the energy of the flow, which in turn can dampen out the numerical oscillations; however, this can be highly dangerous practice (see the next bullet point)

- the application of the "simplification strategy" considered in this study (i.e. increasing the roughness coefficient in order to improve oscillatory results) is inappropriate and potentially extremely dangerous, as there is no known procedure in determining the value of the Manning's coefficient which will improve on the accuracy of the simulations results to an acceptable level; therefore, such practices should not be used as a flood risk assessment modelling tool when analysing flood events with rapid changes in the flow regime or modelling high Froude number flows, as the corresponding flood simulation results have no scientific or engineering basis; moreover, this is particularly dangerous when modelling in the areas where there is no or limited validation and/or calibration data, which is usually the case when modelling in the areas prone to flash flooding

- in the areas prone to occurrence of extreme flood events, the predictions of flood hazard risk indices should be conducted using criteria derived from a physics-based analysis, such as the physically based and experimentally calibrated method considered in this research; these formulations consider all of the physical forces acting on a human body in floodwaters, take into account the rapid changes in the flow regime, which often occur for extreme flood events, and enable a rapid assessment of the degree of flood hazard risk in a short time period, a feature particularly important when assessing flood hazard indices for high Froude numbers flows; furthermore, these criteria can be adjusted to a specific body type, a specific region, or a specific sub-population group

7.2 Research impact

The research presented in this thesis could have significant impact in the near future on the flood risk assessment procedures currently used in areas prone to occurrence of extreme flood events. For example, the research outcomes have already attracted great interest from Natural Resources Wales (previously Environment Agency Wales), as the majority of Wales is highly prone to flash flooding. The Natural Resources Wales is the governing body in Wales for issuing flood inundation extent

and flood hazard maps, and commissioning flood risk assessment studies for urban communities within Wales. Their interest is to test the findings presented in this study on sites in Wales, and afterwards decide whether the modelling and flood hazard assessment methodologies proposed in this thesis significantly improve on the accuracy of the results when compared to standard modelling techniques (i.e. ADI-type flood inundation models and empirically based flood hazard assessment criteria). This being the case, in collaboration with the Natural Resources Wales the main findings presented in this thesis are currently being tested on two locations in Wales. The modelling of the first site (i.e. Borth, West Wales) has already been completed, and the modelling results are very similar to results obtained for Boscastle and Železniki case studies presented in this thesis. The modelling of the second site (i.e. Ebbw Valley) will commence in due time. If the results for the second site do not differ significantly from the previously obtained results, then the Natural Resources Wales will most likely start wider debate on improving flood risk modelling techniques for areas prone to flash flooding. Consequently, this might change the flood risk modelling procedures currently in use by flood risk practitioners in Wales, and thus lead to implementation of the main research finding presented in this thesis as the standard modelling procedures when modelling in areas prone to the occurrence of flash flooding.

The research presented in this thesis could also have a relatively significant economic impact. In the UK, millions of pounds are spent annually for insurance claims and damage repair. Furthermore, once the property gets flooded its value can drop quite significantly and flood insurance premiums can increase drastically. Also, it can be difficult to sell or secure a mortgage for a property that was flooded or is close to previously flooded areas. All this is particularly problematic in areas prone to occurrence of extreme flood events due to lack of adequate flood risk assessment schemes. Therefore, production of high-resolution flood inundation extent maps for urban communities vulnerable to extreme flooding could better equip Government and the insurance industry in the development of more detailed flood insurance schemes. Such schemes could more accurately define the financial burden due to flood risk, and thus reduce the amount of insecurity that is currently present with people living in, or near, high-risk flood zones. In addition, more accurate flood risk tools could lead to revaluation of property prices, as more detailed flood maps could

show higher degree of flood risk for many existing properties. Even though this could lead to dissatisfaction among general population due to decrease in the values of their property, it would also allow people to become more aware of potential risks when buying a particular property. Furthermore, as high-risk flood zones could be identified more accurately, new homes could be built in areas less endangered from flooding. This being the case, less money would be spent on flood protection design and flood insurances, and such homes would be more attractive for buyers and therefore reach higher prices.

Finally, the research presented in this thesis could also have significant impact on the general population and society. Namely, more accurate flood risk management schemes would lead to a more detailed flood protection design. Furthermore, new housing communities could be developed in such a way that they are completely removed from high-frequency flood zones, as these would be more precisely defined and recognised. All this, in turn, should enhance the quality of life, as it would provide a safer living environment for people living in urban communities in areas prone to occurrence of extreme flood events.

7.3   Recommendations for further study

Even though this thesis addressed several topics, it was not possible to investigate all potential areas of interest due to software and data unavailability, and time constraint. Therefore, a number of considerations are recommended for further research.

Extreme flood events are very poorly monitored events due to their relatively rare and usually sudden occurrence, and extremely violent nature. This makes these flood events very difficult to predict and even harder to model, particularly since there are limited data available to test various models. Due to rapid occurrence and the violent nature of extreme floods, there is little time to respond and acquire data for subsequent model verification. During extreme floods government agencies and emergency services understandably have to concentrate on saving human lives and limiting structural damage, rather than collecting data for future studies. This means

that limited attention can be paid to collecting data for extreme floods, which would be ideal for setting up numerical models and improving flood protections for the future. Therefore, future studies are encouraged to further expand (i) the development of more advance and more enduring measuring equipment (such as stream-gauges), which could survive the devastating force of extreme flooding, and (ii) the development of remote sensing techniques for post-flood surveillance, such as the use of LiDAR or drones for mapping flood inundation extent. In addition, it would be also interesting to develop detailed extreme flooding databases, where there would be collected post-flood measurements and observations for specific flood events.

However, the lack of data for extreme flood events will most likely remain a challenge for flood modellers for the foreseeable future due to the aforementioned limitations and practical difficulties in collecting data for such flood events. Therefore, there is an urgent need to improve our knowledge of extreme flood processes and drivers. This being the case, further research is needed to determine the precise hydrological and topographical conditions as to when shock-capturing algorithms are needed. This should focus on determining the topographical and hydrological indexes in the areas prone to extreme flooding, which would stand as a guide as to when to use regular type flood-modelling (e.g. ADI-type models) or extreme flood event modelling (e.g. shock-capturing models). Determination of these indexes, coupled with the correct flood modelling scheme, would lead to a more realistic flood modelling in river basins prone to occurrence of extreme flood events, and thus better equip flood risk practitioners in their planning and decision making.

Heavy precipitation is generally the main cause of flooding. Even though numerical weather prediction has progressed immensely in last decades, there are still difficulties in predicting local weather extremes and further translating these to model inflows. Therefore, further researchers are also encouraged to improve our knowledge of predicting extreme weather events, which can results into extreme precipitation, rapid runoff and consequently to extreme flooding. Furthermore, once our knowledge of predicting extreme weather events is improved, future research could also concentrate on linking meteorological, hydrological and hydraulic modelling, and thus try to develop an advanced extreme flood alert system, similar to

the European Flood Awareness System for large European watercourses. Such system would aim to predict local weather extremes, estimate potential runoff and finally produce flood elevations and inundation maps for the endangered areas before the actual flooding would even take place. This would then provide the emergency services with enough time to develop efficient flood response and rescue plans, and prepare the general public for the danger of the potential extreme flooding.

There is also need to further improve flood hazard assessment methodologies for areas prone to extreme flooding. The switch from the use of conventional methods to recently introduced physics-based methods should only be considered as the first step. Further studies are encouraged to develop even more accurate methods by including more detailed representations of human body characteristics and more complex flow conditions, such as considering local turbulences in the flow. Furthermore, future research should also concentrate on how to qualitatively include the effect of the floating debris into the flood hazard assessment criteria, as this area of research has been practically unexploited so far. Finally, future experimental studies are encouraged to develop more realistic testing conditions, which would try to exclude the experiment limitations currently present (e.g. training, over-use of safety equipment etc.), and thus provide the researchers with the experimental data that would be more comparable to the real-life situations. Such data could then be used for further development of new and even more sophisticated flood hazard assessment methodologies.

References

ABT, S. R., WITTIER, R. J., TAYLOR, A. & LOVE, D. J. 1989. Human Stability in a High Flood Hazard Zone. *Journal of the American Water Resources Association,* 25**,** 881-890.

ACOSTA, M., ANGUITA, M., FERNÁNDEZ-BALDOMERO, F. J., RAMÓN, C. L., SCHLADOW, S. G. & RUEDA, F. J. 2015. Evaluation of a nested-grid implementation for 3D finite-difference semi-implicit hydrodynamic models. *Environmental Modelling & Software,* 64**,** 241-262.

AHMADIAN, R., FALCONER, R. & BOCKELMANN-EVANS, B. 2012. Far-field modelling of the hydro-environmental impact of tidal stream turbines. *Renewable Energy,* 38**,** 107-116.

AHMADIAN, R. & FALCONER, R. A. 2012. Assessment of array shape of tidal stream turbines on hydro-environmental impacts and power output. *Renewable Energy,* 44**,** 318-327.

AHMADIAN, R., FALCONER, R. A. & WICKS, J. 2015. Benchmarking of flood inundation extent using various dynamically linked one- and two-dimensional approaches. *Journal of Flood Risk Management*.

ALCRUDO, F. 2002. A state of the art review on mathematical modelling of flood propagation. *First IMPACT project Workshop, Wallingford, UK.*

ALCRUDO, F. 2004. Advanced mathematical modelling techniques for flood propagation in natural topographies. *IMPACT Project - WP3 - D3.2.1.* Universidad de Zaragoza, Zaragoza, Spain.

ALLAN, R. P. & SODEN, B. J. 2008. Atmospheric warming and the amplification of precipitation extremes. *Science,* 321**,** 1481-1484.

AMENGUAL, A., HOMAR, V. & JAUME, O. 2015. Potential of a probabilistic hydrometeorological forecasting approach for the 28 September 2012 extreme flash flood in Murcia, Spain. *Atmospheric Research,* 166**,** 10-23.

ANDERSON, J. M., AMARASINGHE, S. P. & LAM, M. S. Data and computation transformations for multiprocessors. ACM SIGPLAN Notices, 1995. ACM, 166-178.

ANDROULIDAKIS, Y. S., KOMBIADOU, K. D., MAKRIS, C. V., BALTIKAS, V. N. & KRESTENITIS, Y. N. 2015. Storm surges in the Mediterranean Sea: Variability and trends under future climatic conditions. *Dynamics of Atmospheres and Oceans,* 71**,** 56-82.

ANTICO, A., TORRES, M. E. & DIAZ, H. F. 2015. Contributions of different time scales to extreme Paraná floods. *Climate Dynamics*.

APEL, H., ARONICA, G., KREIBICH, H. & THIEKEN, A. 2009. Flood risk analyses—how detailed do we need to be? *Natural Hazards,* 49**,** 79-98.

ASHLEY, S. T. & ASHLEY, W. S. 2008. Flood fatalities in the United States. *Journal of Applied Meteorology and Climatology,* 47**,** 805-818.

AURELI, F., DAZZI, S., MARANZONI, A., MIGNOSA, P. & VACONDIO, R. 2015. Experimental and numerical evaluation of the force due to the impact of a dam-break wave on a structure. *Advances in Water Resources,* 76**,** 29-42.

BARIWENI, P., TAWARI, C. & ABOWEI, J. 2012. Some environmental effects of flooding in the Niger Delta region of Nigeria. *International Journal of Fisheries and Aquatic Sciences,* 1**,** 35-46.

BATES, P., TRIGG, M., NEAL, J. & DABROWA, A. 2013. LISFLOOD-FP User manual and technical note. *School of Geographical Sciences, University of Bristol, UK*.

BATES, P. D. & DE ROO, A. P. J. 2000. A simple raster-based model for flood inundation simulation. *Journal of Hydrology,* 236**,** 54-77.

BATES, P. D., HORRITT, M. S. & FEWTRELL, T. J. 2010. A simple inertial formulation of the shallow water equations for efficient two-dimensional flood inundation modelling. *Journal of Hydrology,* 387**,** 33-45.

BBC. 2013a. *Cardiff hit by flash flooding chaos on Saturday afternoon* [Online]. Available: http://www.bbc.co.uk/news/uk-wales-south-east-wales-24595500 [Accessed 18/09/2015].

BBC. 2013b. *Flash flooding hits homes after rain across Wale* [Online]. Available: http://www.bbc.co.uk/news/uk-wales-23576219 [Accessed 18/09/2015].

BEDRI, Z., BRUEN, M., DOWLEY, A. & MASTERSON, B. 2011. A three-dimensional hydro-environmental model of Dublin Bay. *Environmental Modeling & Assessment,* 16**,** 369-384.

BEDRI, Z., BRUEN, M., DOWLEY, A. & MASTERSON, B. 2013. Environmental consequences of a power plant shut-down: a three-dimensional water quality model of Dublin Bay. *Marine pollution bulletin,* 71**,** 117-128.

BEGNUDELLI, L. & SANDERS, B. F. 2006. Unstructured grid finite-volume algorithm for shallow-water flow and scalar transport with wetting and drying. *Journal of Hydraulic Engineering,* 132**,** 371-384.

BEGNUDELLI, L. & SANDERS, B. F. 2007. Simulation of the St. Francis dam-break flood. *Journal of Engineering Mechanics,* 133**,** 1200-1212.

BELTAOS, S. 2014. Comparing the impacts of regulation and climate on ice-jam flooding of the Peace-Athabasca Delta. *Cold Regions Science and Technology,* 108**,** 49-58.

BENISTON, M. 2009. Trends in joint quantiles of temperature and precipitation in Europe since 1901 and projected for 2100. *Geophysical Research Letters,* 36.

BERGMAN, N., SHOLKER, O., ROSKIN, J. & GREENBAUM, N. 2014. The Nahal Oz Reservoir dam-break flood: Geomorphic impact on a small ephemeral loess-channel in the semi-arid Negev Desert, Israel. *Geomorphology,* 210**,** 83-97.

BEVEN, K. J. 2000. Uniqueness of place and process representations in hydrological modelling. *Hydrology and Earth System Sciences Discussions,* 4**,** 203-213.

BISCARINI, C., FRANCESCO, S. D. & MANCIOLA, P. 2010. CFD modelling approach for dam break flow studies. *Hydrology and Earth System Sciences,* 14**,** 705-718.

BLADÉ, E., GÓMEZ-VALENTÍN, M., DOLZ, J., ARAGÓN-HERNÁNDEZ, J., CORESTEIN, G. & SÁNCHEZ-JUNY, M. 2012. Integration of 1D and 2D finite volume schemes for computations of water flow in natural channels. *Advances in Water Resources,* 42**,** 17-29.

BLEASDALE, A. 1963. The distribution of exceptionally heavy daily falls of rain in the United Kingdom, 1960-1963. *Instn Wat. Engrs,* 17**,** 45-55.

BOCKELMANN, B., FENRICH, E. K., LIN, B. & FALCONER, R. A. 2004. Development of an ecohydraulics model for stream and river restoration. *Ecological Engineering,* 22**,** 227-235.

BORGA, M., ANAGNOSTOU, E., BLÖSCHL, G. & CREUTIN, J.-D. 2011. Flash flood forecasting, warning and risk management: the HYDRATE project. *Environmental Science & Policy,* 14**,** 834-844.

BORGA, M., GAUME, E., CREUTIN, J. D. & MARCHI, L. 2008. Surveying flash floods: gauging the ungauged extremes. *Hydrological processes,* 22**,** 3883.

BORGA, M., STOFFEL, M., MARCHI, L., MARRA, F. & JAKOB, M. 2014. Hydrogeomorphic response to extreme rainfall in headwater systems: flash floods and debris flows. *Journal of Hydrology,* 518**,** 194-205.

BOUILLOUD, L., DELRIEU, G., BOUDEVILLAIN, B., BORGA, M. & ZANON, F. 2009. Radar rainfall estimation for the post-event analysis of a Slovenian flash-flood case: application of the Mountain Reference Technique at C-band frequency. *Hydrology and Earth System Sciences,* 13**,** 1349-1360.

BOYE, B. A. 2014. *Integrated modelling of hydrodynamic processes, faecal indicator organisms and related parameters with improved accuracy using parallel (GPU) computing.* PhD, Cardiff University.

BRAKENRIDGE, G. 2012. *Global Active Archive of Large Flood Events, Dartmouth Flood Observatory, University of Colorado* [Online]. Available: http://floodobservatory.colorado.edu/Archives/index.html [Accessed 17/08/2015].

BRASINGTON, J. & RICHARDS, K. 2007. Reduced-complexity, physically-based geomorphological modelling for catchment and river management. *Geomorphology,* 90**,** 171-177.

BREILH, J.-F., BERTIN, X., CHAUMILLON, É., GILOY, N. & SAUZEAU, T. 2014. How frequent is storm-induced flooding in the central part of the Bay of Biscay? *Global and Planetary Change,* 122**,** 161-175.

BRUWIER, M., ERPICUM, S., PIROTTON, M., ARCHAMBEAU, P. & DEWALS, B. 2015. Assessing the operation rules of a reservoir system based on a detailed modelling chain. *Natural Hazards and Earth System Science,* 15**,** 365-379.

BURT, S. 2005. Cloudburst upon Hendraburnick Down: the Boscastle storm of 16 August 2004. *Weather,* 60**,** 219-227.

BUTLER, I. R., SOMMER, B., ZANN, M., ZHAO, J. X. & PANDOLFI, J. M. 2015. The cumulative impacts of repeated heavy rainfall, flooding and altered water quality on the high-latitude coral reefs of Hervey Bay, Queensland, Australia. *Marine Pollution Bulletin,* 96**,** 356-367.

CALIANNO, M., RUIN, I. & GOURLEY, J. J. 2013. Supplementing flash flood reports with impact classifications. *Journal of Hydrology,* 477**,** 1-16.

CARTER, H. 2009. *Northern England and Wales mop up after flash floods* [Online]. Available: http://www.theguardian.com/uk/2009/jun/11/flash-floods-northern-england-wales [Accessed 18/09/2015].

CASSE, C., GOSSET, M., PEUGEOT, C., PEDINOTTI, V., BOONE, A., TANIMOUN, B. A. & DECHARME, B. 2015. Potential of satellite rainfall products to predict Niger River flood events in Niamey. *Atmospheric Research,* 163**,** 162-176.

CASTELLARIN, A., DOMENEGHETTI, A. & BRATH, A. 2011. Identifying robust large-scale flood risk mitigation strategies: a quasi-2D hydraulic model as a tool for the Po river. *Physics and Chemistry of the Earth, Parts A/B/C,* 36**,** 299-308.

CH2M. 2016. *Flood Modeller Pro User Manual* [Online]. Available: http://help.floodmodeller.com/floodmodeller/ [Accessed 15/11/2016].

CHADWICK, A., MORFETT, J. & BORTHWICK, M. 2013. *Hydraulics in civil and environmental engineering, 5th edition*, CRC Press.

CHANSON, H. 2004. *Hydraulics of open channel flow*, Butterworth-Heinemann.

CHANSON, H., BROWN, R. & MCINTOSH, D. 2014. Human body stability in floodwaters: the 2011 flood in Brisbane CBD. *Proceedings of the 5th International Symposium on Hydraulic Structures: Engineering Challenges and Extremes.* Brisbane, Australia: The University of Queensland.

CHAU, V. N., HOLLAND, J., CASSELLS, S. & TUOHY, M. 2013. Using GIS to map impacts upon agriculture from extreme floods in Vietnam. *Applied Geography,* 41**,** 65-74.

CHEN, Y. 1992. *Numerical Modeling of Solute Transport Processes Using Higher Order Accurate Finite Difference Schemes.* PhD, University of Bradford.

CHEN, Y., WANG, Z., LIU, Z. & ZHU, D. 2011. 1D–2D coupled numerical model for shallow-water flows. *Journal of hydraulic engineering,* 138**,** 122-132.

CHENG, Y., LIEN, F., YEE, E. & SINCLAIR, R. 2003. A comparison of large eddy simulations with a standard k–ε Reynolds-averaged Navier–Stokes model for the prediction of a fully developed turbulent flow over a matrix of cubes. *Journal of Wind Engineering and Industrial Aerodynamics,* 91**,** 1301-1328.

CHOI, S. U., JUNG, S. & KIM, S. K. 2015. A quasi-2D and quasi-steady hydraulic model for physical habitat simulations. *Ecohydrology,* 8**,** 263-272.

CHOW, V. T. 1959. Open channel hydraulics, 1959. *MacGraw-Hill, New York*.

CHRISTENSEN, J. H. & CHRISTENSEN, O. B. 2007. A summary of the PRUDENCE model projections of changes in European climate by the end of this century. *Climatic Change,* 81**,** 7-30.

CLARK, C. 1995. New estimates of probable maximum precipitation in South West England. *Meteorological Applications,* 2**,** 307-312.

COBBY, D. M., MASON, D. C., HORRITT, M. S. & BATES, P. D. 2003. Two-dimensional hydraulic flood modelling using a finite-element mesh decomposed according to vegetation and topographic features derived from airborne scanning laser altimetry. *Hydrological processes,* 17**,** 1979-2000.

COLELLA, P. & WOODWARD, P. R. 1984. The piecewise parabolic method (PPM) for gas-dynamical simulations. *Journal of computational physics,* 54**,** 174-201.

COLLIER, C. 2007. Flash flood forecasting: What are the limits of predictability? *Quarterly Journal of the royal meteorological society,* 133**,** 3-23.

COOK, A. & MERWADE, V. 2009. Effect of topographic data, geometric configuration and modeling approach on flood inundation mapping. *Journal of Hydrology,* 377**,** 131-142.

COURANT, R., FRIEDRICHS, K. & LEWY, H. 1967. On the partial difference equations of mathematical physics. *IBM journal of Research and Development,* 11**,** 215-234.

COX, R., SHAND, T. & BLACKA, M. 2010. Revision project 10: Appropriate safety criteria for people. Stage 1 report. *Australian Rainfall and Runoff.* Water Research Laboratory, The University of New South Wales.

COX, R., YEE, M. & BALL, J. Safety of People in Flooded Streets and Floodways. National Conference on Hydraulics in Water Engineering, 2004. Engineers Australia.

CREUTIN, J. D., BORGA, M., GRUNTFEST, E., LUTOFF, C., ZOCCATELLI, D. & RUIN, I. 2013. A space and time framework for analyzing human anticipation of flash floods. *Journal of Hydrology,* 482**,** 14-24.

CROISSANT, T., LAGUE, D. & DAVY, P. Calibration of the 2D Hydrodynamic Model Floodos and Implications of Distributed Friction on Sediment Transport Capacity. AGU Fall Meeting Abstracts, 2014. 3565.

CUNGE, J. & WEGNER, M. 1964. Intégration numérique des équations d'écoulement de Barré de Saint-Venant par un schéma implicite de différences finies. *La Houille Blanche***,** 33-39.

CUNGE, J. A. 2003. Of data and models. *Journal of Hydroinformatics,* 5**,** 75-98.

CUNGE, J. A., HOLLY, F. M. & VERWEY, A. 1980. *Practical aspects of computational river hydraulics*, Pitman Pub.

DAGUM, L. & MENON, R. 1998. OpenMP: an industry standard API for shared-memory programming. *Computational Science & Engineering, IEEE,* 5**,** 46-55.

DANISH HYDRAULIC INSTITUTE (DHI) 2007. MIKE FLOOD User Manual. Hørsholm, Denmark: DHI Water & Environment.

DAVIES, D. 2010. *Heavy rain sparks flash floods in Wales* [Online]. Available: http://www.independent.co.uk/environment/nature/heavy-rain-sparks-flash-floods-in-wales-2057955.html [Accessed 18/09/2015].

DAVIS, S. F. 1984. *TVD finite difference schemes and artificial viscosity*, National Aeronautics and Space Administration, Langley Research Center.

DAWSON, C. & MIRABITO, C. M. 2008. The shallow water equations. *University of Texas, Austin,* 29.

DAWSON, R. J., BALL, T., WERRITTY, J., WERRITTY, A., HALL, J. W. & ROCHE, N. 2011. Assessing the effectiveness of non-structural flood management measures in the Thames Estuary under conditions of socio-economic and environmental change. *Global Environmental Change,* 21**,** 628-646.

DE ALMEIDA, G. A. M., BATES, P., FREER, J. E. & SOUVIGNET, M. 2012. Improving the stability of a simple formulation of the shallow water equations for 2-D flood modeling. *Water Resources Research,* 48**,** W05528.

DE SAINT-VENANT, A. B. 1871. Théorie du mouvement non-permanent des eaux avec application aux crues des rivieres et a l'introduction des marees dans leur lit. *Comptes Rendus des séances de l'Académie des Sciences,* 73**,** 237-240.

DEARDORFF, J. W. 1970. A numerical study of three-dimensional turbulent channel flow at large Reynolds numbers. *Journal of Fluid Mechanics,* 41**,** 453-480.

DELIS, A. & KAMPANIS, N. 2009. Numerical flood simulation by depth averaged free surface flow models. *Environmental Systems–Encyclopedia of Life Support Systems (EOLSS).*

DENBIGHSHIRE COUNTY COUNCIL 2013. Investigation into the November 2012 Floods: Flood Investigation Report - Part 1.

DI BALDASSARRE, G. 2012. *Floods in a Changing Climate: Inundation Modelling*, Cambridge University Press.

DI BALDASSARRE, G., MONTANARI, A., LINS, H., KOUTSOYIANNIS, D., BRANDIMARTE, L. & BLÖSCHL, G. 2010. Flood fatalities in Africa: from diagnosis to mitigation. *Geophysical Research Letters,* 37.

DIMITRIADIS, P., TEGOS, A., OIKONOMOU, A., PAGANA, V., KOUKOUVINOS, A., MAMASSIS, N., KOUTSOYIANNIS, D. & EFSTRATIADIS, A. 2016. Comparative evaluation of 1D and quasi-2D hydraulic models based on benchmark and real-world applications for uncertainty assessment in flood mapping. *Journal of Hydrology.*

DING, D. & WU, S. 2012. Direct numerical simulation of turbulent flow over backward-facing at high Reynolds numbers. *Science China Technological Sciences,* 55**,** 3213-3222.

DOULGERIS, C., GEORGIOU, P., PAPADIMOS, D. & PAPAMICHAIL, D. 2012. Ecosystem approach to water resources management using the MIKE 11 modeling system in the Strymonas River and Lake Kerkini. *Journal of environmental management,* 94**,** 132-143.

DRILLIS, R., CONTINI, R. & BLUESTEIN, M. 1964. Body segment parameters. *Artificial limbs,* 8**,** 44-66.

DUFFAUT, P. 2013. The traps behind the failure of Malpasset arch dam, France, in 1959. *Journal of Rock Mechanics and Geotechnical Engineering,* 5**,** 335-341.

DUMBSER, M. & CASULLI, V. 2016. A conservative, weakly nonlinear semi-implicit finite volume scheme for the compressible Navier– Stokes equations with general equation of state. *Applied Mathematics and Computation,* 272**,** 479-497.

DURACK, P., WIJFFELS, S. & MATEAR, R. 2012. Ocean salinities reveal strong global water cycle intensification during 1950 to 2000. *Science,* 336**,** 455-458.

DURBIN, P. A. & REIF, B. A. P. 2010. Reynolds Averaged Navier–Stokes Equations. *Statistical Theory and Modeling for Turbulent Flows.* John Wiley & Sons, Ltd.

ELLIS, T. M. R., PHILIPS, I. R. & LAHEY, T. M. 1994. *Fortran 90 programming*, Addison-Wesley Wokingham, England.

ENDOH, K. & TAKAHASHI, S. 1994. Numerically modeling personnel danger on a promenade breakwater due to overtopping waves. *Coastal Engineering Proceedings,* 1.

FALCONER, R. A. 1986. Water quality simulation study of a natural harbor. *Journal of Waterway, Port, Coastal, and Ocean Engineering,* 112**,** 15-34.

FALCONER, R. A. & LIN, B. 2003. Hydro-environmental modelling of riverine basins using dynamic rate and partitioning coefficients. *International Journal of River Basin Management,* 1**,** 81-89.

FALCONER, R. A., LIN, B. & KASHEFIPOUR, S. M. 2005. Modelling Water Quality Processes in Estuaries. *Computational Fluid Dynamics.* John Wiley & Sons, Ltd.

FAULKNER, H., PARKER, D., GREEN, C. & BEVEN, K. 2007. Developing a translational discourse to communicate uncertainty in flood risk between science and the practitioner. *AMBIO: a Journal of the Human Environment,* 36**,** 692-704.

FENN, C., BETTESS, R., GOLDING, B., FARQUHARSON, F. & WOOD, T. 2005. The Boscastle flood of 16 August 2004: Characteristics, causes and consequences. *40th Defra Flood & Coastal Management Conference, University of York, 5-7 July.*

FERZIGER, J. H. & PERIC, M. 2002. *Computational methods for fluid dynamics, 3rd edition*, Springer Science & Business Media.

FEWTRELL, T., BATES, P., HORRITT, M. & HUNTER, N. 2008. Evaluating the effect of scale in flood inundation modelling in urban environments. *Hydrological Processes,* 22**,** 5107-5118.

FEWTRELL, T. J., DUNCAN, A., SAMPSON, C. C., NEAL, J. C. & BATES, P. D. 2011. Benchmarking urban flood models of varying complexity and scale using high resolution terrestrial LiDAR data. *Physics and Chemistry of the Earth, Parts A/B/C,* 36**,** 281-291.

FINAUD-GUYOT, P., DELENNE, C., GUINOT, V. & LLOVEL, C. 2011. 1D–2D coupling for river flow modeling. *Comptes Rendus Mécanique,* 339**,** 226-234.

FOSTER, D. & COX, R. 1973. Stability of children on roads used as floodways. Technical Report No.73/13. Water Research Laboratory of the University of New South Wales, Manly Vale, Australia.

FOUDI, S., OSÉS-ERASO, N. & TAMAYO, I. 2015. Integrated spatial flood risk assessment: The case of Zaragoza. *Land Use Policy,* 42**,** 278-292.

FOULDS, S. A., MACKLIN, M. G. & BREWER, P. A. 2014. The chronology and the hydrometeorology of catastrophic floods on Dartmoor, South West England. *Hydrological Processes,* 28**,** 3067-3087.

FRANCHELLO, G. 2010. Shoreline tracking and implicit source terms for a well balanced inundation model. *International journal for numerical methods in fluids,* 63**,** 1123-1146.

FREEMAN, J. A. & ROY, C. J. 2014. Verification and validation of Reynolds-averaged Navier–Stokes turbulence models for external flow. *Aerospace Science and Technology,* 32**,** 84-93.

FREI, C. & SCHÄR, C. 1998. A precipitation climatology of the Alps from high-resolution rain-gauge observations. *International Journal of Climatology,* 18**,** 873-900.

FROLKOVIČ, P., MIKULA, K. & URBÁN, J. 2015. Semi-implicit finite volume level set method for advective motion of interfaces in normal direction. *Applied Numerical Mathematics,* 95**,** 214-228.

FU, G. & BUTLER, D. 2014. Copula-based frequency analysis of overflow and flooding in urban drainage systems. *Journal of Hydrology,* 510**,** 49-58.

FULTON, S. R. 2004. Semi-implicit time differencing. Potsdam, New York, USA: Department of Mathematics and Computer Science, Clarkson University.

GALECZKA, I., EIRIKSDOTTIR, E. S., HARDARDOTTIR, J., OELKERS, E. H., TORSSANDER, P. & GISLASON, S. R. 2015. The effect of the 2002 glacial flood on dissolved and suspended chemical fluxes in the Skaftá river, Iceland. *Journal of Volcanology and Geothermal Research,* 301**,** 253-276.

GAO, G., FALCONER, R. A. & LIN, B. 2011. Numerical modelling of sediment–bacteria interaction processes in surface waters. *Water Research,* 45**,** 1951-1960.

GAUME, E., BAIN, V., BERNARDARA, P., NEWINGER, O., BARBUC, M., BATEMAN, A., BLAŠKOVIČOVÁ, L., BLÖSCHL, G., BORGA, M., DUMITRESCU, A., DALIAKOPOULOS, I., GARCIA, J., IRIMESCU, A., KOHNOVA, S., KOUTROULIS, A., MARCHI, L., MATREATA, S., MEDINA, V., PRECISO, E., SEMPERE-TORRES, D., STANCALIE, G., SZOLGAY, J., TSANIS, I., VELASCO, D. & VIGLIONE, A. 2009. A compilation of data on European flash floods. *Journal of Hydrology,* 367**,** 70-78.

GHOSTINE, R., HOTEIT, I., VAZQUEZ, J., TERFOUS, A., GHENAIM, A. & MOSE, R. 2015. Comparison between a coupled 1D-2D model and a fully 2D model for supercritical flow simulation in crossroads. *Journal of Hydraulic Research,* 53**,** 274-281.

GILLES, D. & MOORE, M. 2010. Review of Hydraulic Flood Modeling Software used in Belgium, The Netherlands, and The United Kingdom. *International Perspectives in Water Resources Management*.

GODUNOV, S. K. 1959. A difference method for numerical calculation of discontinuous solutions of the equations of hydrodynamics. *Matematicheskii Sbornik,* 89**,** 271-306.

GOLDING, B., CLARK, P. & MAY, B. 2005. The Boscastle flood: Meteorological analysis of the conditions leading to flooding on 16 August 2004. *Weather,* 60**,** 230-235.

GOURLEY, J. J., FLAMIG, Z. L., HONG, Y. & HOWARD, K. W. 2014. Evaluation of past, present and future tools for radar-based flash-flood prediction in the USA. *Hydrological Sciences Journal,* 59**,** 1377-1389.

GOURLEY, J. J., HONG, Y., FLAMIG, Z. L., ARTHUR, A., CLARK, R., CALIANNO, M., RUIN, I., ORTEL, T., WIECZOREK, M. E. & KIRSTETTER, P.-E. 2013. A unified flash flood database across the United States. *Bulletin of the American Meteorological Society,* 94**,** 799-805.

GOUTA, N. & MAUREL, F. 2002. A finite volume solver for 1D shallow-water equations applied to an actual river. *International Journal for Numerical Methods in Fluids,* 38**,** 1-19.

GRILLAKIS, M., TSANIS, I. & KOUTROULIS, A. 2010. Application of the HBV hydrological model in a flash flood case in Slovenia. *Natural Hazards and Earth System Science,* 10**,** 2713-2725.

GROPP, W., LUSK, E. & SKJELLUM, A. 1999. *Using MPI: portable parallel programming with the message-passing interface*, MIT press.

HABERT, J., RICCI, S., LE PAPE, E., THUAL, O., PIACENTINI, A., GOUTAL, N., JONVILLE, G. & ROCHOUX, M. 2016. Reduction of the uncertainties in the water level-discharge relation of a 1D hydraulic model in the context of operational flood forecasting. *Journal of Hydrology,* 532**,** 52-64.

HAJDUKIEWICZ, H., WYŻGA, B., MIKUŚ, P., ZAWIEJSKA, J. & RADECKI-PAWLIK, A. 2015. Impact of a large flood on mountain river habitats, channel morphology, and valley infrastructure. *Geomorphology*.

HALL, J. W., MEADOWCROFT, I. C., SAYERS, P. B. & BRAMLEY, M. E. 2003. Integrated flood risk management in England and Wales. *Natural Hazards Review,* 4**,** 126-135.

HARLOW, F. H. & WELCH, J. E. 1965. Numerical calculation of time-dependent viscous incompressible flow of fluid with free surface. *Physics of fluids,* 8**,** 2182.

HARTEN, A. 1983. High resolution schemes for hyperbolic conservation laws. *Journal of computational physics,* 49**,** 357-393.

HARTEN, A., ENGQUIST, B., OSHER, S. & CHAKRAVARTHY, S. R. 1987. Uniformly high order accurate essentially non-oscillatory schemes, III. *Journal of computational physics,* 71**,** 231-303.

HARTEN, A. & HYMAN, J. M. 1983. Self adjusting grid methods for one-dimensional hyperbolic conservation laws. *Journal of Computational Physics,* 50**,** 235-269.

HARTEN, A. & OSHER, S. 1987. Uniformly high-order accurate nonoscillatory schemes. I. *SIAM Journal on Numerical Analysis,* 24**,** 279-309.

HARTEN, A., OSHER, S., ENGQUIST, B. & CHAKRAVARTHY, S. R. 1986. Some results on uniformly high-order accurate essentially nonoscillatory schemes. *Applied Numerical Mathematics,* 2**,** 347-377.

HARTMANN, H. & ANDRESKY, L. 2013. Flooding in the Indus River basin — A spatiotemporal analysis of precipitation records. *Global and Planetary Change,* 107**,** 25-35.

HE, H., TIAN, Y. Q., MU, X., ZHOU, J., LI, Z., CHENG, N., ZHANG, Q., KEO, S. & OEURNG, C. 2015. Confluent flow impacts of flood extremes in the middle Yellow River. *Quaternary International,* 380–381**,** 382-390.

HERGET, J., KAPALA, A., KRELL, M., RUSTEMEIER, E., SIMMER, C. & WYSS, A. 2015. The millennium flood of July 1342 revisited. *Catena,* 130**,** 82-94.

HERGET, J. & MEURS, H. 2010. Reconstructing peak discharges for historic flood levels in the city of Cologne, Germany. *Global and Planetary Change,* 70**,** 108-116.

HERVOUET, J.-M. 2007. *Hydrodynamics of free surface flows: modelling with the finite element method*, John Wiley & Sons.

HILL, C. & VERJEE, F. 2010. Flash flood early warning system reference guide 2010. *University Corporation for Atmospheric Research.*

HIRT, C. W. & NICHOLS, B. D. 1981. Volume of fluid (VOF) method for the dynamics of free boundaries. *Journal of computational physics,* 39**,** 201-225.

HORRITT, M. S. & BATES, P. D. 2002. Evaluation of 1D and 2D numerical models for predicting river flood inundation. *Journal of Hydrology,* 268**,** 87-99.

HOU, J., LIANG, Q., ZHANG, H. & HINKELMANN, R. 2015. An efficient unstructured MUSCL scheme for solving the 2D shallow water equations. *Environmental Modelling & Software,* 66**,** 131-152.

HOUGH, A. 2012. *Welsh village evacuated as flash floods strike Britain* [Online]. Available: http://www.telegraph.co.uk/topics/weather/9322889/Weather-Welsh-village-evacuated-as-flash-floods-strike-Britain.html. [Accessed 18/09/2015].

HR WALLINGFORD 2005. Flooding in Boscastle and North Cornwall, August 2004 (Phase 2 Studies Report). Report EX 5160. Wallingford.

HUANG, S., VOROGUSHYN, S. & LINDENSCHMIDT, K.-E. 2007. Quasi 2D hydrodynamic modelling of the flooded hinterland due to dyke breaching on the Elbe River. *Advances in Geosciences,* 11**,** 21-29.

HUNTER, N., BATES, P., NEELZ, S., PENDER, G., VILLANUEVA, I., WRIGHT, N., LIANG, D., FALCONER, R. A., LIN, B. & WALLER, S. Benchmarking 2D hydraulic models for urban flood simulations. Proceedings of the Institution of Civil Engineers: Water Management, 2008. Thomas Telford (ICE publishing), 13-30.

HUNTER, N. M., BATES, P. D., HORRITT, M. S. & WILSON, M. D. 2007. Simple spatially-distributed models for predicting flood inundation: A review. *Geomorphology,* 90**,** 208-225.

HUNTINGTON, T. G. 2006. Evidence for intensification of the global water cycle: review and synthesis. *Journal of Hydrology,* 319**,** 83-95.

INSTITUTE OF RIVER AND COASTAL ENGINEERING 2006. Two-dimensional flow calculation. *Lecture material - Environmental Hydraulic Simulation* Hamburg, Germany: Hamburg University of Technology.

INTEL. 2013. *Intel® Fortran Compiler XE 13.1 User and Reference Guide.*

ISAACSON, E., STOKER, J. J. & TROESCH, A. 1958. Numerical solution of flow problems in rivers. *Journal of the Hydraulics Division,* 84**,** 1-18.

IZEM, N., SEAID, M. & WAKRIM, M. 2016. A discontinuous Galerkin method for two-layer shallow water equations. *Mathematics and Computers in Simulation,* 120**,** 12-23.

JANSSEN, J. A., HOEKSTRA, A. Y., DE KOK, J.-L. & SCHIELEN, R. M. 2009. Delineating the model-stakeholder gap: framing perceptions to analyse the information requirement in river management. *Water resources management,* 23**,** 1423-1445.

JHA, A. K., AKIYAMA, J. & URA, M. 2000. Flux-difference splitting schemes for 2D flood flows. *Journal of hydraulic engineering,* 126**,** 33-42.

JI, B., LUO, X., WU, Y., PENG, X. & XU, H. 2012. Partially-Averaged Navier–Stokes method with modified k–ε model for cavitating flow around a marine propeller in a non-uniform wake. *International Journal of Heat and Mass Transfer,* 55**,** 6582-6588.

JONGMAN, B., HOCHRAINER-STIGLER, S., FEYEN, L., AERTS, J. C., MECHLER, R., BOTZEN, W. W., BOUWER, L. M., PFLUG, G., ROJAS, R. & WARD, P. J. 2014. Increasing stress on disaster-risk finance due to large floods. *Nature Climate Change,* 4**,** 264-268.

JONKMAN, S. N., KOK, M. & VRIJLING, J. K. 2008. Flood risk assessment in the Netherlands: A case study for dike ring South Holland. *Risk Analysis,* 28**,** 1357-1373.

JONKMAN, S. N. & PENNING-ROWSELL, E. 2008. Human instability in flood flows. *Journal of the American Water Resources Association,* 44**,** 1208-1218.

JONKMAN, S. N., VAN GELER, P. H. A. J. M. & VRIJLING, J. K. Loss of life models for sea and river floods. *In:* WU, B., WANG, Z.-Y., WANG, G., HUANG, G. G. H., FARIG, H. & HUANG, J., eds. Flood Defence 2002, 2002. Science Press, New York, 196-206.

KARVONEN, R., HEPOJOKI, H., HUHTA, H. & LOUHIO, A. 2000. The Use Of Physical Models In Dam-Break Flood Analysis, Development of Rescue Actions Based on Dam-Break Flood Analysis (RESCDAM). Final report of Helsinki University of Technology. *Finnish Environment Institute.*

KATOPODES, N. D. & SCHAMBER, D. R. 1983. Applicability of dam-break flood wave models. *Journal of Hydraulic Engineering,* 109**,** 702-721.

KATOPODES, N. D. & STRELKOFF, T. 1978. Computing two-dimensional dam-break flood waves. *Journal of the Hydraulics Division,* 104**,** 1269-1288.

KAUFFELDT, A., WETTERHALL, F., PAPPENBERGER, F., SALAMON, P. & THIELEN, J. 2016. Technical review of large-scale hydrological models for implementation in operational flood forecasting schemes on continental level. *Environmental Modelling & Software,* 75**,** 68-76.

KAŹMIERCZAK, A. & CAVAN, G. 2011. Surface water flooding risk to urban communities: Analysis of vulnerability, hazard and exposure. *Landscape and Urban Planning,* 103**,** 185-197.

KELLER, R. J. & MITSCH, B. 1993. *Safety aspects of the design of roadways as floodways*, Urban Water Research Association of Australia.

KESSERWANI, G. & LIANG, Q. 2012. Influence of total-variation-diminishing slope limiting on local discontinuous galerkin solutions of the shallow water equations. *Journal of Hydraulic Engineering,* 138**,** 216-222.

KHAN, Z. & JOSHI, J. B. 2015. Comparison of k–ε, RSM and LES models for the prediction of flow pattern in jet loop reactor. *Chemical Engineering Science,* 127**,** 323-333.

KIRK, D. NVIDIA CUDA software and GPU parallel computing architecture. ISMM, 2007. 64.

KLIMEŠ, J., BENEŠOVÁ, M., VILÍMEK, V., BOUŠKA, P. & RAPRE, A. C. 2014. The reconstruction of a glacial lake outburst flood using HEC-RAS and its significance for future hazard assessments: an example from Lake 513 in the Cordillera Blanca, Peru. *Natural hazards,* 71**,** 1617-1638.

KNUTH, D. E. 1974. Structured Programming with go to Statements. *ACM Computing Surveys (CSUR),* 6**,** 261-301.

KOBOLD, M. 2011. Comparison of floods in September 2010 with registered historic flood events (in Slovenian). *Ujma,* 25**,** 48-56.

KOBOLD, M., SUŠNIK, M., ROBIČ, M., ULAGA, F. & LALIĆ, B. Hydrological analysis of high waters and flash floods occurred in September 2007 in Slovenia. IOP Conference Series: Earth and Environmental Science, 2008. IOP Publishing, 012008.

KOLKER, A. S., LI, C., WALKER, N. D., PILLEY, C., AMEEN, A. D., BOXER, G., RAMATCHANDIRANE, C., ULLAH, M. & WILLIAMS, K. A. 2014. The impacts of the great Mississippi/Atchafalaya River flood on the oceanography of the Atchafalaya Shelf. *Continental Shelf Research,* 86**,** 17-33.

KOLMOGOROV, A. N. 1962. A refinement of previous hypotheses concerning the local structure of turbulence in a viscous incompressible fluid at high Reynolds number. *Journal of Fluid Mechanics,* 13**,** 82-85.

KOMAC, B., NATEK, K. & ZORN, M. 2008. *Geographical aspects of floods in Slovenia (in SLovenian),* Ljubljana, Slovenia, Založba ZRC.

KOMAC, B. & ZORN, M. 2013. Extreme floods in Slovenia in September 2010. *Geomorphological impacts of extreme weather.* Springer.

KOPMANN, R. & MARKOFSKY, M. 2000. Three-dimensional water quality modelling with TELEMAC-3D. *Hydrological Processes,* 14**,** 2279-2292.

KOTLARSKI, S., HAGEMANN, S., KRAHE, P., PODZUN, R. & JACOB, D. 2012. The Elbe river flooding 2002 as seen by an extended regional climate model. *Journal of Hydrology,* 472–473**,** 169-183.

KUNDZEWICZ, Z. W. 2008. Climate change impacts on the hydrological cycle. *Ecohydrology & Hydrobiology,* 8**,** 195-203.

KUNDZEWICZ, Z. W., PIŃSKWAR, I. & BRAKENRIDGE, G. R. 2013. Large floods in Europe, 1985–2009. *Hydrological Sciences Journal,* 58**,** 1-7.

LAMB, R., MANTZ, P., ATABAY, S., BENN, J. & PEPPER, A. Recent advances in modelling flood water levels at bridges and culverts. Proceedings of 41st Defra Flood and Coastal Risk Management Conference, 2006. 4-6.

LAMOVEC, P., OŠTIR, K. & MIKOŠ, M. 2012. Flash floods and peak discharge estimation: The Selška Sora River flash flood in September 2007, W Slovenia. *12th Congress INTERPRAEVENT.* Grenoble, France.

LAUNDER, B., REECE, G. J. & RODI, W. 1975. Progress in the development of a Reynolds-stress turbulence closure. *Journal of fluid mechanics,* 68**,** 537-566.

LAX, P. 2006. Gibbs Phenomena. *Journal of Scientific Computing,* 28**,** 445-449.

LAX, P. D. 1973. *Hyperbolic systems of conservation laws and the mathematical theory of shock waves*, SIAM.

LAX, P. D. & WENDROFF, B. 1960. Systems of conservation laws. *Communications on Pure and Applied Mathematics,* 13**,** 217-237.

LENDERINK, G. & VAN MEIJGAARD, E. 2008. Increase in hourly precipitation extremes beyond expectations from temperature changes. *Nature Geoscience,* 1**,** 511-514.

LEOPARDI, A., OLIVERI, E. & GRECO, M. 2002. Two-dimensional modeling of floods to map risk-prone areas. *Journal of water resources planning and management,* 128**,** 168-178.

LESKENS, J., BRUGNACH, M., HOEKSTRA, A. & SCHUURMANS, W. 2014a. Why are decisions in flood disaster management so poorly supported by information from flood models? *Environmental modelling & software,* 53**,** 53-61.

LESKENS, J. G., BRUGNACH, M., HOEKSTRA, A. Y. & SCHUURMANS, W. 2014b. Why are decisions in flood disaster management so poorly supported by information from flood models? *Environmental Modelling & Software,* 53**,** 53-61.

LI, G., DONG, G., WEN, L. & CHEN, F. 2014a. Overbank flooding and human occupation of the Shalongka site in the Upper Yellow River Valley, northeast Tibet Plateau in relation to climate change since the last deglaciation. *Quaternary Research,* 82**,** 354-365.

LI, N., KINZELBACH, W., LI, W. & DONG, X. 2015. Box model and 1D longitudinal model of flow and transport in Bosten Lake, China. *Journal of Hydrology,* 524**,** 62-71.

LI, Y., RYU, D., WESTERN, A. W., WANG, Q., ROBERTSON, D. E. & CROW, W. T. 2014b. An integrated error parameter estimation and lag-aware data assimilation scheme for real-time flood forecasting. *Journal of hydrology,* 519**,** 2722-2736.

LIANG, D., FALCONER, R. A. & LIN, B. 2006. Comparison between TVD-MacCormack and ADI-type solvers of the shallow water equations. *Advances in water resources,* 29**,** 1833-1845.

LIANG, D., FALCONER, R. A. & LIN, B. Linking one-and two-dimensional models for free surface flows. Proceedings of the Institution of Civil Engineers-Water Management, 2007a. Thomas Telford Ltd, 145-151.

LIANG, D., LIN, B. & FALCONER, R. A. 2007b. A boundary-fitted numerical model for flood routing with shock-capturing capability. *Journal of hydrology,* 332**,** 477-486.

LIANG, D., LIN, B. & FALCONER, R. A. 2007c. Simulation of rapidly varying flow using an efficient TVD-MacCormack scheme. *International journal for numerical methods in fluids,* 53**,** 811-826.

LIANG, D., WANG, X., FALCONER, R. A. & BOCKELMANN-EVANS, B. N. 2010. Solving the depth-integrated solute transport equation with a TVD-MacCormack scheme. *Environmental Modelling & Software,* 25**,** 1619-1629.

LIANG, D., XIA, J., FALCONER, R. A. & ZHANG, J. 2014. On the refinement of a boundary-fitted shallow water model. *Coastal Engineering Journal,* 56**,** 1450001.

LIANG, Q., DU, G., HALL, J. W. & BORTHWICK, A. G. 2008. Flood inundation modeling with an adaptive quadtree grid shallow water equation solver. *Journal of Hydraulic Engineering,* 134**,** 1603-1610.

LIN, B., WICKS, J. M., FALCONER, R. A. & ADAMS, K. 2006. Integrating 1D and 2D hydrodynamic models for flood simulation. *Proceedings of the Institution of Civil Engineers: Water Management,* 159**,** 19-25.

LIND, N., HARTFORD, D. & ASSAF, H. 2004. Hydrodynamic models of human stability in a flood. *Journal of the American Water Resources Association,* 40**,** 89-96.

LINDENSCHMIDT, K.-E., HUANG, S. & BABOROWSKI, M. 2008. A quasi-2D flood modeling approach to simulate substance transport in polder systems for environment flood risk assessment. *Science of the total environment,* 397**,** 86-102.

LITRICO, X. & FROMION, V. 2009. Chapter 2: Modeling of Open Channel Flow. *Modeling and Control of Hydrosystems.* Springer London.

LIU, Q., QIN, Y., ZHANG, Y. & LI, Z. 2015. A coupled 1D–2D hydrodynamic model for flood simulation in flood detention basin. *Natural Hazards,* 75**,** 1303-1325.

LIU, X.-D., OSHER, S. & CHAN, T. 1994. Weighted essentially non-oscillatory schemes. *Journal of computational physics,* 115**,** 200-212.

LOWE, C. 2013. *Homes evacuated in Treorchy after flash flooding* [Online]. Available: http://www.walesonline.co.uk/news/wales-news/homes-evacuated-treorchy-after-flash-6407007 [Accessed 18/09/2015].

MA, G., SHI, F. & KIRBY, J. T. 2012. Shock-capturing non-hydrostatic model for fully dispersive surface wave processes. *Ocean Modelling,* 43–44**,** 22-35.

MACCORMACK, R. W. 1969. The effect of viscosity in hypervelocity impact cratering. *Hypervelocity impact conference.* Cincinnati, Ohio, USA: American Institute of Aeronautics and Astronautics, New York, USA.

MACCORMACK, R. W. 1976. An efficient numerical method for solving the time-dependent compressible Navier-Stokes equations at high Reynolds number. Moffett Field, California, USA: NASA Ames Research Center.

MACHALINSKA-MURAWSKA, J. & SZYDŁOWSKI, M. 2014. Lax-Wendroff and McCormack Schemes for Numerical Simulation of Unsteady Gradually and Rapidly Varied Open Channel Flow. *Archives of Hydro-Engineering and Environmental Mechanics,* 60**,** 51-62.

MAHMOOD, K., YEVJEVICH, V. M. & MILLER, W. A. 1975. *Unsteady flow in open channels*, Water Resources Publications Fort Collins, Colorado,, USA.

MAIJALA, T., HUOKUNA, M. & HONKAKUNNAS, T. 2001. Development of rescue actions based on dam-break flood analysis. *RESCDAM, Final report*.

MARCHE, F., BONNETON, P., FABRIE, P. & SEGUIN, N. 2007. Evaluation of well-balanced bore-capturing schemes for 2D wetting and drying processes. *International Journal for Numerical Methods in Fluids,* 53**,** 867-894.

MARCHI, L., BORGA, M., PRECISO, E. & GAUME, E. 2010. Characterisation of selected extreme flash floods in Europe and implications for flood risk management. *Journal of Hydrology,* 394**,** 118-133.

MARCHI, L., BORGA, M., PRECISO, E., SANGATI, M., GAUME, E., BAIN, V., DELRIEU, G., BONNIFAIT, L. & POGAČNIK, N. 2009. Comprehensive post-event survey of a flash flood in Western Slovenia: observation strategy and lessons learned. *Hydrological processes,* 23**,** 3761-3770.

MARTIN, C. S. & DEFAZIO, F. G. 1969. Open-channel surge simulation by digital computer. *Journal of the Hydraulics Division,* 95**,** 2049-2070.

MARTIN, C. S. & ZOVNE, J. J. 1971. Finite-difference simulation of bore propagation. *Journal of the Hydraulics Division,* 97**,** 993-1010.

MARTÍNEZ IBARRA, E. 2012. A geographical approach to post-flood analysis: The extreme flood event of 12 October 2007 in Calpe (Spain). *Applied Geography,* 32**,** 490-500.

MASON, D. C., COBBY, D. M., HORRITT, M. S. & BATES, P. D. 2003. Floodplain friction parameterization in two-dimensional river flood models using vegetation heights derived from airborne scanning laser altimetry. *Hydrological Processes,* 17**,** 1711-1732.

MASON, D. C., HORRITT, M. S., HUNTER, N. M. & BATES, P. D. 2007. Use of fused airborne scanning laser altimetry and digital map data for urban flood modelling. *Hydrological Processes,* 21**,** 1436-1447.

MCGAHEY, C., SAMUELS, P. G. & KNIGHT, D. W. A practical approach to estimating the flow capacity of rivers - Application and analysis. Proceedings of the International Conference on Fluvial Hydraulics - River Flow 2006, 2006. 303-312.

MCGAHEY, C., SAMUELS, P. G., KNIGHT, D. W. & O'HARE, M. T. 2008. Estimating river flow capacity in practice. *Journal of Flood Risk Management,* 1**,** 23-33.

MENSENCAL, Y. 2012. Use of TELEMAC software system as a technical modelling tool for coastal zone development studies. *SOGREAH Eau-Energie-Environnement-SPICOSA project.*

MERKURYEVA, G., MERKURYEV, Y., SOKOLOV, B. V., POTRYASAEV, S., ZELENTSOV, V. A. & LEKTAUERS, A. 2015. Advanced river flood monitoring, modelling and forecasting. *Journal of Computational Science,* 10**,** 77-85.

MICHOT, D., WALTER, C., ADAM, I. & GUÉRO, Y. 2013. Digital assessment of soil-salinity dynamics after a major flood in the Niger River valley. *Geoderma,* 207–208**,** 193-204.

MIGNOT, E., PAQUIER, A. & HAIDER, S. 2006. Modeling floods in a dense urban area using 2D shallow water equations. *Journal of Hydrology,* 327**,** 186-199.

MIHAESCU, M., MURUGAPPAN, S., KALRA, M., KHOSLA, S. & GUTMARK, E. 2008. Large Eddy Simulation and Reynolds-Averaged Navier–Stokes modeling of flow in a realistic pharyngeal airway model: An investigation of obstructive sleep apnea. *Journal of biomechanics,* 41**,** 2279-2288.

MILANESI, L., PILOTTI, M. & RANZI, R. 2015. A conceptual model of people's vulnerability to floods. *Water Resources Research,* 51**,** 182-197.

MIN, S.-K., ZHANG, X., ZWIERS, F. W. & HEGERL, G. C. 2011. Human contribution to more-intense precipitation extremes. *Nature,* 470**,** 378-381.

MINISTRY OF THE ENVIRONMENT AND SPATIAL PLANNING OF THE REPUBLIC OF SLOVENIA. 2015. *LIDAR* [Online]. Available: http://evode.arso.gov.si/indexd022.html?q=node/12 [Accessed 10/10/2015 2015].

MIRZAEI, M., KRAJNOVIĆ, S. & BASARA, B. 2015. Partially-Averaged Navier–Stokes simulations of flows around two different Ahmed bodies. *Computers & Fluids,* 117**,** 273-286.

MOGOLLÓN, B., FRIMPONG, E. A., HOEGH, A. B. & ANGERMEIER, P. L. 2016. An empirical assessment of which inland floods can be managed. *Journal of Environmental Management,* 167**,** 38-48.

MOHAMMADI, A., RYU, D. & COSTELLOE, J. 2013. Mapping of flow paths in large, anastomosing arid zone rivers: Cooper Creek, Australia. *Modelling & Simulation Society of Australia & New Zealand***,** 2485-2491.

MOIN, P. & MAHESH, K. 1998. Direct numerical simulation: a tool in turbulence research. *Annual review of fluid mechanics,* 30**,** 539-578.

MORALES-HERNÁNDEZ, M., GARCÍA-NAVARRO, P., BURGUETE, J. & BRUFAU, P. 2013. A conservative strategy to couple 1D and 2D models for shallow water flow simulation. *Computers & Fluids,* 81**,** 26-44.

MORALES-HERNÁNDEZ, M., PETACCIA, G., BRUFAU, P. & GARCÍA-NAVARRO, P. 2016. Conservative 1D–2D coupled numerical strategies applied to river flooding: The Tiber (Rome). *Applied Mathematical Modelling,* 40**,** 2087-2105.

MOUSSA, R. & BOCQUILLON, C. 2009. On the use of the diffusive wave for modelling extreme flood events with overbank flow in the floodplain. *Journal of Hydrology,* 374**,** 116-135.

MUDELSEE, M., BÖRNGEN, M., TETZLAFF, G. & GRÜNEWALD, U. 2004. Extreme floods in central Europe over the past 500 years: Role of cyclone pathway "Zugstrasse Vb". *Journal of Geophysical Research: Atmospheres (1984–2012),* 109.

MUIS, S., GÜNERALP, B., JONGMAN, B., AERTS, J. C. & WARD, P. J. 2015. Flood risk and adaptation strategies under climate change and urban expansion: A probabilistic analysis using global data. *Science of The Total Environment,* 538**,** 445-457.

NASH, J. E. & SUTCLIFFE, J. V. 1970. River flow forecasting through conceptual models part I—A discussion of principles. *Journal of hydrology,* 10**,** 282-290.

NEAL, J., VILLANUEVA, I., WRIGHT, N., WILLIS, T., FEWTRELL, T. & BATES, P. 2012. How much physical complexity is needed to model flood inundation? *Hydrological Processes,* 26**,** 2264-2282.

NEELZ, S. & PENDER, G. 2009. Desktop review of 2D hydraulic modelling packages. Bristol: Environment Agency.

NEELZ, S. & PENDER, G. 2013. Benchmarking the latest generation of 2D hydraulic modelling packages. Bristol: Environment Agency.

NEWTON, I. 1687. *Mathematical Principles of Natural Philosophy,* California, Berkeley University Press.

NIKOLOVA, G. S. & TOSHEV, Y. E. 2007. Estimation of male and female body segment parameters of the Bulgarian population using a 16-segmental mathematical model. *Journal of biomechanics,* 40**,** 3700-3707.

NORBIATO, D., BORGA, M., DEGLI ESPOSTI, S., GAUME, E. & ANQUETIN, S. 2008. Flash flood warning based on rainfall thresholds and soil moisture conditions: An assessment for gauged and ungauged basins. *Journal of Hydrology,* 362**,** 274-290.

NORMANT, C. L. 2000. Three-dimensional modelling of cohesive sediment transport in the Loire estuary. *Hydrological processes,* 14**,** 2231-2243.

OERTEL, M. 2015. Numerical Modeling of Free-Surface Flows in Practical Applications. *In:* ROWIŃSKI, P. & RADECKI-PAWLIK, A. (eds.) *Rivers – Physical, Fluvial and Environmental Processes.* Cham: Springer International Publishing.

OKAZE, T., TAKANO, Y., MOCHIDA, A. & TOMINAGA, Y. 2015. Development of a new k–ε model to reproduce the aerodynamic effects of snow particles on a flow field. *Journal of Wind Engineering and Industrial Aerodynamics,* 144**,** 118-124.

OUYANG, C., HE, S., XU, Q., LUO, Y. & ZHANG, W. 2013. A MacCormack-TVD finite difference method to simulate the mass flow in mountainous terrain with variable computational domain. *Computers & Geosciences,* 52**,** 1-10.

OWEN, S. J. & SHEPHARD, M. S. 2003. Special Issue: Trends in Unstructured Mesh Generation. *International Journal for Numerical Methods in Engineering,* 58**,** 159-160.

OZDEMIR, H., SAMPSON, C., DE ALMEIDA, G. A. & BATES, P. 2013. Evaluating scale and roughness effects in urban flood modelling using terrestrial LIDAR data. *Hydrology and Earth System Sciences,* 10**,** 5903-5942.

PALL, P., AINA, T., STONE, D. A., STOTT, P. A., NOZAWA, T., HILBERTS, A. G. J., LOHMANN, D. & ALLEN, M. R. 2011. Anthropogenic greenhouse gas contribution to flood risk in England and Wales in autumn 2000. *Nature,* 470**,** 382-385.

PAPPENBERGER, F., BEVEN, K., HORRITT, M. & BLAZKOVA, S. 2005. Uncertainty in the calibration of effective roughness parameters in HEC-RAS using inundation and downstream level observations. *Journal of Hydrology,* 302**,** 46-69.

PARK, D. & MARKUS, M. 2014. Analysis of a changing hydrologic flood regime using the Variable Infiltration Capacity model. *Journal of Hydrology,* 515**,** 267-280.

PEIRÓ, J. & SHERWIN, S. 2005. Finite difference, finite element and finite volume methods for partial differential equations. *Handbook of materials modeling.* Springer.

PENDER, G. 2006. Briefing: Introducing the flood risk management research consortium. *Proceedings of the ICE-Water Management,* 159**,** 3-8.

PENDER, G. & NÉELZ, S. 2011. Flood Inundation Modelling to Support Flood Risk Management. *Flood Risk Science and Management.*

PENNING-ROWSELL, E., FLOYD, P., RAMSBOTTOM, D. & SURENDRAN, S. 2005. Estimating injury and loss of life in floods: a deterministic framework. *Natural Hazards,* 36**,** 43-64.

PERKO, D. 1998. Krška ravan (in Slovenian). *In:* PERKO, D. & ADAMIČ, M. O. E. (eds.) *Slovenija: pokrajina in ljudje.* Ljubljana, Slovenia: Mladinska knjiga.

PHILLIPS, I. & MCGREGOR, G. 2001. The relationship between synoptic scale airflow direction and daily rainfall: a methodology applied to Devon and Cornwall, South West England. *Theoretical and Applied Climatology,* 69**,** 179-198.

PHILLIPS, I. D. & MCGREGOR, G. R. 2002. The relationship between monthly and seasonal South-west England rainfall anomalies and concurrent North Atlantic sea surface temperatures. *International Journal of Climatology,* 22**,** 197-217.

PINSON, F., GRÉGOIRE, O. & SIMONIN, O. 2006. k–ε Macro-scale modeling of turbulence based on a two scale analysis in porous media. *International Journal of Heat and Fluid Flow,* 27**,** 955-966.

POTTER, M., WIGGERT, D. & RAMADAN, B. 2012. *Mechanics of Fluids, SI Edition, 5th Edition*, Cengage Learning.

PURWANDARI, T., HADI, M. P. & KINGMA, N. C. 2011. A GIS modelling approach for flood hazard assessment in part of Surakarta city, Indonesia. *Indonesian Journal of Geography,* 43.

RAHIMPOUR, M. & TAVAKOLI, A. 2011. Multi-grid Beam and Warming scheme for the simulation of unsteady flow in an open channel. *Water SA,* 37.

RAJAR, R. 1980. *Hydromechanics (in Slovenian),* Ljubljana, Slovenia, University of Ljubljana, Faculty of Civil and Geodetic Engineering.

RAMSBOTTOM, D., FLOYD, P. & PENNING-ROWSELL, E. 2003. *Flood risks to people: Phase 1. R&D Technical Report FD2317*, Department for the Environment, Food and Rural Affairs (DEFRA), UK Environment Agency.

RAMSBOTTOM, D., WADE, S., BAIN, V., HASSAN, M., PENNING-ROWSELL, E., WILSON, T., FERNANDEZ, A., HOUSE, M. & FLOYD, P. 2006. *Flood risks to people: Phase 2. R&D Technical Report FD2321/IR2*, Department for the Environment, Food and Rural Affairs (DEFRA), UK Environment Agency.

RANSOM, O. & YOUNIS, B. A. 2015. Selective application of a total variation diminishing term to an implicit method for two-dimensional flow modelling. *Journal of Flood Risk Management,* 8**,** 52-61.

RANSOM, O. T. & YOUNIS, B. A. 2016. Explicit GPU Based Second-Order Finite-Difference Modeling on a High Resolution Surface, Feather River, California. *Water Resources Management,* 30**,** 261-277.

RAŠKA, P. & EMMER, A. 2014. The 1916 catastrophic flood following the Bílá Desná dam failure: The role of historical data sources in the reconstruction of its geomorphologic and landscape effects. *Geomorphology,* 226**,** 135-147.

REDDY, J. N. 1993. *An introduction to the finite element method*, McGraw-Hill New York.

REZOUG, M., EL MEOUCHE, R., HAMZAOUI, R., KHREIM, J., FENG, Z. & BASSIR, D. 2010. Optimal Modeling Study of Flooding Phenomenon in Urban Area (Dam break case). *International Journal for Simulation and Multidisciplinary Design Optimization,* 4**,** 149-158.

ROCA, M. & DAVISON, M. 2010. Two dimensional model analysis of flash-flood processes: application to the Boscastle event. *Journal of Flood Risk Management,* 3**,** 63-71.

RODI, W. 1993. *Turbulence models and their application in hydraulics: A state-of-the-art review*, CRC Press.

ROE, P. & PIKE, J. Efficient construction and utilisation of approximate Riemann solutions. Proc. of the sixth int'l. symposium on Computing methods in applied sciences and engineering, VI, 1985. North-Holland Publishing Co., 499-518.

ROE, P. L. 1981. Approximate Riemann solvers, parameter vectors, and difference schemes. *Journal of computational physics,* 43**,** 357-372.

ROE, P. L. 1992. Sonic flux formulae. *SIAM journal on scientific and statistical computing,* 13**,** 611-630.

ROGERS, B. D., BORTHWICK, A. G. & TAYLOR, P. H. 2003. Mathematical balancing of flux gradient and source terms prior to using Roe's approximate Riemann solver. *Journal of Computational Physics,* 192**,** 422-451.

ROJAS, R., FEYEN, L. & WATKISS, P. 2013. Climate change and river floods in the European Union: Socio-economic consequences and the costs and benefits of adaptation. *Global Environmental Change,* 23**,** 1737-1751.

ROSATTI, G., BONAVENTURA, L., DEPONTI, A. & GAREGNANI, G. 2011. An accurate and efficient semi-implicit method for section-averaged free-surface flow modelling. *International Journal for Numerical Methods in Fluids,* 65**,** 448-473.

ROSEVEARE, N. & TRAPMORE, G. The sustainable regeneration of Boscastle. BHS 10th National Hydrology Symposium, Exeter, 2008.

ROZALIS, S., MORIN, E., YAIR, Y. & PRICE, C. 2010. Flash flood prediction using an uncalibrated hydrological model and radar rainfall data in a Mediterranean watershed under changing hydrological conditions. *Journal of hydrology,* 394**,** 245-255.

RUSJAN, S., KOBOLD, M. & MIKOŠ, M. 2009. Characteristics of the extreme rainfall event and consequent flash floods in W Slovenia in September 2007. *Natural Hazards and Earth System Science,* 9**,** 947-956.

RYABEN'KII, V. S. & TSYNKOV, S. V. 2006. *A theoretical introduction to numerical analysis*, Chapman and Hall/CRC Press.

SAJIKUMAR, N. & REMYA, R. S. 2015. Impact of land cover and land use change on runoff characteristics. *Journal of Environmental Management,* 161**,** 460-468.

SALEH, F., DUCHARNE, A., FLIPO, N., OUDIN, L. & LEDOUX, E. 2013. Impact of river bed morphology on discharge and water levels simulated by a 1D Saint–Venant hydraulic model at regional scale. *Journal of Hydrology,* 476**,** 169-177.

SÁNCHEZ-LINARES, C., DE LA ASUNCIÓN, M., CASTRO, M. J., MISHRA, S. & ŠUKYS, J. 2015. Multi-level Monte Carlo finite volume method for shallow water equations with uncertain parameters applied to landslides-generated tsunamis. *Applied Mathematical Modelling,* 39**,** 7211-7226.

SANDERS, B. F. 2007. Evaluation of on-line DEMs for flood inundation modeling. *Advances in Water Resources,* 30**,** 1831-1843.

SANTOS, M., SANTOS, J. & FRAGOSO, M. 2015. Historical damaging flood records for 1871–2011 in Northern Portugal and underlying atmospheric forcings. *Journal of Hydrology,* 530**,** 591-603.

SAVAGE, J. T. S., BATES, P., FREER, J., NEAL, J. & ARONICA, G. 2015. When does spatial resolution become spurious in probabilistic flood inundation predictions? *Hydrological Processes.*

SCHÄFER, M. 2006. Finite-Volume Methods. *Computational engineering - Introduction to numerical methods.* Berlin, Germany: Springer.

SCHRÖTER, K., KUNZ, M., ELMER, F., MÜHR, B. & MERZ, B. 2015. What made the June 2013 flood in Germany an exceptional event? A hydro-meteorological evaluation. *Hydrology and Earth System Sciences,* 19**,** 309-327.

SENE, K. 2008. *Flood warning, forecasting and emergency response*, Springer Science & Business Media.

SHIMADA, K. & ISHIHARA, T. 2002. Application of a modified k–ε model to the prediction of aerodynamic characteristics of rectangular cross-section cylinders. *Journal of fluids and structures,* 16**,** 465-485.

SHRESTHA, K. Y., WEBSTER, P. J. & TOMA, V. E. 2014. An atmospheric-hydrologic forecasting scheme for the Indus River basin. *Journal of Hydrometeorology,* 15**,** 861-890.

SHU, C.-W. & OSHER, S. 1988. Efficient implementation of essentially non-oscillatory shock-capturing schemes. *Journal of Computational Physics,* 77**,** 439-471.

ŠIFRER, M., LOVRENČAK, F. & NATEK, M. 1980. *Geographical characteristics of the flood areas in the Krka River Basin below Otočec (in Slovenian),* Ljubljana, Slovenia, Založba ZRC.

SLOVENIAN ENVIRONMENT AGENCY. 2008. *Viskoe vode in poplave 18. septembra 2007 (in Slovenian)* [Online]. Available: http://www.arso.gov.si/vode/poro%C4%8Dila%20in%20publikacije/Visoke%20vode%20in%20poplave%2018.%20septembra%202007.pdf [Accessed 15/10/2015].

SLOVENIAN ENVIRONMENT AGENCY. 2010a. *Hidrološko porocilo o povodnji v dneh od 17. do 21. septembra 2010 (in Slovenian)* [Online]. Available: http://www.arso.gov.si/vode/poro%C4%8Dila%20in%20publikacije/Poplave%2017.%20-%2021.%20september%202010.pdf [Accessed 15/10/2015].

SLOVENIAN ENVIRONMENT AGENCY. 2010b. *Porocilo o izjemno obilnih padavinah od 16. do 19. septembra 2010 (in Slovenian)* [Online]. Available: http://meteo.arso.gov.si/uploads/probase/www/climate/text/sl/weather_events/padavine_16-19sep10.pdf [Accessed 15/10/2015].

SLOVENIAN ENVIRONMENT AGENCY. 2013. *Povratne dobe velikih in malih pretokov za merilna mesta državnega hidrološkega monitoringa površinskih voda (in Slovenian)* [Online]. Available: http://www.arso.gov.si/vode/podatki/Povratne%20dobe%20Qvk,Qnp.pdf [Accessed 15/10/2015].

SLOVENIAN ENVIRONMENT AGENCY. 2015a. *Hydrological archive - Krka, Podbočje (in Slovenian)* [Online]. Available: http://vode.arso.gov.si/hidarhiv/pov_arhiv_tab.php?p_vodotok=Krka&p_post aja=7160&p_leto=2010&b_arhiv=Prika%C5%BEi [Accessed 20/10/2015].

SLOVENIAN ENVIRONMENT AGENCY. 2015b. *Hydrological archive - Selška Sora, Železniki (in Slovenian)* [Online]. Available: http://vode.arso.gov.si/hidarhiv/pov_arhiv_tab.php?p_vodotok=Sel%C5%A1 ka+Sora&p_postaja=4270&p_leto=2007&b_arhiv=Prika%C5%BEi [Accessed 20/10/2015].

SMITH, G. & WASKO, C. 2012. Revision Project 15: Two Dimensional Simulations in Urban Areas - Representation of Buildings in 2D Numerical Flood Models. *In:* BALL, J. (ed.) *Australian Rainfall and Runoff.* Canberra, Australia: Engineers Australia.

SPADA, E., TUCCIARELLI, T., SINAGRA, M., SAMMARTANO, V. & CORATO, G. 2015. Computation of vertically averaged velocities in irregular sections of straight channels. *Hydrology and Earth System Sciences,* 19**,** 3857-3873.

SPARKS, T. D., BOCKELMANN-EVANS, B. N. & FALCONER, R. A. 2013. Development and analytical verification of an integrated 2-D surface water—Groundwater model. *Water resources management,* 27**,** 2989-3004.

STELLING, G. S. 2012. Quadtree flood simulations with sub-grid digital elevation models. *Proceedings of the Institution of Civil Engineers - Water Management,* 165**,** 567-580.

STELLING, G. S. & VERWEY, A. 2005. Numerical Flood Simulation. *In:* ANDERSON, M. G. (ed.) *Encyclopedia of Hydrological Sciences.* John Wiley & Sons, Ltd.

STELLING, G. S., WIERSMA, A. & WILLEMSE, J. 1986. Practical aspects of accurate tidal computations. *Journal of Hydraulic Engineering,* 112**,** 802-816.

STRANG, G. 1968. On the construction and comparison of difference schemes. *SIAM Journal on Numerical Analysis,* 5**,** 506-517.

SWEBY, P. K. 2001. Godunov Methods. *In:* TORO, E. F. (ed.) *Godunov Methods: Theory and Applications.* Boston, MA: Springer US.

SZYMKIEWICZ, R. 2010. *Numerical modeling in open channel hydraulics*, Springer Science & Business Media.

TAKAHASHI, S., ENDOH, K. & MURO, Z. 1992. Experimental study on people's safety against overtopping waves on breakwaters. *Report on the Port and Harbour Institute,* 34**,** 4-31.

TANNEHILL, J. C., ANDERSON, D. & PLETCHER, R. H. 1997. *Computational Fluid Mechanics and Heat Transfer, Second edition,* Washington DC, USA, CRC Press.

THERRELL, M. D. & BIALECKI, M. B. 2015. A multi-century tree-ring record of spring flooding on the Mississippi River. *Journal of Hydrology,* 529, Part 2**,** 490-498.

THIELEN, J., BARTHOLMES, J., RAMOS, M. H. & DE ROO, A. 2009. The European flood alert system - Part 1: Concept and development. *Hydrology and Earth System Sciences,* 13**,** 125-140.

THOMAS, H. & NISBET, T. 2007. An assessment of the impact of floodplain woodland on flood flows. *Water and Environment Journal,* 21**,** 114-126.

TIMMERMAN, J., BEINAT, E., TERMEER, C. & COFINO, W. 2010. A methodology to bridge the water information gap. *Water Science & Technology,* 62.

TRIGG, M. A., WILSON, M. D., BATES, P. D., HORRITT, M. S., ALSDORF, D. E., FORSBERG, B. R. & VEGA, M. C. 2009. Amazon flood wave hydraulics. *Journal of Hydrology,* 374**,** 92-105.

TSAKIRIS, G. & BELLOS, V. 2014. A Numerical Model for Two-Dimensional Flood Routing in Complex Terrains. *Water Resources Management,* 28**,** 1277-1291.

TSUBAKI, R. & FUJITA, I. 2010. Unstructured grid generation using LiDAR data for urban flood inundation modelling. *Hydrological processes,* 24**,** 1404-1420.

UN 2014. World Urbanizations Prospects: The 2014 revision. *Population Division of the Department of Economic and Social Affairs of the United Nations Secretariat, New York.*

UN 2015. World Population Prospects: The 2015 revision. *Population Division of the Department of Economic and Social Affairs of the United Nations Secretariat, New York.*

VACONDIO, R., DAL PALÙ, A. & MIGNOSA, P. 2014. GPU-enhanced Finite Volume Shallow Water solver for fast flood simulations. *Environmental Modelling & Software,* 57**,** 60-75.

VAN LEER, B. 1977. Towards the ultimate conservative difference scheme. IV. A new approach to numerical convection. *Journal of computational physics,* 23**,** 276-299.

VAN LEER, B. 1979. Towards the ultimate conservative difference scheme. V. A second-order sequel to Godunov's method. *Journal of computational Physics,* 32**,** 101-136.

VAN LEER, B. 1997. Godunov's method for gas-dynamics: Current applications and future developments. *Journal of Computational Physics,* 132**,** 1-2.

VERWEY, A. Latest developments in floodplain modelling-1D/2D integration. 6th Conference on Hydraulics in Civil Engineering: The State of Hydraulics; Proceedings, 2001. Institution of Engineers, Australia, 13.

VILLARET, C., HERVOUET, J.-M., KOPMANN, R., MERKEL, U. & DAVIES, A. G. 2013. Morphodynamic modeling using the Telemac finite-element system. *Computers & Geosciences,* 53**,** 105-113.

VOJINOVIC, Z. & TUTULIC, D. 2009. On the use of 1D and coupled 1D-2D modelling approaches for assessment of flood damage in urban areas. *Urban Water Journal,* 6**,** 183-199.

VOS, R. & FAROKHI, S. 2015. Introduction to Transonic Aerodynamics. *In:* THESS, A. (ed.) *Fluid Mechanics and Its Applications.* Springer.

VRHOVEC, T., RAKOVEC, J. & GREGORIČ, G. 2004. Mesoscale diagnostics of prefrontal and frontal precipitation in the Southeast Alps during MAP IOP 5. *Meteorology and Atmospheric Physics,* 86**,** 15-29.

WANG, F. & LIN, B. 2013. Modelling habitat suitability for fish in the fluvial and lacustrine regions of a new Eco-City. *Ecological modelling,* 267**,** 115-126.

WANG, Y. 2011. *Numerical improvements for large-scale flood simulation.* PhD, Newcastle University.

WANG, Z.-L. & GENG, Y.-F. 2013. Two-dimensional shallow water equations with porosity and their numerical scheme on unstructured grids. *Water Science and Engineering,* 6**,** 91-105.

WARMING, R. & BEAM, R. M. 1976. Upwind second-order difference schemes and applications in aerodynamic flows. *AIAA Journal,* 14**,** 1241-1249.

WARREN, R. A., KIRSHBAUM, D. J., PLANT, R. S. & LEAN, H. W. 2014. A 'Boscastle-type' quasi-stationary convective system over the UK Southwest Peninsula. *Quarterly Journal of the Royal Meteorological Society,* 140**,** 240-257.

WETTERHALL, F., PAPPENBERGER, F., ALFIERI, L., CLOKE, H. L., THIELEN-DEL POZO, J., BALABANOVA, S., DAŇHELKA, J., VOGELBACHER, A., SALAMON, P., CARRASCO, I., CABRERA-TORDERA, A. J., CORZO-TOSCANO, M., GARCIA-PADILLA, M., GARCIA-SANCHEZ, R. J., ARDILOUZE, C., JURELA, S., TEREK, B., CSIK, A., CASEY, J., STANKUNAVIČIUS, G., CERES, V., SPROKKEREEF, E., STAM, J., ANGHEL, E., VLADIKOVIC, D., ALIONTE EKLUND, C., HJERDT, N., DJERV, H., HOLMBERG, F., NILSSON, J., NYSTRÖM, K., SUŠNIK, M., HAZLINGER, M. & HOLUBECKA, M. 2013. HESS Opinions "forecaster priorities for improving probabilistic flood forecasts". *Hydrology and Earth System Sciences,* 17**,** 4389-4399.

WHITTAKER, P. 2014. *Modelling the hydrodynamic drag force of flexible riparian woodland.* PhD, Cardiff University.

WOOD, M., KOVACS, D., BOSTROM, A., BRIDGES, T. & LINKOV, I. 2012. Flood risk management: US Army Corps of Engineers and layperson perceptions. *Risk analysis,* 32**,** 1349-1368.

WORNI, R., HUGGEL, C. & STOFFEL, M. 2013. Glacial lakes in the Indian Himalayas—From an area-wide glacial lake inventory to on-site and modeling based risk assessment of critical glacial lakes. *Science of the Total Environment,* 468**,** S71-S84.

WU, W. & LIN, Q. 2015. A 3-D implicit finite-volume model of shallow water flows. *Advances in Water Resources,* 83**,** 263-276.

XIA, J., FALCONER, R. A., LIN, B. & TAN, G. 2011. Numerical assessment of flood hazard risk to people and vehicles in flash floods. *Environmental Modelling & Software,* 26**,** 987-998.

XIA, J., FALCONER, R. A., WANG, Y. & XIAO, X. 2014. New criterion for the stability of a human body in floodwaters. *Journal of Hydraulic Research,* 52**,** 93-104.

YATHEENDRADAS, S., WAGENER, T., GUPTA, H., UNKRICH, C., GOODRICH, D., SCHAFFNER, M. & STEWART, A. 2008. Understanding uncertainty in distributed flash flood forecasting for semiarid regions. *Water Resources Research,* 44.

YEE, H. C. 1989. A class of high-resolution explicit and implicit shock-capturing methods. Moffett Field, California, 94035 USA: NASA Ames Research Center, Computational Fluid Dynamics Branch.

YOON, T. H. & KANG, S.-K. 2004. Finite volume model for two-dimensional shallow water flows on unstructured grids. *Journal of Hydraulic Engineering,* 130**,** 678-688.

YOSHIDA, H. & DITTRICH, A. 2002. 1D unsteady-state flow simulation of a section of the upper Rhine. *Journal of Hydrology,* 269**,** 79-88.

YU, H., HUANG, G. & WU, C. 2015. Efficient Finite-Volume Model for Shallow-Water Flows Using an Implicit Dual Time-Stepping Method. *Journal of Hydraulic Engineering,* 141**,** 04015004.

ZANON, F., BORGA, M., ZOCCATELLI, D., MARCHI, L., GAUME, E., BONNIFAIT, L. & DELRIEU, G. 2010. Hydrological analysis of a flash flood across a climatic and geologic gradient: The September 18, 2007 event in Western Slovenia. *Journal of Hydrology,* 394**,** 182-197.

ZHANG, T., FENG, P., MAKSIMOVIĆ, Č. & BATES, P. D. 2016. Application of a Three-Dimensional Unstructured-Mesh Finite-Element Flooding Model and Comparison with Two-Dimensional Approaches. *Water Resources Management,* 30**,** 823-841.

ZHI-YONG, W., GUI-HUA, L., ZHI-YU, L., JIN-XING, W. & HENG, X. 2013. Trends of Extreme Flood Events in the Pearl River Basin during 1951–2010. *Advances in Climate Change Research,* 4**,** 110-116.

ZHOU, F., CHEN, G., HUANG, Y., YANG, J. Z. & FENG, H. 2013. An adaptive moving finite volume scheme for modeling flood inundation over dry and complex topography. *Water Resources Research,* 49**,** 1914-1928.

ZIENKIEWICZ, O. C. & TAYLOR, R. L. 1977. *The finite element method*, McGraw-hill London.

Publication list

Journal papers

Kvočka, D., Falconer, R. A. & Bray, M. (2016). Flood hazard assessment for extreme flood events. *Natural Hazards*, 84, 1569-1599.

Kvočka, D., Falconer, R. A. & Bray, M. (2015). Appropriate model use for predicting elevations and inundation extent for extreme flood events. *Natural Hazards*, 79, 1791-1808.

Conference Proceedings

Kvočka, D., Falconer, R. A., & Bray, M. (2016). Flood hazard assessment in areas prone to flash flooding. *EGU General Assembly Conference Abstracts*, Vol. 18, p. 4564.

Kvočka, D., Falconer, R. A., & Bray, M. (2015). Appropriate flood risk assessment tools for predicting flood inundation extent and assessing flood hazard risk for flash flood events. *E-proceedings of the 36th IAHR World Congress, The Hagues, the Netherlands*.